UNIVERSITY OF OKLAHOMA

GRADUATE COLLEGE

CUCURBIT[7]URIL MEDIATED VIOLOGEN-FLUOROPHORE DYAD FOR FLUORESCENCE OFF/ON SWITCH

A DISSERTATION

SUBMITTED TO THE GRADUATE FACULTY

in partial fulfillment of the requirements for the

Degree of

DOCTOR OF PHILOSOPHY

By

ANURADHA SINGH
Norman, Oklahoma
2012

CUCURBIT[7]URIL MEDIATED VIOLOGEN-FLUOROPHORE DYAD FOR FLUORESCENCE OFF/ON SWITCH

A DISSERTATION APPROVED FOR THE
DEPARTMENT OF CHEMISTRY AND BIOCHEMISTRY

BY

_____
Dr. Ronald L. Halterman, Chair

_____
Dr. Kenneth Nicholas

_____
Dr. Daniel Glatzhofer

_____
Dr. Wai Tak Yip

_____
Dr. Lloyd Bumm

I dedicate this dissertation to my parents
Dr. Bhrigu Nath Singh and Dropati Devi Singh

Acknowledgments

I would like to express my very great appreciation to my advisor Dr. Ronald Halterman for his excellent encouragement, guidance, support and instruction. The work presented here would not be possible without his knowledge and vision.

I also want to thank my graduate committee members Dr. Kenneth Nicholas, Dr. Daniel Glatzhofer, Dr. Wai Tak Yip, and Dr. Lloyd Bumm for their advice throughout the past five years.

I offer my special thanks to the University of Oklahoma, Department of Chemistry and Biochemistry. My special thanks go to Dr. Kalani Gunawardana, for her wonderful friendship and Dr. Halterman's research group, Shawna Ellis, Nathan Green, Sarvanan Ramaswamy and Justin Garret for their help and encouragement. Thanks also go to Dr. Daminda Dahanayake and Loius Jackson for their support in my research. I express thanks to my friend Dr. Sitaram Acharya for his assistance in technical issues. I would also like to thank to all of my friends without listing their names for their encouragement.

Special thanks to my parents, Dr. Bhrigu Nath Singh and Dropati Devi Singh for their never-ending love, support, and encouragement. Thanks also to my brother Shambhu Nath Singh and my sister Anjali Singh for their endless love and support. Finally, I wish to thank my husband Shanta Bahadur Karki and my two daughters Sara and Ashika for making my life easier even in hard days.

Table of Contents

Abstract

CUCURBIT[7]URIL MEDIATED VIOLOGEN-FLUOROPHORE DYAD FOR FLUORESCENCE OFF/ON SWITCH

Due to the advancement of fluorescence spectroscopy, fluorescence techniques have been applied in biological imaging and sensing. In biological imaging, biomolecules are labeled with fluorophore which allow us to track them. However, this procedure limits its implication where localized emission is stronger than the background one due to background fluorescence of nonspecific adsorbed fluorophore. Design of fluorescence-on binding sensors could be a better approach to overcome this disadvantage in which emission is quenched extensively until the sensing events occur. Our aim was targeted to develop the bright fluorescence probes by utilizing two different approaches: metal-enhanced fluorescence and photoinduced electron transfer.

To study the first approach it was necessary to obtain a well-ordered, good quality, high-density, and crystalline $(\sqrt{3}x\sqrt{3})R30^{o}$, corresponds to spacing in lattice, self assembled monolayer (abbreviated as SAM) on gold surface. We have developed a simple methodology for the generation of ordered SAMs by the cleavage of alkanethioacetate at bench top conditions. The extent of cleavage of decanethioacetate was investigated by the NMR spectroscopy experiments. The scanning tunnel microscope (STM) study was carried out on SAMs obtained *in situ* cleavage of thioacetate. According to the data obtained as a result of our

investigations, a well ordered SAM was produced with the reagents that cleave thioacete fast and more complete within 2 h whereas slow cleavage of the thioacetate resulted in a poor ordered SAM. The developed methodology for obtaining well-ordered SAM was utilized to attach bodipy fluorophore on the gold surface.

The bodipy dye was incorporated to the gold surface by precleaving thioacetate tethered to bodipy with potassium hydroxide to investigate its optical properties. The gold/bodipy sol was stabilized by employing competing ligands. The molar fluorescence of bodipy on the gold nanoparticles was determined. In addition to this, the gold/bodipy sol was used to study ligand exchange on the gold surface.

As the second approach of our study, the photoinduced electron transfer was utilized to achieve fluorescence-on sensors. We were able to develop a novel and more general fluorescence-on signal unit in which the quencher tethered to fluorophore, dyad, switches from fluorescence-off to fluorescence-on state due to disruption of electron transfer from the excited fluorophore to the quencher upon binding of the latter with a host molecule, cucurbit[7]uril. The viologen-rhodamine B and viologen-bodipy dyads were synthesized to investigate their fluorescence off-on efficacy. According to our finding, complexation of CB7 with viologen caused 14 and 30 fold fluorescence enhancement of viologen-rhodamine B and viologen-bodipy dyad, respectively.

In continuation of the work towards the development of real time sensors, it was necessary to investigate the fluorescence off-on mechanism of dyads in the presence of competing binding molecules with CB7 at the different pH. For this purpose, we chose 1,4-diaminobenzene as it has lower pK_a and comparable binding constant with viologen. It was observed that at lower pH, binding of CB7 with viologen as well as protonated diaminobenzene resulted in a small fluorescence enhancement. However, complete recovery of fluorescence was observed at higher pH because of complexation of CB7 with the viologen alone.

In conclusion, investigations were carried out for the development of next generation optoelectronic devices and novel real world applicable biosensors.

Chapter I: Introduction

Over the past two decades tremendous efforts towards the development of biosensors have been focused by chemists and biologists.[1,2] Continuous monitoring of biomolecules or ions in cells provides valuable information.[3,4,5] Biosensor have two components, a receptor component to interact with the analytes, and a signal transduction component to convert the ligand-binding event into measurable signals, such as fluorescence, chemiluminescence, colorimetric, and electrochemical responses. Fluorescence detection techniques have received extensive attention due to their high sensitivity and selectivity, temporal and spatial resolution, and relatively low cost.[6]

The goals of our work are to improve the functioning of biosensors and methodology for the assembly of fluorophores into functional units. In the First Chapter the fundamentals of fluorescence and assembly techniques through host guest interactions and covalent attachment are covered. In the Second Chapter, the assembly methodology of organothioacetate on gold surface is covered. A discussion on optical properties of fluorophore incorporated to gold surface by utilizing the methodology described in chapter two is presented in Chapter III. Covalent attachment techniques of fluorophore with quencher to provide a novel dyad and its efficacy to switch fluorescence off-on through host-guest interaction are described in Chapter IV. In Chapter V, fluorescence off-on of dyads in response to pH via displacement of intial guest from a host is presented.

Some molecules, fluorophores or fluorescent dyes, absorb light of specific wave length and emit light back called fluorescence. Most often the emitted light has longer wavelength than absorbed wavelength. This phenomenon can be explained in terms of graphic, well known Jablonski diagram (Figure 1.1). A fluorophore absorbs energy and is excited to a higher electronic level S_1'. Thus excited fluorophore vibrationally relaxes to the lowest vibrational state S_1 and back to S_0 with the emission light. However, the excited fluorophore can also undergo several other deactivating non-radioactive pathways such as intersystem crossing, internal conversion or vibrational relaxation. A wide range of fluorophores from UV to near IR are reported such as fluoresceins, rhodamine, 4,4-difluoro-4-bora-3a,4a-diaza-*s*-indacenes (BODIPY dyes), squarines, and cyanines. These fluorescent dyes have wide range of applications from paints and textiles to advanced photonic devices,[7] biomedical researches[8] such as labeling of biomolecules,[9] and construction of biosensors[10].

Due to the advancement of fluorescent spectroscopy, fluorescence has become the most powerful signal transduction mechanism.[11] Several features of fluorophores such as lifetime, intensity, anisotropy and energy transfer could be employed to get a signal output.[12] Intensity change as a signal transduction component seems most promising. Significant change in intensity could be obtained by applying FRET[13] or photoinduced electron transfer to suppress the signal. We have utilized photoinduced electron transfer mechanism as a signal unit as it provides massive change in intensity of fluorophores.

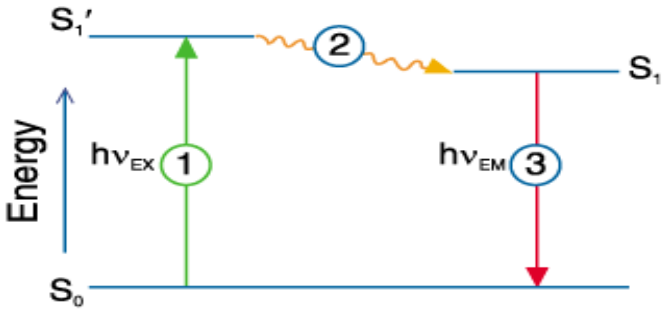

Figure 1.1. Jablonski Diagram. Adapted from *The Molecular Probes® Handbook—A Guide to Fluorescent Probes and Labeling Technologies.*

1.1 Photoinduced Electron Transfer

Photoinduced electron transfer (PET) is well established mechanism in which the fluorescence of a fluorophore is quenched (reduced fluorescence intensity of fluorophore) due to electron transfer from donor moiety to acceptor fluorophore.[13] PET sensors consist of three important components, fluorophore, spacer, and receptor (Figure 1.2).[14] The spacer keeps fluorophore and receptor in proximity but separate from each other. In the presence of an analyte, the fluorescence of the fluorophore turns on (Figure 1.3b) as arresting of the non-bonding electron transfer from receptor to the proximate excited fluorophore (Figure 1.3a). Weller studied the thermodynamic features of the PET mechanism. He stated that electron transfer is only possible if excited-state of the fluorophore has sufficient energy to oxidize the receptor and reduce the fluorophore. The fluorescence-on state PET becomes thermodynamically disfavored because of an increase in oxidation potential of the receptor on binding with an analyte.[15]

.

Figure 1.2. The 'fluorophore–spacer–receptor' format of fluorescent PET sensors. Adapted from reference 14.

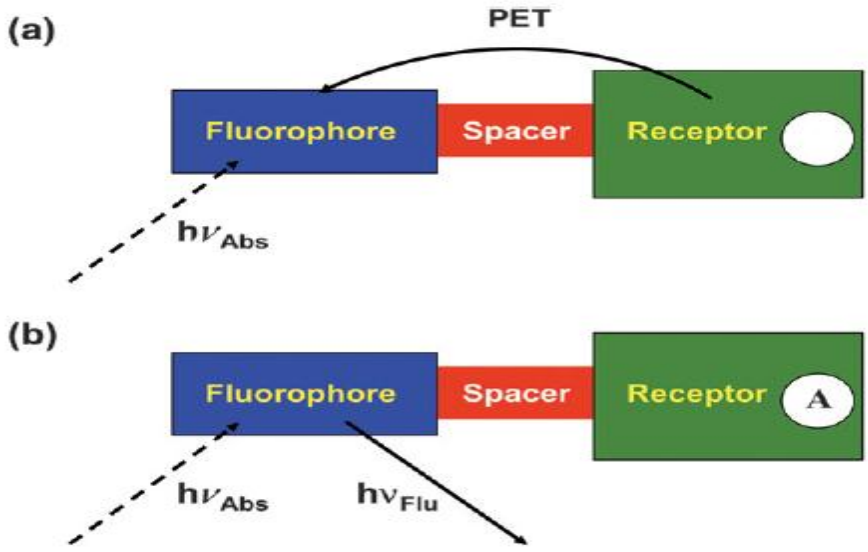

Figure 1.3. **(a)** An electron transfer from receptor to the photo-excited fluorophore provides the 'off' state of the sensor. **(b)** Halting of electron transfer from the analyte-bound receptor provides the 'on' state of the sensor. Adapted from reference 14.

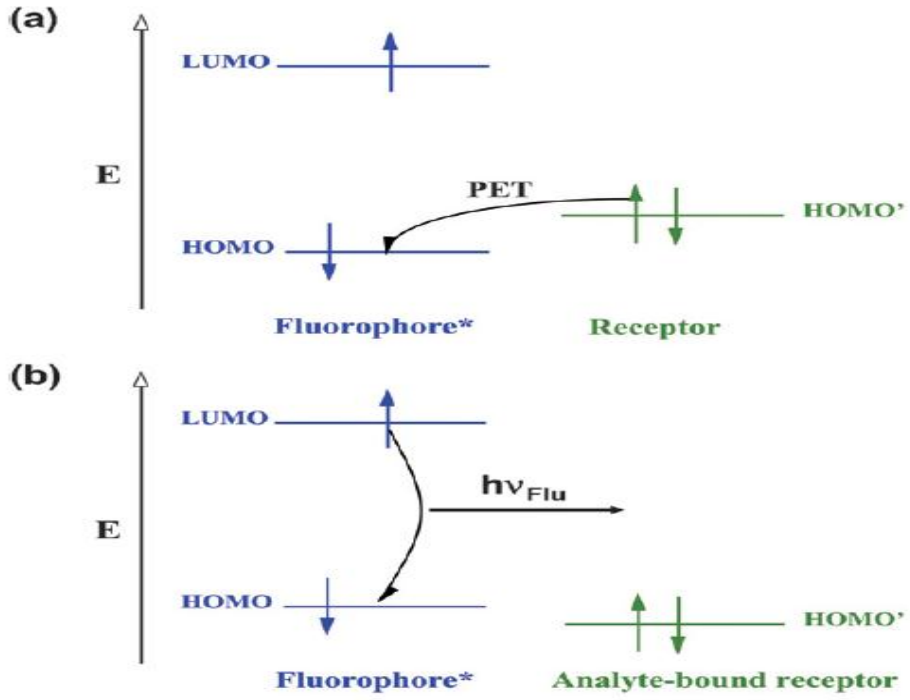

Figure 1.4. Molecular orbital energy diagrams which show the relative energetic dispositions of the frontier orbitals of the fluorophore and the receptor in **(a)** the analyte-free state and **(b)** the analyte-bound state. Adapted from reference 14.

Fluorescence off-on phenomenon has also been described in terms of molecular orbital energy diagram.[16] The low lying of HOMO of the excited fluorophore lower than that of HOMO of receptor facilitates the electron transfer (Figure 1.4a) and results in quenching of fluorescence. Coordination of receptor with an analyte alters the fluorescence on (Figure 4b) because of low lying HOMO of analyte bound receptor than HOMO of fluorophore. Thus PET occurs when the oxidation potential of the receptor is smaller in magnitude than that of the fluorophore.[14,17] The opposite applies in the case of fluorescence on-off sensors.

The selectivity of a receptor for the interested analyte is a big challenge for designing sensors. To improve selectivity, extensive use of development of macrocyclic hosts has been introduced to enhance signals. Crown ether, cryptands, cyclophanes, calixarenes, cyclodextrin, and cucurbiturils have been so utilized. A PET sensor containing macroycle receptor, diaza-18-crown-6, and fluorophore, benzofurans shows excellent selectivity with K^+ and responds very efficiently as fluorescent off- on (Figure 1.5). Therefore, this sensor has been commercialized to detect concentration of K^+ ion in blood.[18] Similarly, highly selective PET sensors for Na^{+}[19] and Ca^{++} [20] ions have already been commercialized. Recently reported PET metal ion sensors could be used to image ions in living cells by the use of fluorescence microscopy.[21] Although massive development of PET metal ion sensors there are very few reports could be found on PET biosensors. In this case fluorescence on state achieves due to conformational change in protein move the quencher away from the fluorophore. [22]

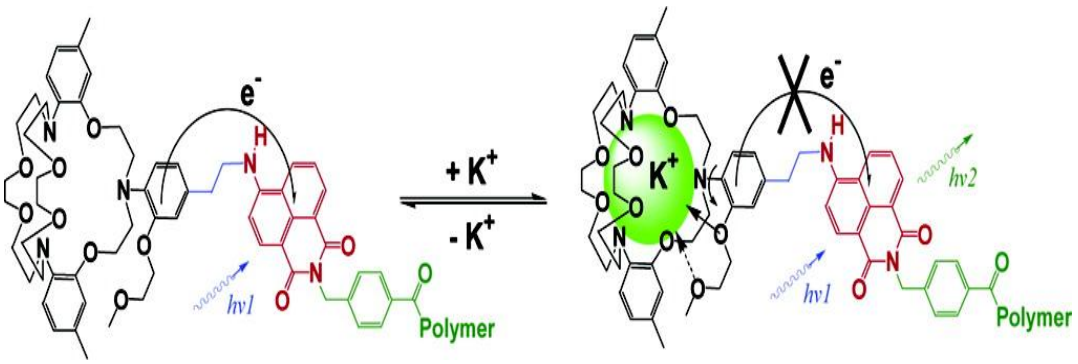

Figure 1.5. Potassium free sensor at Fluorescent off state and switch to on state in presence of potassium. Adapted from reference 18.

1.2 Macrocyclic Host, Cucurbit[7]uril

Excellent binding of crown ether to alkali metal ions demonstrated by Pederson inspired intensive development of host-guest chemistry.[23] Biological processes such as catalysis and ion transport especially work on molecular recognition processes. These processes are driven by non-covalent interactions such as hydrogen bonding, ion dipole interactions, π-π dispersion interaction, Van der Waals interaction, and hydrophobic interaction.[24] Host-guest complexation is also known as supramolecular chemistry as it deals with weak interaction to assemble subunits.[25]

Similar to hydrophobic pocket of several enzymes, most of macrocyclic hosts possess concave interior.[26] Due to the mimicry of these hosts with enzymes these can have potential application in the development of sensors, catalysis, information technology, removal of contaminants, nuclear waste treatment, drug delivery.[24] Therefore examination of the intermolecular non-covalent interaction between host and guest has grown a major area of study. Until now different types of molecular hosts have been developed, e.g., cryptands, cyclophane, cavitands, carcerands, calixarene, cyclodextrin, and recently cucurbituril.[27]

Cucurbiturils are macrocyclic methylene-bridged glycouril oligomer that we will apply in our studies.[28] The name cucurbiturils came from Latin word *cucurbitaceae* due to its shape resemblance to that of pumpkin. These were first synthesized in 1901 by Behrend and co-workers by the condensation of glycoluril

with formaldehyde in concentrated HCl and known as "Behrend's polymer".[29] Later on in 1981, Mock and co-workers were able to characterize this polymer as a macrocycle of

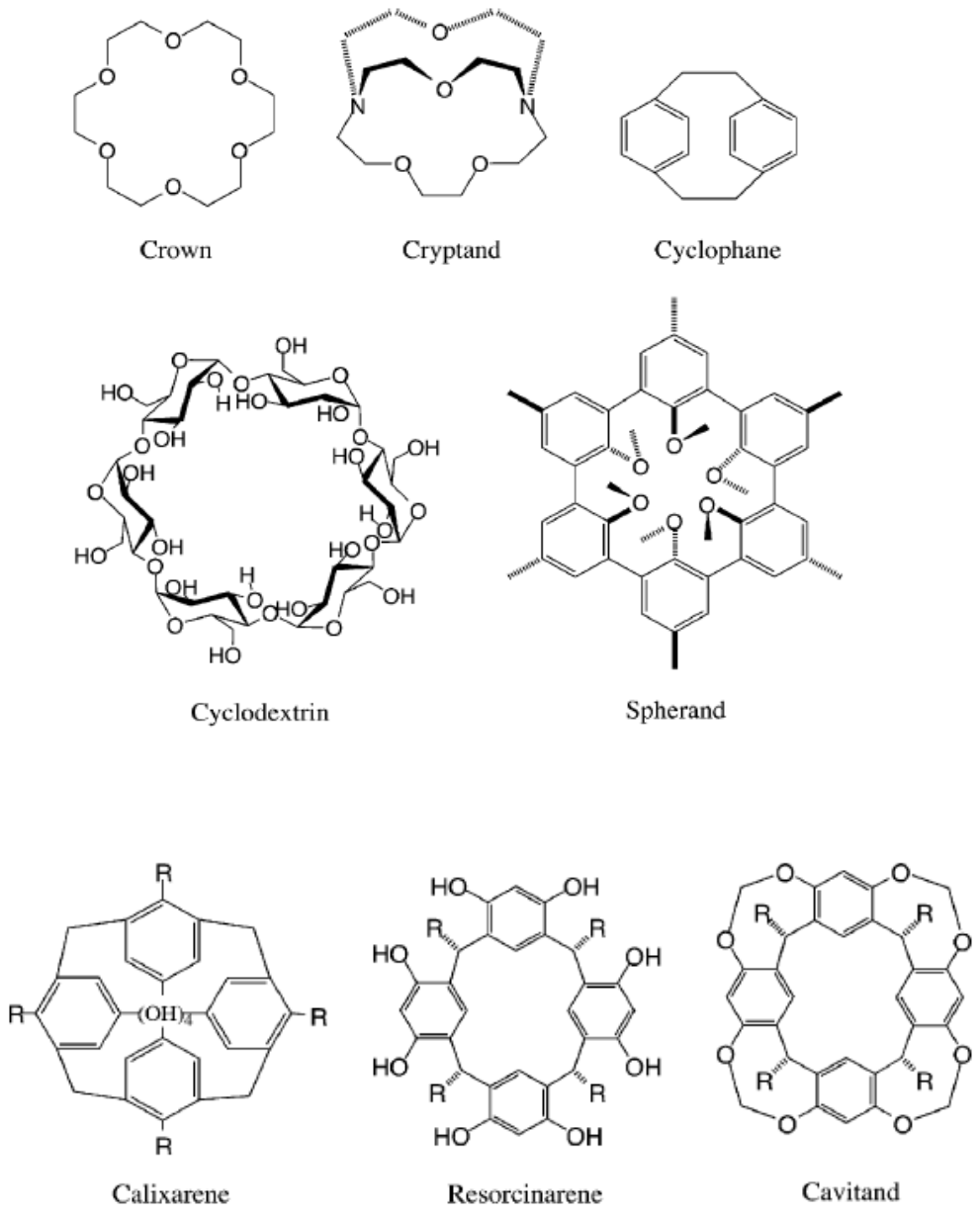

Figure 1.6. Line drawing of some reported host macromolecules. Adapted from Sherman.[30]

six glycouril unit and named as cucurbit[6]uril. Cucurbiturils were able to gain huge attention from a large number of research groups after their convenient synthesis and isolation procedure developed by Kim[31] and Day[32]. Several homologous of cucurbiturils have been synthesized by performing the condensation under milder kinetically controlled conditions and isolated as CB[*n*] (*n* = 5, 6, 7, 8, and 10; *n* represents the number glycouril monomer).

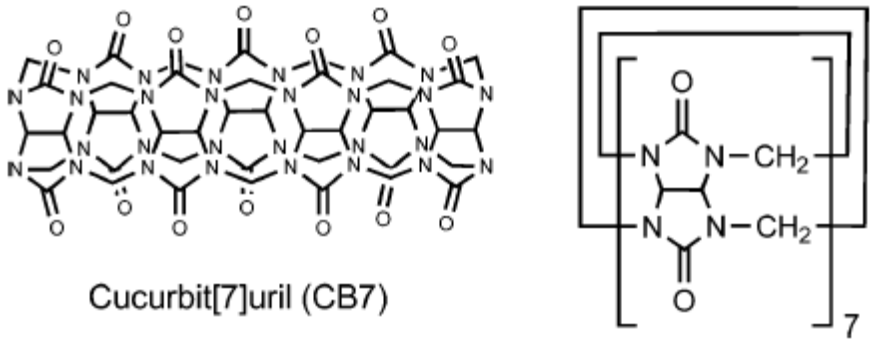

Figure 1.7. Line drawing of CB7. Adapted from Halterman and co-workers. [46]

Cucurbiturils possesses hydrophobic cavity similar to cyclodextrins. Cyclodextrins are the oligomers of glucopyranose units.[33] Three homologs of cyclodextrins have been reported and they are described as α, β, and γ on the basis of number of glucopyranose units 6, 7, and 8 respectively. Cyclodextrins are synthesized from starch in the presence of bacteria *Bacillus macerans.*[34] Cyclodextrins (CDs) are known to be very important and promising macrocyclic hosts due to their excellent solubility in water, inexpensive, readily availability commercially, non-toxicity, and easy functionalization.[34] Cyclodextrin

encapsulates a variety of hydrophobic compounds in water via hydrophobic and Van der Waals interaction.[34] Though cyclodextrins have multiple benefits, their limited selectivity, especially for cationic guest compounds, has driven the research towards the search for another macrocyclic host for cationic molecules.

Similar to cyclodextrins, some oligomers of cucurbiturils (CB5 and CB7) are sparingly soluble in water. They have negligible toxicity *in vitro* and *vivo*.[35] More importantly, unlike cyclodextrins these have excellent selectivity for cationic species.[27b] These hosts form inclusion complexes with cationic organic moieties through ion-dipole, hydrogen bonding, and hydrophobic interactions. The presence of electron rich carbonyl portals and inner hydrophobic cavity on these hosts drives the complexation with organic cationic guest.

Mock identified CB6 as a host and reported its high binding affinity for ammonium species.[36] Moreover, his and Tuncel's group described the shuttling feature of CB6 from one docking site to another with external stimuli such as pH opened new route for their aplications in catalysis, supramolecular switches etc.[37]

However, the small cavity (Table 1.1) of CB6 limits its application as it can accommodate only the small guests. CB7 can bind with a large range of guests as its portal diameter and inner cavity is larger than CB6 and comparable to β-cyclodextrin (Table 1.1). A large number of research groups such as Kaifer, Macartney, Isaacs, Nau, and others have put their effort to gain information regarding to inclusion complexes of CB7 with other cationic group so that CB7 can

be applied to various application such as catalysis, drug delivery, sensors, and biological probes.

Table 1.1. Cavity dimensions and aqueous solubilities of CB[*n*] and CD hosts, Adapted from Wyman's thesis. [38]

Host	Portal Diameter (Å)	Interior Cavity Diameter (Å)	Height (Å)	Cavity Volume (Å^3)	Solubility in Water (mM)
CB[5]	2.4	4.4	9.1	82	20-30
CB[6]	3.9	5.8	9.1	164	0.018
CB[7]	5.4	7.3	9.1	279	20-30
CB[8]	6.9	8.8	9.1	479	<0.01
CB[10]	9.5-10.6	11.3-12.4	9.1	870	Not reported
α-CD	4.7	5.3	7.9	174	297
β-CD	6.0	6.5	7.9	262	16
γ-CD	7.5	8.3	7.9	427	293

Kaifer and coworkers has investigated the mode of binding of aliphatic as well as aromatic substituents viologen (4,4'-bipyridinium) by using NMR spectroscopy.[39] CB7 produces very stable inclusion complexes with viologen that has short alkyl chain in which the aromatic unit of the bipyridinium species fits tightly inside the host cavity and two positively charged nitrogen atoms encircled by portal carbonyl oxygens of CB7. In support of this fact, they showed the large upfield shift (Figure 1.7a) of the β protons of methyl viologen (abbreviated as MV^{2+}) upon CB7 inclusion, similar binding mode reported by Kim.[40] In continuation, they published external complexation with longer alkyl substituted viologen and benzyl substituted viologen, where CB7 docked at one of aliphatic chains or benzyl moiety. [39b]

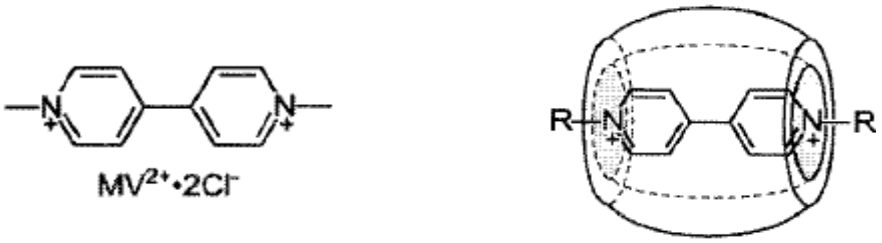

Figure 1.7a. Inclusion complex. Adapted from Kaifer and co-workers.[39]

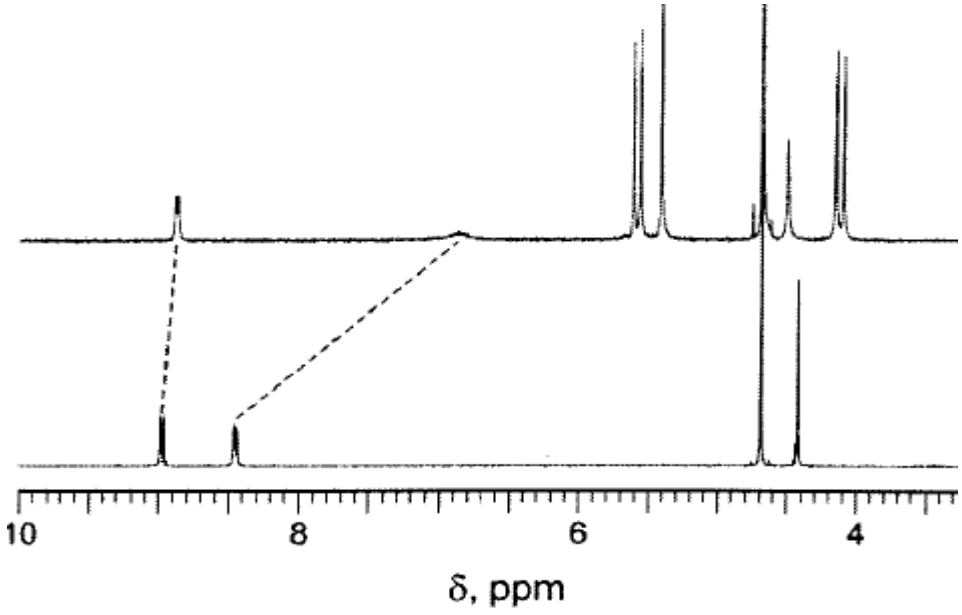

Figure 1.7. ^{1}H NMR spectra (300 MHz, 0.2 M NaCl-D_2O) of MV^{2+} in the absence (bottom) and in the presence (top) of 1 equiv of CB7. Adapted from Kaifer and co-workers.[39a]

In further support of their findings, they employed NMR titration upfield shifts of aromatic protons of benzylic unit and splitting of their singlet into three separated peaks indicated engulfing of benzyl group into the cavity of CB7(Figure 1.8) and interaction of positively charged nitrogen with the carbonyl oxygens of

CB7.[41] Recently, their group has developed a pH controlled pseudorotaxane in which shuttling of CB7 from one binding to another site could be observed upon change of pH.[42]

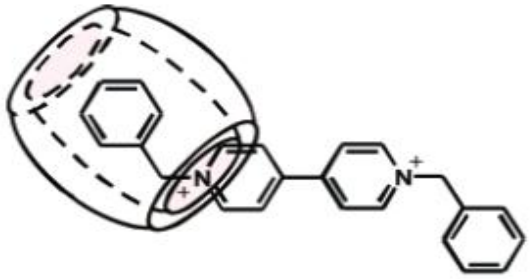

Figure 1.8. External Complexation of benzylviologen with CB7. Adapted from Kaifer and co-workers.[41]

Isaac and co-workers have reported 1:1 complexation of CB7 with a large variety of guest molecules (Figure 1.9).[43] By employing ^{1}H NMR competition experiments they were able to determine the binding constant in aqueous solution and found from a range 10^{4} to 10^{12} M^{-1}. This extraordinarily high selectivity and affinity of CB7 with several cationic species is due to a combination of electrostatic, hydrophobic and steric interactions.[44]

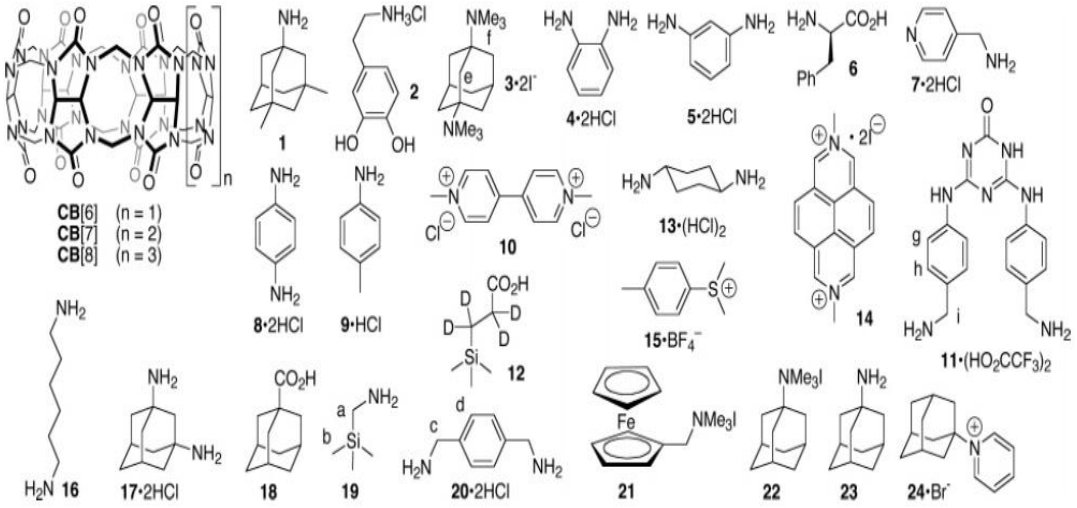

Figure 1.9. List of guest compounds used by Isaacs and co-workers to study complexation with CB7. Adapted from Isaacs and co-workers.[43]

Nau and co-workers reported the advantages of complexed fluorophore, rhodamine 6G with CB7. The increase in photo-stability of rhodamine 6G, fluorescence enhancement, reduction of nonspecific adsorption and aggregation effects are due to complexation dye with CB7.[45] A two fold enhancement of dodecane- tethered rhodamine B complexed with CB7 has already been reported by us.[46] Complexation of CB7 with tethered rhodamine B decreases the H-dimer aggregation and results increase in brightness. Interestingly our lab investigated the photophysics of single CB7/rhodamine 6G molecules by immobilizing CB7 on glass surface and noticed strong binding with rhodamine 6G with increase in brightness because of suppression of solvent induced nonradiative relaxations.[46b]

1.3 Self Assembled Monolayer on Gold Nanoparticles

Though complexation of rhodamine B with CB7 is beneficial in terms of brightness, a mere two fold enhancement cannot be applied in the construction of biosensors. When a fluorophore is placed in proximity to metal nanoparticles like gold, silver, the fluorescence of fluorophore is dramatically changed. A fluorophore within 5 nm from gold surface experiences quenching whereas greater than this distance cause dramatic fluorescence enhancement.[47] The quenching phenomenon has been utilized to develop fluorescence off-on biosenors. Initially fluorescence is off due to energy transfer, orelectron transfer from excited fluorophore to metal nanoparticles. Binding of an analyte with a recognition unit moves the fluorophore away from metal and turns the fluorescence on.[48] Gold nanoparticles are better candidates for biological applications because of its chemical inertness and can readily incorporate to fluorophores or biomolecules. [49] For the incorporation of invaluable molecules on gold it is necessary to be familiar with the properties of gold.

Organic molecules having suitable functionality spontaneously adsorb on metal surface to yield well ordered monolayer known as self assembled monolayer (abbreviated as SAM).[50] Since gold has high affinity to thiol, alkane thiol

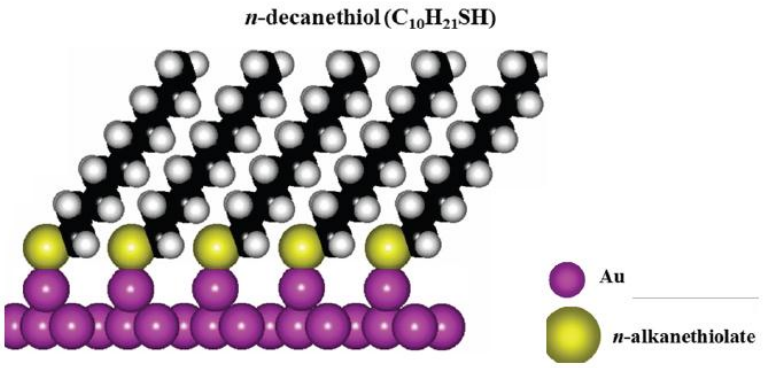

Figure 1.10. Self assembled monolayer of alkanethiols on gold surface. (Diagram produced by Lloyd Bumm).

chemisorbed on gold surface to provide SAM.[50] Fluorophore or biomolecules possessing thiol functionality can easily be attached to gold surface. Desirable molecules can also be successfully coupled to the gold surface by performing ligand exchange. High affinity ligand replaces weakly bound phosphines or citrate ions with thiols.[51] In addition, complex thiols or disulfides are able to replace simple thiols.[50,52] Fluorophores or biomolecules can also be connected to gold by performing mild chemical reactions, such as nucleophilic substitution, amide coupling, metathesis, on SAM.[53] The surface of the SAM can conveniently be tailored by employing suitable functionality on terminal end of alkanethiol. Similarly fluorophores or biomolecules could be modified with suitable functionality to couple with the functionality of alkanethiol so as to attach to gold nanoparticles.

1.4 Research Focus

This thesis describes our effort towards the development of methodology for generating self assembled monolayer on gold nanoparticles. Investigation of optical properties of directly attached bodipy to gold surface is described. The extension of this project to develop procedure for place exchange by employing several ligands on gold nanoparticles is documented. Second part of the body covers our effort to design novel fluorescence off-on dyads as a signal unit and to investigate their fluorescence off-on efficacy. Finally investigation of fluorescence off-on efficacy of dyads through competitive binding of guest molecule with host at different pH is presented.

1.5 References

1. Tainaka, K.; Sakaguchi, R.; Hayashi, H.; Nakano, S.; Liew, F.; Morii, T**.** Design Strategies of Fluorescent Biosensors Based on Biological Macromolecular Receptors *Sensors* **2010**, *10*, 1355-1376.

2. Johnson, I. Fluorescent Probes for Living Cells. *Histochem. J.* **1998**, *30*, 123-140.

3. Domaille, D.W.; Que, E.L.; Chang, C.J. Synthetic Fluorescent Sensors for Studying the Cell Biology of Metals. *Nat. Chem. Biol.* **2008**, *4*, 168-175.

4. Terai, T.; Nagano, T. Fluorescent Probes for Bioimaging Applications. *Curr. Opin. Chem. Biol.* **2008**, *12*, 515-521.

5. (a) Giepmans, B.N.; Adams, S.R.; Ellisman, M.H.; Tsien, R.Y. The Fluorescent Toolbox for Assessing Protein Location and Function. *Science* **2006**, *312*, 217-224. (b) Johnsson, N.; Johnsson, K. Chemical Tools for Biomolecular Imaging. *ACS Chem. Biol.* **2007**, *2*, 31-38. (c) Rao, J.; Dragulescu-Andrasi, A.; Yao, H. Fluorescence Imaging *in vivo*: Recent Advances. *Curr. Opin. Biotechnol.* **2007**, *18*, 17-25. (d) Johnsson, K. Visualizing Biochemical Activities in Living Cells. *Nat. Chem. Biol.* **2009**, *5*, 63-65. (e) Wang, H.; Nakata, E.; Hamachi, I. Recent Progress in Strategies for the Creation of Protein-Based Fluorescent Biosensors. *ChemBioChem* **2009**, *10*, 2560-2577.

6. (a) Halaoui, L. I.; Abrams, N. M.; Mallouk, T. E. Increasing the Conversion. Efficiency of Dye-Sensitized TiO2 Photoelectrochemical Cells by Coupling to Photonic Crystals *J. Phys. Chem. B* **2005**, *109*, 6334-6342. (b) Gvishi, R.; Narang, U.; Ruland, G.; Kumar, D. N.; Prasad, P. N. Novel, Organically Doped, Sol–Gel-DerivedMaterials for Photonics: Multiphasic Nanostructured Composite Monoliths andOptical Fibers . *Appl. Organomet. Chem.* **1997**, *11*, 107-127. (c) Gfeller, N.; Calzaferri, G. Energy Migration in Dye-Loaded Hexagonal Microporous Crystals. *J. Phys. Chem. B* **1997**, *101*, 1396-1408.

7. Irvine, D. J.; Purbhoo, M. A.; Krogsgaard, M.; Davis, M. M. Direct observation of ligand recognition by T cells *Nature* **2002**, *419*, 845–849.

8. Gonçalves, S. T. M**.** Fluorescent labeling of biomolecules with organic probes. *Chem. Rev.* **2009**, *109*, 190–212.

9. (a) Steemers, F. J.; Ferguson, J. A.; Walt, D. R. Screening unlabeled DNA targets with randomly ordered fiber-optic gene arrays *Nat. Biotechnol*. **2000**, *18*, 91–94. (b) De Lorimier, R. M.; Smith, J. J.; Dwyer, M. A.; Looger, L. L.; Sali, K. M.; Paavola, C. D.; Rizk, S. S.; Sadigov, S.; Conrad, D. W.; Loew, L.; Hellinga, H.

W. Construction of a fluorescent biosensor family *Protein Sci.* **2002**, *11*, 2655–2675. (c) Hellinga, H. W.; Marvin, J. S. Protein engineering and the development of generic biosensors *Trends Biotechnol.* **1998**, *16*, 183–189. (d) Arora, P.; Sindhu, A.; Dilbaghi, N.; Chaudhury, A**.** Biosensors as innovative tools for the detection of food borne pathogens *Biosensors and Bioelectronics* **2011**, *28*, 1– 12.

10. Lakowicz, J. R. Topics in Fluorescence Spectroscopy, Vol. 2, Principles, Plenum Press, New York, 1991.

11. (a) Lakowicz, J. R. Topics in Fluorescence Spectroscopy, vol. 4, Techniques, Plenum Press, New York, 1991. (b) Lakowicz, J. R. Topics in Fluorescence Spectroscopy, vol. 3, Application, Plenum Press, New York, 1991. (c) Pope, A.J.; Haupts, U. M.; Moore, K. J. *Drug Discovery Today* **1999**, *4*, 350–362.

12. (a) Piston, D.W.; Kremers, G.J. Fluorescent Protein FRET: The Good, the Bad and the Ugly. *Trends Biochem. Sci.* **2007**, *32*, 407-414. (b) Carlson, H.J.; Campbell, R.E. Genetically Encoded FRET-Based Biosensors for Multiparameter Fluorescence Imaging. *Curr. Opin. Biotechnol.* **2009**, *20*, 19-27.

13. de Silva, A. P.; Gunaratne, H. Q. N.; Gunnlaugsson, T.; Huxley, A. J. M.; McCoy, C. P.; Rademacher, J. T.; Rice, T. E. Signaling Recognition Events with Fluorescent Sensors and Switches. *Chem. Rev.* **1997**, *97*, 1515- 1566.

14. de Silva, P.; Moody, T. S. ; Wright, G. D. Fluorescent PET (Photoinduced Electron Transfer) sensors as potent analytical tools. *Analyst* **2009**, *134*, 2385–2393.

15**.** *(a)* Weller, A. Electron-transfer and complex formation in the excited state *Pure Appl. Chem.* **1968**, *16*, 115-124. (b) Rehm, D.; Weller, A. Kinetics of fluorescence quenching by electron and hydrogen-atom transfer. *Isr. J. Chem.* **1970**, *8*, 259-271.

16. Fahrni, C.J.; Yang, L.C.; Van Derveer, D.G. Tuning the Photoinduced Electron-Transfer Thermodynamics in 1,3,5-Triaryl-2-Pyrazoline Fluorophores: X-Ray Structures, Photophysical Characterization, Computational Analysis, and *in vivo* Evaluation. *J. Am. Chem. Soc.* **2003**, *125*, 3799-3812.

17. Chatterjee, A.; Suzuki, T.M.; Takahashi, Y.; Tanaka, D. A. P. A Density Functional Study to Choose the Best Fluorophore for Photon-Induced Electron-Transfer (PET) Sensors. *Chem. Eur. J.* **2003**, *9*, 3920-3929.

18. He, H.; Mortellaro, M. A.; Leiner, M. J. P.; Fraatz, R. J.; Tusa, J. K. A Fluorescent Sensor with High Selectivity and Sensitivity for Potassium in Water. *J. Am. Chem. Soc.* **2003**, *125*, 1468-1469.

19. He, H.; Mortellaro, M.A.; Leiner, M.J.P.; Young, S.T.; Fraatz, R.J.; Tusa, J. K. A Fluorescent Chemosensor for Sodium Based on Photoinduced Electron Transfer. *Anal. Chem.* **2003**, *75*, 549-555.

20. Tusa, J. K.; He, H. Critical Care Analyzer with Fluorescent Optical Chemosensors for Blood Analytes. *J. Mater. Chem.* **2005**, *15*, 2640-2647.

21. (a) Wu, Y.; Peng, X.; Guo, B.; Fan, J.; Zhang, Z.; Wang, J.; Cui, A.; Gao, Y. Boron dipyrromethene fluorophore based fluorescence sensor for the selective imaging of Zn(II) in living cells. *Org.Biomol.Chem.* **2005**, *3*, 1387-1392. (b) He, G.; Zhao, X.; Zhang, X.; Fan, H.; Wu, S.; Li, H.; Hea, C.; Duan, C. A turn-on PET fluorescence sensor for imaging Cu^{2+}. *New J. Chem.* **2010**, *34*, 1055–1058. (c) Dodani, S. C.; He, Q.; Chang, C. J. "A Turn-On Fluorescent Sensor for Detecting Nickel in Living Cells" *J. Am. Chem. Soc.* **2009,** *131*, 18020-18021.

22. (a) Doose, S.; Neuweiler, H.; Sauer, M. *ChemPhysChem* **2009**, *10* (9_10), 1389–1398. (b) Gray, H. B.;Winkler, J.R. Long-range electron transfer *Proc.Natl. Acad. Sci. U.S.A.* **2005**, *102*, 3534–3539. (c)Yang, H.;Luo,G.; Karnchanaphanurach, P.; Louie, T.-M.; Rech, I.;Cova, S.; Xun, L.; Xie, X. S. Protein Conformational Dynamics Probed by Single-Molecule Electron Transfer *Science* **2003**, *302*, 262–266. (d)Marquez, C.;Huang,F.; Nau,W.M. Cucurbiturils: Molecular Nanocapsules for Time-Resolved Fluorescence-based Assays *IEEETrans.Nanobiosci.* **2004**, *3*, 39–45.

23. Pedersen, C. J. The discovery of crown ethers. *Angew.Chem., Int.Ed.* **1988**, *27*, 1021-1027.

24. Cram, D. J. Molecular container compounds. *Nature* **1992**, *356*, 29-36.

25. Lehn, D. J. Supramolecular Chemistry, scope and perspectives molecules, supramolecules, and molecular devices. *Angew. Chem., Int. Ed.* **1988**, *27*, 89-112.

26. Marquez, C.; Huang, F.; Nau, W. M. Cucurbiturils: Molecular nanocapsules for Time-Resolved Fluorescence-Based Assays *IEEE Trans. Nanobiosci.***2004**, *3*, 39–45.

27. (a) Stewart, D. R.; Gutsche, C. D. *J. Am. Chem. Soc.* **1999**, *121*, 4136. (b) Szejtli, J. Introduction and General Overview of Cyclodextrin Chemistry. *Chem. Rev.* **1998**, *98*, 1743. (c) Dsouza, R. N.; Pischel, U.; Nau, W. M. Fluorescence dyes

and their supramolecular host/guest complexes with macrocycles in aqueous solution. *Chem. Rev.* **2011**, *111*, 7941-7980.

28**.** Freeman, W. A.; Mock, W. L.; Shih, N. Y. Cucurbituril *J. Am. Chem. Soc.* **1981**, *103*, 7367.

29. Behrend, R.; Meyer, E.; Rusche, F. Ueber Condensationsproducte aus Glycoluril und Formaldehyd Justus Liebigs *Ann. Chem.* **1905,** *339*, 1-37.

30. Sherman, J. Molecules that can't resist templation *Chem.Commun.* **2003**, 1617-1623.

31. Kim, J.; Jung, I.-S.; Kim, S.-Y.; Lee, E.; Kang, J.-K.; Sakamoto, S.; Yamaguchi, K.; Kim, K. New Cucurbituril Homologues: Syntheses, Isolation, Characterization, and X-ray Crystal Structures of Cucurbit[n]uril (n = 5, 7, and 8) *J. Am. Chem. Soc.* **2000,** *122*, 540.

32. Day, A.; Arnold, A. P.; Blanch, R. J.; Snushall, B. Controlling Factors in the Synthesis of Cucurbituril and Its Homologues *J. Org. Chem.* **2001**, *66*, 8094-8100.

33. (a) Dodziuk, H. In Molecules with Holes –Cyclodextrins, In Cyclodextrins and Their Complexes, H. Dodziuk (ed.), Wiley-VCH Verlag GmbH & Co. KGaA: Weinheim, 2006; pp. 1-30. (b) Ogoshi, T.; Harada, A. Chemical Sensors Based on Cyclodextrin Derivatives. *Sensors* **2008**, *8*, 4961-4982. (c) Nepogodiev, S. A.; Stoddart, J. F. Cyclodextrin-based catenanes and rotaxanes. *Chem. Rev.* **1998**, *98*, 1959-1976.

34**.** (a) French, D. The Schardinger dextrins *Adv. Carbohydr. Chem*. **1957**, *12*, 189-260. (b) Gattuso, G.; Nepogodiev, S. A.; Stoddart, J. F. Synthetic cyclic oligosaccharides. *Chem. Rev.* **1998,** *98*, 1919-1958. (c) Khan, A. R.; Forgo, P.; Stine, K. J.; D'Souza, V. T. Methods for selective modifications of cyclodextrins. *Chem. Rev.* **1998**, *98*, 1977-1996.

35. Saleh, N.; Al-Soud, Y. A.; Al-Kaabi, L.; Ghosh, I.; Nau, W. M. A coumarin-based fluorescent PET sensor utilizing supramolecular pKa shifts *Tetrahedron Lett.* **2011,** *52*, 5249-5254.

36**.** (a) Mock, W, L.; Shih, N.-Y**.** Host-guest binding capacity of cucurbiturilJ. Org. Chem. **1983**, 48, 3618. (b) Mock, W, L.; Shih, N.-Y. Structure and selectivity in host-guest complexes of cucurbituril *J. Org. Chem.* **1986,** *51*, 4440-4446.

37. (a) Mock, W, L.; Pierpont, J**.** A cucurbituril-based molecular switch *J. Chem.Soc., Chem. Commun.* **1990**, 1509. (b) Tuncel, D.; Steinke, J. H. G. Catalytically self threading polyrotaxanes *Chem. Commun.* **1999**, 1509-1510.

38. Wyman, I. W. Host-Guest chemistry between cucurbit[7]uril and neutral and cationic guests. Ph. D. thesis, Queen's University, 2010.

39. (a) Ong, W.; Kaifer, A. E. Cucurbit[7]uril: a very effective host for viologens and their cation radicals. *Org. Lett*. **2002**, *4*, 1791. (b) Moon, K.; Kaifer, A. E. Modes of Binding Interaction between Viologen Guests and the Cucurbit[7]uril Host. *Org. Lett.* **2004**, *2*, 185-188.

40. Kim, H.-J.; Jeon, W. S.; Ko, Y. H.; Kim, K. Inclusion of methylviologen in cucurbit[7]uril *Proc. Natl. Acad. Sci. U.S.A.* **2002**, *99*, 5007-5011.

41. Sindelar, V.; Moon, K.; Kaifer, A. E. Binding Selectivity of Cucurbit[7]uril:Bis(pyridinium)-1,4-xylylene versus 4,4'-Bipyridinium Guest Sites *Org. Lett.* **2004,** *6*, 2665-2668.

42. Sindelar, V.; Silvi, S.; Kaifer, A. E. Switching a molecular shuttle on and off: simple, pH-controlled pseudorotaxanes based on cucurbit[7]uril. *Chem. Commun.* **2006**, 2185–2187.

43. Liu, S.; Ruspic, C.; Mukhopadhyay, P.; Chakrabarti, S. Zavalij, P. Y. ; Isaacs, L. The Cucurbit[n]uril Family: Prime Components for Self-Sorting Systems. *J. Am. Chem. Soc.* **2005**, *127*, 15959-15967.

44. (a) Isaacs, L. Cucurbit[n]urils: from mechanism to structure and function. *Chem. Commun.* **2009**, 619–629 (b) Lagona, J.; Mukhophadhyay, P.; Chakrabarti, S.; Isaacs, L. The CB[n] Family: Prime Components for Self-Sorting Systems *Angew. Chem., Int. Ed.* **2005**, *44*, 4844. (c) Lee, J. W. ; Samal, S. ; Selvapalam, N. ; Kim, H.-J. ; Kim, K. Cucurbituril Homologues and Derivatives: New Opportunities in Supramolecular Chemistry *Acc. Chem. Res.* **2003**, *36*, 621–630. (d) Ong, W. ; Kaifer, A. E. Unusual Electrochemical Properties of the Inclusion Complexes of Ferrocenium and Cobaltocenium with Cucurbit[7]uril *Organometallics* **2003**, *22*, 4181–4183.

45. (a) Mohanty, J., Nau, W.M.: Ultrastable rhodamine with cucurbituril. *Angew. Chem., Int. Ed.* **2005**, *44*, 3750–3754. (b) Mohanty, J., Pal, H., Ray, A.K., Kumar, S., Nau, W.M.: Supramolecular dye laser with cucurbit[7]uril in water. *Chem. Phys.Chem.* **2007**, *8*, 54–56. (c) Nau, W. M.; Mohanty, J. Taming fluorescent dyes with cucurbit[7]uril. *Inter. J. Photoenergy* **2005**, *7*, 717-726. (d) Marquez, C.; Hudgins, R. R.; Nau, W. M. The Mechanism of Host-Guest Complexation by Cucurbituril *J. Am. Chem. Soc.* **2004**, *126*, 5806-5816. (e) Mohanty, J.; Bhasikuttan, A. C.; Nau, W. M.; Pal, H. Host-guest complexation of neutral red with macrocyclic host molecules: contrasting pK (sub a) shifts and binding

affinities for cucurbit[7]uril and b-cyclodextrin. *J. Phys. Chem. B* **2006**, *110*, 5132-5138.

46. Halterman, R. L.; Moore, J. L.; Mannel, L., M. Disrupting Aggregation of Tethered Rhodamine B Dyads through Inclusion in Cucurbit[7]uril *J. Org. Chem.* **2008**, *73*, 3266-3269. (b) Martyn, T.A.; Moore, J.L.; Halterman, R.L.; Yip, W.T. Cucurbit[7]uril induces superior probe performance for single-molecule detection. *J. Am. Chem. Soc.* **2007**, *129*, 10338–10339. (c) Halterman, R. L.; Moore, J.L.; Yakshe, K. A. ; Halterman, J. A. I.; Woodson, K. A. Inclusion complexes of cationic xanthene dyes in cucurbit[7]uril. *J Incl Phenom Macrocycl Chem.* **2010**, *66*, 231–241.

47. Aslan, K.;. Malyn, S. N.; Geddes, C. D. Metal-Enhanced Fluorescence from Gold Surfaces: Angular Dependent Emission *J. Fluoresc.* **2007**, *17*, 7–13.

48. (a) Phillips, R. L.; Miranda, O. R. , You, C. C.; Rotello, V. M. Bunz, U. H. F. Rapid and Efficient Identification of Bacteria Using Gold-Nanoparticle–Poly(para-phenyleneethynylene) Constructs *Angew. Chem,. Int. Ed*. **2008**, *47*, 2590 –2594. (b) You, C. C.; Miranda, O. ; Gider, B. ; Ghosh, P. S.; Kim, I.B.; Erdogan, B.; Krovi, S.; Bunz, U. H. F.; Rotello, V. M. Detection and identification of proteins using nanoparticle–fluorescent polymer 'chemical nose' sensors *Nat. Nanotech.* **2007,** *2*, 318-323.

49. (a) Kang, K. A; Wang, J.; Jasinski, J. B.; Achilefu, S. Fluorescence Manipulation by Gold Nanoparticles: From Complete Quenching to Extensive Enhancement. *J. Nanobiotech.* **2011**, *9*, 16. (b) Davis ME, Chen Z, Shin DM: Nanoparticle therapeutics: an emerging treatment modality for cancer. Nature Reviews *Drug Discovery* **2008**, *7*, 771-782. (c) Jiang W, Kim BYS, Rutka JT, Chan WCW: Nanoparticle-mediated cellular response is size-dependent. *Nat. Nanotech.* **2008**, *3*, 145-150. (d) Hong B, Kang KA: Biocompatible, nanogold-particle Fluorescence enhancer for fluorophore mediated, optical immunosensor. *Biosensorsand Bioelectronics* **2006**, *21*, 1333-1338.

50. Love, J. C.; Estroff, L. A.; Kriebel, J. K.; Nuzzo, R. G.; Whitesides, G. M., Self-assembled monolayers of thiolates on metals as a form of nanotechnology. *Chem.Rev.-Columbus* **2005**, 105.

51. (a) Kim, B.; Steven L.; Tripp, S. L.; Wei, A. Self-Organization of Large Gold Nanoparticle Arrays *J. Am. Chem. Soc.* **2001,** *123*, 7955-7956. (b) Warner, M. G. ; Reed, S. M.; Hutchison, J. E. Small, Water-Soluble, Ligand-Stabilized GoldNanoparticles Synthesized by Interfacial Ligand Exchange Reactions. *Chem. Mater.* **2000**, *12*, 3316-3320.

52. (a) Templeton, A. C.; Wuelfing, W. P. ; Murray, R. W. Monolayer-Protected Cluster Molecules *Acc. Chem. Res.* **2000**, *33*, 27-36. (b) Hostetler, M. J.; ingate, J. E.; Zhong, C. J. ; Harris, J. E. ; Vachet, R. W.; Clark, M. R. J.; Londono, D. ; Green, S. J.; Stokes, J. J.; Wignall, G. D.; Glish, G. L. ; Porter, M. D.; Evans, N. D. ; Murray, R. W. Alkanethiolate Gold Cluster Molecules with Core Diameters from 1.5 to 5.2 nm: Core and Monolayer Properties as a Function of Core Size. *Langmuir* **1998**, *14*, 17-30.

53. Templeton, A. C.; Hostetler, M. J.; Warmoth, E. K.; Chen, S.; Hartshorn, C. M.; Krishnamurthy, V. M.; Forbes, M. D. E.; Murray, R. W. Gateway Reactions to Diverse, Polyfunctional Monolayer-Protected Gold Clusters *J. Am. Chem. Soc.* **1998**, *120*, 4845.

Chapter II: NMR and STM Study of Efficacy of Various Cleaving Agents for Thioacetate Cleavage and Molecular Order of SAM Prepared in the Presence of those Agents

2.1 Chapter Overview

This chapter presents the development of a simple methodology for obtaining high-quality, well-ordered, and high-density crystalline $(\sqrt{3}x\sqrt{3})R30^{o}$ organothiolate SAMs from organothioacetate under ambient benchtop conditions. Organothiols are typically chemisorbed on the gold nanoparticles spontaneously to give an ordered monolayer known as self-assembled monolayer (SAM). However, the high reactivity of the thiol functionality can limit the direct use of organothiol. Thus acetyl protected thiol was reported to be deprotected in mild acidic or basic solutions before or during formation of SAMs.[19] Formation of SAMs *in situ* deprotection of thioacetate have already been reported and characterized by ellipsometry X-ray photoelectron spectroscopic (XPS), infrared reflection absorption spectroscopy (IRRAS), near-edge X-ray absorption fine structure (NEXAFS), electrochemistry, contact angle, and/or surface plasmon resonance (SPR) measurements.[16] Though these techniques measure the average bulk properties of SAMs, molecular order of SAMs could not be analyzed. Lack of study of molecular order of SAM produced *in situ* cleavage of thioacetate with several cleaving agents inspired us to put our efforts in this direction. We used an NMR study to study the cleaving ability of thioacetate with several reagents. Also, STM study was done on SAMs obtained during *in situ* cleavage of thioacetate with

those reagents to correlate reagents with surface quality. A simple method was established to produce well-ordered SAMs. A work described in this chapter has been published.[1]

2.2 Introduction

Organic molecules spontaneously adsorb on the substrates in an ordered array to produce crystalline or semicrystalline structures known as self-assembled monolayer (SAM).[2] Organic molecules that have functionality, called head groups, with specific affinity for substrates drive the formation of SAM. For example, Pd, Ag, and Au have high affinity to sulfur in thiols. There are several well known SAMs (Figure 2.1) such as silanes on silicon, phosphines on platinum or palladium, and siloxanes on glass.[3,4,5,6] SAMs have become important tools in surface science as these provide a convenient, flexible, and simple system.2 Several applications of SAMs can be found ranging from engineering to biology.[7] Their invaluable importance can be found in the construction of biomolecular and molecular electronic devices,[8, 9] protection of metal against corrosion,[10] preparation of biocompatible platforms,[11] or immobilization of biological species.[12]

Alkanethiol SAMs on Au (111) have been intensively studied for the past two decades because of their high stability to air and moisture. In contrast silane SAMs can hydrolyze and form polymers.[3-7] The physical and chemical properties of the SAM surface can be tailored with suitable functionality by adding a tail group or terminal group, on the opposite end of the thiol molecule.[13] Furthermore,

SAMs are gaining more attention because of their ease of preparation and low cost of solution deposition. When Au (111) is treated with pure alkanethiol molecules well ordered, crystalline structure ($\sqrt{3}x\sqrt{3})R30^{o}$ SAM is formed due to both strong chemisorption of thiol on gold and van der Waal interaction between the alkyl chains.

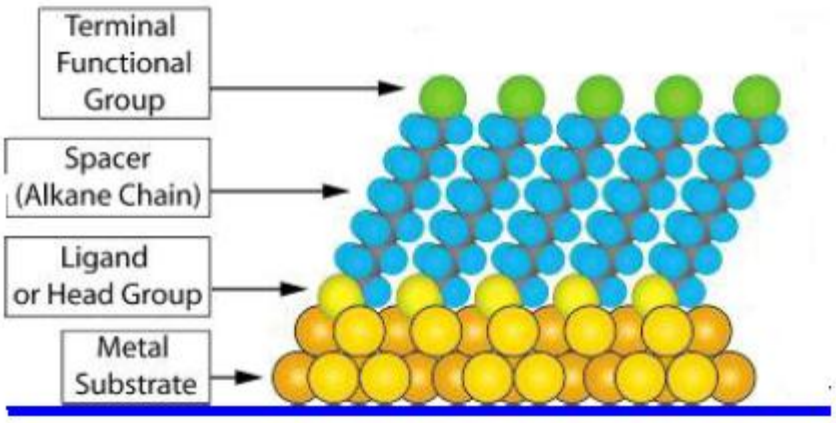

Figure 2.1. Schematic diagram of SAM, adapted from ref. 2.

The chemisorption of organothiols from solution or vapor onto the gold is a widely used method to form molecularly –ordered organothiolate monolayers.2 It is well known that under ambient and benchtop conditions organothiol samples can be easily oxidized to form disulfides. The lower solubility and vapour pressure of disulfide compared to parent thiol may affect the nature of SAMs formation. The presence of disulfide in the thiol samples can result SAMs with high defect density[14] and poor molecular order.[15] Also, dithiols are prone to polymerization

both in solution and on the surface that leads to the formation of multilayers rather than monolayers.[16]

2.2.1 Protection of Thiol Derivatives

Disulfide formation could be minimized by protectting the thiols and the deprotecting before or during the formation of SAM *in situ*. This approach has been employed by several groups using thiocyanates,[17, 12] S- tritylalkanethiols,[18] and acetyl- protected thiols[16,19] as a precursor for thiol and allowing their facile deprotection and monoayer formation. Especially, acetyl-protected thiols (thioacetates) have gained much attention due to their ease of preparation from alkyl halides and deprotection with mild reagents to the parent thiol. Furthermore, thioacetates do not oxidize to disulfide upon storage.

2.2.2 Deprotection of Thioacetates

Tour *et al.*[16] reported that the thioacetate group could be a useful precursor for thiol in the formation of monolayer. ^{1}H and ^{13}C NMR analysis in THF $-d_8$ indicated the complete hydrolysis within 10 min whereas other bases such as *N*,*N*-dipropylamine or 4-*N*,*N*-dimethylaminopyridine (DMAP) were found to be less effective. The researches allowed acetyl-protected arylthiol to react with NH_4OH in THF prior to exposure to gold surface and found that the thickness (ellipsometry and XPS) of monolayer of the resulting SAM matched the expected full monolayer.[16] Additionally, this group also attempted the preparation of SAMs from arylthioacetate without using exogeneous base.[16] The thickness of these

SAM's did not match the thickness of the expected monolayer. This anomaly could be due to the presence of higher concentration of thiolate in base catalyzed thioacetate hydrolysis.[16] The absence of the carbonyl stretch in SAM from IR studies supported that the SAM formation takes place only after the cleavage of acetyl group to thiolate.[16] Furthermore, IR analysis of phenylene ethynylene molecules showed that these rigid-rod molecules were standing up, oriented within 20^{o} of the surface normal, and had infrared intensities consistent with a full monolayer. Direct adsorption of thioacetate suggested to be occurred possibly due to the hydrolysis of thioacetate by trace amount of water or enols of the thioesters.[16] This results indicated that arylthiol produced after the hydrolysis would go to gold surface to form monolayer. However limited concentration of arythiol in arylthioacetate, as no exogeneous base was used, would not result well ordered monolayer.

Inspired from Tour's initial work[16] notable studies could be found on SAM formation *in situ* cleavage of arylthioacetate and alkanethioacetates by using a number of exogenous bases in different solvents. Several reagents in different solvents are known for cleaving of thioacetate NH_4OH or conc. H_2SO_4 in EtOH,[19a] NH_4OH in EtOH, THF, or acetone/MeOH, Cs_2CO_3 in acetone/MeOH or conc. H_2SO_4 in CH_2Cl_2/MeOH,[19b] triethylamine or NH_4OH in DMF,[20] NaOH in EtOH,[21] or EtOH/H_2O.[22] The cleaving reactions were done in a range of 0.1-1 mM thioacetate in the presence of 0.1 mM-0.2 M of cleaving reagents. The molar ratio

of cleaving agent to the thioacetate could be found from unity to over a thousand-fold excess.

Tour *et al.*[16] and other subsequent groups[19-22] characterized the produced SAM through in situ cleavage of thioacetate by calculating thickness using ellipsometry, X-ray photoelectron spectroscopy (XPS), infrared reflection absorption spectroscopy (IRRAS), near-edge X-ray absorption fine structure (NEXAFS), electrochemistry, contact angle, and/or surface plasmon resonance (SPR)measurements.2, [16] However, these techniques only measured the bulk properties such as thickness and molecular tilt. An advancement in direct imaging techniques such as STM (Scanning Tunneling Microscope) or a surface diffraction technique such as grazing incident X-ray diffraction (GIXRD) make it possible to measure the molecular order and crystallinity of the SAM. Niklewski *et al.*[22] unsuccessfully attempted STM measurement to characterize the SAM produced by an *in situ* cleavage of thioacetate. To the best of our knowledge, no systematic characterization of molecular order on SAM formed by deprotection of thioacetates has been reported.

2.2.3 Direct Use of Thioacetates

Few reports have claimed that thioacetate can be directly employed in the formation of SAM.[16, 19,23,24,25] Direct deprotection of thioacetate can take place in the presence of gold.[19d] Formation of a monolayer of 1,8-octane-dithioacetate and 1,4-di(phenylethynyl-4',4''-diacetylthio)-benzene in ethanol : THF or 1: 1

dichloromethane : ethanol has also been reported.[19d] Thus prepared monolayer was confirmed by SPR, XPS, and TOF-SIMS measurements. Lee's group also carried out direct adsorption of alkylthioacetate on gold surface and characterized the resulted SAM by XPS and IRRAS techniques. The group concluded that with a less densely packed and less ordered SAM was produced from alkylthioacetate than from their parent thiol.[24] In another report, the alkylthioacetate was carefully purified to remove any residual thiols.[25] Thus obtained thioacetate was directly used to obtain SAM and characterized by infrared reflection absorption spectroscopy (IRRAS), X-ray photoelectron spectroscopy (XPS), near-edge X-ray absorption fine structure (NEXAFS) spectroscopy, optical ellipsometry, contactangle measurements, and STM. STM imaging indicated the high density of ordered flat lying molecules and very small regions for upright standing molecules especially at the edges and defect sites. Thus, if direct cleavage occurs, it is not expected to occur at a rate sufficient to allow formation of large region of dense upright phases. Furthermore, XPS and IRRAS studies indicate the presence of thiolate mostly at the molecule-gold interface in thioacetate-derived SAMs and may be occassionally due to trace thioacetate.[25] In summary, SAM obtained from thioacetates with or without cleavage by exogenous base, has been previously shown to produce thiolate SAMs with monolayer coverage, but with a large degree of uncertainty regarding long-range crystalline molecular ordering.

2.2.4 Functionalization of Tail Group

Since all the molecules of interest cannot produce good SAMs, they can be introduced after the formation of SAMs. This can be done by two ways: (a) insertion of synthesized thiol into defect site of SAMs (Fig 2.1.2a) or (b) modification of the terminal functional group (Fig 2.1.2b) of SAMs.[2] The second method is the most widely used. In this method SAMs having specific terminal functional groups can be used to couple with the molecule of interest having suitable functionality. Modification of terminal group in a controlled manner is a subject of great interest as it provides the possibility to tailor the surface properties, e.g. wettability, friction, adhesion and conductivity.[13,26] These surfaces find many applications in various fields, such as microelectronics, optoelectronics, thin-film technology, protective coatings, chemical sensors, biosensors, nanotechnology, bioactive surfaces, cell adhesion, protein adsorption and others.[27] The coupling could be done through the noncovalent interactions as well as by forming the covalent bond. A monolayer of the polypeptide poly- (L-lysine) (PL) was reported onto a SAM of 11- mercaptoundecanoic acid (MUA) through electrostatic interaction between the MUA carboxylate and the lysine ammonium groups as well as through covalent linkage, amide coupling.[28] Mrksich's group [29] has used SAMs with maleimide functionality to attach peptides and carbohydrates having thiols functionality. Several other groups have utilized the amide coupling, nucleophilic substitution for anchoring the desired molecules on SAM.[30]

Recently Collman's group reported the use of click chemistry on the Au(111) to immobilize ferrocene.[31] Sharpless click chemistry works under mild conditions in a wide range of pH and regioselectively in the presence of copper (I) catalyst.[32] Furthermore, introduction of azide and alkyne functionality is convenient and also these possess extraordinary tolerance of other functionality. Collman's group studied click chemistry on gold surface using ellipsometry, grazing angle infrared spectroscopy, and electrochemistry. However, these techniques could not provide enough information on molecular order and reactivity of click chemistry. Therefore, we used STM techniques to gain more insight on molecular order and reactivity of click chemistry to introduce desired molecules in a more controlled manner.

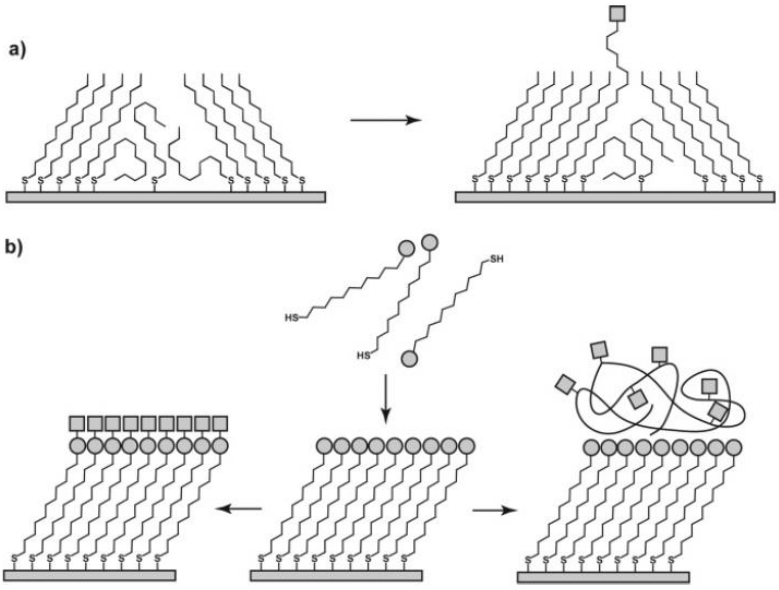

Figure 2.2a and b. Introduction of molecules after the formation of SAMs (Figures are adapted from ref 2).

2.3 Results and Discussion

In spite of a wide range of applications of SAMs, there was still missing data on molecular order of SAMs of acetyl-protected alkanethiol and *in situ* cleavage of alkanethioacetate. Thus we thought to carry out the NMR study of cleavage of decanethioacetate with various cleaving agents and compare the molecular order of SAMs formed in the absence and as well as in the presence of cleaving agents. Distinct differences were observed in the quality of high density, upright-standing SAMs formed in the presence of several cleaving agents. SAMs produced in the presence of different thioacetate cleaving agents ranged from almost completely disordered to almost completely ordered regions. Though the exact percentages of molecularly ordered SAM regions were not quantified, this qualitative information is sufficient in setting procedures that favor the formation of well-ordered SAMs on Au(111).

Decanethioacetate (C10SAc) was prepared by the reaction of 1-bromodecane with potassium thioacetate in ethanol at room temperature for overnight and purified by simple bulb- to-bulb vacuum distillation (scheme 2.1). The ^{1}H NMR spectra matched with that described in the precedent literature.[24, 33] The purified acetyl-protected decanethiol was found to contain 0.04% decanethiol and 0.01% decanedisulfide by GC-MS integration using total ion current. All the STM measuremnts were performed by Daminda H. Dahanayaka in Dr. Bumm's lab. All the samples were prepared under ambient benchtop conditions with no attempts to

exclude oxygen. For STM studies concentration of decylthioacetate and cleaving agents was limited to 2.5 mM in absolute ethanol. The solution of the mixture was allowed to stand for 1 h for deprotecton of thioacetate prior to exposure with Au(111) substrates. Freshly H_2 flame annealed (cleaned) Au(111)/mica substrates were immersed in that solution for 16 h. Au(111) substrates were then removed, rinsed in absolute EtOH, and blown dry with dry N_2. All sample preparation was performed at room temperature under ambient atmospheric conditions. Constant current STM imaging was performed in a dry N_2 purged atmosphere, as this condition known to routinely produce excellent molecularly resolved images of decanethiol/Au(111) SAMs.[34]

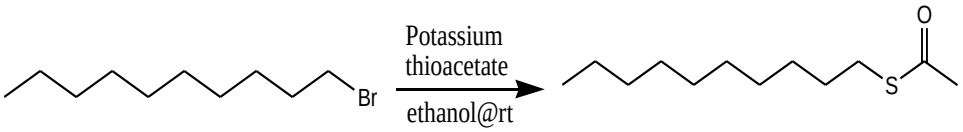

Scheme 2.1. Synthesis of decanethioacetate.

2.3.1 STM Studies of Direct Adsorption of C10SAc

Decylthioacetate solution was exposed to Au(111) for the formation of SAM and thus resulted SAM was studied under STM. STM image of acetyl-protected decanethiol demonstrates the high density upright chains with almost no molecular ordering. Very small islands of expected crystalline structure $(\sqrt{3}x\sqrt{3})R30^o$ were observed (Fig 2.3) whereas similar conditions in the case of decanethiol leads to well-ordered monolayers composed of $(\sqrt{3} \times \sqrt{3})R30^o$ domains. Molecular ordering

of SAM of decanethioacetate exhibited no improvement when molecularly disordered SAM of decylthioacetate was re-exposed to decanethiol (vapor or in ethanol at 60 ^{o}C). This could be attributed to kinetic stability of disordered, high-coverage, and standing-up monolayers. Also, SAM of decylthioacetate produced at higher temperature (60 ^{o}C) with a fresh substrate did not increase the molecular ordering.

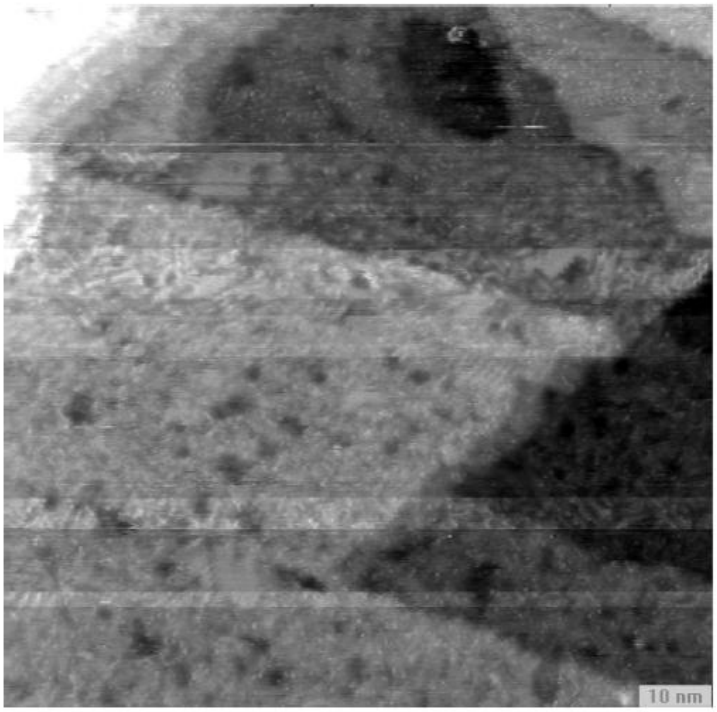

Figure 2.3. STM image of SAM on Au(111) grown for 16 h from C10SAc. The image is 100 nm X 100 nm. Tunneling conditions are V_{sample} = - 1 V and i_{tunnel} = 1 pA. STM image provided courtesy of Daminda H. Dahanayaka.

2.3.2 Cleavage of C10SAc by NH_4OH

Most literature reports mentioned the use of NH_4OH in situ cleavage of acetyl protected of arylthiol or alkylthiol. Therefore, we thought to carry out STM measurement of deprotected decylthioacetate with NH_4OH. In this initial experiment decanethioacetate was deprotected to decanethiol *in situ* with NH_4OH for 1 h and then the Au substrate was immersed in the solution to produce SAM.[19] Thus produced SAM was analyzed with STM data with which it had poor, but an improved order (Figure 2.4) of SAM. The structure is composed of with two distinct regions with different heights. No molecularly resolved imaging was noticed especially in the lower regions whereas sometimes $(\sqrt{3} \times \sqrt{3})R30^{o}$ domain in higher regions were noticed. The statistical percentage of molecularly ordered domains was not determined.

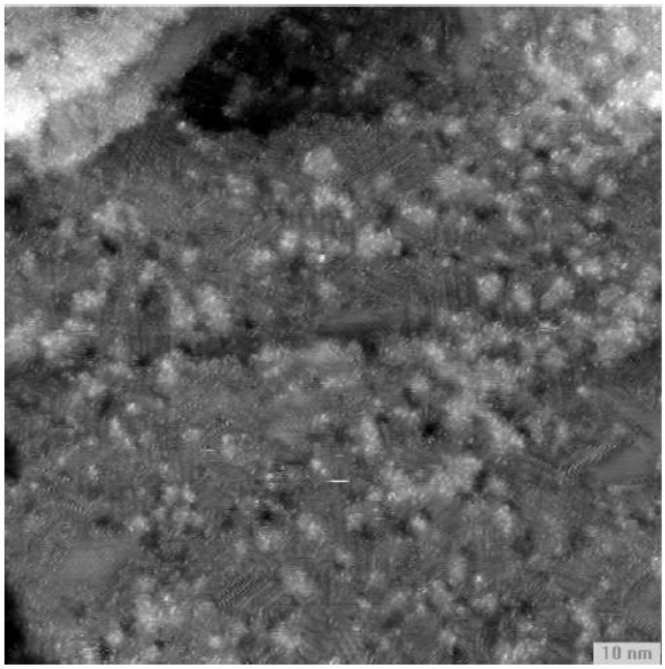

Figure 2.4. STM image of SAM on Au(111) grown for 16 h from C10SAc, precleaved for 1 h in NH_4OH. The image is 100 nm X 100 nm. Tunneling conditions are V_{sample} = -1 V and i_{tunnel} = 1pA. STM image provided courtesy of Daminda H. Dahanayaka.

Our results for the formation of highly disordered SAMs were found to be consistent with those of Tour and others [16,19] who found near-monolayer coverages of high-density, standing-up molecules of undetermined molecular ordering. While our results contradict to those of Wöll *et al.*[35] where high density of well-ordered flat or lying-down phase of decanethiolate were observed with highly pure thioacetate sample. We purified C10SAc sample by bulb-to-bulb vacuum distillation and stored in glass vials. Though NMR mesurements did not indicate the presence of thiol and disulphide, GC-MS measurements, more sensitive, do

show the presence of traces of decanethiol (0.04%) and decanedisulfide (0.01%) in our distilled decanethioacetate sample. This trace thiol could be present through co-distillation or through trace hydrolysis on the glassware. We believed that trace thiol, or disulfide, could adsorb in preference to thioacetate, might be responsible for formation of the monolayers. In the case of formation of SAM *in situ* cleavage of decylthioacetate with NH_4OH, the concentration of decanethiolate was not enough to produce well-ordered monolayer. Furthermore, low concentrations of decanethiol present in our samples, initially physisorbed thioacetate could inhibit formation of wellordered crystalline regions, in a manner analogous to that reported for disulfides.

2.3.3 NMR Studies of C10SAc Cleavage

High concentration of thiolate is required to form well ordered crystalline SAM as can be seen with decanethiols. Therefore, we wanted to investigate the ability of NH_4OH in the cleavage of decylthioacetate. The reaction was monitored by ^1H NMR spectroscopy by integrating the methylene hydrogen atoms adjacent to the sulfur atom. These hydrogen atoms give characteristic and different signals in CD_3OD for the thioacetate ($AcSCH_2$-, 2.85 ppm), the thiol ($HSCH_2$-, 2.50 ppm) and the disulfide (-CH_2S-SCH_2-, 2.68 ppm) groups (Figure 2.5 and 2.6). The disappearance of the acetyl methyl group (2.30 ppm) can also be monitored for the extent of thioacetate cleavage. The detailed hydrolysis or methanolysis of the acetate group was not determined. Our results showed slow exchange of deceylthioacetate (58 mM) with NH_4OH (115 mM) in CD_3OD with only 54%

cleavage (Figure 2.7) after 48 h at room temperature in the presence of air which contradict to literatures[17] where cleavage of arylthioacetate was completely hydrodyzed in THF-d_8 within 10 min. Also, the concentration of formation of disulfide was continuously increasing (31% after 48 h) with time (Figure 2.8). However, complete cleavage (Figure 2.9) was noted with the higher concentration of NH_4OH (575 mM) within 6 h.

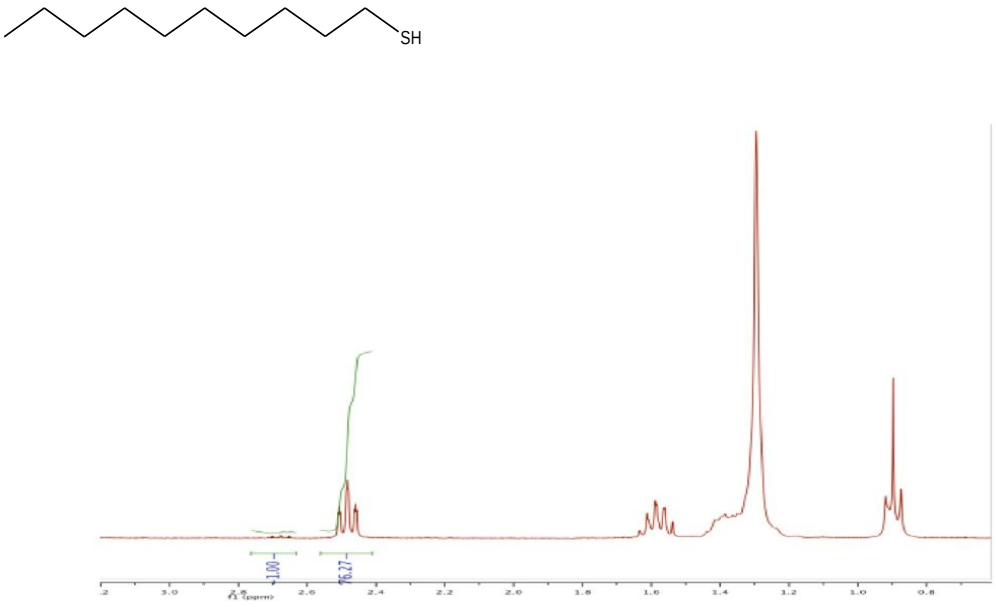

Figure 2.5. NMR spectrum of C10SH in CD_3OD.

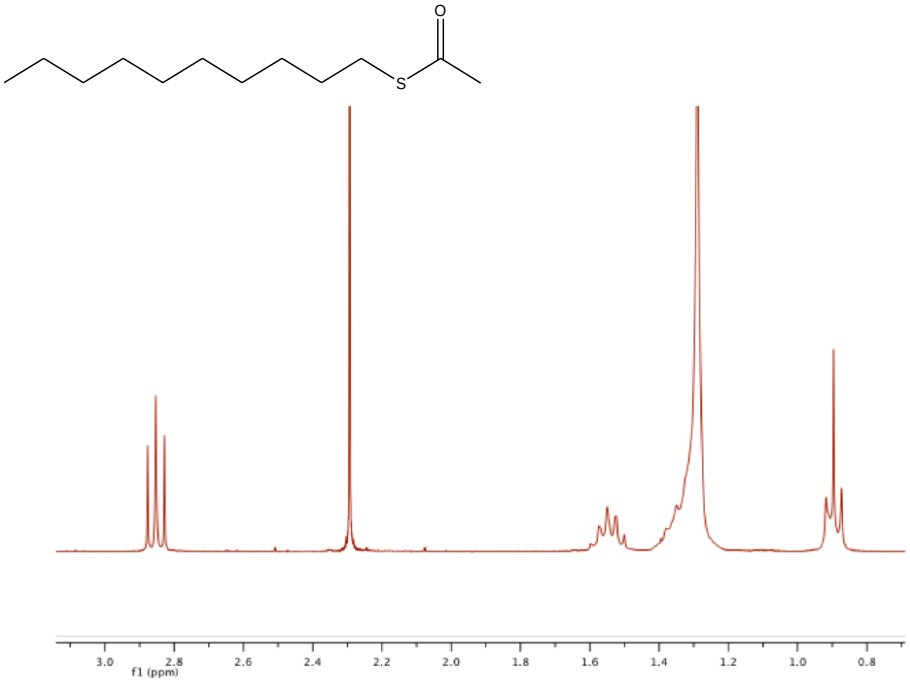

Figure 2.6. NMR spectrum of C10SAc in CD_3OD.

The 2.5 mM solutions we employed to grow SAM were not able to provide higher concentration of decylthiolate and ended with poor ordering monolayer. This result correlates to our expectations should have sufficient amount of thiolate in the solution to form well ordered SAMs similar to decanethiol. In such a low concentration of NH_4OH most of the decylthioacetate remains uncleaved and thus resulted to only small regions of well-ordered monolayer.

Since our major goal was to find a simple methodology for obtaining high density, well-defined, and molecularly ordered decanethiolate monolayers on gold nanoparticles, we used several bases for *in situ* cleavage of the acetyl-protected decanethiol. The extent of cleavage of decylthioacetate was examined by using

various cleaving agents, mostly reported in the literature for thioacetate cleavage, by NMR spectroscopy. Methanol-d_4 was chosen as a model solvent because we were growing our SAM in absolute ethanol. Since decanethiol gives well-ordered monolayers we hypothesized that reagents and conditions that led to faster and more complete cleavage of the thioacetate to form decanethiolate would be better for the formation of the well-ordered monolayers.

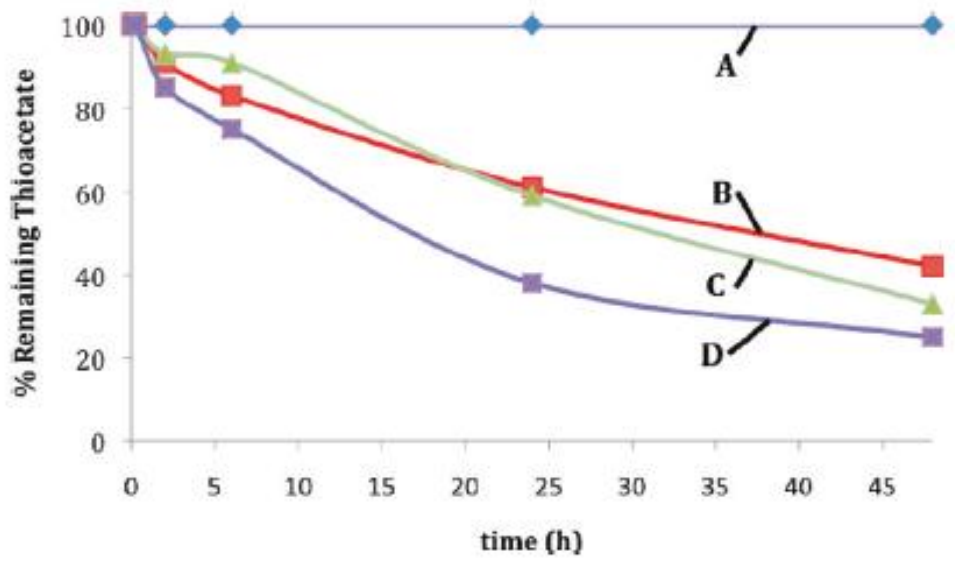

Figure 2.7. C10SAc (46 mM in CD_3OD) cleavage by NMR monitoring. **A**: no additive. **B**: NH_4OH (115 mM). **C**: HCl (250 mM). **D**: propylamine (70 mM).

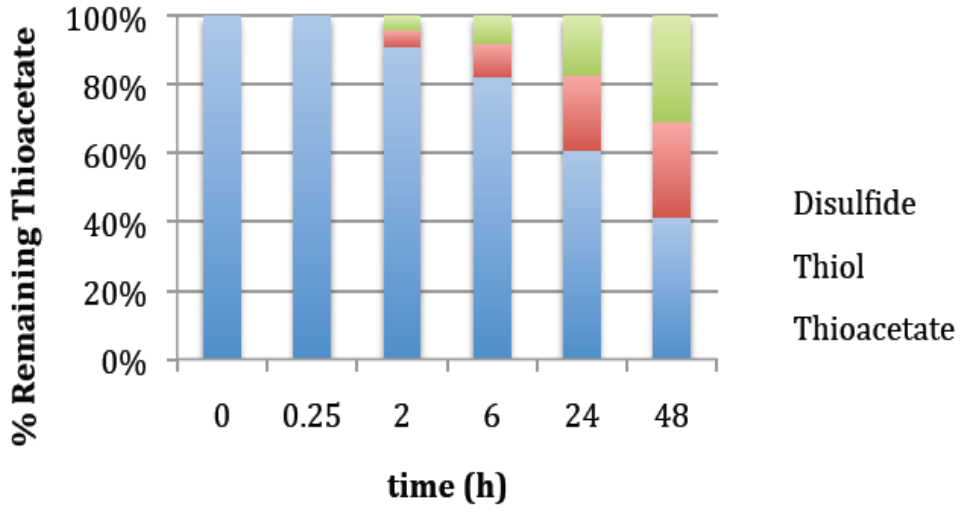

Figure 2.8. ^{1}H NMR monitored cleavage of C10SAc (46 mM) by NH_4OH (115 mM) in CD_3OD.

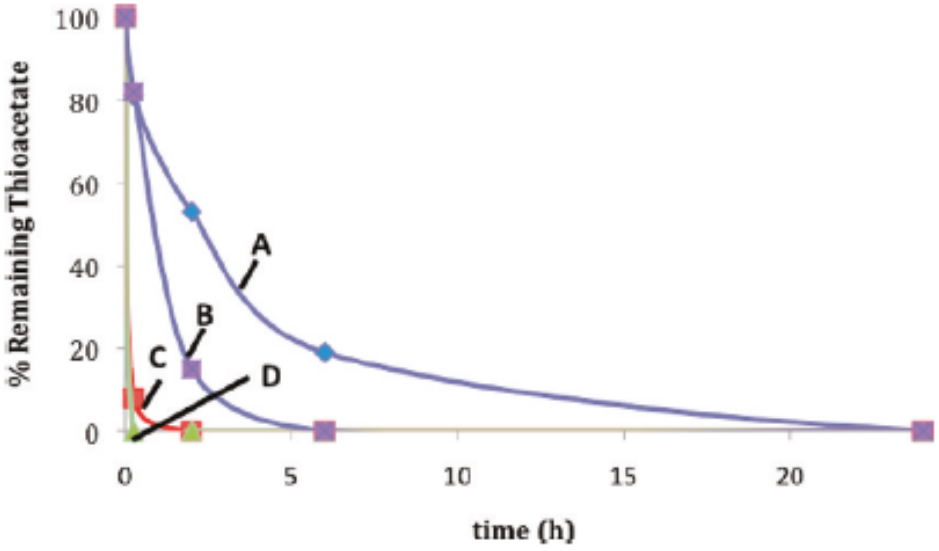

Figure 2.9. C10SAc (46 mM in CD_3OD) cleavage by NMR monitoring. **A**: K_2CO_3 (46 mM). **B**: NH_4OH (575 mM). **C**: DBU (58 mM). **D**: KOH (58 mM).

The mechanism of cleavage of thioacetate had already been studied under basic conditions.[36, 37] Initially tetrahedral intermediate was produced due to the slow addition of hydroxide to the thioacetate, formed by the reaction of bases like amines to water, followed by fast decomposition of the intermediate to form thiol. In the acid catalyzed cleavage, protonation of carbonyl of thioacetate dictate towards addition of water or alcohols and form tetrahedral intermediates which subsequently decomposed to thiol.

We started to study acid catalyzed cleavage and base catalyzed cleavage of decylthioacetate by using HCl (250 mM) and n-propylamine (70 mM) in CD_3OD respectively side by side. Some extent of cleavage of decylthioacetate was observed (Figure 2.7) but the reaction did not go to completion within 48 h even at these relatively higher concentrations required for the NMR measurement for better signals. Furthermore, the concentration disulfide steadily increased to 11% after 48 h with HCl (Figure 2.10) and 48% with propylamine (Figure 2.11).

We thought to investigate the ability of cleavage with the weak base sodium citrate as this reagent is usually used in the synthesis of gold nanoparticles.[38] Our results indicate no cleavage of thioacetate over 48 h which are similar to the reaction of thioacetate with methanol-d_4 (Figure 2.7) only.

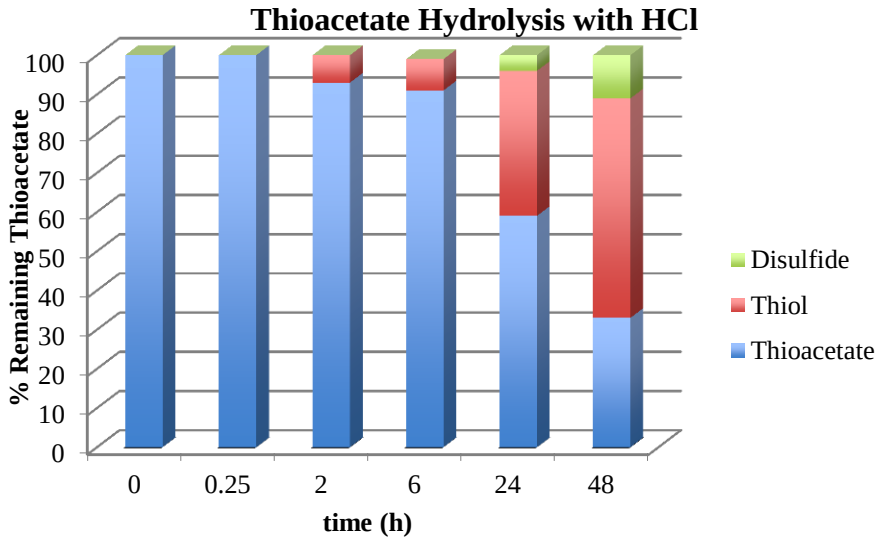

Figure 2.10. ^{1}H NMR monitored cleavage of C10SAc (46 mM) by HCl (250 mM) in CD_3OD.

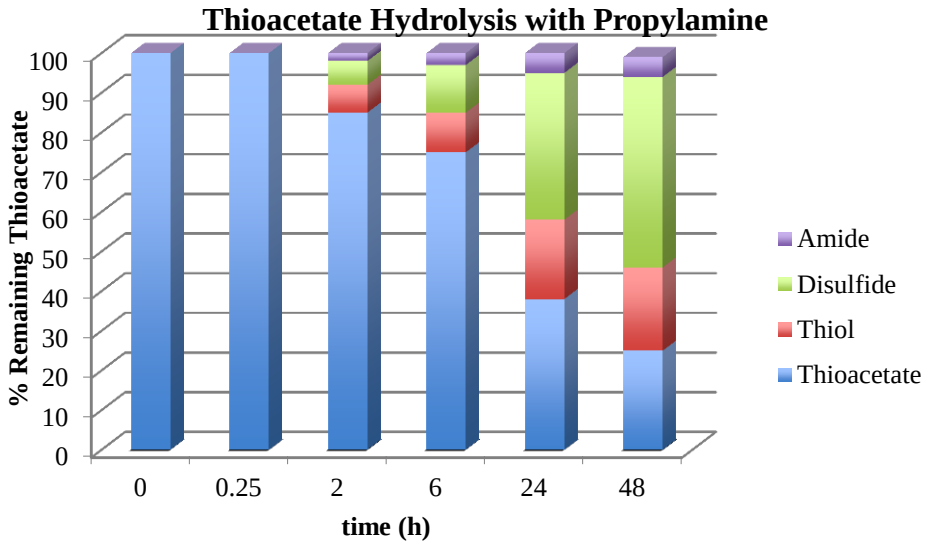

Figure 2.11. ^{1}H NMR monitored cleavage of C10SAc (46 mM) by propylamine (70 mM) in CD_3OD.

Due to incomplete cleavage of thioacetate with HCl and propyl amine, we examined the efficacy of cleavage of decylthioacetate with stronger bases. We used K_2CO_3 as a cleaving agent for cleaving decylthioacetate and found complete cleavage within 24 h (Figure 2.9) and with19% disulfide (Figure 2.12) after 48 h. The reason for more effective cleavage could be due to the presence of higher concentration of nuccleophilic CD_3O^- K^+ species. We also examined the efficacy of cleavage of decyl thioacetate with the strongest bases, KOH and DBU, and observed the complete cleavage of the thioester within minutes for KOH and within 2 h for DBU (Figure 2.9). Both the reactions were continously monitored to find the amount of formation of disulfide over 48 h and observed 30% in KOH (Figure 2.13) and 46% in DBU (Figure 2.14). Such type of fast cleavage of thioacetate by these two reagents could be due to their basicity (aqueous p*K*a of conjugate acid is about 16 in each case) high concentration of CD_3O^- (K^+ or H-DBU$^+$) present in the solution.

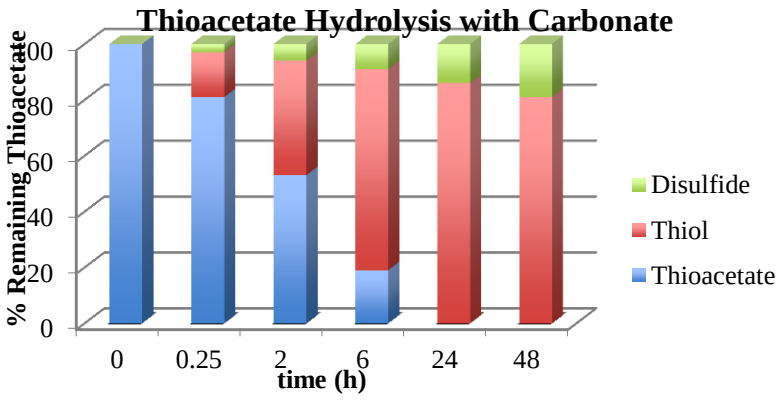

Figure 2.12. ^{1}H NMR monitored cleavage of C10SAc (46 mM) by K_2CO_3 (46 mM) in CD_3OD.

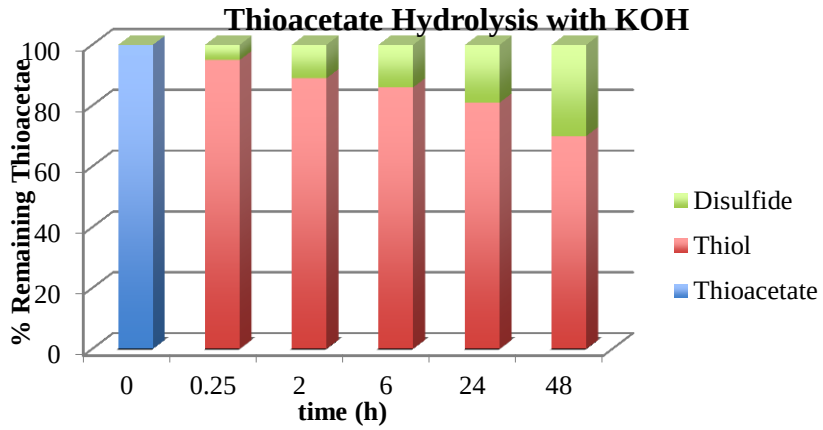

Figure 2.13. ^{1}H NMR monitored cleavage of C10SAc (46 mM) by KOH (58 mM) in CD_3OD.

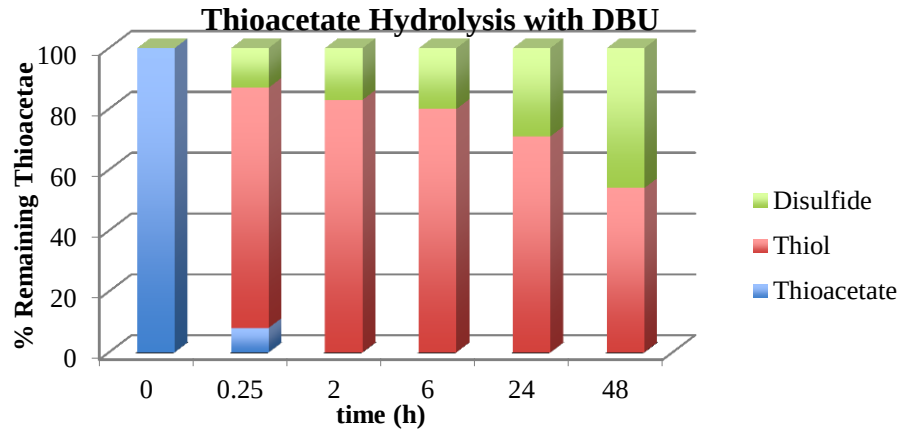

Figure 2.14. ^{1}H NMR monitored cleavage of C10SAc (46 mM) by DBU (58 mM) in CD_3OD.

Also, the extent of cleavage of decylthiolate was studied by NMR spectroscopy in THF-d_8 by using NH_4OH, Cs_2CO_3, and DBU to compare our results to those reported in the literatures. However, we did not use the decylthioacetate solution in THF-d_8 for the growth of SAM. No cleavage was

observed in the case of decylthioacetate in THF-d_8 solvent only over 48 h. Similar result was observed when Cs_2CO_3 (46 mM) or NH_4OH (58 mM) were used as cleaving agent for decylthioacetate over 48 h. While lower extent of cleavage of decylthioacetate was observed with more concentrated NH_4OH (173 mM) or DBU (58 mM) as compared to cleavage in methanol-d_4 (29% and 72% cleavage at 24 h, respectively).

2.3.4 STM Imaging of *in situ* Deprotected C10SAc

SAM was grown by following the same procedure described above in this work (for the NH_4OH cleaved SAMs) with different cleaving agents. The SAMs produced this way were analyzed by taking their STM measurements. Formation of SAM was repeated many times with those cleaving agents under identical condition and took hundreds of images. However, only one image from each cleaving agents as a representative of that agents has been shown in Figure 2.15. As in alkanethiol SAMs, all samples contained Au(111) substrate steps and vacancy islands. As expected, in the case of SAM produced by HCl-reacted thioacetate only small ordered regions could be observed as in NH_4OH. Our result of poor ordered monolayer was found to be consistent with the NMR data where we could see the low extent of cleavage of decylthioacetate with HCl as in NH_4OH. Unsurprisingly, *n*-$PrNH_2$ produced slightly better order SAM as the extent cleavage of thioacetate with amine was more than that of HCl. Additionally, SAM produced by K_2CO_3-treated thioacetate was found to be more ordered whereas high degree of ordered SAMs were observed in DBU and KOH (Figure 2.15).

Qualitative molecular order can be visualized by looking at structural domain boundaries. This is observed between the crystalline domain of different orientation and the position of substrate. The well ordered SAM has lack of zigzag row and mostly with straight lines between the different domains and run in the Au (110) crystallographic directions. Poor ordered domains do not have structural boundaries whereas well-ordered regions do have the crystalline islands which are surrounded by lower disordered regions. As the crystalline order increases to an intermediate level, the structural domain boundaries appear between neighbouring crystalline domains. The disordered regions appear interstitial to some ordered regions, existing as connected areas and expanded domain boundaries. A very well-ordered SAMs have a high degree of crystalline order and the entire surface is composed of domains with crystalline order directly separated by domain boundaries, but with little or no disordered regions.

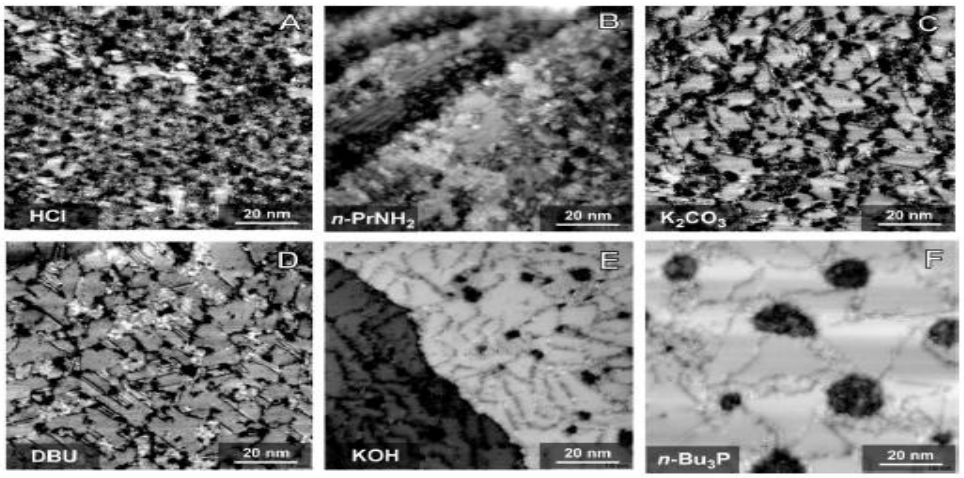

Figure 2.15. STM images SAMs on Au(111) grown for 16 h in 2.5mMC10SAc in EtOH grown from a solution premixed for 1 h with 2.5mM of (A) HCl, (B) $PrNH_2$, (C) K_2CO_3, (D) DBU, (E) KOH, and (F) Bu_3P. Each sample was grown from 2.5 mM each in ethanol (1 h premix, 16 h immersion of Au/mica). All STM images are 100 nm X 100 nm. Tunneling conditions are V_{sample} = -1 V and i_{tunnel} = 1 pA. STM image provided courtesy of Daminda H. Dahanayaka.

Also, we noticed that in a low to intermediate degree of order the disorder regions are lower than the crystalline regions while in a high degree of order the scattered or isolated disoredered regions appear higher. This effect was observed in the DBU STM image (Figure 2.15 D). To gain more insight of this effect more characterization of the chemical composition of disordered regions could be needed.

2.3.5 Cleavage of Phenylthioacetates

We also carried out the NMR measurement experiments for cleavage of arylthioacetate to aryl thiol with NH_4OH, HCl, KOH, and DBU as the most of the literature reports are based on *in situ* cleavage of arylthioacetate. However growth of SAM with phenylthioacetate was not performed. The extent of cleavage is similar as with C10SAc (Figure 2.16) and this NMR results are consistent with reports in literatures.[37] UV analysis shows the complete cleavage of arythioacetate (0.5 mM) by NH_4OH (37.5 mM) in acetone/MeOH after 30 min.[19b] Furthermore, cyclic voltammetry studies demonstrate at least 1 h precleavage of arylthioacetate with strong base at low concentration (0.27 mM NaOH in EtOH) necessary for the saturated adsorption on the electrode. When the levels of electrode passivation by adsorption were studied using cyclic voltammetry, it was found that more than an hour of precleavage was required for the adsorption rate to saturate when strong base at low concentrations (aryl thioacetate 0.1 mM with 0.27 mM NaOH in EtOH) was used.[20]

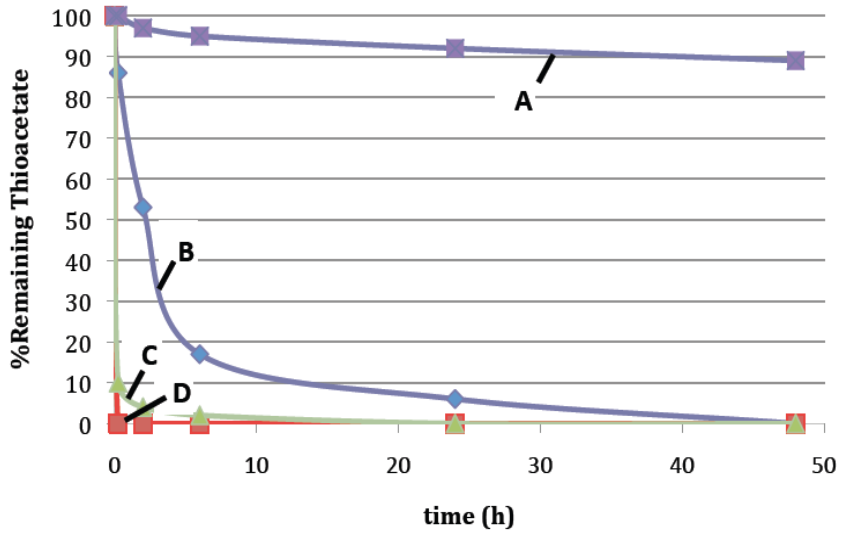

Figure 2.16. ^{1}H NMR monitored cleavage of phenylthioacetate C_6H_5SAc (46 mM) by: **A.** NH_4OH (58 mM), **B.** HCl (58 mM), **C.** KOH (58 mM), and **D.** DBU (58 mM) in CD_3OD.

2.3.6 Effect of Added Tributylphosphine

Our procedure for forming a well ordered SAM is technically simple as it can be done at ambient temperature in air. We also noticed that on increasing the time the formation of amount of disulfide keep on increasing under more basic conditions which could change the molecular order of SAM. It is well known that tributylphosphine (Bu_3P) can reduce aryl or alkyl disulfides to their respective thiol.[39] Thus we used Bu_3P as a sacrificial reductant to convert disulfides to thiols.[40] Initially we monitored the cleavage of C10SAc (46 mM) by DBU (58 mM) in the presence of Bu_3P (58 mM) by NMR spectroscopy. As in the previous results, cleavage was almost complete within 15 min and was found to be complete by 2 h. As assumed no disulfide was observed even after 48 h (Figure 2.17). The

SAM grown on gold nanoparticles (C10SAc 2.5 mM, DBU 2.5 mM, Bu_3P 2.5 mM in ethanol, 1 h premixing, 16 h immersion) contains well-ordered domains (Figure 2.18) as in DBU alone. STM experiments were carried out by Daminda H. Dahanayaka. Furthermore, DBU and Bu_3P were not interfering in the formation ordered monolayer.

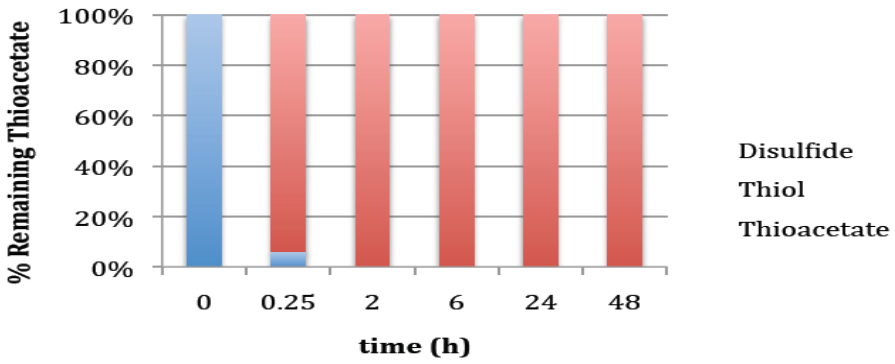

Figure 2.17. ^1H NMR monitored cleavage of C10SAc (46 mM) by DBU (58 mM) and Bu_3P (58 mM) in CD_3OD.

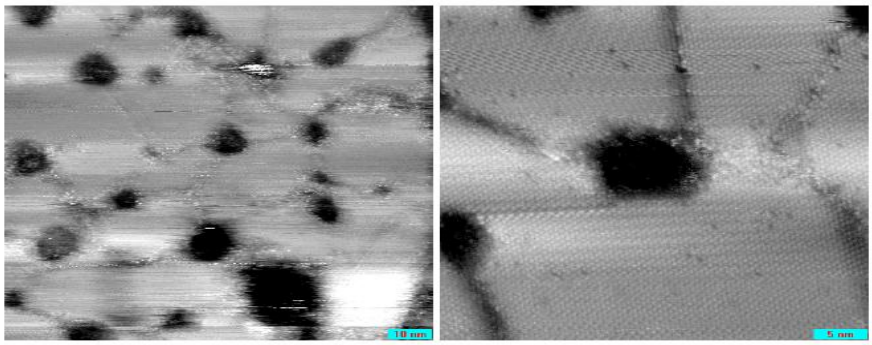

Figure 2.18. STM image of C10SAc + DBU + Bu_3P (2.5 mM each in ethanol, 1 h

premix, 16 h immersion of Au/mica). Two scan sizes are shown: left 100 nm × 100 nm, and right 50 nm × 50 nm. STM image provided courtesy of Daminda H. Dahanayaka.

The cleavage efficiency of Bu_3P on C10SAc was examined in CD_3OD by NMR spectroscopy. No cleavage of C10SAc was observed within 48 h. We propose two reasons for this result. First, Bu_3P may not be able to deprotonate the methanol to provide enough methoxide to cause cleavage as it is a weak base. Secondly, Bu_3P alone may not become so effective nucleophile to cleave thioacetate directly in methanol solution.

Interestingly, when SAM was grown in C10SAc and Bu_3P, as a cleaving agent, solution, a well-ordered SAM (Figure 2.15 F) was obtained. The quality of molecular order of this SAM (Figure 2.15 F) was similar to the SAM produced from the strong bases DBU and KOH (Figure 2.15 D and E). However, the sizes of the vacancy islands in the Bu_3P SAM are significantly larger than in the other images. Having larger size of vacancy islands is not the characteristic of the Bu_3P but is unique for this particular sample.

Though Bu_3P alone is not able to cleave the acetyl-protected thiol, the formation of well-ordered SAM with this led us to think the mechanism of cleavage in the presence of gold. Bu_3P is a weak base but a good nucleophile. The thioacetate can coordinate to the gold surface and activate the carbonyl. Nucleophilic addition of Bu_3P to the activated carbonyl followed by the leaving of

acetylphophonium group leads to the formation of thiolate. Additionally, Bu_3P can reduce the disulfide to thiols. The trace disulfide present in our sample could produce poor order SAM from the mixture of disulfide and thioacetate or mixture of thiol, disulfide and thioacetate. Complete conversion of disulfide to thiol may allow thiol to displace the any initially adsorbed thioacetate more effectively. While phosphines can also adsorb weakly on Au surfaces, they can be easily displaced by more strongly binding thiols that are responsible to give well-oredered monolayer.[41]

2.3.7 Click Chemistry on Gold Surface

After establishing a method for preparing well-ordered SAMs, we pursued our investigation towards the click reaction on SAMs. Excellent stereospecific and requirement of mild condition attracted us towards this reaction.[42] The product, 10-azido decanethioacetate was synthesized by following Scheme 2.2. The compound, 10-bromodecan-1-ol was obtained from the reaction of 1, 10-decanediol and hydrobromic acid. Nucleophilic substitution on monobromodecanol with sodium azide followed by conversion of hydroxyl to mesylate and further converted to 10-azido-decanethioacetate simply by nucleophilic substituition with potassium thioacetate.

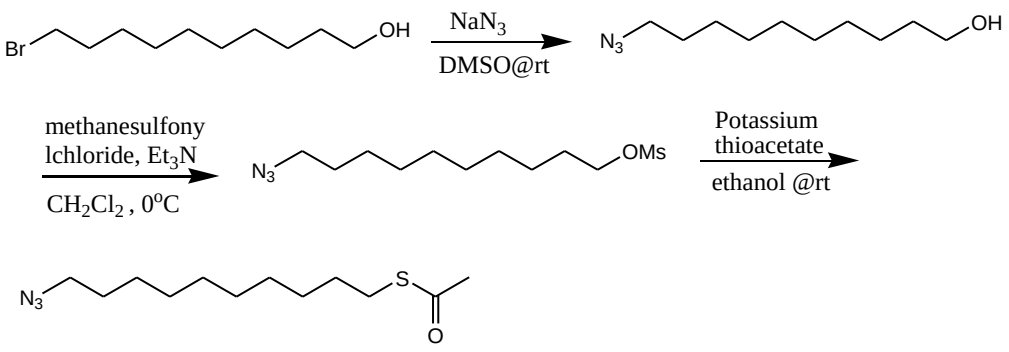

Scheme 2.2. Synthesis of 10-azido decanethioacetate.

The crude product, 10-azido decanethioacetate was purified by column chromatography. This compoumd and decylthioacetate (precleaved in KOH) was used to prepare binary SAMs with islands of a longer azide terminated SAMs surrounded by a shorter inert alkyl SAMs (Figure 2.19). Mixed SAM preparation and STM experiments were carried out by Daminda H. Dahanayaka. The click chemistry was performed with *p*-tolylacetylene in the presence of catalyst IMesCu(I)Br in 3:1 *t*-BuOH/H_2O at 45 ^oC for 2 h. The Cu (I) catalyzed alkyne-azide reaction (click-reaction) was found to occur 4-10 times faster at the edges of these islands. The bulky transition state could sterically prevent the reaction in the inner region. Click chemistry was successfully achieved on well ordered SAMs without any damage on their molecular order.

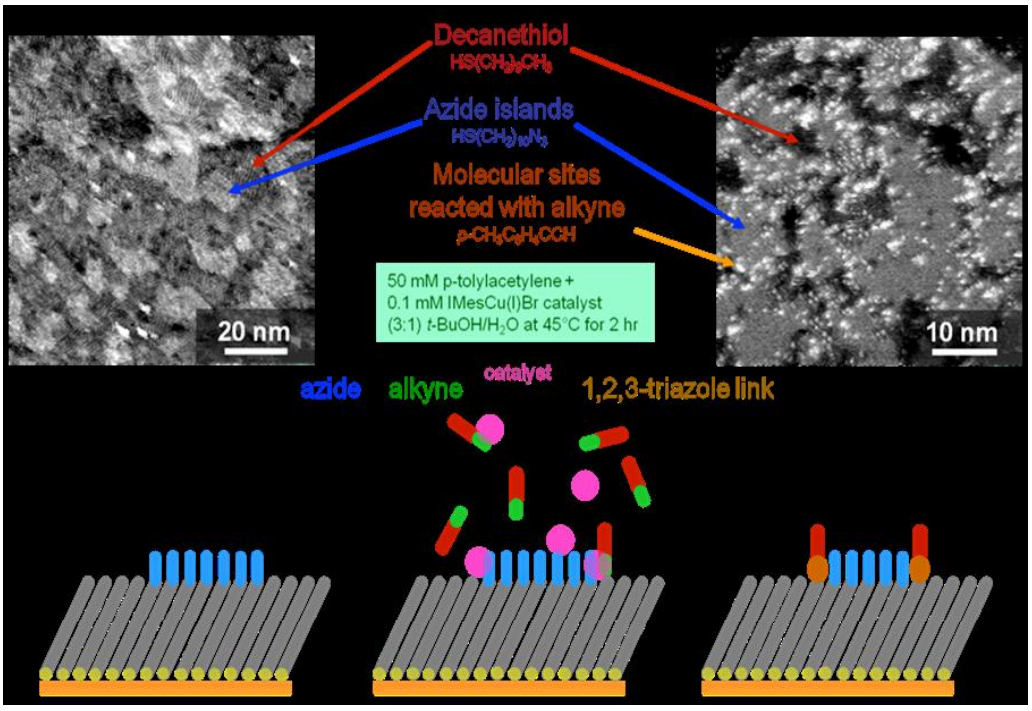

Figure 2.19. Binary SAMs. Image provided courtesy of Daminda H. Dahanayaka.

2.4 Chapter Summary

We were able to establish a simple methodology for the formation of well-ordered crystalline ($\sqrt{3}$ x $\sqrt{3}$)R30^{o} SAM on Au(111) under ambient benchtop condition. The reagents that cleave decylthioacetate fast, as detected by means of NMR spectroscopy were found to produce well-ordered crystalline decanethiolate monolayers on Au(111) as determined by the STM measurements. The results from the NMR measurements can be correlated to the STM measurements. Poorly ordered SAM was obtained in the case of HCl, NH_4OH, and propyl amine as these reagents were not able to provide high enough concentration of decanethiolate. These reactions were not completed within 48 h for the formation of well-ordered SAM whereas well-ordered SAM was produced with cleaving agents that cleave decylthioacetate completely within 2 h. Addition Bu_3P was also found to be beneficial as a sacrificial reductant for getting a well-ordered SAM. The poor SAM molecular order produced in the presence of a large excess of uncleaved thioacetate is likely caused by initial physisorption of the thioacetate onto the surface in a way that inhibits highly ordered phases from forming. In conclusion, ordinary pure thioacetates can give well-ordered monolayer like alkanethiol by precleaving the thioacetate with bases such as DBU, KOH etc. Additionally, molecules of interest can be covalently attached on the gold nanoparticles by performing click chemistry without the destruction of the ordered SAM.

2.5 Experimental Section

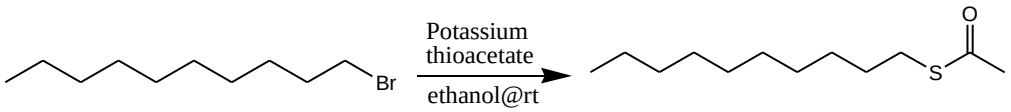

Preparation of C10SAc. Following literature precedent, potassium thioacetate (2.0 g, 17.5 mmol) was added to 1-bromodecane (2.0 g, 9.0 mmol) in absolute ethanol (50 mL) at room temperature under nitrogen. After stirring for 24 h, the solvent was removed *in vacuo*. The residue was partitioned between icecold water (100 mL) and diethyl ether (3x50 mL). The combined organic portion was washed with water (3x50 mL), dried ($MgSO_4$), and the solvent removed by rotary evaporation. The crude C10SAc containing decanethiol (0.6%) and decanedisulfide (2%) as determined byGC-MS measurements was purified through two bulb-to-bulb distillation cycles under vacuum (0.2 mm) to give 1-decanethioacetate as a pale yellow liquid (1.09 g, 56% yield). The 1H NMR spectrum matched that reported in the literature.[24] GC-MS analysis of the purified decanethioacetate determined that trace decanethiol (0.04%) and decanedisulfide (0.01%) were present in the sample.

^{1}H NMR Spectroscopic Monitoring of Thioacetate Cleavage. Separate solutions of C10SAc (92 mM in methanol-d_4) and the reagent to be investigated (typically 116 mM in methanol-d_4) were mixed in equal portions to give final concentrations of 46 mM in C10SAc and typically 58 mM in reagent just prior to measuring the first NMR spectrum. These samples in methanol-d_4 were left in capped NMR tubes at room temperature and were periodically monitored by NMR spectroscopy. The

ratios of thioacetate, thiol, and disulfide were based on the integration of the methylene signals at 2.85, 2.48, and 2.67 ppm for these three compounds in CD_3OD, respectively.

Preparation of Samples for STM. Separate solutions of C10SAc and the reagent to be investigated (KOH, DBU, K_2CO_3, aqueous concentrated HCl, aqueous 30% NH_4OH, and DBU/Bu_3P) were freshly prepared in absolute ethanol with initial concentrations at 7.5 mM. The solutions of C10SAc and the reagent were mixed with additional ethanol to give final concentrations of 2.5 mM in each. The mixture was allowed to stand for 1 h prior to use allowing time for cleavage to occur. All solution work was carried out under benchtop (ambient) conditions, with no attempts to exclude oxygen. H_2 flame-annealed (cleaned) Au(111)/mica substrates were then immersed in this solution for 16 h. They were then removed, rinsed in absolute EtOH, and blown dry with dry N_2. All sample preparation was performed at room temperature under ambient atmospheric conditions. STM measurements were conducted by Daminda H. Dahanayaka and Lloyd Bumm as described in reference 1 and Daminda H. Dahanayaka's thesis.

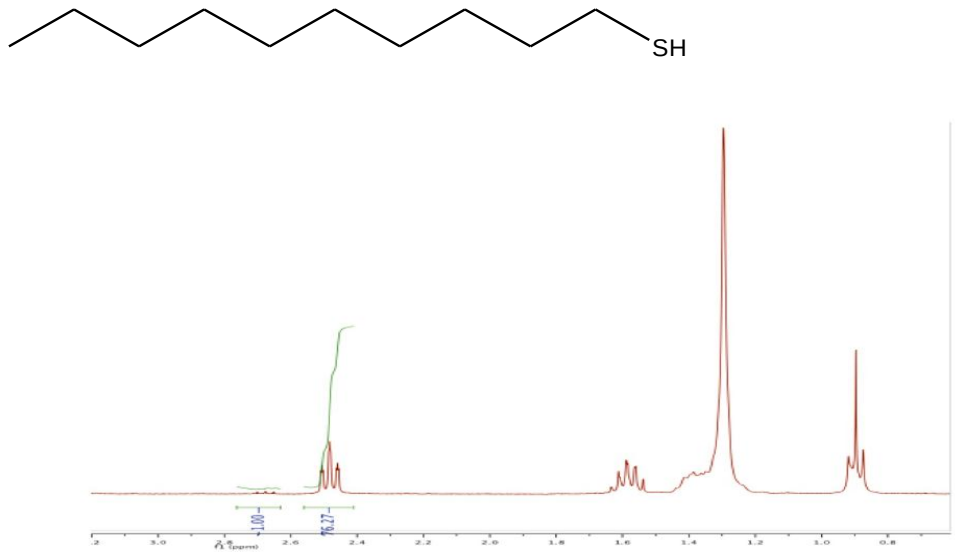

Figure 2.20. ^{1}H NMR spectrum of C10SH in CD_3OD.

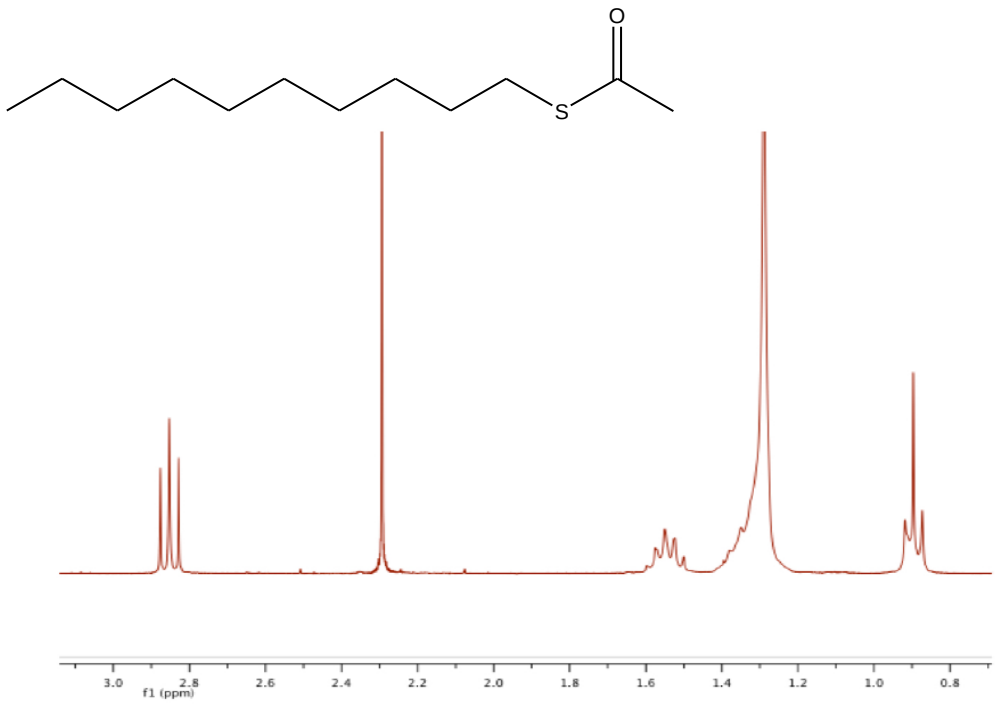

Figure 2.21. ^{1}H NMR spectrum of C10SAc in CD_3OD.

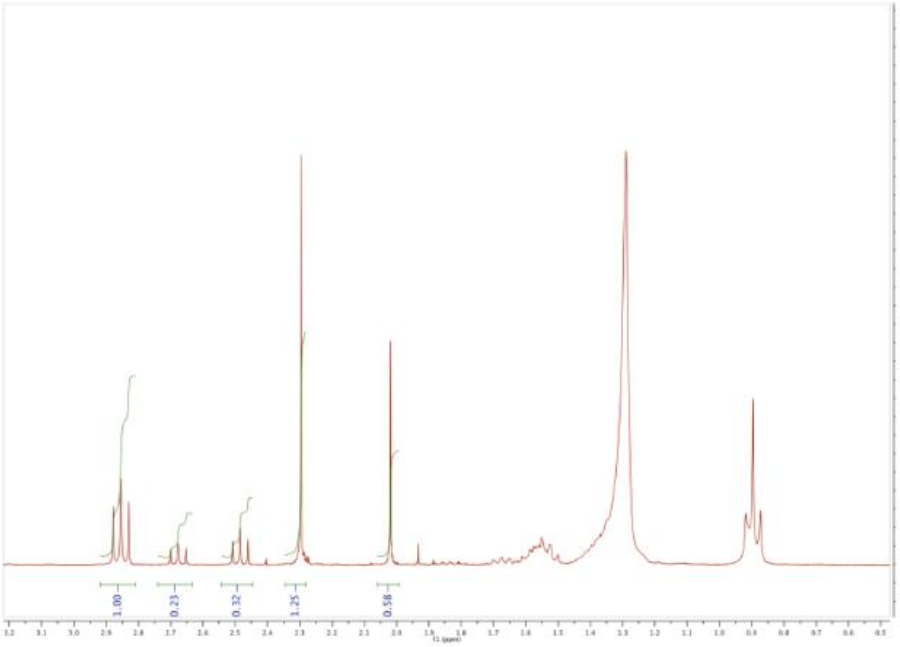

Figure 2.22. ^{1}H NMR spectrum of C10SAc (46 mM) sample mixture (K_2CO_3, 46 mM) after 2 h in CD_3OD.

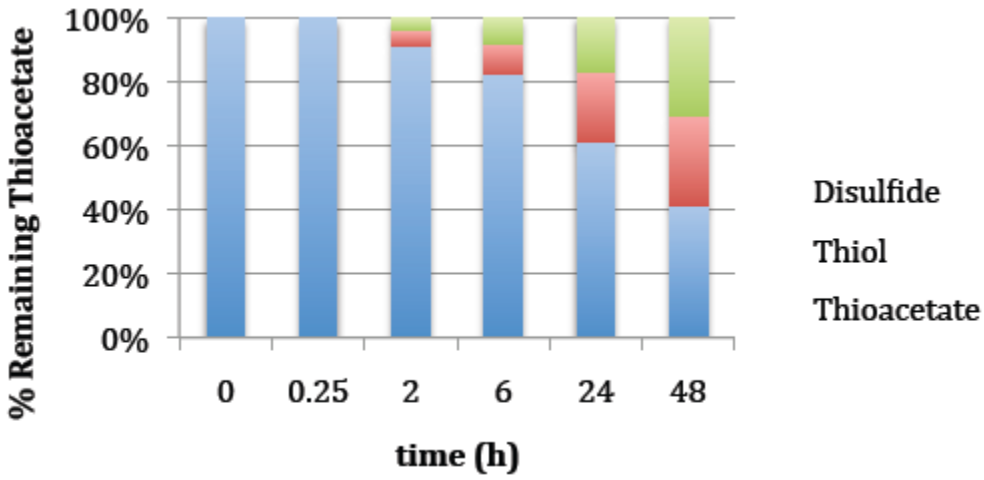

Figure 2.23. ^{1}H NMR monitored cleavage of C10SAc (46 mM) by NH_4OH (115 mM) in CD_3OD.

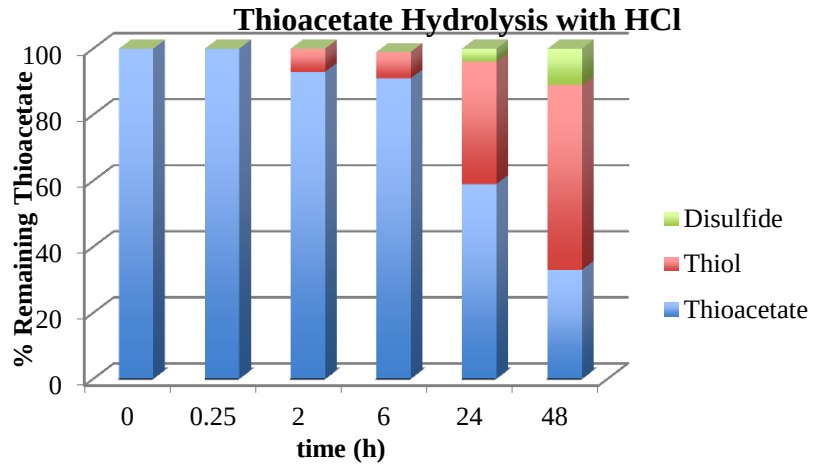

Figure 2.24. ^{1}H NMR monitored cleavage of C10SAc (46 mM) by HCl (250 mM) in CD_3OD.

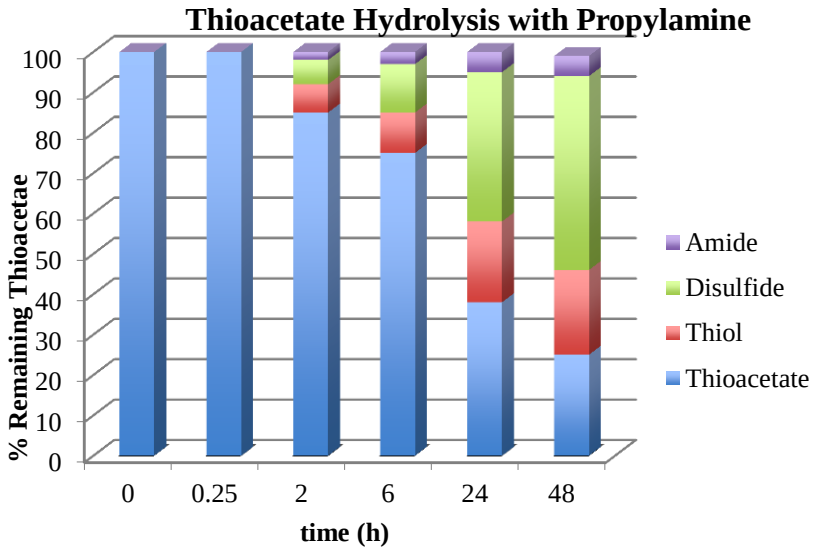

Figure 2.25. ^{1}H NMR monitored cleavage of C10SAc (46 mM) by propylamine (70 mM) in CD_3OD.

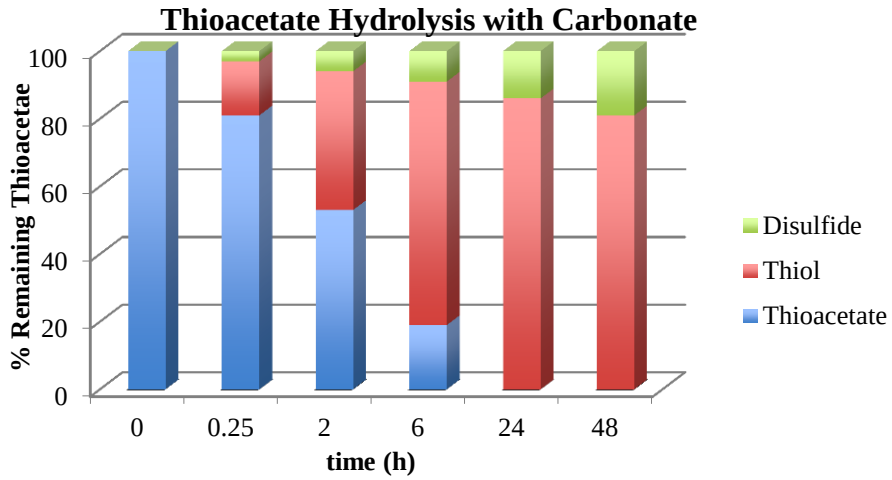

Figure 2.26. ^{1}H NMR monitored cleavage of C10SAc (46 mM) by K_2CO_3 (46 mM) in CD_3OD.

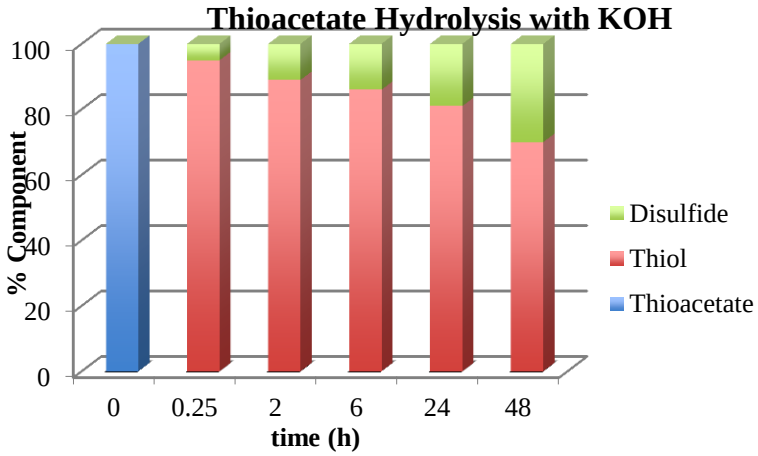

Figure 2.27a. ^{1}H NMR monitored cleavage of C10SAc (46 mM) by KOH (58 mM) in CD_3OD.

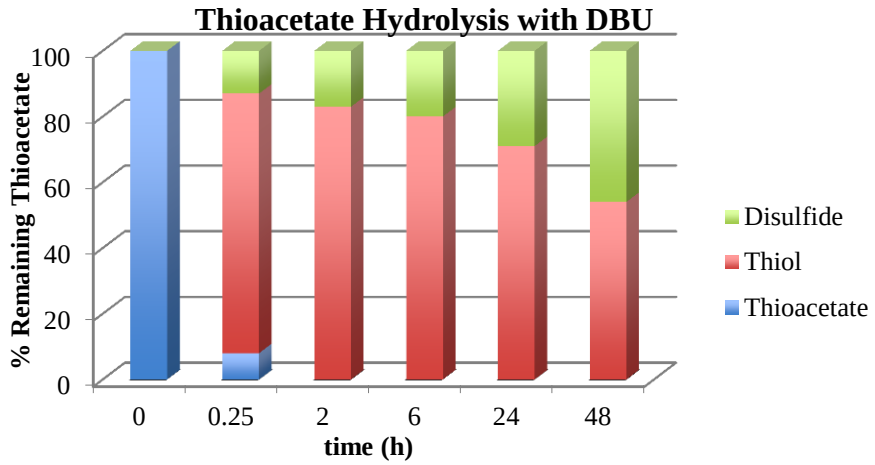

Figure 2.27b. ^{1}H NMR monitored cleavage of C10SAc (46 mM) by DBU (58 mM) in CD_3OD.

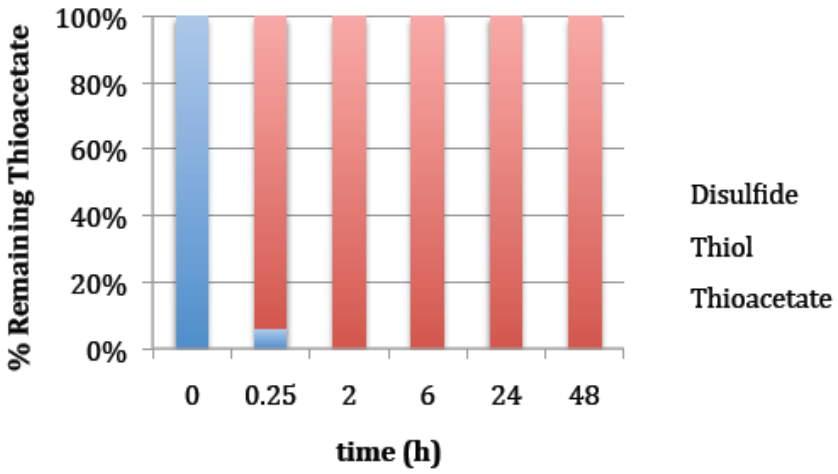

Figure 2.28. ^{1}H NMR monitored cleavage of C10SAc (46 mM) by DBU (58 mM) and Bu_3P (58mM) in CD_3OD.

Following STM images were obtained by Daminda Dahanayaka (reference 1 and Daminda Dahanayaka's thesis).

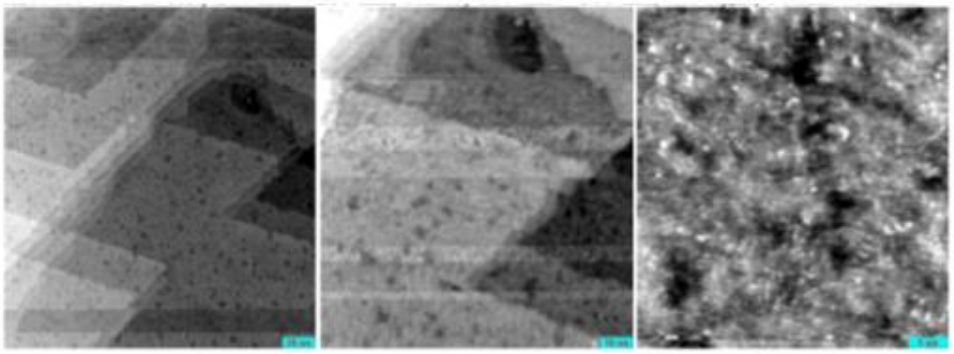

Figure 2.29. STM image of C10SAc (2.5 mM in ethanol, 16 h immersion of Au/ mica). Three scan sizes are shown : left 200 nm x 200 nm, center 100 nm x 100 nm, and right 50 nm x 50 nm.

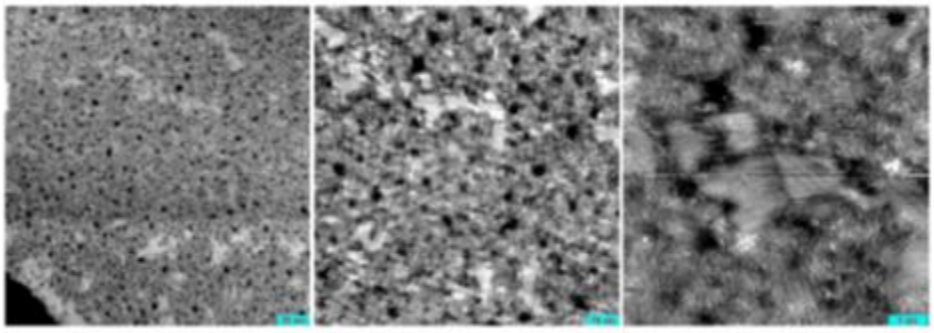

Figure 2.30. STM image of C10SAc + HCl (2.5 mM in ethanol, 16 h immersion of Au/ mica). Three scan sizes are shown : left 200 nm x 200 nm, center 100 nm x 100 nm, and right 50 nm x 50 nm.

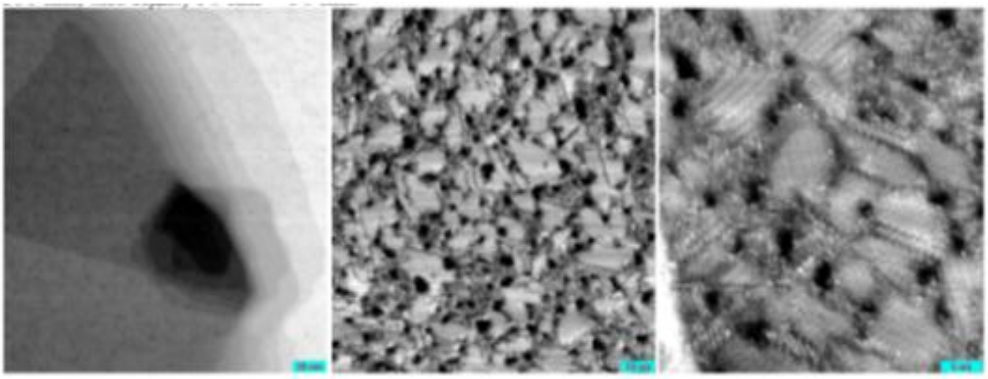

Figure 2.31. STM image of C10SAc + K_2CO_3 (2.5 mM in ethanol, 16 h immersion of Au/ mica). Three scan sizes are shown: left 200 nm x 200 nm, center 100 nm x 100 nm, and right 50 nm x 50 nm.

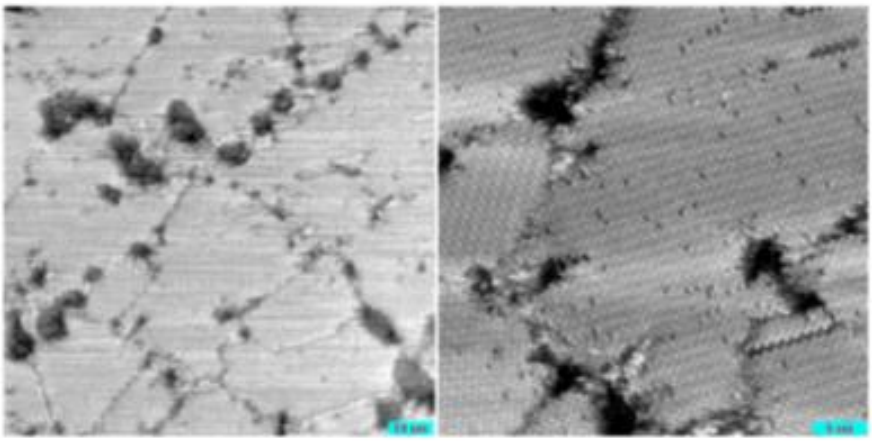

Figure 2.32. STM image of C10SAc + DBU (2.5 mM in ethanol, 16 h immersion of Au/ mica). Two scan sizes are shown : left 100 nm x 100 nm, and right 50 nm x 50 nm.

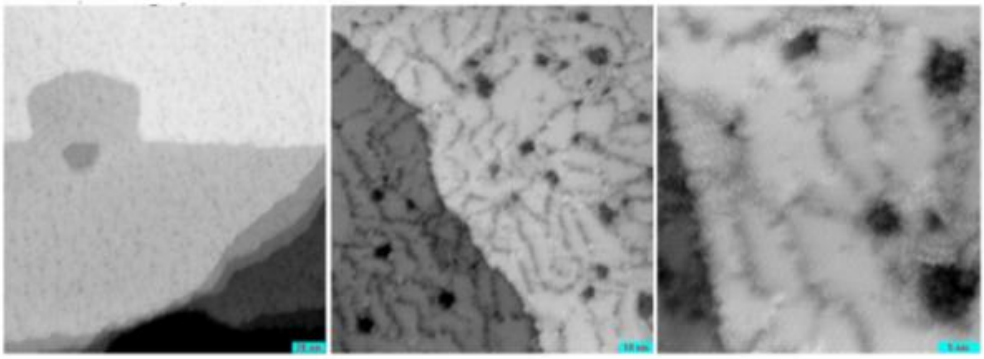

Figure 2.33. STM image of C10SAc + KOH (2.5 mM in ethanol, 16 h immersion of Au/ mica). Three scan sizes are shown: left 200 nm x 200 nm, center 100 nm x 100 nm, and right 50 nm x 50 nm.

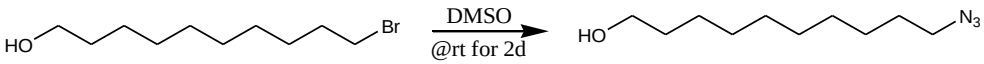

10-azido-1-decanol. To the solution of sodium azide (0.819 g, 12.6 mmol) and dimethyl sulfoxide(20 mL), 10-bromo-1-decanol (2 g, 8.4 mmol) was added stirred at room temperature for 2 days. 50 mL of distilled water was added and stirred it for 30 mintutes and extracted with dichloromethane (3×10 mL). The organic portion was combined and washed with water (2× 20 mL) and brine (20 mL). The organic phase was dried over anhydrous $MgSO_4$, filtered and concentrated to obtain colorless oily liquid with 94% (1.7g) yield. ^{1}H NMR ($CDCl_3$, 300 MHz): δ 3.5 (t, 2H, J = 6 Hz), 3.2 (t, 2H, J = 6 Hz), 2.2 (s, 1H), 1.4-1.6 (m, 4H), 1.2-1.4 (b, 12H); ^{13}C NMR ($CDCl_3$, 75 MHz): δ 62.75, 51.42, 32.68, 29.44, 29.37, 29.09, 28.77, 26.65, 25.71. MS (ESI) $[M+Na]^+$ calcd for $C_{10}H_{21}N_3ONa$ 222.28 ; found 222.2.

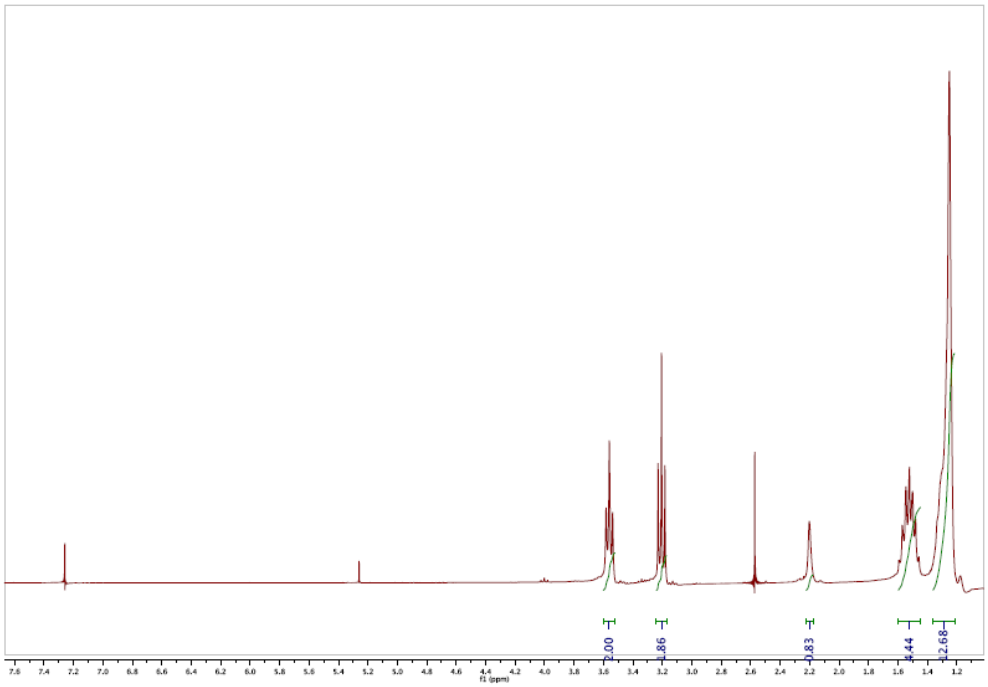

Figure 2.34a. ^{1}H NMR spectrum of 10-azidodecan-1-ol.

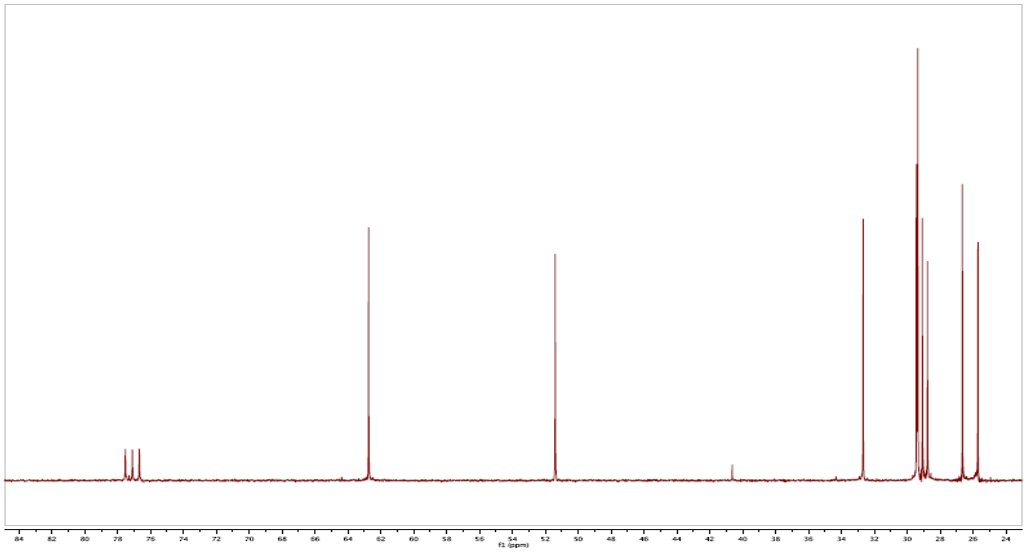

Figure 2.34b. ^{13}C NMR spectrum of 10-azidodecan-1-ol.

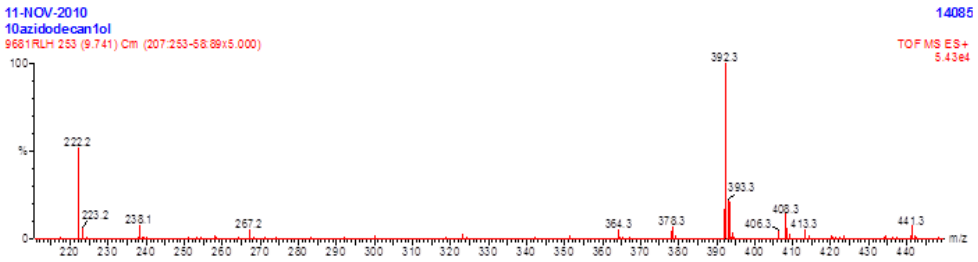

Figure 2.34c. Mass spectrum of 10-azidodecan-1-ol.

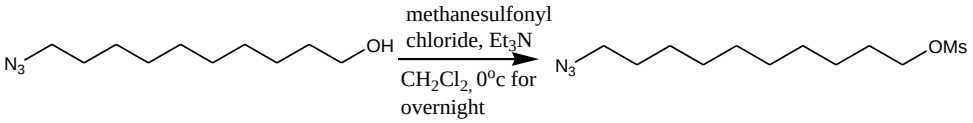

10-azidodecane-1-mesylate. 10-Azido-1-decanol (1.6 g, 8.02 mmol), methanesulfonylchloride (2.348 g, 20.5 mmol) and dichloromethane (50 mL) were added to 250 mL reaction flask kept in icebath and stirred. The solution of triethylamine (2.8 mL, 20.5 mmol) in 1 mL of dichloromethane was added to the cooled reaction flask dropwise through syringe over 5 min and stirred it for overnight. The reaction was quenched by the addition of 50 mL of ice-cold water and stirred for 15 min. The organic phase was collected and the aqueous phase was taken for extraction with dichloromethane (2×20 mL). The organic portions were combined, washed with 1M HCl (1×25 mL), $NaHCO_3$ (1×25 mL), brine (1×25 mL), and water(2×25 mL), dried over anhydrous sodium sulfate, filtered, and evaporated the solvent via rotary evaporation to get pale yellow oily liquid (92% yield, 2.074 g). ^{1}H NMR ($CDCl_3$, 300 MHz): δ 4.2 (t, 2H, J = 6 Hz), 3.2 (t, 2H, J =

6 Hz), 3.0 (s, 3H), 1.7-1.8 (m, 2H), 1.6 (m, 2H), 1.2-1.4 (b, 12H); ^{13}C NMR ($CDCl_3$, 75 MHz): δ 70.22, 52.55, 51.43, 37.32, 29.31, 29.28, 29.06, 28.96, 28.80, 26.65, 25.37. MS (ESI) $[M+Na]^+$calcd for $C_{11}H_{23}N_3O_3SNa$ 300.37; found 299.2.

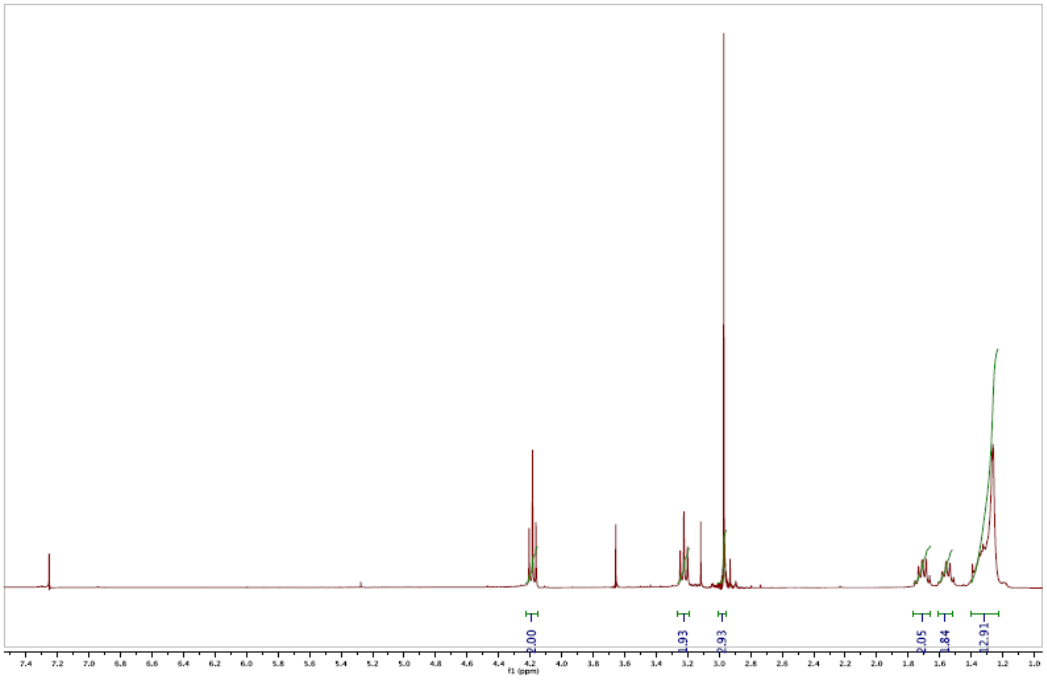

Figure 2.35a. ^{1}H NMR spectrum of 10-azidodecane-1-mesylate.

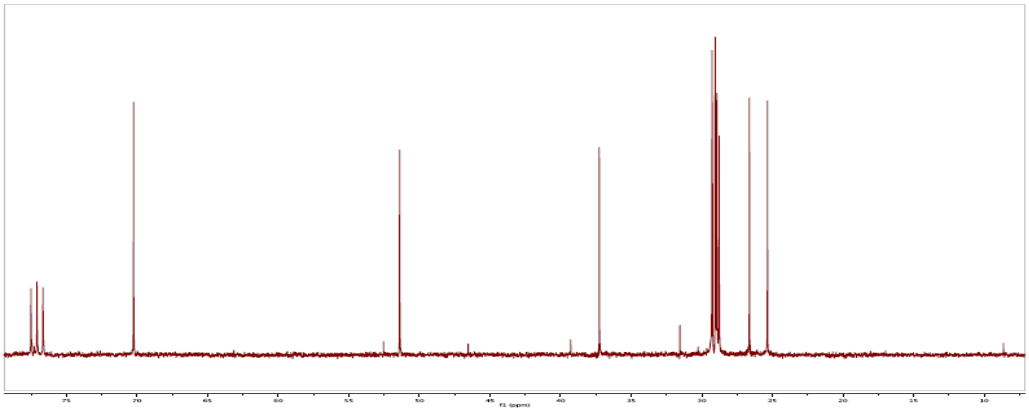

Figure 2.35b. ^{13}C NMR spectrum of 10-azidodecane-1-mesylate.

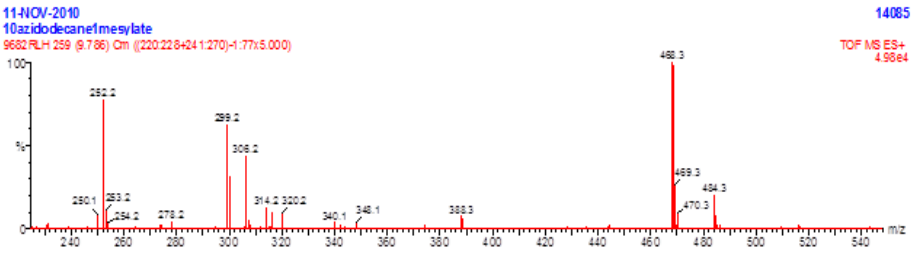

Figure 2.35c. Mass spectrum of 10-azidodecane-1-mesylate.

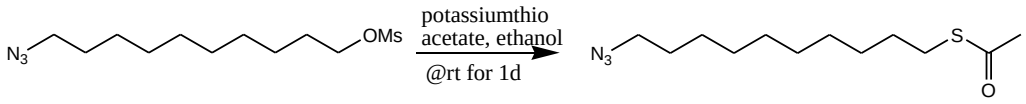

10-azidodecane-1-thioacetate. 10-azidodecane-1-mesylate (3.68 g, 13.27 mmol), potassium thioacetate (3g, 26.54 mmol), and 75 mL of abs. ethanol were taken in a 250 mL of reaction flask and stirred for 1 d at room temperature under nitrogen atmosphere. Ethanol was removed via rotary evaporation. 150 mL of ice-cold water was added to the raction flask and extracted with diethylether (3×50 mL). The combined organic portion was washed with water (3×50 mL) and dried over anhydrous $MgSO_4$, filtered, and concentrated to obtain 2.5 g of 10-azidodecane-1-thioacete. It was purified by column chromatography using 2 : 1 petroleum ether and dichloromethane as eluent to get yellow oily liquid (1.85 g, 54% yield). ^{1}H NMR ($CDCl_3$, 300 MHz): δ 3.2 (t, 2H, J = 6 Hz), 2.8 (t, 2H, J = 6 Hz), 2.3 (s, 3H), 1.6 (m, 4H), 1.2-1.4 (b, 12H); ^{13}C NMR ($CDCl_3$, 75 MHz): δ 196.13, 51.49, 30.69,

29.52, 29.41, 29.37, 29.14, 29.09, 28.86, 28.82, 26.73. MS (ESI) $[M+Na]^+$ calcd for $C_{12}H_{23}N_3OSNa$ 280.39; found 280.2.

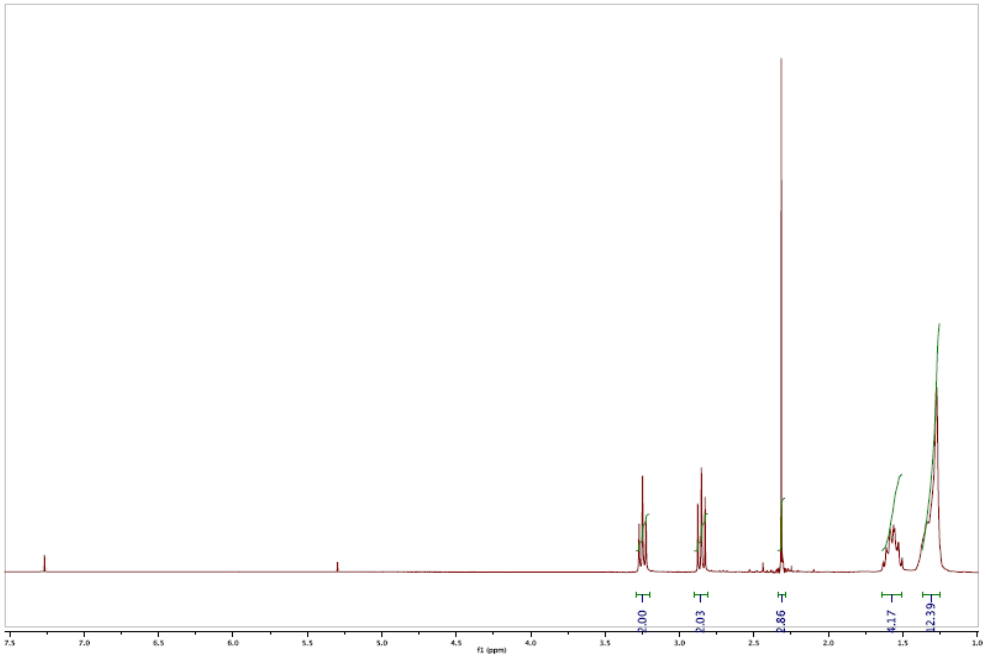

Figure 2.36a. ^1H NMR spectrum of 10-azidodecane-1-thioacetate.

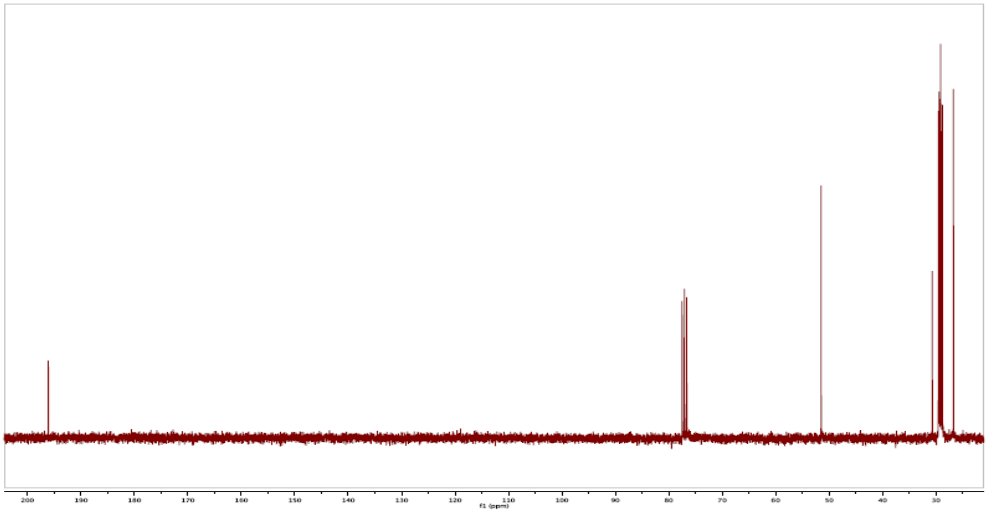

Figure 2.36b. ^{13}C NMR spectrum of 10-azidodecane-1-thioacetate.

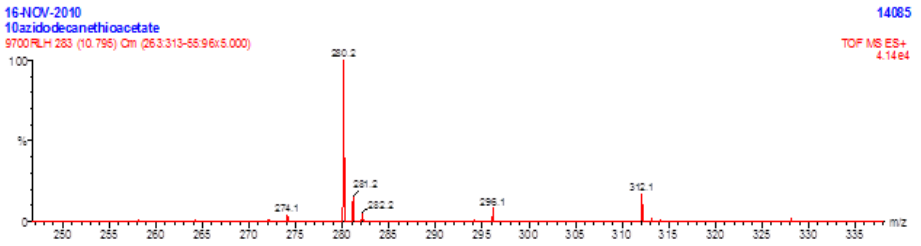

Figure 2.36c. Mass spectrum of 10-azidodecane-1-thioacetate.

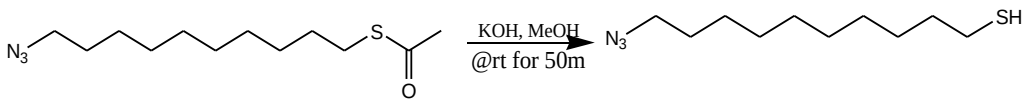

10-azido-decanethiol. 10-azidodecane-1-thioacetate (100 mg, 0.39 mmol), potassium hydroxide (26 mg, 0.47 mmol), and 5 mL of methanol were taken in a 50 mL reaction flask and stirred it for 50 min under nitrogen at room temperature. 10 mL of water was added to the reaction flask and extracted with diethylether (3×10 mL). The organic phase was washed with water (3×10 mL), dried over anhydrous $MgSO_4$, and filtered. The solvent was removed via rotary evaporation. A colorless oily liquid was obtained (80 mg, 94% yield). ^{1}H NMR ($CDCl_3$, 300 MHz): δ 3.2 (t, 2H, J = 6 Hz), 2.5 (q, 2 H, J = 9 Hz), 1.6 (m, 4H), 1.2-1.4 (b, 12H); ^{13}C NMR ($CDCl_3$, 75 MHz): δ 51.46, 34.02, 29.38, 29.11, 29.02, 28.82, 28.35, 26.69, 24.65. MS (ESI) $[M+Na]^+$ calcd for $C_{10}H_{21}N_3SNa$ 238.35; found 451.3.

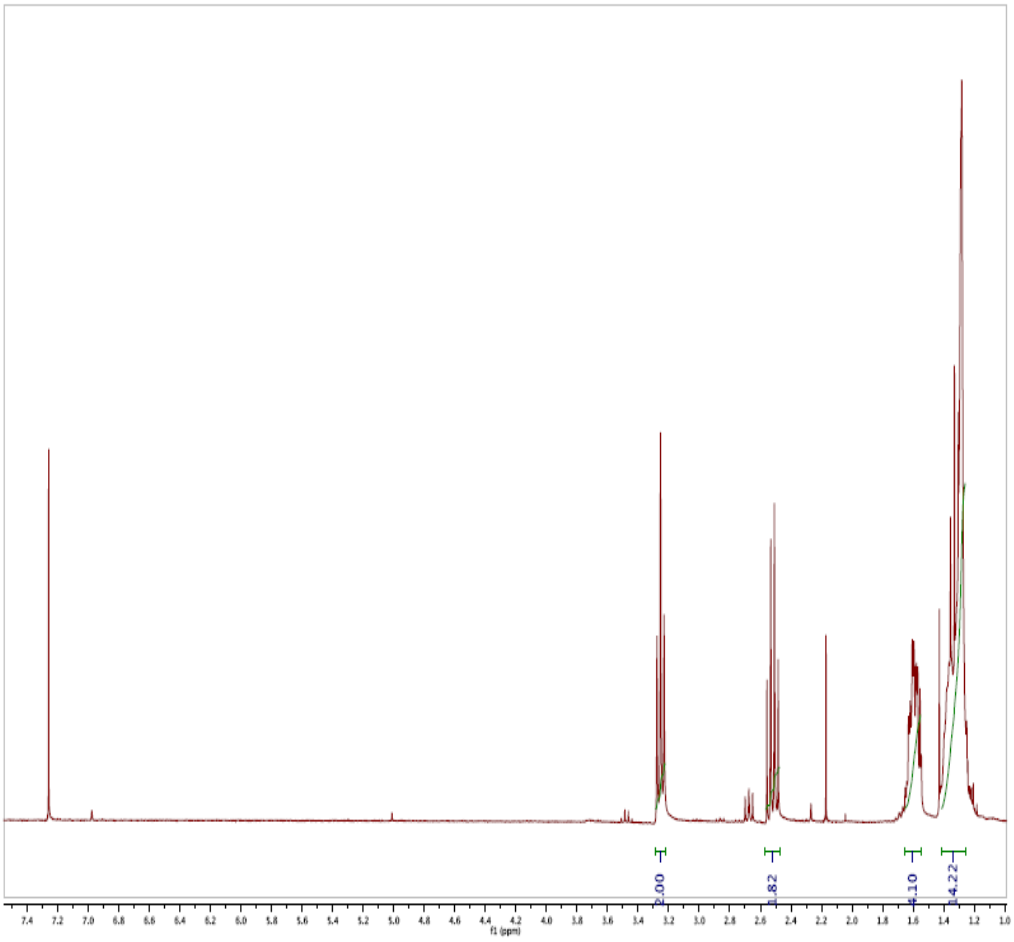

Figure 2.37a. ^{1}H NMR spectrum of 10-azidodecane-1-thiol.

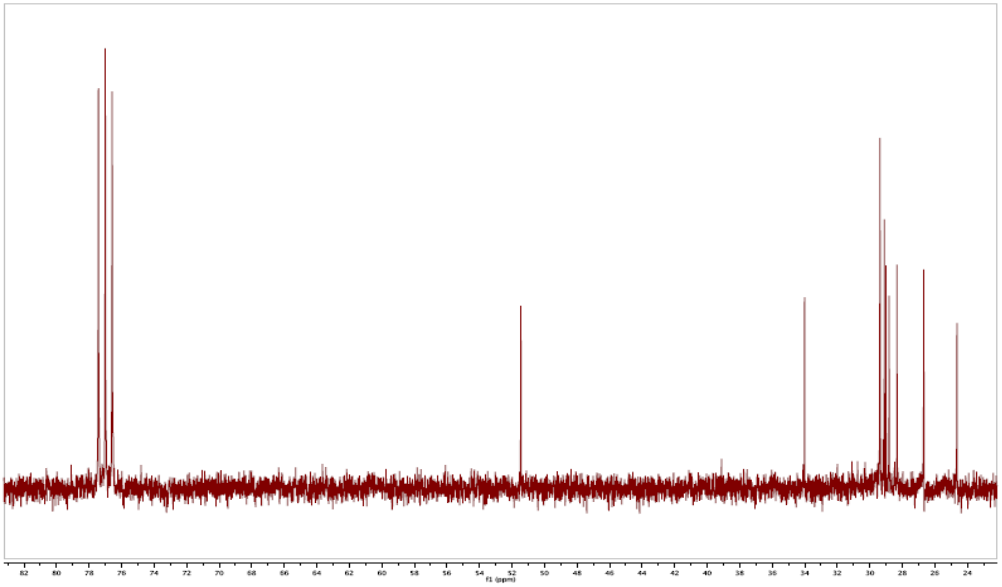

Figure 2.37b. ^{13}C NMR spectrum of 10-azidodecane-1-thiol.

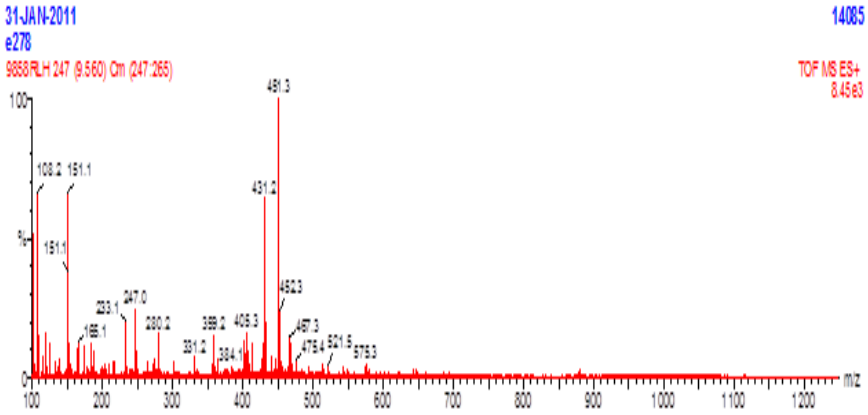

Figure 2.37c. Mass spectrum of 10-azidodecane-1-thiol.

2.6 References

1. Halterman, R. L.; Singh, A.; Dahanayaka, D. H.; Biswas, A.; Bumm, L. A. Molecularly Ordered Decanethiolate Self-Assembled Monolayers on Au(111) from in Situ Cleaved Decanethioacetate: An NMR and STM Study of the Efficacy of Reagents for Thioacetate Cleavage *Langmuir* **2010,** *26*, 13221.

2. Love, J. C.; Estroff, L. A.; Kriebel, J. K.; Nuzzo, R. G.; Whitesides, G. M. Self-assembled monolayers of thiolates on metals as a form of nanotechnology.*Chem. Rev.* **2005,** 105, 1103-1169**.**

3. Vericat, C.; Vela, M. E.; Salvarezza, R. C. Self-assembled monolayers of alkanethiols on Au(111): surface structures, defects and dynamics *Phys. Chem. Chem. Phys.* **2005,** 3258-3268.

4. Ulman, A. An Introduction to Ultrathin Organic Films: from Langmuir-Blodgett to Self-assembly, Academic Press, San Diego, CA, 1991.

5. Nuzzo, R. G.; Allara, D. L. Adsorption of bifunctional organic disulfides on gold surfaces *J. Am. Chem. Soc.* **1983,** *105*, 4481-4483.

6. Sagiv, J. Organized monolayers by adsorption. 1. Formation and structure of oleophobic mixed monolayers on solid surfaces *J. Am. Chem. Soc.* **1980,** *102*, 92-98.

7. Dreesen, L.; Volcke, C.; Sartenaer, Y.; Peremans, A. ; Thirty, P.A.; Humbert, C.; Grugier, J.; Marchand –Brynaert, J. Comparative study of decyl thiocyanate and decanethiol self-assembled monolayers on gold substrates *Surf. Sci.* **2006,** *600*, 4052-4057.

8. Singhvi, R.; Kumar, A.; Lopez, Z. P.; Stephanopolous, G.N.; Wang, D. I.; Whitesides, G. M.; Ingber, D. E. Engineering cell shape and function. *Science* **1994,** *264*, 696-698.

9. Wirth, M. J.; Fairbank, R.W.; Fatunmbi, H. O. Mixed Self-Assembled Monolayers in Chemical Separations *Science* **1997,** *275*, 44-47.

10. Laibnis, P. E.; Whitesides, G. M. Self-assembled monolayers of *n*-alkanethiolates on copper are barrier films that protect the metal against oxidation by air *J. Am. Chem. Soc.* **1992,** *114*, 9022-9028.

11. Prime, K.L.; Whitesides, G.M. Self-assembled organic monolayers: model systems for studying adsorption of proteins at surfaces *Science* **1991,** *252*, 1164-1167.

12. Dreesen, L.; Sartenaer, Y.; Humbert, C.; Mani, A. A.; Lemaire, J.-J; Méthivier, C.; Pradier, C.-M.; Thiry, P.A.; Peremans A. *Thin Solid Films* **2004,** *373*, 464.

13. Schreiber, F. Structure and growth of self-assembling Monolayers *Prog. Surf. Sci.* **2000**, *65*, 151-256.

14. Porter, M. D.; Bright, T. B.; Allara, D. L.; Chidsey, C. E. D. Spontaneously organized molecular assemblies. 4. Structural characterization of n-alkyl thiol monolayers on gold by optical ellipsometry, infrared spectroscopy, and electrochemistry *J. Am. Chem. Soc*. **1987**, *109*, 3559-3568.

15. Love, J. C.; Wolfe, D. B.; Haasch, R.; Chabinyc, M. L.; Paul, K. E.; Whitesides, G. M.; Nuzzo, R. G**.** Formation and Structure of Self-Assembled Monolayers of Alkanethiolates on Palladium *J. Am. Chem. Soc.* **2003**, *125*, 2597-2609.

16. Tour, J. M.; Jones, L.; Pearson, D. L.; Lamba, J. J. S.; Burgin, T. P.; Whitesides, G. M.; Allara, D. L.; Parikh, A. N.; Atre, S. Self-Assembled Monolayers and Multilayers of Conjugated Thiols, α,ω-Dithiols, and Thioacetyl-Containing Adsorbates. Understanding Attachments between Potential Molecular Wires and Gold Surfaces *J. Am. Chem. Soc.* **1995,** *117*, 9529-9534.
17. Ciszek, J.W.; Stewart, M. P.; Tour, J. M. *J. Am. Chem. Soc.* **2004**, *20*, 9144.

18. Inman, C. E.; Reed, S. M.; Hutchison, J. E. In Situ Deprotection and Assembly of S-Trityl Alkanethiols on Gold Yields Monolayers Comparable to Those Prepared Directly from Alkanethiols *Langmuir* **2004**, *20*, 9144-9150.

19. (a) Stapleton, J. J.; Harder, P.;Daniel , T.A.; Reinard, M. D.; Yao, Y.; Price, D. W.;Tour, J.M.; Allara, D. L. Self-Assembled Oligo(phenylene-ethynylene) Molecular Electronic Switch Monolayers on Gold: Structures and Chemical Stability. *Langmuir* **2003**, *19,* 8245-8255. (b) Cai, L.; Yao, Y.; Yang, J.; Price, D. W.; Tour, J. M. Chemical and Potential-Assisted Assembly of Thiolacetyl-Terminated Oligo(phenylene ethynylene)s on Gold Surfaces *Chem. Mater.* **2002**, *14*, 2905-2909. (c) Holmes, B. T.; Snow, A. W. Aliphatic thioacetate deprotection using catalytic tetrabutylammonium cyanide. *Tetrahedron* **2005**, *61*, 12339-12342. (d) Lau, K. H. A.; Huang, C.; Yakovlev, N.; Chen, Z. K.; O'Shea, S. J. Direct adsorption and monolayer self-assembly of acetyl-protected dithiols *Langmuir* **2006,** *22,* 2968-2971.

20. Shaporenko, A.; Elbing, M.; Blaszczyk, A.; von Hanisch, C.; Mayor, M.; Zharnikov, M. Self-Assembled Monolayers from Biphenyldithiol Derivatives: Optimization of the Deprotection Procedure and Effect of the Molecular Conformation *J. Phys. Chem. B* **2006,** *110*, 4307-4317.

21. Cheng, L.; Yang, J.; Yao, Y.; Price, D. W.; Dirk, S. M.; Tour, J. M. Comparative Study of Electrochemically Directed Assembly versus Conventional Self-Assembly of Thioacetyl-Terminated Oligo(phenylene ethynylene)s on Gold and Platinum Surfaces. *Langmui*r **2004,** *20,* 1335-1341.

22. Niklewski, A.; Azzam, W.; Strunskus, T.; Fischer, R. A.; Woll, C. Fabrication of self-assembled monolayers exhibiting a thiol-terminated surface *Langmuir* **2004,** *20,* 8620-8624.

23. Nakashima, H.; Furukawa, K.; Ajito, K.; Kashimura, Y.; Torimitsu, K. Selective Chemisorption of End-Functionalized Conjugated Polymer on Macro- and Nanoscale Surfaces. *Langmuir* **2005***, 21*, 511-515.

24. Bethencourt, M. I.; Srisombat, L.-O.; Chinwangso, P.; Lee, T. R. SAMs on Gold Derived from the Direct Adsorption of Alkanethioacetates Are Inferior to Those Derived from the Direct Adsorption of Alkanethiols. *Langmuir* **2009,** *25,* 1265-1271.

25. Kang, Y.; Won, D.-J.; Kim, S. R.; Seo, K.; Choi, H.-S.; Lee, G.; Noh, Z.; Lee, T. S.; Lee, C. Self-assembled monolayer of the aromatic thioacetate on the gold surface *Mater. Sci. Eng. C* **2004,** *24*, 43-46.

26. Smith, R. K.; Lewis, P. A. ; Weiss, P. S. Patterning self-assembled monolayers. *Prog. Surf. Sci*. **2004**, *75*, 1–68.

27. (a) Ruckenstein, E.; Li, Z. F. Surface modification and functionalization through the self-assembled monolayer and graft polymerization. *Adv. Colloid Interface Sci.* **2005**, *113*, 43–63. (b) Chaki, N. K.; Vijayamohanan, K. Self-assembled monolayers as a tunable platform for biosensor applications *Biosens. Bioelectron.* **2002,** *17*, 1–12. (c) Parikh, A. N.; Allara, D. L. ; Azouz, I. B. ; Rondelez, F. An Intrinsic Relationship between Molecular Structure in Self-Assembled n-Alkylsiloxane Monolayers and Deposition Temperature *J. Phys. Chem.* **1994**, *98*, 7577–7590. (d) Aswal, D. K. ; Lenfant, S. ; Guerin, D. ; Yakhmi, J. V. ; Vuillaume, D. Self assembled monolayers on silicon for molecular electronics. *Anal. Chim. Acta* **2006**, *568,* 84–108. (e) Pignataro, B.; Licciardello, A.; Cataldo, S. ; Marletta, G. SPM and TOF-SIMS investigation of the physical and chemical modification induced by tip writing of self-assembled monolayers *Mater. Sci. Eng. C* **2003,** *23*, 7–12. (f) Morgenthaler, S.; Zink, C.; Spencer, N. D. Surface-chemical and -morphological gradients *Soft Matter.* **2008,** *4*, 419–434.

28. (a) Jordan, C. E.; Frey, B. L.; Kornguth, S.; Corn, R. M. Characterization of Poly-L-lysine Adsorption onto Alkanethiol-Modified Gold Surfaces with Polarization-Modulation Fourier Transform Infrared Spectroscopy and Surface

Plasmon ResonanceMeasurements *Langmuir* **1994**, *10*, 3642-3648. (b) Frey, B. L.; Corn, R. M. *Anal. Chem.* **1996,** *68*, 3187-3193.

29. Houseman, T. B.; Gawalt, E. S.; Mrksich, M. Maleimide-Functionalized Self-Assembled Monolayers for the Preparation of Peptide and Carbohydrate Biochips *Langmuir* **200**3**,** 19, 1522-1531**.**

30. (a)Willner, I.; Katz, E.; Riklin, A.; Kasher, L. Mediated electron transfer in gluthathione reductase organized in self-assembled monolayers on gold electrodes *J. Am. Chem. Soc.* **1992**, 114, 10965-10966. (b) Leggett, G. J.; Roberts, C. J.; Williams, P. M.; Davies, M. C.; Jackson, D. E.;Tendler, S. J. B. Approaches to the immobilization of proteins at surfaces for analysis by scanning tunneling microscopy *Langmuir* **1993**, 9, 2356-2362. (c) McNeil, C. J.; Athey, D.; Ho, W. O. Direct electron transfer bioelectronic interfaces: application to clinical analysis. *Biosens. Bioelectron.* **1995**, 10, 75-83. (d) Duan, C.; Meyerhoff, M. E. Separation-Free Sandwich Enzyme Immunoassays Using Microporous Gold Electrodes and Self-Assembled Monolayer/Immobilized Capture Antibodies *Anal. Chem.* **199**4, 66, 1369-1377.

31. Collman, J. P.; Devaraj, N. K.; Chidsey, C. E. D. "Clicking" Functionality onto Electrode Surfaces *Langmuir* **2004**, *20*, 1051-1053.

32. (a) Rostovtsev, V. V.; Green, L. G.; Fokin, V. V.; Sharpless, K. B. A Stepwise Huisgen Cycloaddition Process: Copper(I)-Catalyzed Regioselective "Ligation" of Azides and Terminal Alkyne. *Angew. Chem.* **2002**, *114*, 2708-2711. (b) Rostovtsev, V. V.; Green, L. G.; Fokin, V. V.; Sharpless, K. B. A Stepwise Huisgen Cycloaddition Process: Copper(I)-Catalyzed Regioselective Ligation of Azides and Terminal Alkynes. *Angew. Chem., Int. Ed.* **2002**, *41*, 2596-2599.

33. Evans, R. M.; Owen, L. N. Dithiols. Part II. 2 : 3-Dimercaptopropyl ethers of glycerol and of glycollic acid, with some further observations on "BAL-Intrav."*J. Chem. Soc.* **1949,** 244-248**.**

34. Bumm, L. A.; Arnold, J. J.; Charles, L. F.; Dunbar, T. D.; Allara, D. L.; Weiss, P. S. Directed Self-Assembly to Create Molecular Terraces with Molecularly Sharp Boundaries in Organic Monolayers *J. Am. Chem. Soc*. **1999**, *121*, 8017-8021.
35. Badin, M. G.; Bashir, A.; Krakert, S.; Strunskus, T.; Terfort, A.; Wöll, C. Kinetically stable, flat-lying thiolate monolayers *Angew. Chem., Int. Ed.* **2007**, *46*, 3762-3764.

36. Bruice, T. C.; Fedor, L. R. The Kinetic Demonstration of a Metastable Intermediate in a Nucleophilic Displacement at a Thiol-Ester Bond. *J. Am. Chem. Soc.* **1964**, *86*, 738.

37. Gregory, M. J.; Bruice, T. C. Nucleophilic Displacement Reactions at the Thiol Ester Bond. V. Reactions of 2,2,2- Trifluoroethyl Thiolacetate. *J. Am. Chem. Soc*. **1967**, *89*, 2121.

38. Turkevich, J.; Stevenson, P. C.; Hillier, J. A study of the nucleation and growth processes in the synthesis of colloidal gold. *Discuss. Faraday Soc.* **1951,** *11*, 55-75.

39. Humphrey, R. E.; Potter, J. L**.** Reduction of disulfides with tributylphosphine *Anal. Chem***. 1965,** 37, 164-165.

40. Wrochem, F. v.; Scholz, F.; Schreiber, A.; Nothofer, H.-G.; Ford, W. E.; Morf, P.; Jung, T.; Yasuda, A.; Wessels, J. M. Structure and Conductance of Aromatic and Aliphatic Dithioacetamide Monolayers on Au(111) *Langmuir* **2008,** *24*, 6910-6917.

41. Weare, W. W.; Reed, S. M.; Warner, M. G.; Hutchison, J. E. Improved synthesis of small (dCORE ≈ 1.5 nm) phosphine-stabilized gold nanoparticles. *J. Am. Chem. Soc.* **2000**, *122*, 12890-12891.

42. Kolb, H. C.; Finn, M. G.; Sharpless, K. B. Click Chemistry: Diverse Chemical Function from a Few Good Reactions. *Angew. Chem., Int. Ed.* **2001,** *40*, 2004–2021.

Chapter III: Synthesis of Various Ligand for Capping Gold Nanoparticles and Thioacetate Tethered Fluorescent Dyes to Attach with Gold Nanoparticles Surface

3.1 Chapter Overview

This chapter presents the synthesis of different ligands for coating the gold nanoparticles. Derivatization of different cationic and neutral fluorophores is described so as to incorporate these on gold nanoparticles. The main aim of this work was to achieve brighter fluorophore due to metal-enhanced fluorescence by keeping the fluorophore at hot spot on the gold nanoparticles. Thus preliminary study of optical properties of fluorophore on gold surface was crucial. In addition, information on place exchange of ligands on gold surface was required for providing more stable gold nanoparticles which could be compatible in different solvent system.

3.2 Introduction

Use of organic fluorophore in several areas such as electronic devices,[1] molecular sensors, labeling biomolecules[2] for cell imaging makes them more invaluable. Their continuous growth is due to their versatility, sensitivity and quantitative capabilities. Unfortunately these properties are also coupled with undesirable aggregation, poor photostability, fluorescence blinking and photobleaching, and surface adsorption.[3,4] A number approaches has been

attempted to improve the these issues such as protecting the fluorophore in inorganic matrix, such as zeolite,[5] silica,[6] supramolecular encapsulation.[7]

Nau and coworkers reported the enhancement of brightness and fluorescence lifetimes because of reduction of non-specific adsorption and aggregation when cucurbit[7]uril (abbreviated as CB7) was added to aqueous solutions of rhodamine 6G.[8] Consistent to Nau's finding our group also observed the two fold fluorescent enhancement of tethered rhodamine B dyad upon encapsulating in CB7 due to the unique solvation properties of the cucurbiturils nonpolarizing interior[9], however, for the construction of biological probes and light harvesting devices a bright long-lived fluorescence probes are required. The brightness of fluorophore could be enhanced by keeping it closer to metal nanoparticles such as silver and gold.

3.2.1. Metal-Fluorophore Interactions

When a fluorophore is kept proximate to the metal nanoparticles its spectral properties change distinctly due to the interactions of the surface plasmon resonance of the metal.[10] These interactions are highly dependent on distance between the metal surface and the fluorophore. Fluorophore placed within 5 nm from the metal surface exhibit quenching because of efficient electron transfer or energy transfer from excited fluorophore to metal (Figure 3.1).[11] Quenching could also results from the intermolecular interactions of fluorohpores if fluorophores are tightly packed on the surface, however, dramatic fluorescence enhancement of

fluorophore could be achieved on placing the fluorophores away from quenching region (farther than 5 nm) of metal surface.[12]

3.2.2 Gold Nanoparticles

Noble metal particles in the nanometer size scale show unique size dependent optical, electronic and chemical properties.[13] Gold nanoparticles have gained much attention because of their high extinction coefficient and a broad absorption spectrum in the visible region that overlaps with the emission wavelength of usual energy donors. Additionally, gold nanoparticles are stable under atmospheric conditions and their surface can be functionalized by using ligand having suitable functionality.[14] More often ligands having functional groups, such as thiols, amines, or silanes are exploited to attach electroactive or photoactive molecules, dyes, to the gold surface.[15]

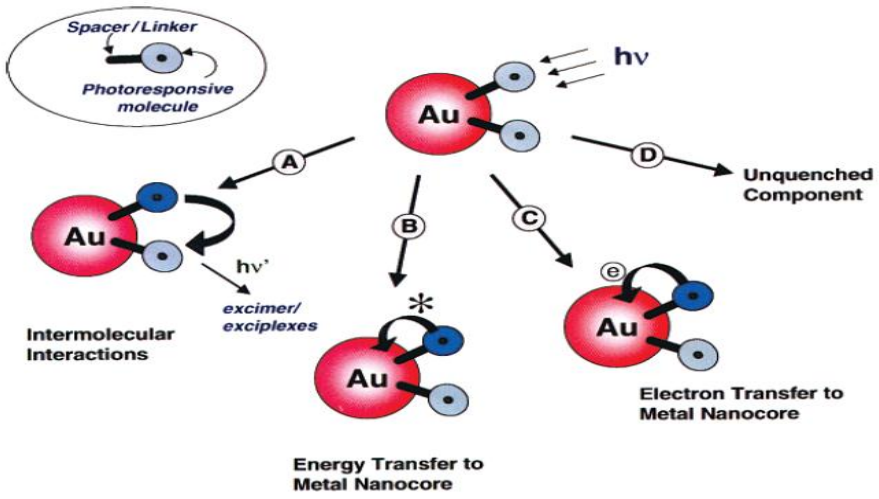

Figure 3.1. Excited-state deactivation processes in fluorophore-metal nanohybrids. Reprinted from reference 10.

Highly fluorescent probes have been reported by the conjugation of rhodamine with gold nanoparticles.[16] *p*-Mercaptophenol, gold has high affinity for

thiol, on gold surface was utilized to immobilize rhodamine by the reaction of hydroxy group of *p*-mercaptophenol and sulfonyl chloride of rhodamine. The immobilization of organic fluorophore can also be achieved after the derivatization of fluorophore with a thiol functionality. Due to reactivity of thiol, acetylprotected thiol fluorophore is better as acetylprotected thiol can be cleaved in situ to provide parent thiol to attach the fluorophore on gold surface. This is a well established method to achieve well-ordered monolayer on gold surface.[17]

3.3 Results and Discussion

Cationic fluorescent dyes, rosamine and malachite green, and neutral dye bodipy were tethered with acetyl protected decanethiol chain. Several ligands possessing acetyl protected thiol functionality were synthesized. Thioacetate readily hydrolyzes to provide parent thiol in the presence of acid or base. Additionally, thiols have high affinity to gold surface and KOH cleaved acetyl protected thiol results well-ordered monolayer on gold surface. These ligands and fluorophore were modified with acetyl protected thiol functionality. Synthesized compounds were characterized by NMR spectroscopy.

Following the literature precedent,[18] 10- thioacetyldecyltriethylene glycol 2 was synthesized by following the scheme 3.1. First mononucleophilic substitution on 1,10-dibromodecane was performed by using triethyleneglycol in the presence sodium hydride base in dimethyl formaldehyde (DMF) solvent. Compound **1** was isolated from the crude through silica chromatography by using 20-50% ethyl

acetate/ hexane eluent. This ligand was synthesized to cap the gold nanoparticles for better stability and compatibility of nanoparticles in water as it possesses hydrophilic glycol.

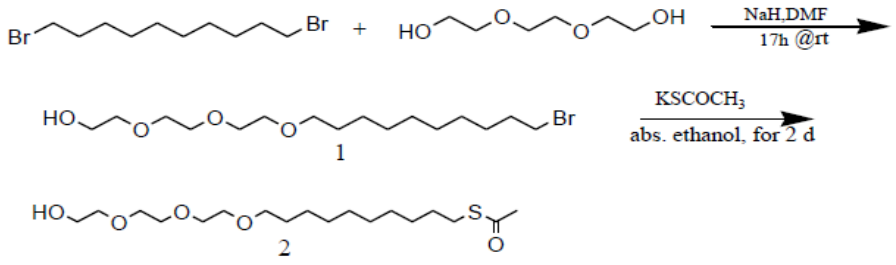

Scheme 3.1. Synthetic routes for the synthesis of 10- thioacetyldecyltriethylene glycol **2**.

Bodipy dye was synthesized by following the literature procedure.[19] As shown in scheme 3.2 first pyrole was reacted with 10-bromodecanoyl chloride to obtain bromo bodipyC9. This compound was isolated by column chromatography using petroleum ether : methylene chloride (v/v 4/1) as an eluent. Finally nucleophilic substitution of bromine with potassium thiacetate provided bodipyC9thioacetate. This compound was isolated as an orange solid by column chromatography using petroleum ether : methylene chloride (v/v 4/1) as an eluent. Bodipy is a neutral dye with an absorbance and fluorescence emission maximum at 521 nm and 530 nm (Figure 3.4) respectively. The gold nanoparticles were synthesized and all the measurements with nanoparticles were carried out by Kalani Gunawardana. Monodisperse gold nanoparticles were synthesized by reducing

$HAuCl_4$ with trisodium citrate in boiling water.[20] Thus synthesized gold nanoparticles were found to be 13 nm in size by transmission electron microscopy (TEM) measurements. These gold nanoparticles were coated with negatively charged citrate so as to stabilize gold nanoparticles in water, preventing aggregation. Gold nanoparticles suspended solution is known as sol.

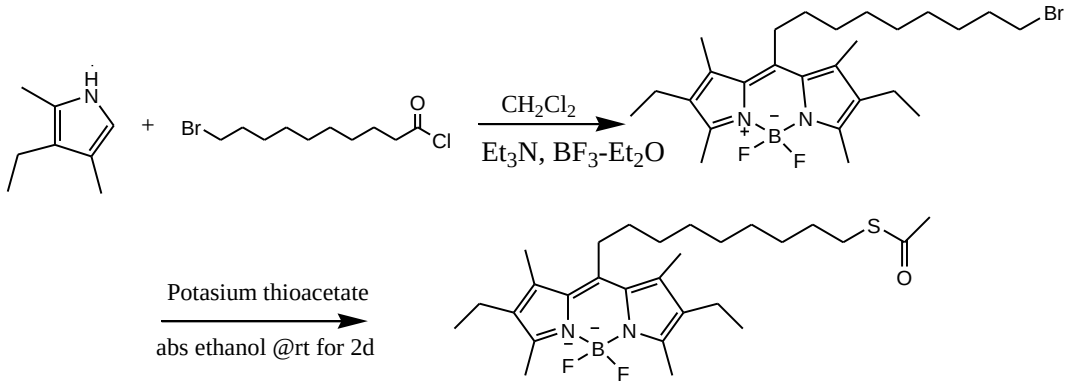

Scheme 3.2. Synthetic routes for the synthesis bodipyC9SAc.

Bodipydecylthioacetate was precleaved with KOH before exposing to gold nanparticles for 30 minutes. Loosely bound citrate was successfully displaced by thiolate of decylbodipy on gold surface. Poor solubility of bodipy in water resulted aggregation in the mixture of sol and dye therefore 95% ethanol was used as a solvent. However after few hours aggregation was observed in sol/dye mixture. Therefore, to further improve the stability of mixture and prevent aggregation a competing deprotonated ligand, 11-mercaptoundecanioc acid, was exploited. Introduction of this ligand was beneficial for regaining the stability of sol/dye

mixture as well as successfully attaching neutral dye to AuNP surface.

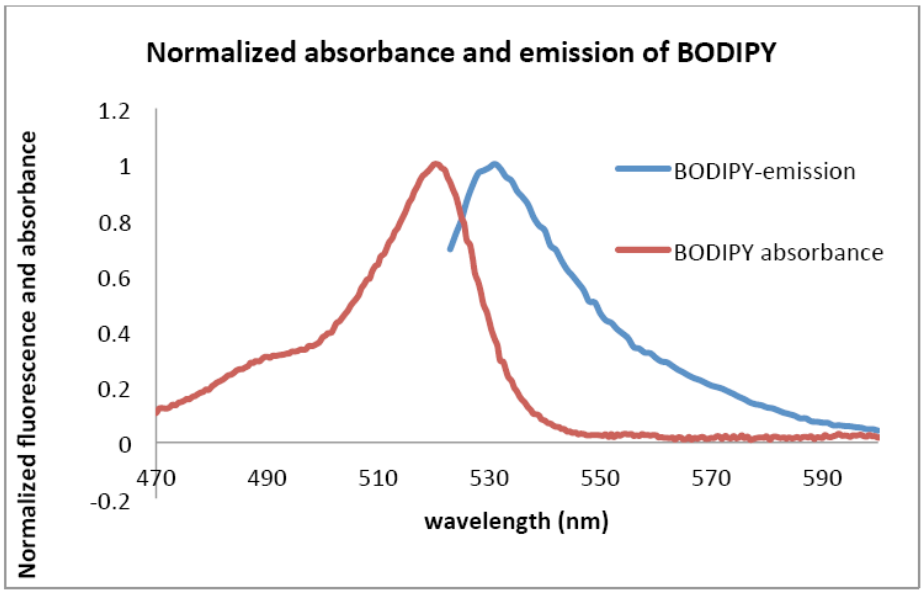

Figure 3.4. Normalized absorbance and emission of Bodipy decylthioacetate. Courtesy of Dr. Kalani Gunawardana.

Spectral properties of dye loaded on gold surface were studied in the presence of 11- mercaptoundecanoic acid as a competing ligand. As expected, emission of fluorophore was quenched as it is in quenching region. Also, there was no distinct shift in fluorescence emission maxima of dye on gold surface. We were interested in studying the molar fluorescence of dye on gold surface. Molar fluorescence of dye remains constant in same solvent system at low concentration. However we found continuous decrease in molar fluorescence (Figure 3.5) on increasing the concentration dye on gold surface. If gold was the only factor for quenching, the molar fluorescence would remain constant. The decrease in molar

fluorescence could be due to dye-dye intermolecular interaction, resulted quenching at higher dye loading on gold nanoparticles surface.

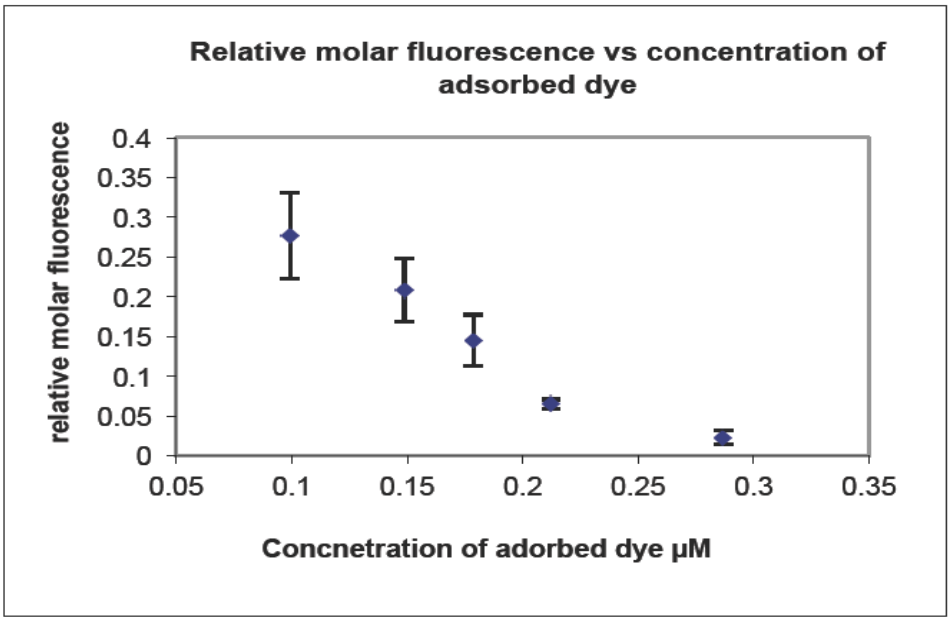

Figure 3.5. Variation of relative molar fluorescence of the absorbed dye against the concentration of the dye absorbed dye on AuNP surface (0.1-0.3 µM). Adapted from Kalani Gunawardana's thesis.

Furthermore, bodipy decylthioacetate was utilized to investigate the place exchange by 11- mercaptoundecanioc acid. For this study, gold nanoparticles were precoated with bodipy followed by the introduction of 11- mercaptoundecanioc acid. 11-mercaptoundecanoic acid was able to exchange bodipy rapidly at higher concentration and slowly at lower concentration.

After investigating the place exchange of bodipy by negatively charged mercaptodecanoic acid, neutral ligand, thiol tethered diethyleneglycol **2** was used

for place exchange study. Additionally, use of ligand **2** in the case of rosamine[21] or malachite green[22] could cause aggregation due to electrostatic interaction between cations of dye and anions of ligands. Therefore, we synthesized 10-thioacetyldecyl diethylene glycol ether **4** by following scheme 3.3. Monosubstitution on 1, 10-dibromodecane with diethylene glycol ether followed by nucleophilic substitution by potassium thioacetate provided acetyl protected decyl diethylene glycol ether **4** (ether ligand). Pure compound **4** was obtained through silica gel column chromatography by using 20-40% ethyl acetate and hexane solvent system.

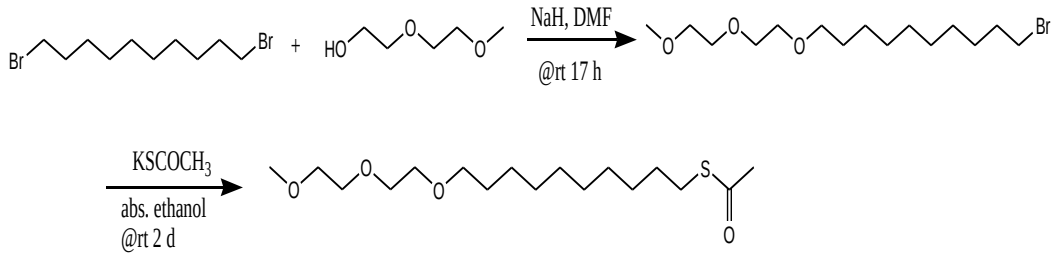

Scheme 3.3. Synthetic routes for the synthesis of S-10-[2-(2 methoxyethoxy)ethoxy] decyl ethanethioate, **4**.

This ligand was also able to exchange bodipy dye. Experiments for place exchange study of thiols by disulfide were also performed. Compound, 11-(2-(11-aminoundecyl)disulfanyl)undecan-1-amine **5** (diaminoun decyl disulfide) was synthesized by following Scheme 3.4. Ether capped gold nanoparticles were exposed with diamino decyl disulfide ligand. Aggregation occurred at higher concentration of diamino decyl disulfide due to high affinity of gold for amine.

However, ammonium decyl disulfide was successfully and rapidly replaced ether on controlling the concentration of amine disulfide ligand.[23]

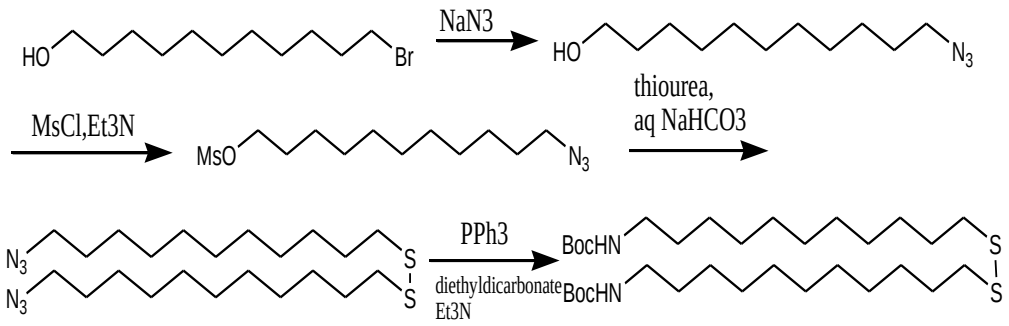

Scheme 3.4. Synthetic routes for the synthesis amineundecanedisulfide.

3.4 Chapter Summary

In this chapter we have successfully synthesized several neutral and cationic dyes and derivatized with decylthioacetate functionality. We were able to attach bodipy dye on gold surface. Additionally, variation of the molar fluorescence of bodipy on gold surface was investigated. Several ligands were synthesized and investigated place exchange of thiol tethered bodipy with those ligands as well as 11- mercaptoundecanioc acid. This effort was crucial for the development of metal enhanced fluorescence probes.

3.5 Experimental

General Procedure. All the reactions were performed under nitrogen atmosphere in a Schlenk-line apparatus unless specified otherwise. *N,N*-dimethylaniline, formylbenzoic acid, dimethylaminopyridine, 1,10-decanediol, 10-bromodecanoic acid, thionyl chloride, 3-ethyl 2,4-dimethylpyrrole, borontrifluoridediethyletherate and potassium thioacetate were purchased from Sigma-Aldrich Co. Triehylamine was purchased from Fisher Scientific Co. The NMR spectra were recorded on Varian Unity 300 MHz or 400 MHz instrument.

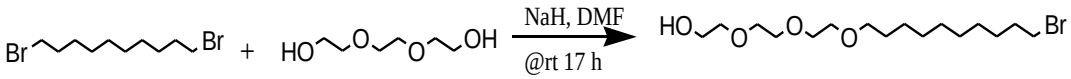

Synthesis of HO $(CH_2CH_2O)_3(CH_2)_{10}Br$; (10-bromodecyl) triethylene glycol.[24] To a solution of tri(ethylene glycol) (2.8 g, 18.48 mmol) in 50 mL of DMF, NaH (132 mg, 3.3 mmol) dispersed in mineral oil (60%) was added portion by portion. After stirring the mixture for 70 min., 1,10-dibromodecane (1 g, 3.3 mmol) was added. The mixture was stirred for 17 h @ rt. The mixture was diluted with 50 mL of water and 40 mL of diethyl ether and stirred for 15 min. The ether layer was separated and the aqueous portion was extracted with (4 x 20 mL) of diethyl ether. The organic portion was washed with water and dried over anhydrous sodium sulfate then concentrated. The crude product was purified on silica gel column with 20-50% ethyl acetate/ hexane solvent system. The desired fractions were cooled and concentrated to get the title product (223 mg, 18%) as an oily colorless liquid. ^{1}H NMR (400 MHz, $CDCl_3$): δ 3.57–3.76 (m, 12H), 3.45 (t, 2H, J = 7.2

Hz), 3.41 (t, 2 H, *J* = 7.2 Hz,), 2.5 (t, 1 H, *J* = 6 Hz) 1.84 (m, 2 H), 1.6 (m, 2 H), 1.24-1.46 (m, 12H).

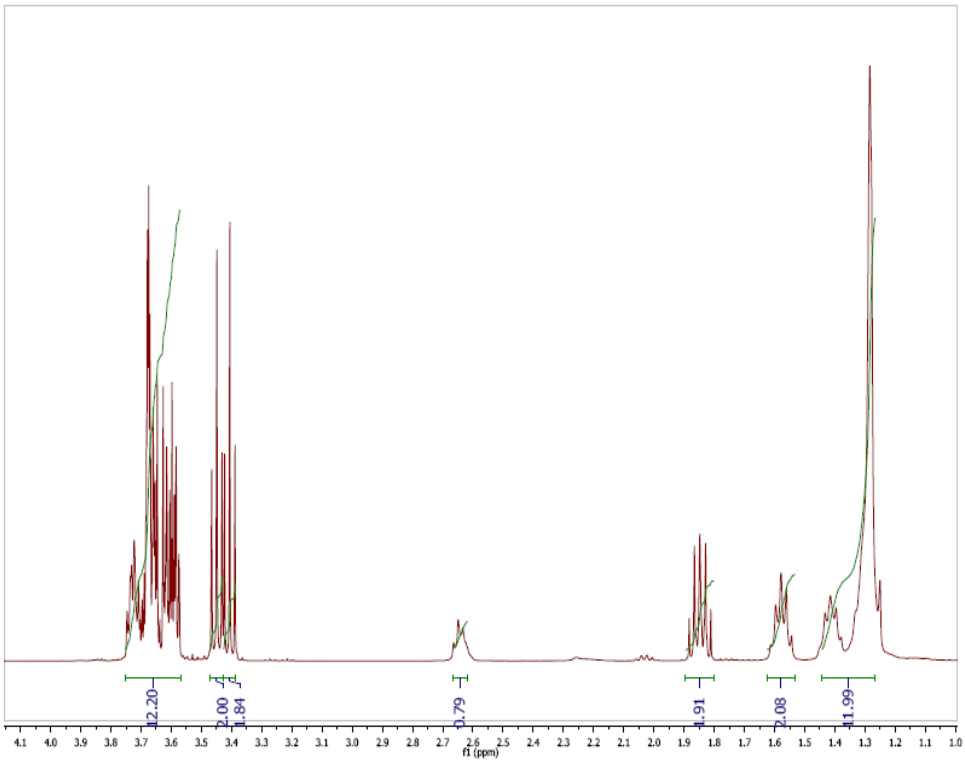

Figure 3.8. ^{1}H NMR of (**10-bromodecyl) triethylene glycol.**.

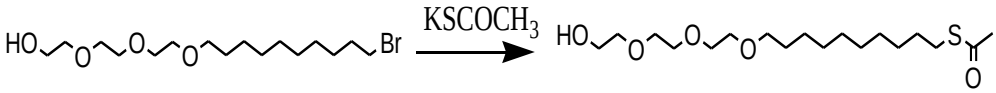

Synthesis of $OH(CH_2CH_2O)_3(CH_2)_{10}SCOCH_3$; (10–thioacetyldecyl) triethylene glycol). To a 100 mL reaction flask, 10-bromodecyltriethylene glycol (223 mg, 0.603 mmol), potassium thioacetate (138 mg, 1.206 mmol) and 15 mL of abs. ethanol were taken and stirred for 2 d @ rt. The ethanol was removed by

rotary evaporation. Then 15 mL of ice cold water was added to the reaction flask and stirred for 10 min. After that 10 mL of diethyl ether was added and stirred for 5 min. The organic portion was separated and two more times organic portion was extracted from aqueous portion. The organic portions were combined and washed with water three times and organic portion was dried over magnesium sulfate. The organic portion was concentrated and crude was purified on silica gel column with 30-70% ethyl acetate and hexane solvent system. The required fractions were cooled and concentrated to afford the product (105 mg, 48%) as a colorless oily liquid. ^{1}H NMR (400 MHz, $CDCl_3$): δ 3.57-3.75 (m, 12H), 3.45 (t, 2H , *J* = 7.2 Hz), 2.86 (t, 2H , *J* = 7.2 Hz), 2.58 (b, 1H), 2.32 (s, 3H), 1.5-1.6 (m, 4H), 1.2-1.4 (m, 12H).

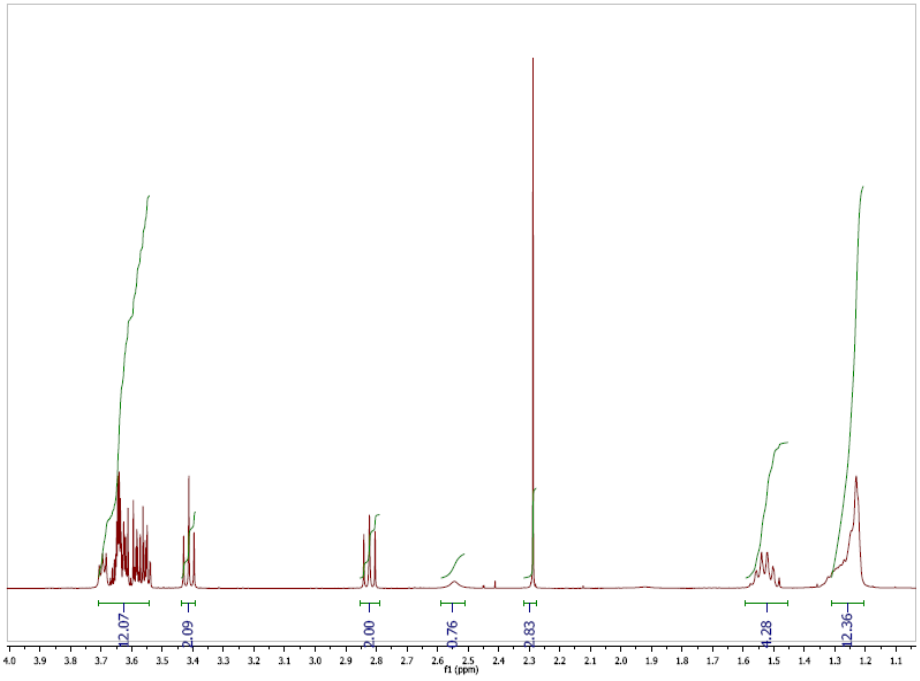

Figure 3.9. ^{1}H NMR of **(10 –thioacetyldecyl) triethylene glycol), 2.**

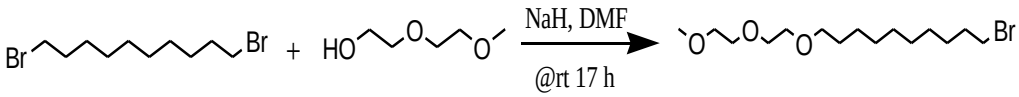

Synthesis of $OCH_3(CH_2CH_2O)_2(CH_2)_{10}Br$; (10-bromodecyl) diethylene glycolmonomethyl ether.[24] To a solution of diethylene glycolmonomethyl ether (1g, 8.3 mmol) in 50 mL of DMF, NaH (432 mg, 10.7 mmol) dispersed in mineral oil (60%) was added portion by portion. The mixture was stirred for 30 min. and then 1,10-dibromodecane was added. The reaction mixture was stirred for 17 min @ rt. After addition of 20 mL of water, the solution was extracted with (4 x 20 mL) of diethyl ether and the organic phases were combined. Combined organic portion was washed with 20 mL of water for three times and dried over magnesium sulfate. The organic portion was concentrated and the crude product was purified on silica gel by using 5-45% ethyl acetate and petroleum ether. The needed fractions were concentrated to obtain the expected product (600mg, 21%) as a colorless liquid. ^{1}H NMR (400 MHz, $CDCl_3$): δ 3.62-3.65 (m, 4H), 3.53-3.59 (m, 4H), 3.42 (t, J = 6.8 Hz, 2H), 3.38 (t, J = 6.8 Hz, 2H), 3.36 (s, 3H), 1.83 (m, 2H), 1.56 (m, 2H), 1.4 (m, 2H), 1.26 (m, 10H); ^{13}C NMR (100 MHz, $CDCl_3$): δ 71.89, 71.38, 70.61, 70.48, 70.00, 58.89, 33.97, 32.77, 29.56, 29.41, 29.37, 29.32, 28.70, 28.10, 26.01.

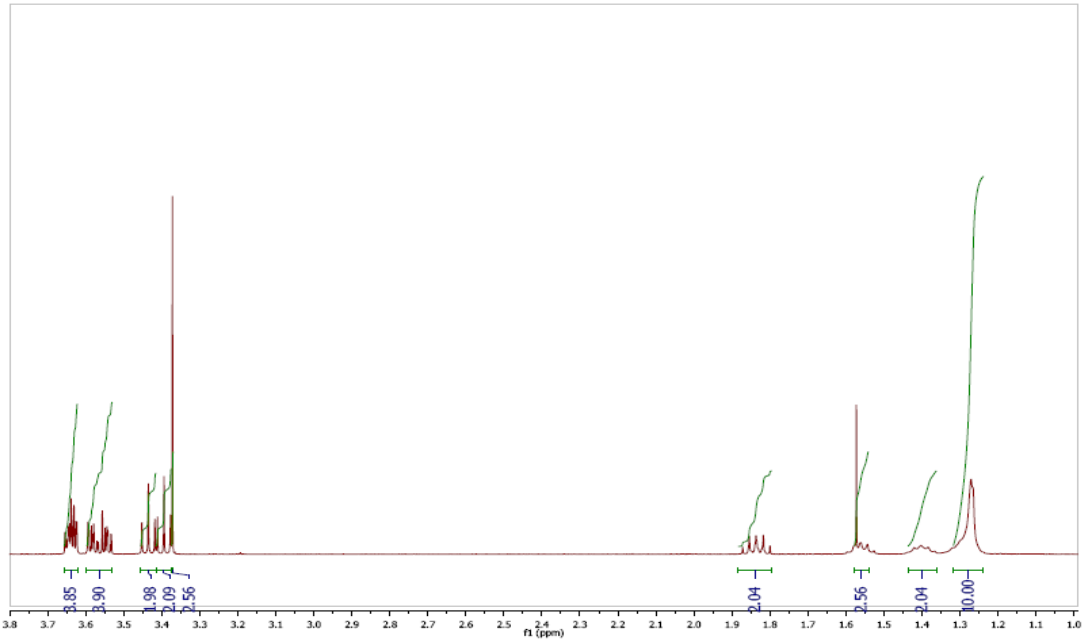

Figure 3.10a. ^{1}H NMR of **(10-bromodecyl) diethylene glycolmonomethyl ether.**

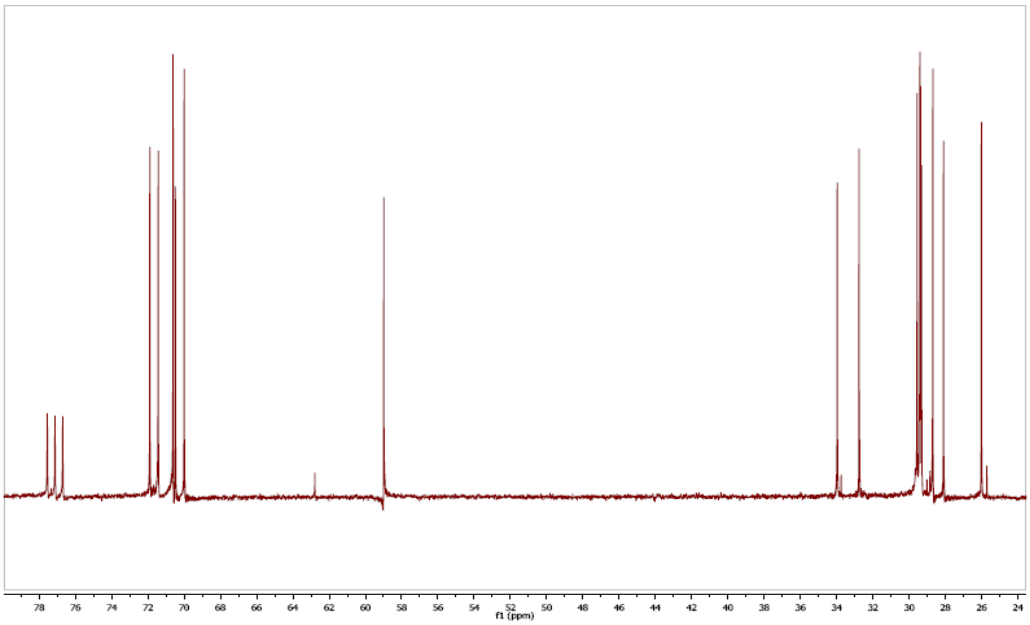

Figure 3.10b. ^{13}C NMR of (**10-bromodecyl) diethylene glycolmonomethyl ether.**

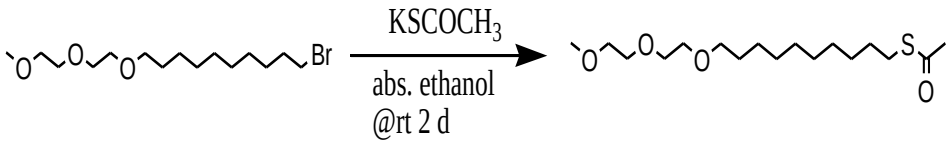

Synthesis of $OCH_3(CH_2CH_2O)_2(CH_2)_{10}SCOCH_3$; (10–thioacetyldecyl) diethylene glycolmonomethyl ether. (10-bromodecyl) diethylene glycolmonomethyl ether (600 mg, 1.77 mmol), potassium thioacetate (404 mg, 3.54 mmol) and 25 mL of abs. ethanol were taken in a 100 mL reaction flask and stirred for 2 days @rt. The abs. ethanol was removed via rotary evaporation and 20 mL of ice cold water was added to the residue and stirred for 10 min. After that 20 mL of diethyl ether was added and stirred for the next 5 min. The organic phase was separated and again ether was used to extract two more times (2x20 mL) from the aqueous portion. The organic phases were combined and washed with water (3x20 mL) and dried over anhydrous magnesium sulfate. The organic phase was concentrated and the crude product was purified on silica gel column by using 20-40% ethyl acetate and hexane solvent system. The required fractions were concentrated to get the desired product (378 mg, 64%). ^{1}H NMR (400 MHz, $CDCl_3$): δ 3.52-3.65 (m, 8H), 3.42 (t, *J* = 7.2 Hz, 2H), 3.35 (s, 3H), 2.83 (t, *J* = 8 Hz), 2.29 (s, 3 H), 1.5 (m, 4 H), 1.2 (m, 12 H). ; ^{13}C NMR (75 MHz, $CDCl_3$): δ 195.92, 71.88, 71.43, 70.58, 70.46, 69.97, 58.95, 30.57, 29.53, 29.42, 29.36, 29.32, 29.04, 28.72, 25.99. MS (ESI) $[M+Na]^+$ calcd for $C_{17}H_{34}O_4SNa$ 357.2075; found 357.2074.

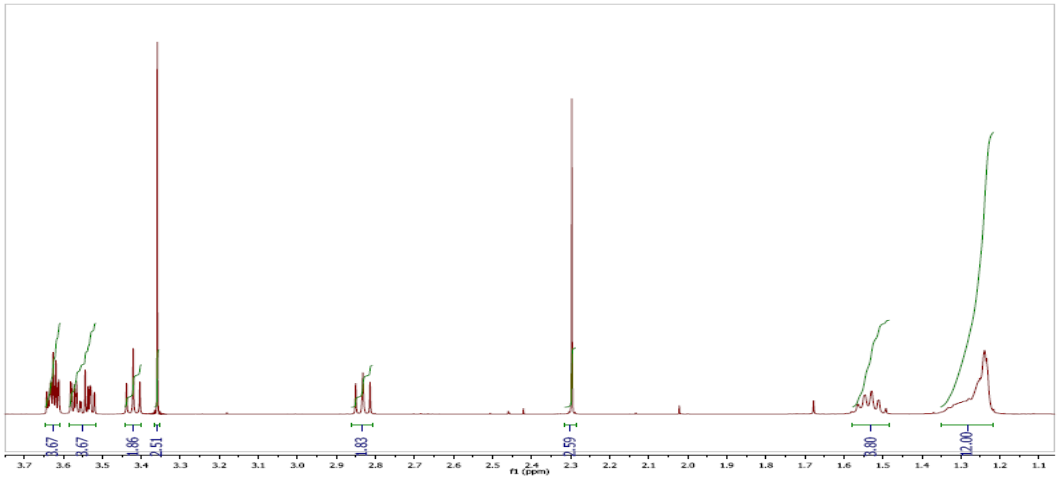

Figure 3.11a. ^{1}H NMR of **(10–thioacetyldecyl) diethylene glycolmonomethyl ether.**

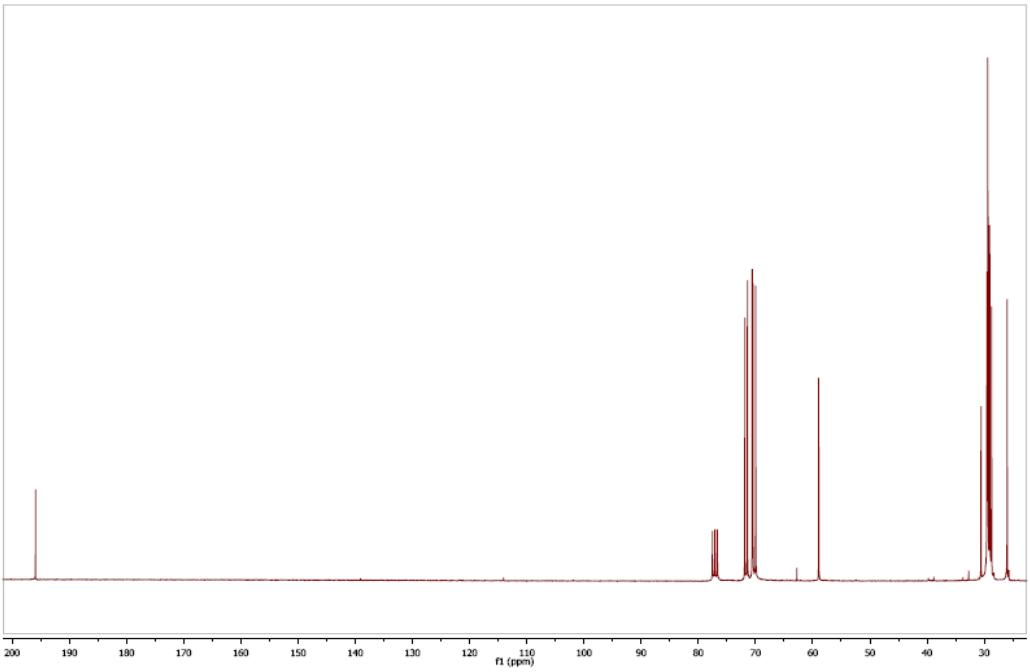

Figure 3.11b. ^{13}C NMR of **(10–thioacetyldecyl) diethylene glycolmonomethyl ether.**

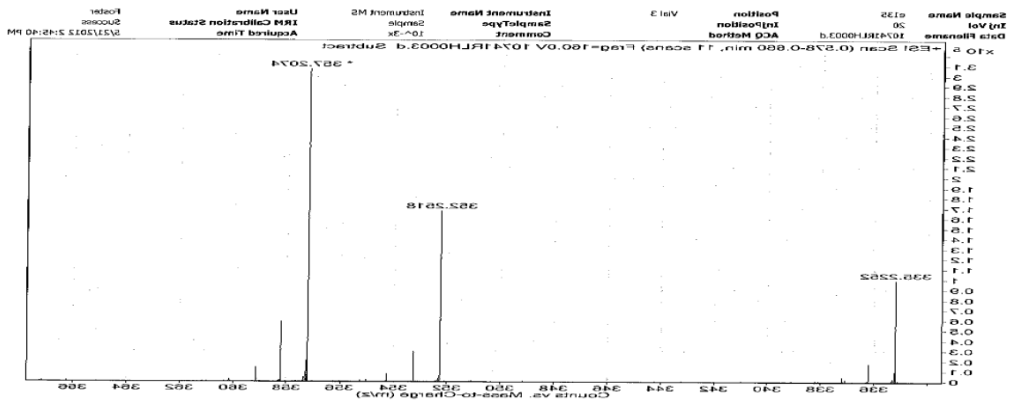

Figure 3.11c. Mass spectra of **(10–thioacetyldecyl) diethylene glycolmonomethyl ether.**

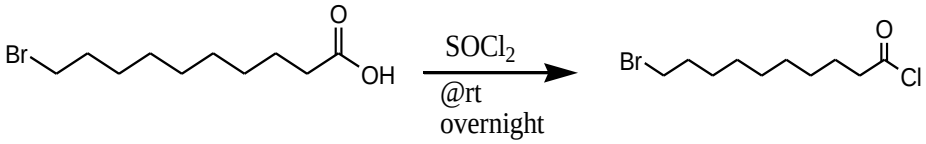

Synthesis of 10-bromodecanoyl chloride. A mixture of 10-bromodecanoic acid (2.5 g, 9.95 mmol) and thionyl chloride (2.4 g, 19.9 mmol) was stirred under nitrogen at room temperature for overnight. Excess of thionyl chloride was removed via vacuum evaporation to provide 10-bromodecanoyl chloride (1.9 g, 73%) as a colorless liquid. ^{1}H NMR (300 MHz, $CDCl_3$): δ 3.4 (2H, t, *J* = 6.9 Hz), 2.8 (2H, t, *J* = 7.2 Hz), 1.8-1.2 (15H, m).

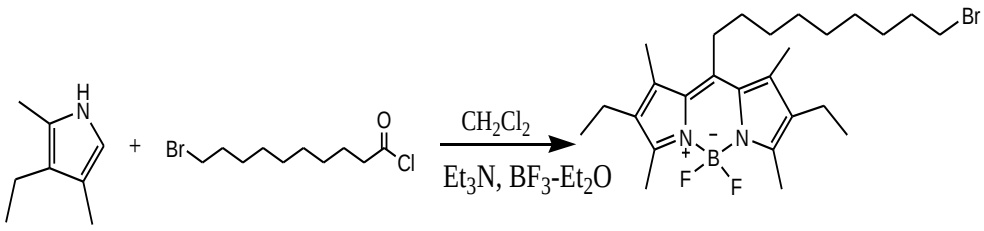

Synthesis of bromo bodipyC9.[19] To a 250 ml reaction flask 3-ethyl 2,4-dimethyl pyrrole (0.99 g, 8 mmol), and methylene chloride (45 mL) was added. The mixture was stirred under nitrogen at room temperature for 10 m. Then 10-bromodecanoyl chloride (1.08 g, 4 mmol) was added slowly to the flask through a syringe. The mixture was heated at 50 ^{o}C for 3 h under nitrogen with continuous stirring. Methylene chloride was removed via vacuum evaporation. To the residue of toluene (95 mL), methylene chloride (5 mL), and triethylamine (1.94 g, 19 mmol) were added to and the mixture was stirred under nitrogen at room temperature for 30 m. After that boron trifluoride diethyl etherate (3.9 g, 27.5 mmol) was added and heated at 50^{0}C for 1.5 h. The cooled mixture was washed with water (2 x 20 mL) and dried over anhydrous Na_2SO_4. The crude product was purified via silica gel column chromatography (4:1 petroleum ether/methylene chloride) to give pure bromoundecylbodipy (122 mg, 6%) as an orange solid. ^{1}H NMR (300 MHz, $CDCl_3$): δ 3.4 (2 H, t, *J* =6.9 Hz), 3.0 (2 H, s), 2.48 (6 H, s), 2.4 (q, 4 H, *J* = 6 Hz), 2.3 (6 H, s), 1.6 (14 H, b), 1.01 (6 H, t, *J* =7.8 Hz); ^{19}F NMR (300 MHz, $CDCl_3$): δ -146 (2F, q).

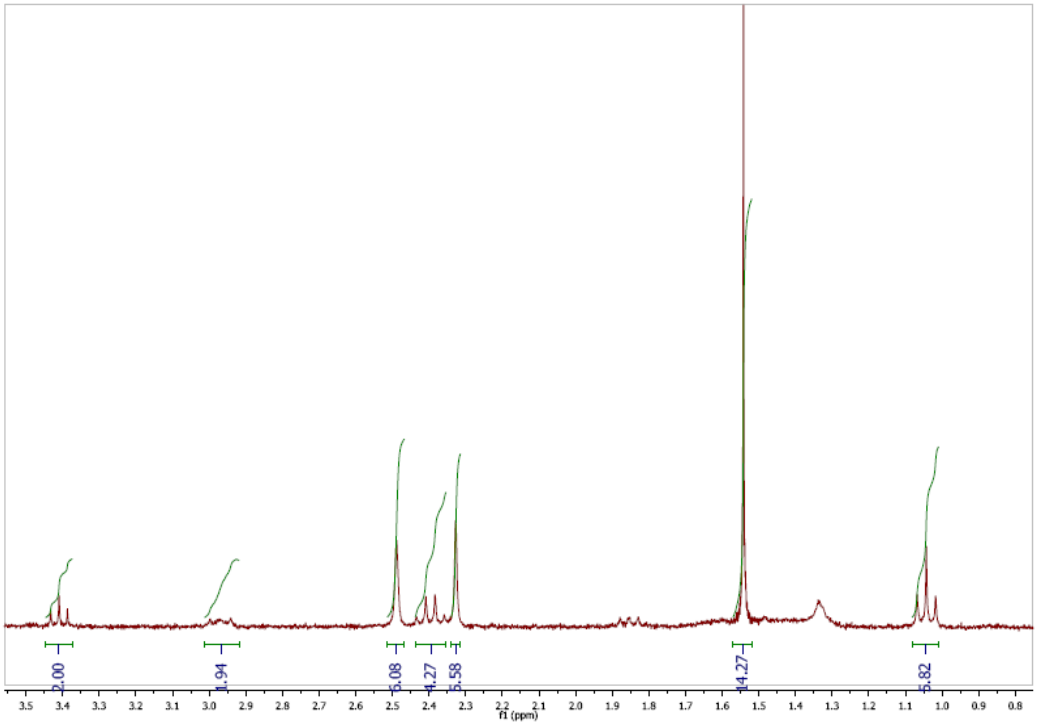

Figure 3.12. ^{1}H NMR of **bromo bodipyC9.**

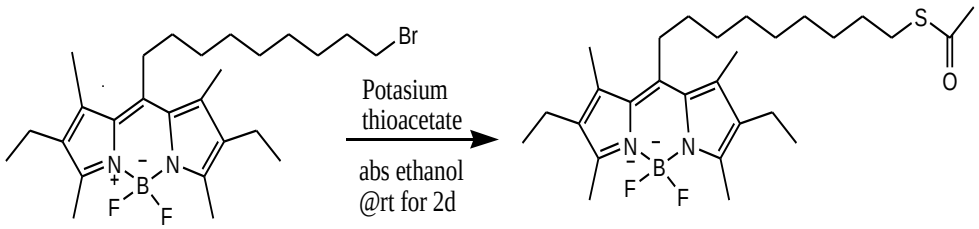

Synthesis of bodipyC9thioacetate. A mixture of bodipyundecylbromide (111mg, 0.22mmol), absolute ethanol (20mL), and potassium thioacetate (50 mg, 0.44mmol) was stirred under nitrogen at room temperature for 2 d. Ethanol was removed via vacuum evaporation. To the residue ice-cold water (10mL) was added and then extracted with diethyl ether (3 × 10 mL). The combined ether phase was washed with water (3 × 10 mL), dried over anhydrous $MgSO_4$, filtered via vacuum filtration, and concentrated via rotary evaporation. The crude product was purified

by silica gel column chromatography (4:1 petroleum ether /dichloromethane) to obtain orange solid (67mg, 60%). ^{1}H NMR ($CDCl_3$, 400MHz): δ 2.9 (t, 2H, *J* = 4 Hz), 2.78 (2H, t, *J* = 4 Hz), 2.4 (s, 6H), 2.3 (q, 4H, *J* = 8Hz), 2.26 (s, 9H), 1.5 (m, 4H), 1.4 (m,2H) , 1.2-1.3 (b, 9H), 0.98 (t, 6H, *J* = 8Hz); ^{13}C NMR ($CDCl_3$, 400MHz): δ 196.09, 151.97, 144.94, 135.63, 132.49, 130.89, 31.8, 30.65, 30.32, 29.47, 29.41, 29.35, 29.08, 29.03, 28.74, 28.53, 17.18, 14.86, 13.35, 12.39; ^{19}F NMR($CDCl_3$, 300 MHz): δ -146 (2F, q). MS (ESI): calcd 527 for, found 527.3 $[M+K]^+$.

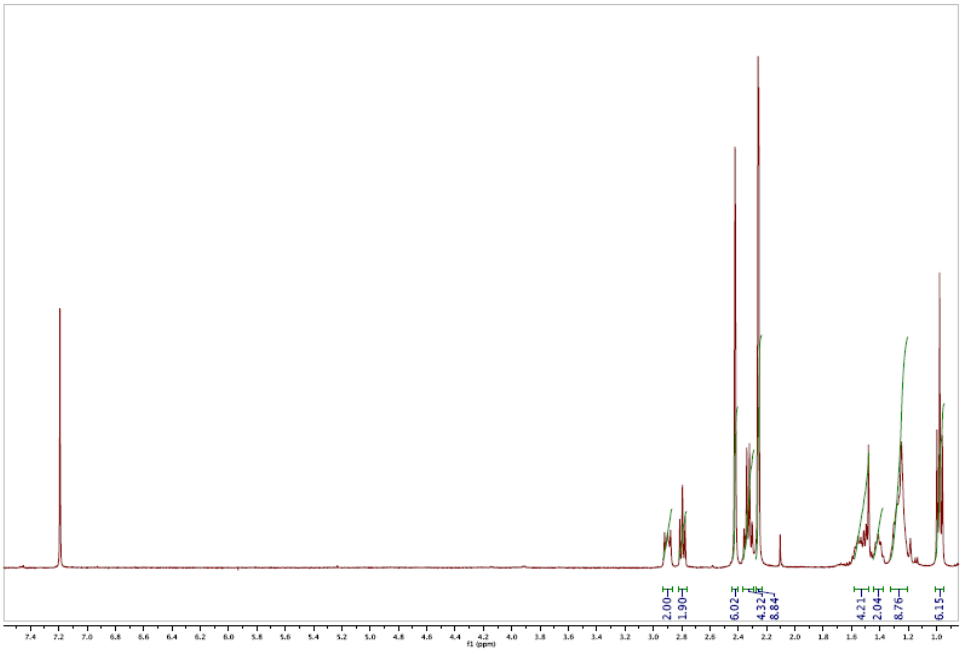

Figure 3.13a. ^{1}H NMR spectrum of **bodipyC9Sac.**

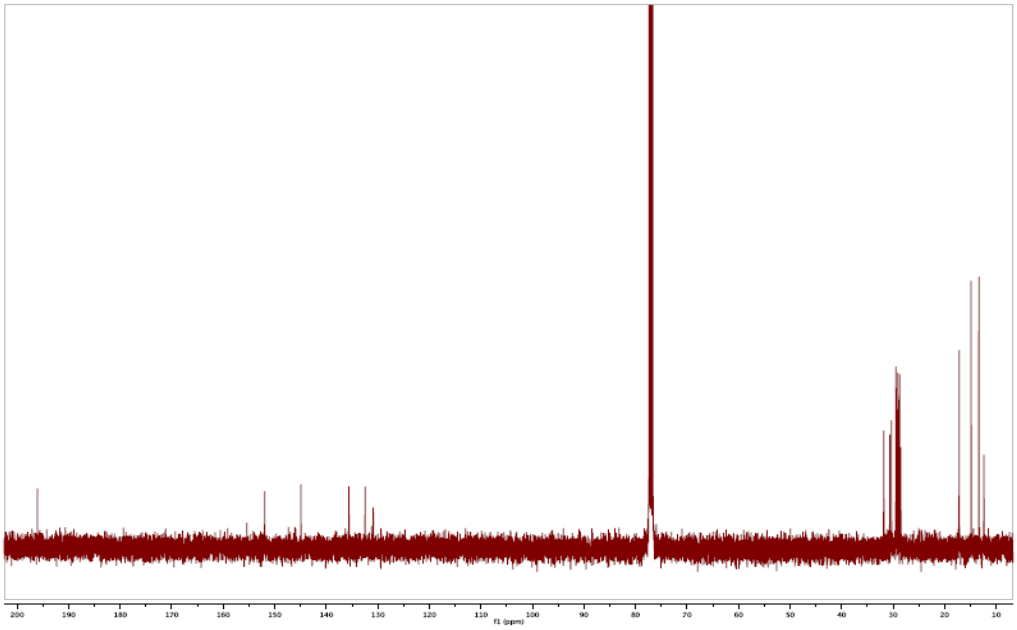

Figure 3.13b. ^{13}C NMR spectrum of **bodipyC9Sac.**

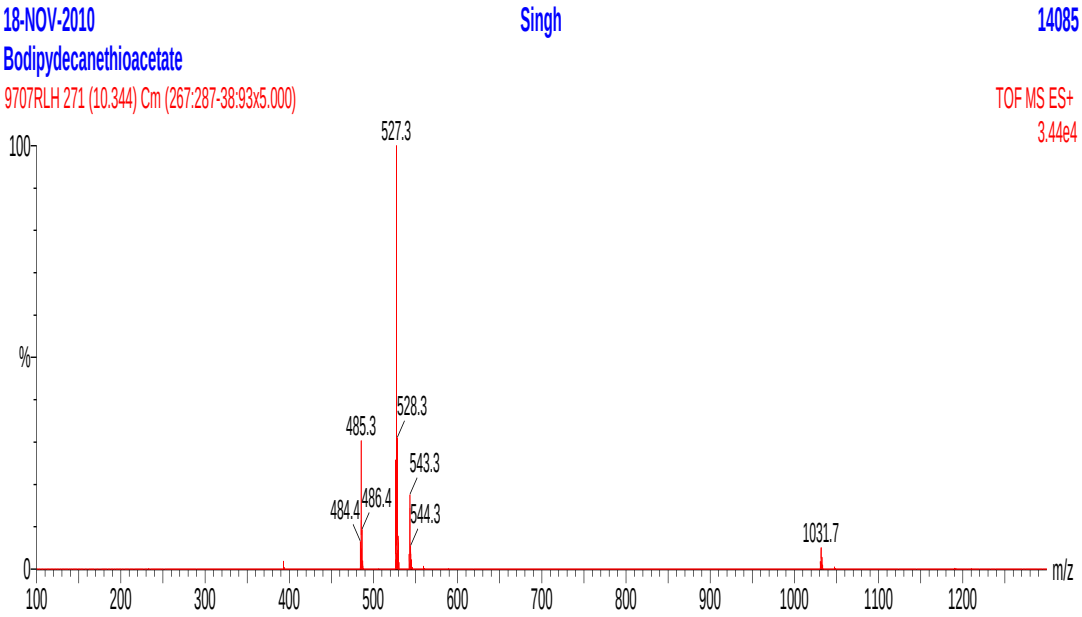

Figure 3.13c. Mass spectrum of **bodipyC9Sac.**

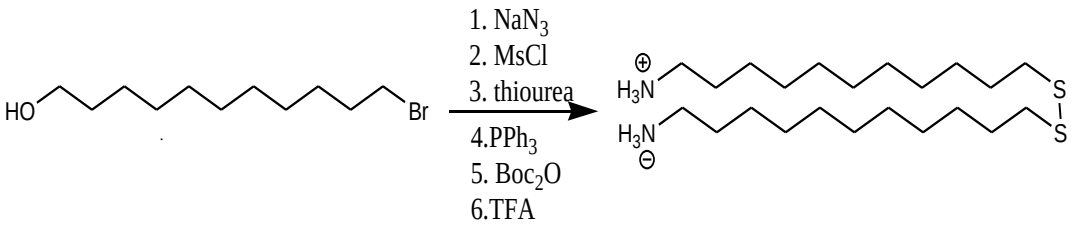

(11-(2-(11-aminoundecyl)disulfanyl)undecan-1-amine).[24] To a 250 mL reaction flask, 11-bromoundecanol (5 g, 20 mmol), sodium azide (4.2 g, 64 mmol), and DMSO (80 mL) were added and stirred for 24 h at room temperature . 200 ml of distilled water was added and stirred it for 30 mintutes and extracted with dichloromethane (3×20 mL). The organic portion was combined and washed with water (2× 20mL) and brine (1× 20 mL). The organic phase was dried over anhydrous $MgSO_4$, filtered and concentrated to obtain pure 11-azidoundecanol (3.9 g, 93%) as a colorless oily liquid. The NMR spectrum matched with literatue. To a 250 mL reaction flask, 11- azidoundecanol (3.9 g, 18.3 mmol), methanesulfonyl chloride (5.5 g, 47.6 mmol), dichloromethane (50 mL) were added and stirred at 0 ^{o}C. The solution of triethylamine (4.9 g, 47.6 mmol) in 1 mL of dichloromethane was added to the cooled reaction flask dropwise through syringe over 5 min and stirred it for overnight at room temperature . The reaction was quenched by the adding ice-cold water (50 mL) and stirred for 15 min. The organic phase was separated and the aqueous phase was further extracted with dichloromethane (2×20 mL). The organic portions were combined, washed with 1M HCl (1×20 mL), $NaHCO_3$ (1×20 mL), brine (1×20 mL), and water (2×20 mL), dried over anhydrous sodium sulfate, filtered, and evaporated the solvent via rotary evaporation to provide pale yellow oily liquid(98% yield, 5.2 g). The obtained 1-

azidoundecanemesylate (2 g, 6.7 mmol) was refluxed with thiourea (1 g, 13.4 mmol), and ethanol (25 mL) for 4h. The flask was cooled and concentrated. The residue was treated with water (50 mL) and extracted with dichloromethane (3×20 mL). The combined organic phase was dried over Na_2SO_4 and concentrated to obtain bis-(azidoundecane)disulfide (1.2 g, 20%) as a colorless liquid. Azidoundecanedisulfide (1.2 g, 2.63 mmol) was reduced to amine by stirring with triphenyl phosphine (6.9 g, 26.3 mmol) in THF (25 mL)/ water (1 mL) at room temperature for 24 h. Triethyl amine (1.5 g, 15 mmol) and ditertbutyldicarbonate (2.84 g, 13 mol) were added to the same flask and continued stirring at room temperature for more 18 h. The crude was extracted with ether (3×20 mL), and washed with water (2×20 mL). The combined organic phase was dried over $MgSO_4$ and concentrated via rotary evaporation. The bocprotected aminedisulfide was purified through silica gel column chromatography (9:1 CH_2Cl_2/ MeOH) to provide pure compound (482 mg, 30%) as a colorless solid. Boc was deprotected by stirring boc proptected disulfide (0.482 g, 0.80 mmol) with TFA (5 mL) and dichloromethane (5 mL) at room temperature for more 0.5 h. The TFA was removed through vacuum evaporation in the presence of methanol couple of times to provide pure aminedisulfide (.387 g, 77%) as a colorless oily liquid. ^{1}H NMR (300 MHz, CD_3OD): δ 7.86 (b, 6H), 2.9 (m, 4H), 2.7 (t, 4H, J = 7.35 Hz), 1.66 (m, 8H), 1.28 (m, 28 H).

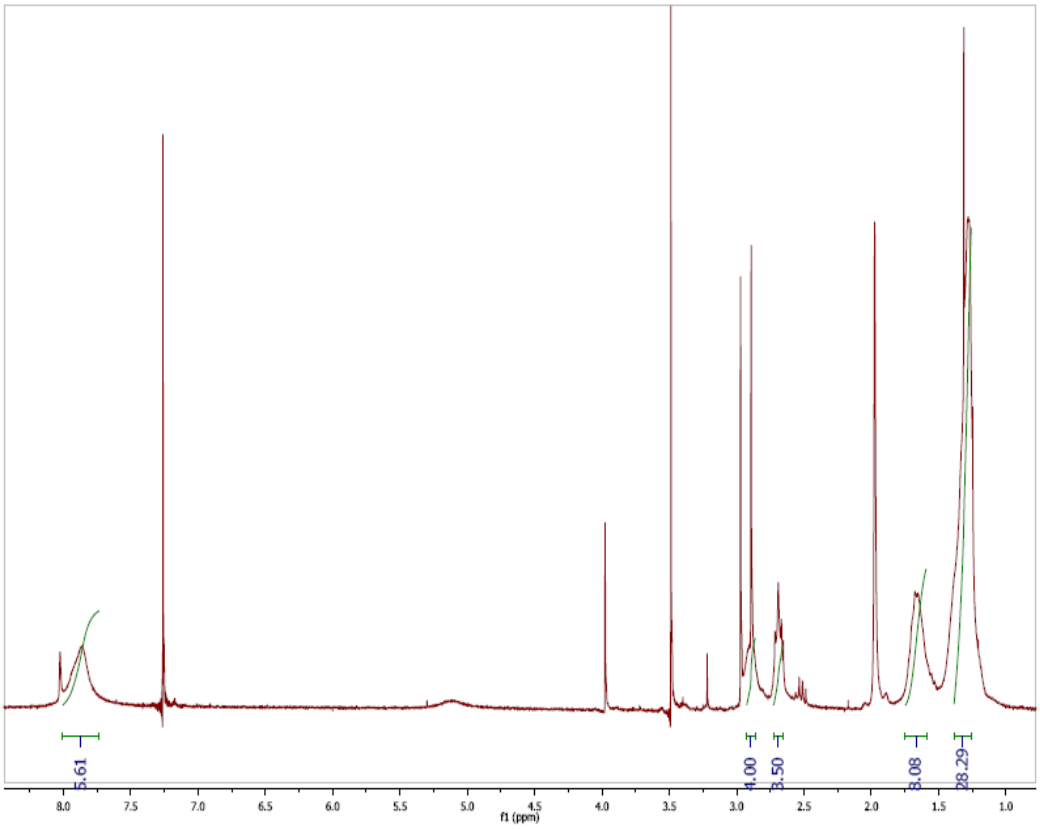

Figure 3.14. ^{1}H NMR of bis-(amineundecane)disulfide.

3.6 References

1. Hara, K.; Sayama, Y.; Ohga, A.; Shinpo, S.; Arakawa, H. A coumarin-derivative dye sensitized nanocrystalline TiO2 solar cell having a high solar-energy conversion efficiency up to 5.6%. *Chem. Commun.2***001,** 569-570.

2. Kobayashi, H.; Ogawa, M.; Alford, R.; Choyke, P. L.; Urano, Y. New Strategies for Fluorescent Probe Design in Medical Diagnostic Imaging *Chem. Rev.* **2010,** *110*, 2620–2640.

3. Arunkumar, E.; Forbes, C.C.; Smith, B.D.: Improving the properties of organic dyes by molecular encapsulation. *Eur. J. Org.Chem.* **2005**, 4051–4059.

4. (a)Mohanty, J.; Bhasikuttan, A. C.; Nau, W. M.; Pal, H. Host-guest complexation of neutral red with macrocyclic host molecules: Contrasting pKa shifts and binding affinities for cucurbit[7]uril and β-cyclodextrin. *J. Phys. Chem. B* **2006**, *110*, 5132–5138. (b) Rohatgi, K.K.; Singhal, G.S. Nature of bonding in dye aggregates. *J. Phys. Chem.* **1996**, *70*, 1695–1701. (c) Selwyn, J.E.; Steinfeld, J.I. Aggregation of equilibriums of xanthene dyes. *J. Phys. Chem.* **1972,** *76*, 762–774. (d) Nau, W.M.; Mohanty, J. Taming fluorescent dyes with cucurbituril. *Inter. J. Photoenergy* **2005,** *7*, 133-141.

5. Ramamurthy, V.; Sanderson, D. R.; Eaton, D. F. Control of dye assembly within zeolites: role of water. *J. Am. Chem.Soc.* **1993**, *115*, 10438-10439.

6. Lian, W.; Litherland, S. A.; Badrane, H.; Tan, W.; Wu, D.; Baker, H. V.; Gulig, P. A.; Lim, D. V.; Jin, S. Ultrasensitive detection of biomolecules with fluorescent dye-doped nanoparticles *Anal. Biochem.* **2004,** *334*, 135-144.

7. (a) Wagner, B. D.; Fitzpatrick, S. J.; Gill, M. A.; MacRae, A. I.; Stojanovic, **N.** A fluorescent host-guest complex of cucurbituril in solution: a molecular Jack O'Lantern *Can. J. Chem.* **2001**, *79*, 1101-1104. (b) Jon, S. Y.; Selvapalam, N.; Oh, D. H.; Kang, J.-K. ; Kim, S.-Y. ; Jeon, Y. J.; Lee, J. W.; Kim, K. Facile Synthesis of Cucurbit[n]uril Derivatives via Direct Functionalization: Expanding Utilization of Cucurbit[n]uril *J. Am. Chem. Soc*. **2003**, *125*, 10186-10187. (c) Marquez, C.; Nau, W. M. Polarisierbarkeiten im Inneren von molekularen Containern. *Angew. Chem.* **2001,** *113*, 4515-4518. (d) Marquez, C.; Huang, F.; Nau, W. M. Cucurbiturils: Molecular Nanocapsules for Time-Resolved Fluorescence-based Assays. IEEE *Trans. Nanobiosci.* **2004**, *3*, 39-45. (e) Mohanty, J.; Nau, W. M. Refractive Index Effects on the Oscillator Strength and Radiative Decay Rate of 2,3-Diazabicyclo[2.2.2]oct-2-ene. *Photochem. Photobiol. Sci.* **2004**, *3*, 1026-1031. (f) Rankin, M. A.; Wagner, B. D. Fluorescence Enhancement of Curcumin upon Inclusion into Cucurbituril. *Supramol. Chem.* **2004,** *16*, 513-519.

8. (a) Mohanty, J.; Nau, W. M. Ultrastable rhodamine with cucurbituril .*Angew. Chem., Int. Ed.* **2005,** *44*, 3750–3754. (b) Mohanty, J.; Pal, H.; Ray, A. K.; Kumar, S.; Nau, W. M. Supramolecular dye laser with cucurbit[7]uril in water *Chem. Phys. Chem.* **2007**, *8*, 54–56.

9. Halterman, R. L.; Moore, J. L.; Mannel, L. M.: Disrupting Aggregation of Tethered Rhodamine B Dyads through Inclusion in Cucurbit[7]uril. *J. Org. Chem.* **2008,** *73*, 3266-3269.

10. Thomas, K. G.; Kamat, P. V.: Chromophore-functinalized gold nanoparticles. *Acc. Chem.Res.* **2003**, *36*, 888-898.

11. Eustis, S.; El-Sayed, M. A.: Why gold nanoparticles are more precious than pretty gold: Noble metal surface plasmon resonance and its enhancement of the radiative and nonradiative properties of nanocrystals of different shapes. *Chem. Soc. Rev*. **2006**, *35*, 209–217.

12. (a) Gedes, C. D.; Lakowicz, J. R. Editorial: Metal-enhanced fluorescence . *J. fluoresc.* **2002**, *12*, 121-129. (b) Tam, F.; Goodrich, G. P.; Johnson, B. R.; Halas, N. J.: Plasmonic enhancement of molecular fluorescence. *Nano Lett.***2007**, *7*, 496-501.

13. Waldeck, D. H.; Alivisatos, A. P.; Harris, C. B. Nonradiative damping of molecular electronic excited states by metal surfaces. *Surf. Sci.* **1985**, *158*, 103-125.

14. Ghosh, S. K.; Pal, T. Photophysical aspects of molecular probes near nanostructured gold surfaces. *Phys. Chem. Chem. Phys.* **2009**, *11*, 3831-3844.

15. Love, C. J.; Estroff, L. A. ; Jennah, K.; Kriebel, J. K.; Nuzzo, R. G.; Whitesides, G. M.: Self-Assembled Monolayers of Thiolates on Metals as a Form of Nanotechnology. *Chem. Rev.* **2005,** *105*, 1103-1169.

16. Stephane, R.; Tillement, O.; Billotey, C.; Coll, J.-C.; Le Duc, G.; Christopher;, A.; Marquette, P. P. Multifunctional nanoparticles: from the detection of biomolecules to the therapy. *J. Nanotech.* **2010**, *7*, 781 – 801.

17. Halterman, R. L.; Singh, A.; Dahanayaka, D. H.; Biswas, A.; Bumm, L. A.: Molecularly Ordered Decanethiolate Self-Assembled Monolayers on Au(111) from *in situ* Cleaved Decanethioacetate: An NMR and STM Study of the Efficacy of Reagents for Thioacetate Cleavage. *Langmuir* **2010**, *26*, 13221-13226.

18. Canaria, C. A.; Smith, C. J.; Yu, S. E.; Fraser, R. L. New syntheses for 11-(mercaptoundecyl)triethylene glycol and mercaptododecyltriethyleneoxy biotin amide *Tetrahedron Lett.* **2005**, *46*, 4813-4816.

19. Loudet, A.; Burgess, K.: Bodipy Dyes and Their Derivatives: Syntheses and Spectroscopic Properties. *Chem. Rev.* **2007,** *107*, 4891-4932.

20. (a) Turkevich, J.; Stevenson, P. C.; Hillier, J.: A study of the nucleation and growth processes in the synthesis of colloidal gold. *Discuss. Faraday Soc.* **1951,** *11*, 55-75. (b) Frens, G.: Controlled nucleation for the regulation of the particle size in monodisperse gold suspensions. *Nature* **1973,** *241*, 20-22.

21. (a) Wu, L.; Burgess, K., Synthesis and Spectroscopic Properties of Rosamines with Cyclic Amine Substituents. *J. Org. Chem.* **2008,** *73* (22), 8711-8718. (b) Gibson, S. L.; Hilf, R.; Donnelly, D. J.; Detty, M. R., Analogues of tetramethylrosamine as transport molecules for and inhibitors of P-glycoprotein-mediated multidrug resistance. *Bioorg. Medic. Chem.* **2004,** *12* (17), 4625-4631.

22. Yang, M.-C.; Fang, J.-M.; Kuo, T.-F.; Wang, D.-M.; Huang, Y.-L.; Liu, L.-Y.; Chen, P.-H.; Chang, T.-H., Production of Antibodies for Selective Detection of Malachite Green and the Related Triphenylmethane Dyes in Fish and Fishpond Water. *J. Agric. Food Chem.* **2007,** *55* (22), 8851-8856.

23. Lu, Y.; Dasog, M.; Leontowich, A. F. G.; Scott, R. W. J.; Paige, M. F.: Fluorescently Labeled Gold Nanoparticles with Minimal Fluorescence Quenching. *J. Phys. Chem. C* **2010,** *114*, 17446–17454

24. Canaria, C. A.; Smith, J. O.; Yu, C. J.; Fraser, S.E.; Lansford, R.New syntheses for 11-(mercaptoundecyl)triethylene glycol and mercaptododecyltriethyleneoxy biotin amide. *Tetrahedron Lett.***2005**, 46, 4813-4816

Chapter IV: Investigation of Fluorescence-on Efficacy of Benzylviologen Fluorophore Dyads

4.1 Chapter Overview

This chapter presents the fluorescence on response upon binding of cucurbit[7]uril (CB7) to a viologen guest to displace the quencher from the tethered fluorophore. Bulk of prior research has been done on fluorescence off-on sensors for metal ion detection. Initially fluorphore quenching would be attributed to photoinduced electron transfer from nonbonded electron receptor (such as nitrogen) to the fluorophore. Binding of metal ions to the receptor lone pair shut off the transfer of electrons which turned on the fluorescence. This procedure can be extended for sensing biomolecules where fluorescence switches on due to disruption of electron transfer from the excited fluorophore to the quencher upon binding of host to the quencher of a dyad. This chapter describes our effort to design and synthesize novel fluorescence off-on pseudorotaxane for this purpose. The change in emission intensity, of dyads was measured by conducting UV-Vis absorbance and steady-state fluorescence titration experiments. Collected data were further examined by curve fit modeling to determine the association constant. In addition, NMR titration experiments were perfomed to gain insight the binding mode of CB7 to dyads. Portions of the work done for this chapter has been published.[1]

4.2 Introduction

Advancement in fluorescence spectroscopy molecular fluorescence has gained extensive attention by chemists and biologists.[2,3] Fluorescence sensing is highly sensitive, selective, and inexpensive[4,5,6,7,8] and has been employed in ion sensing,[9] detection of war-fare agent, [10] and also in biomolecule labeling for real time tracking.[11] In biological imaging, biomolecules of interest are labeled by either natural fluorophore such as green fluorescent proteins or synthetic fluorophores to visualize the target using optical microscopy.[12,13] However, this approach is limited to the cases where localized emission is stronger than the background due to the nonspecific adsorption of fluorophore. For these cases fluorescence-on binding sensors could be designed in which emission of fluorophore is substantially quenched until the sensing event takes place to prevent the quenching. Photoinduced electron transfer mechanism has been extensively applied to achieve fluorescence-on sensors.[14]

Conventional fluorescent-on sensors contain three components: a fluorophore as a signal transduction unit (provides fluorescence signal before and after the recognition event takes place), a receptor responsible for complexation and decomplexation with analyte, and spacer that keeps fluorophore and receptor close to but separate from each other. The electron transfer process is distance dependent and efficient electron transfer can be observed when fluorophore and receptor are at van der Waals contact.[15] Quenching of fluorescence (fluorescence-off) of

fluorphore due to nonbonded electron transfer from receptor to the excited fluorophore could be switched to fluorescence-on by complexation of analyte to the receptor which results no longer electron transfer to the excited fluorophore as depicted in Figure 4.1a.[14]

Extensive development of PET (photoinduced electron transfer) sensors for metal ions[16] could be found such as BDA (Figure 4.2 a) for zinc,[17] bodipy-based sensor (Figure 4.2b) for mercury.[18] In each case fluorescence is initially off due to the nonbonded electron transfer from nitrogen to the excited fluorophore. Once the metal comes into the system fluorescence turns on since transfer of electron shut off from nitrogen to the excited fluorophore as nonbonded electron of nitrogen coordinates to the metal. Both sensors have been utilized in imaging of metals in living cell. Though employment of this approach could be seen enormously for metal ion detection, following only this approach cannot be directly employed for macromolecular sensing.[19]

A more general approach of fluorescence-on could be achieved by disrupting the contact between fluorophore and quencher. Although this approach has not been explored much, considerable effort has been done in detecting conformational changes in proteins that move away the quencher from the fluorophore or disrupt the aggregation of fluorophore-quencher.[20] A novel and more general fluorescence-on response can be achieved by the disruption of quenched aggregate through the binding of host to guest quencher. When the host is displaced from initial binding site to the new guest due to external stimuli, the

aggregation between quencher and fluorophore gets disrupted and turns the fluorescence on (Figure 4.1b). This unique approach can be utilized to construct sensors that have one site for binding with analytes and another site responsible for the fluorescence signal. The fluorescence signal unit is structurally independent with the binding unit and thus binding unit can be varied without any change in the signaling unit make this approach more attractive.

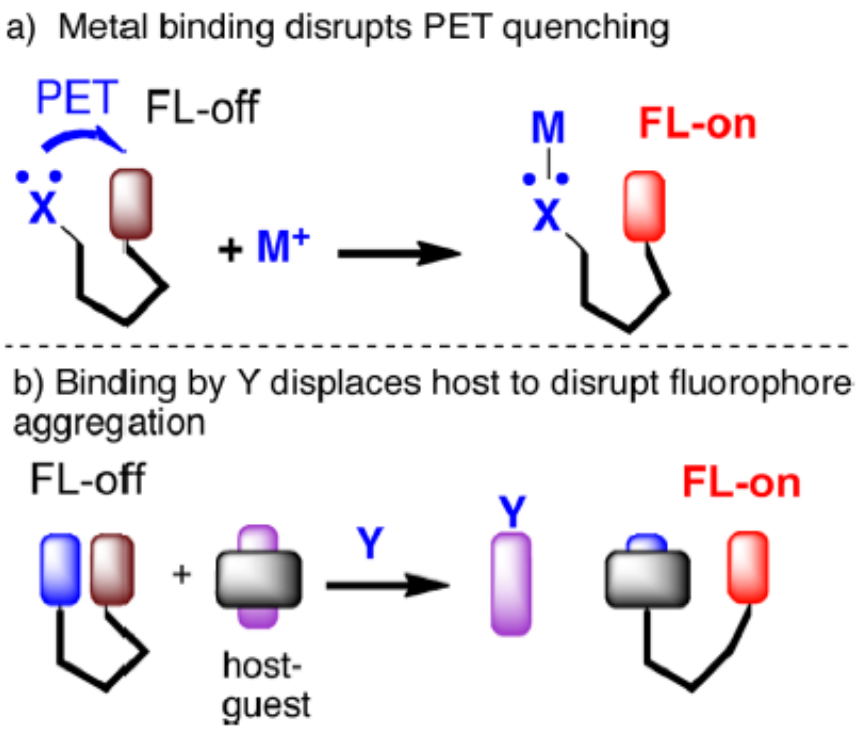

Figure 4.1. Mechanisms to disrupt fluorescence quenching. Diagram produced by Ronald L. Halterman.

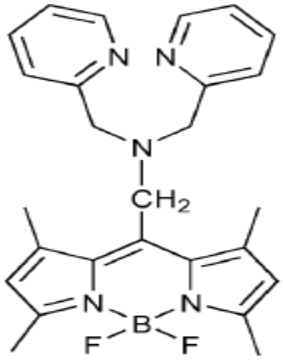

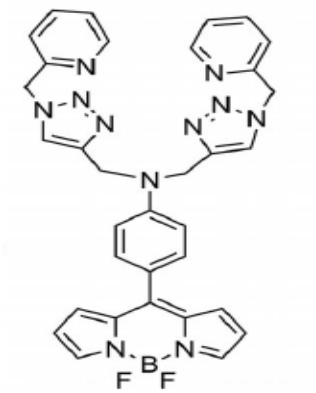

Figure 4.2a. (Left) BDA zinc sensor (Adapted from ref 8) and **Figure 4.2b.** (Right) Bodipy based mercury sensor (Adapted from ref 9).

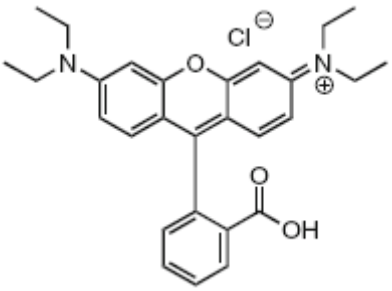

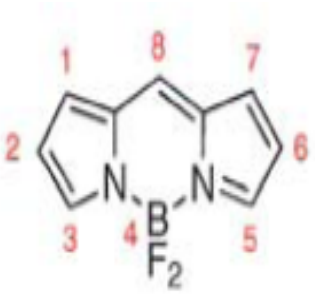

Figure 4.3a. Rhodamine B **Figure 4.3b.** Bodipy.

A well studied monocationic xanthaene dye, organic fluorophore, rhodamine B (Rh B) (Fig 4.3a), has widely been used in lasers, solar cells, staining and labeling of biomolecules, and as a fluorescent probes due to its high quantum yield and excellent solubility in organic solvents as well as in water.[21] Unlike rhodamine B, Bodipy (Fig 4.3b) is neutral dye and has sharp emission peaks as well as high quantum yield.[22] This organic dye has been extensively employed in intracellular imaging, labeling of biomolecules, switches, sensors, and lasers.[23]

Quenching of fluorescent dyes due to their homoaggregation in solution has been studied well and been reported its prevention by the inclusion of dye in macrocyclic hosts.[24]

Several studies on cone-shaped hosts such as cyclodextrin and calixarene included fluorescent dye are available.[25,26] Inclusion of fluorescent dyes in these host molecules results in increase in photostability of dye and also enhancement in emission. As reviewed in chapter one, recent development on convenient synthetic methodology of cucurbit[7]uril (abbreviated as CB7) has been gained more attraction.[27] Its name originated from the Latin word *cucurbitaceae* as its shape is similar to pumpkin. CB7 has electron rich carbonyl portals at two rims and inner hollow cavity is hydrophobic (Figure 4.4). Due to this property binding of CB7 to cationic species, such as cationic fluorescent dyes, viologen, and ammonium compounds, is driven by hydrophobic interaction as well as ion-dipole interaction.[28] Binding affinity of CB7 with several ammonium species is reported from a range of 10^4 to 10^{12} .[29] Our group has reported the increse in emission intensity of tethered rhodamine B dyad upon CB7 binding by two fold due to disruption of less fluorescent H-dimers aggregates.[30] This two fold change in intensity is too weak for the construction of sensors. Therefore, we wanted to extend this complexation method to achieve higher change in emission intensity so that it can be utilized as a signal transduction unit in making biosensors. For this purpose we aimed to construct pseudorotaxane dyad which turns the fluorescence of fluorophore on upon binding of CB7 to the quencher as shown in Figure 4.1b.

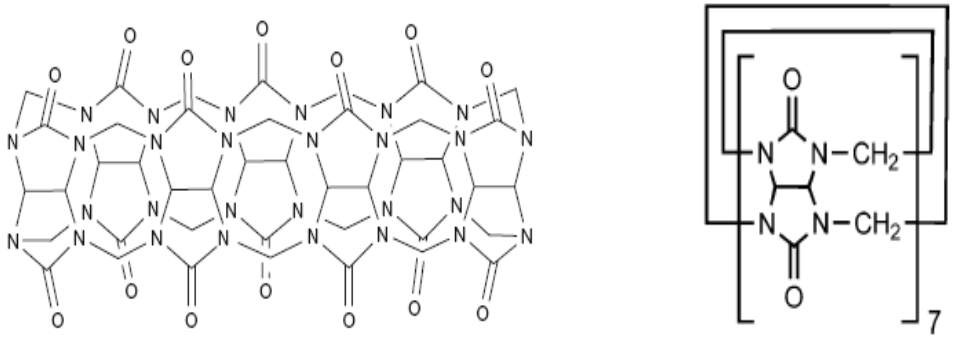

Figure 4.4. Line drawing of CB7, adapted from reference 30.

Rhodamine B quenches due to the electron transfer from the excited dye to 1, 4-dipyridinium viologen dications when these are present in the polymer matrix.[31] Furthermore, the mode of binding and binding affinity of CB7 with viologen has been documented well.[32] Recently our group has reported the formation and dissociation rate constants; $k_1 = 6.01 \times 10^6\ M^{-1}s^{-1}$ and $k_{-1} = 52.7\ s^{-1}$, respectively for 1:1 binding of viologen with CB7 adduct by performing stopped flow kinetic experiments.[33] By combining such information we envisioned to design fluorescence-on signal upon addition of CB7 to the tethered viologen-rhodamine (Figure 4.5a, b) and viologen-bodipy (Figure 4.5c).

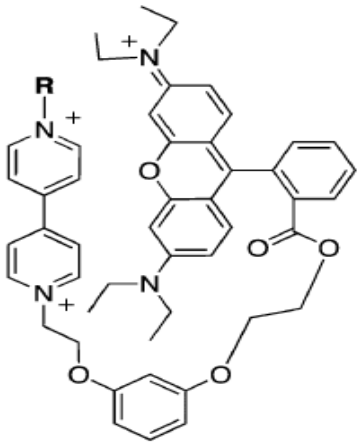

Figure 4.5a and b.

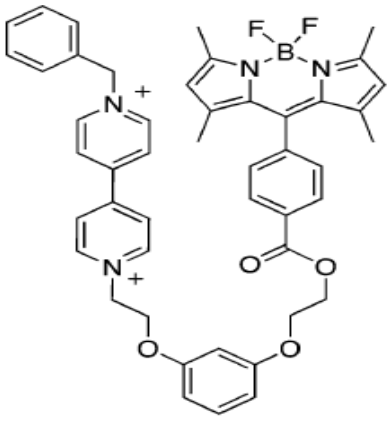

Figure 4.5c.

Figure 4.5a and b: tethered viologen-rhodamine (**a**. R=CH_3, **b.** R=$CH_2C_6H_5$) and **4.5 c:** tethered viologen-bodipy.

4.3 Results and Discussion

The three dyads, methylviologen-rhodamine B (Fig. 4.5a), benzylviologen-rhodamine B (Fig. 4.5b), and benzylviologen-bodipy (Fig. 4.5c), were synthesized as shown in scheme 1. One hydroxy group of resorcinol was alkylated with 2-chloroethanol followed by second alkylation of another hydroxy functionality with 1,2-dibromoethane. Esterification was performed to couple rhodamine B with hydroxyl terminated alkylated resorcinol and another bromine terminated alkylated resorcinol was utilized to incorporate viologens. Finally, the second pyridine molecule of monosubstituted dipyridyl complex was alkylated by using methyl iodide or benzyl bromide to provide the molecules as shown in Figures 4.5a and 4.5b respectively. All reactions were carried out under mild conditions because of cleavage of ester or benzylviologen under harsher conditions.

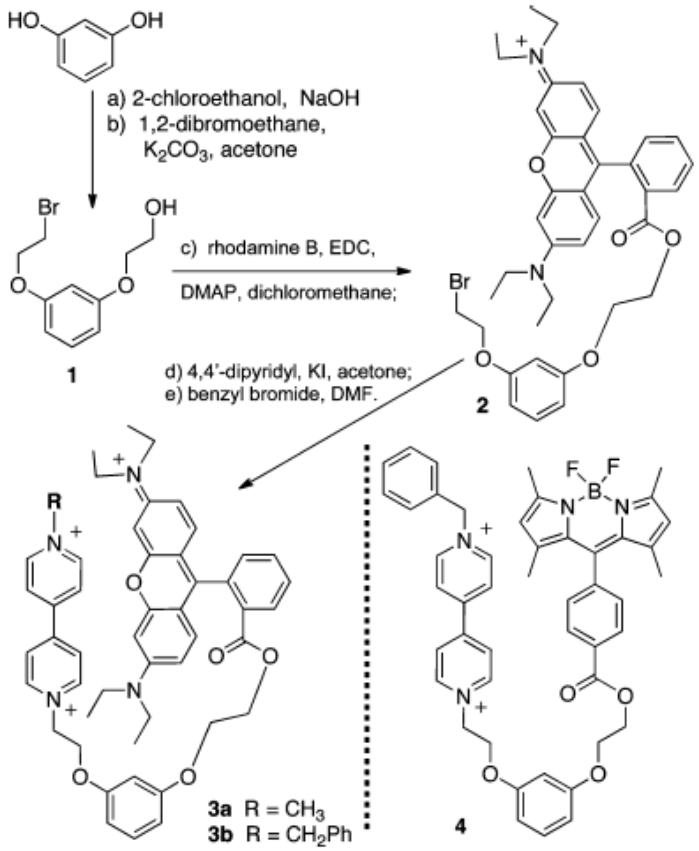

Scheme 1. Synthesis of methylviologen rhodamine B (**3a**), benzylviologen rhodamine B (**3b**), benzylviologen bodipy (**4**).

The polycationic complex was purified through silica gel chromatography by using a mixture of methanol, nitromethane, and aqueous ammonium chloride eluent.[34] Ammonium chloride was removed by dissolving the dyads in dichloromethane followed by filtration. Following literature precedent carboxybodipy[35] and CB7[27, 30] were synthesized. Benzylviologen-bodipy **4.5c** was synthesized with the similar set of reactions as shown in scheme 1. The synthesized dyads were characterized by NMR spectroscopy and mass

spectrometry whereas efficiency of switching fluorescence was studied by measuring the absorbance and fluorescence by UV-visible and fluorescence spectroscopy.

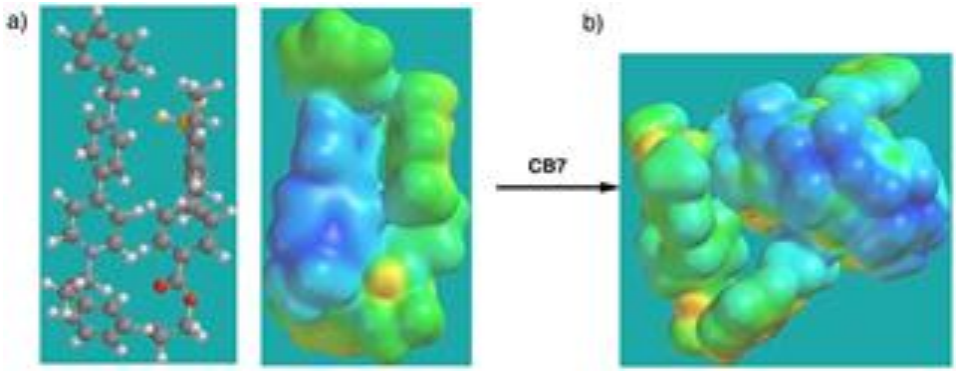

Figure 4.6. (a) PM3-optimized structure/electrostatic surface potential of compound as shown in Figure 4.5c before and (b) after binding with CB7. Image provided courtesy of Ronald L. Halterman.

Semi-emperical calculations using spartan were run on benzylviologen-bodipy to study the aggregation of viologen and bodipy. This calculation was performed by Ronald L. Halterman. Viologen and bodipy were both found to be close enough for the electron transfer in the absence of CB7 (Figure 4.6a). Presence of CB7 allows the disruption of viologen-bodipy as shown in Figure 4.6b.

4.3.1 Spectroscopic Investigation of Methylviologenrhodamine B Dyad with Cucurbit[7]uril

In order to examine the efficiency of fluorescent-on in the methylviologen rhodamine B dyad, spectroscopic titration experiments were performed in aqueous

solution. No significant change in aborbance was for methylviologen rhodamine B observed in the absence and presence of cucurbit[7]uril (CB7) as indicated by the UV-Visible aborbance spectra (Figure 4.7). Additionally, no detectable shift was observed for the λ_{max} in the absence and presence of CB7.

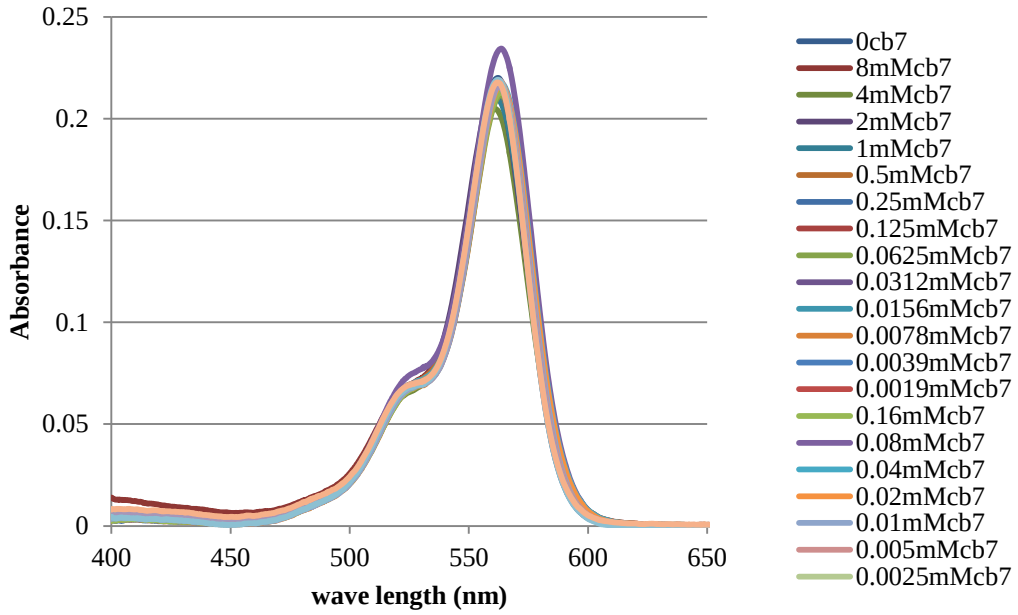

Figure 4.7. UV-Vis absorption spectra of methylviologen rhodamine B dyads (5µM): CB7 (0 mM-8 mM).

From the fluorescence titration curve (Figure 4.8) a continuous increase in intensity of methylviologen rhodamine B dyads with increasing concentration of CB7 was observed. In the absence of CB7, a 10-fold decrease in fluorescence intensity of methylviologen rhodamine B was noticed over non- tethered rhodamine B. Even though quenching was found to be very efficient due to the electron transfer from the excited rhodamine B to the viologen, only a three-fold

enhancement in intensity was observed upon CB7 binding. Binding of CB7 with methyl viologen ($K_a = 10^6\ M^{-1}$)[29,32] has well been documented in the literature.

However, we observed poor fluorescence recovery of the dyad **4.5a**. The lower hydrophobicity of the methyl group may not provide enough energy upon binding to CB7 to disrupt the viologen rhodamine B aggregates. This poor binding of CB7 with methylviogen of dyad led to poor fluorescence recovery.

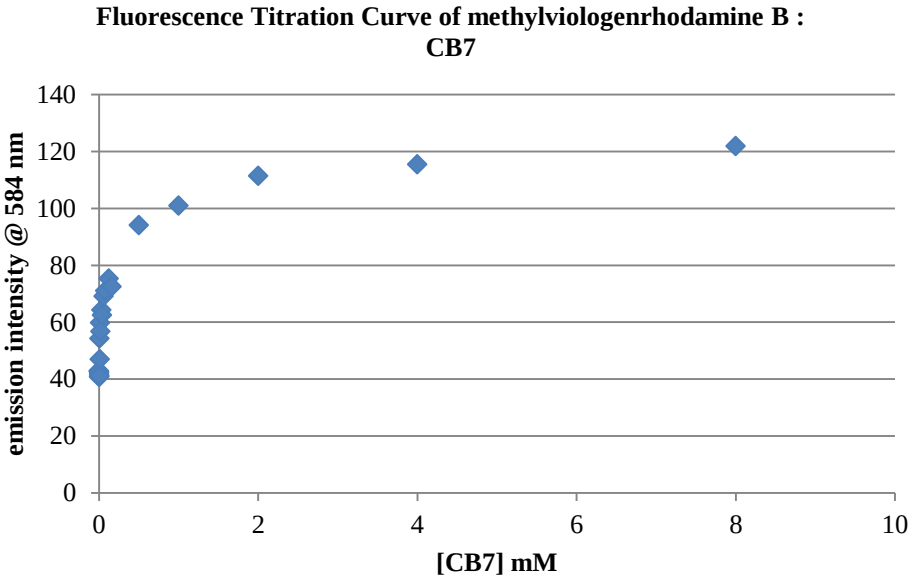

Figure 4.8. Fluorescence titration curve of methylviologenrhodamine B (5 μM) titrated with CB7 (0 mM to 8 mM) in water.

In an attempt to acquire better insight on the nature of the complexation between methylviologen-rhodamine B and CB7, a series of ^{1}H NMR titration experiments (Figure 3.9) were performed. In these experiments, the concentration of the methylviologen-rhodamine B dyad was held constant while the concentration

of CB7 was varied from 0 to 2 mol equivalents. At 0.5 equiv. of CB7, the α protons at 9 ppm in te ^{1}H NMR spectrum slightly shifted upfield to 8.9 ppm whereas upfield shift of the β protons from 8.4 to 7.3 ppm. This shift infers the formation of inclusion complexes between CB7 and viologen.[32] At higher concentrations of 1.5 and 2 eq of CB7, splitting of methylene protons at 3.25 ppm of *N*,*N*-diethyl hydrogens of rhodamone B directed to the binding of CB7 with cationic rhodamine B.[36] Limited amounts of CB7 led to binding with the viologen of dyad whereas excess CB7 concentration also resulted in binding with cationic rhodamine B of dyad. NMR titration data indicated the binding of CB7 with viologen and rhodamine B of dyads. This two competing binding sites for CB7 on dyad **4.5a** was further verified by performing curve fit with fluorescent titration data. Curve fitting experiment was performed by Wai Tak Yip. The data was better fit with two binding sites model on dyad, the first binding site, viologen, has higher binding constant ($k_1 = 6.92 \times 10^4\ M^{-1}$) and the second weaker site, rhodamine B, has lower binding constant ($k_2 = 9.14 \times 10^2\ M^{-1}$).

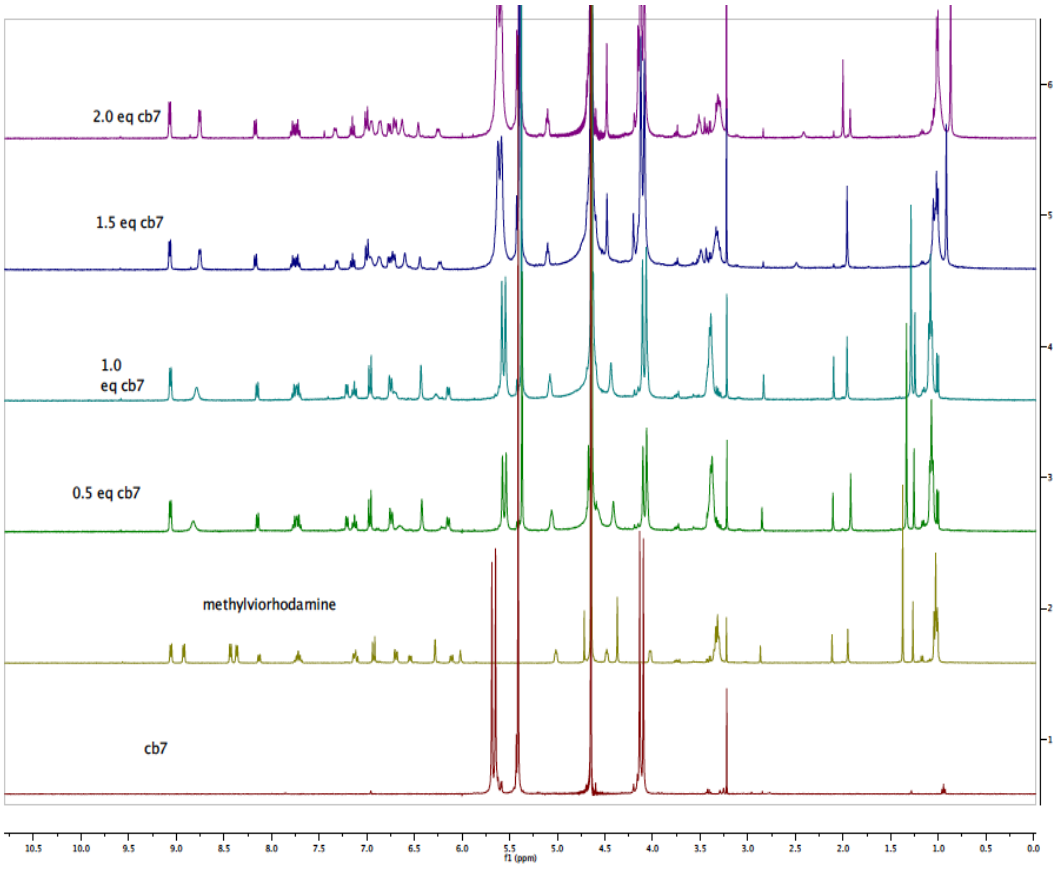

Figure 4.9. ^{1}H NMR spectra (300 MHz, D_2O) of methylviologen-rhodamine B dyad (3.1 mM) with CB7 (0 to 2 equivalent).

4.3.2 Spectroscopic Investigation of Benzylviologen-Rhodamine B Dyad 4.5b : Cucurbit[7]uril

Since binding of CB7 to viologens strongly depends on the substituent on the viologen,[32] the binding occurs due to the ion dipole interaction and hydrophobic interaction. Benzyl viologen geometrically fits beter in CB7 and provides a huge hydrophobic interation than that of short alkyl chain viologen such as methylviologen.[32] Therefore, we postulated that substituting the methyl with benzyl

group on viologen would provide an efficient fluorescent- on dyad. This postulate led to the synthesis of benzylviologen-rhodamine B dyad 4.5b by following the Scheme 1.

In order to obtain the efficacy of fluorescence off-on of benzylviologen-rhodamine B dyad, as shown in Figure 4.5b, CB7 titration experiments were performed by UV-Vis aborbance and fluorescence spectroscopy. An examination of aborbace spectra (Figure 3.10) shows no detectable change in aborbance and also no distinct shift for the λ_{max} in the absence and presence of CB7.

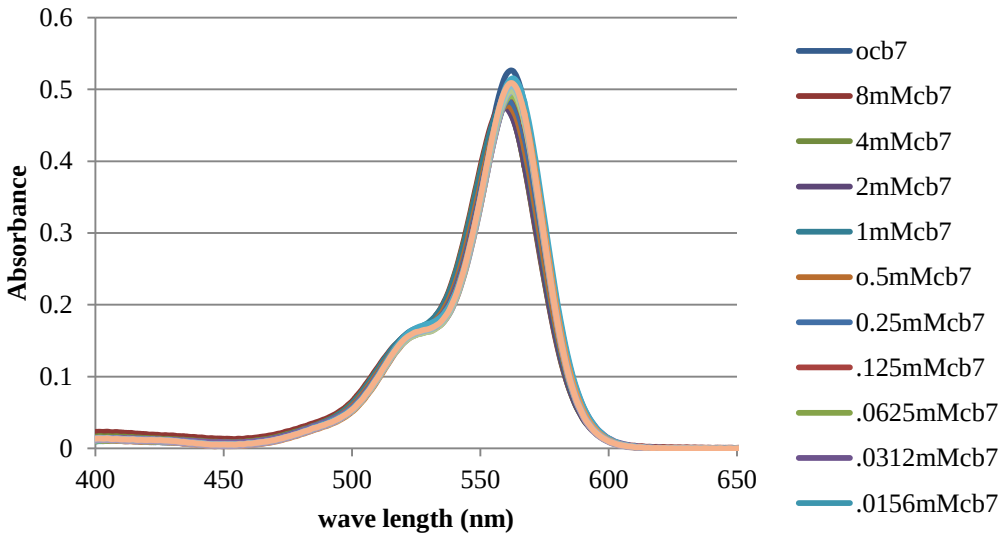

Figure 4.10. UV-Vis absorption spectra of benzylviologen-rhodamine B dyads (5μM): CB7 (0 mM-8 mM).

However, a fourteen-fold enhancement (Figure 4.11) was observed when benzylviologen-rhodamine dyad was titrated with CB7. In addition, this benzyl

containing dyad 4.5b was not saturated even with 8 mM CB7. This strong enhancement indicates the disruption of viologen-rhodamine B aggregates upon complexation of viologen with CB7. In the absence of CB7 the fluorescence of dyad **3.5b** quenches as in that in **3.5a** by about 10 fold due to the electron transfer from excited rhodamine B to the dicationic viologen of dyad. Addition of CB7 results in complexation between CB7 and viologen and prevents the electron transfer from excited rhodamine B to viologen. Thus fluorescence of rhodamine B increases or turns on from fluorescence off. Analysis of fluorescence intensity depicts 88% recovery in fluorescence on comparing to rhodamine B ester, **2**, (Figure3.12) with CB7. CB7 binds strongly to the benzylviologen because it is geometrically more fitted in CB7 due to dipole-ion interaction of carbonyl portal of CB7 to cationic nitrogen of viologen and more especially, hydrophobic interaction of benzyl and inner part of CB7. This strong binding enables to disrupt the interaction between viologen and rhodamine B which results in the prevention of the electron transfer from excited rhodmine B to viologen and switches the fluorescence-off to on.

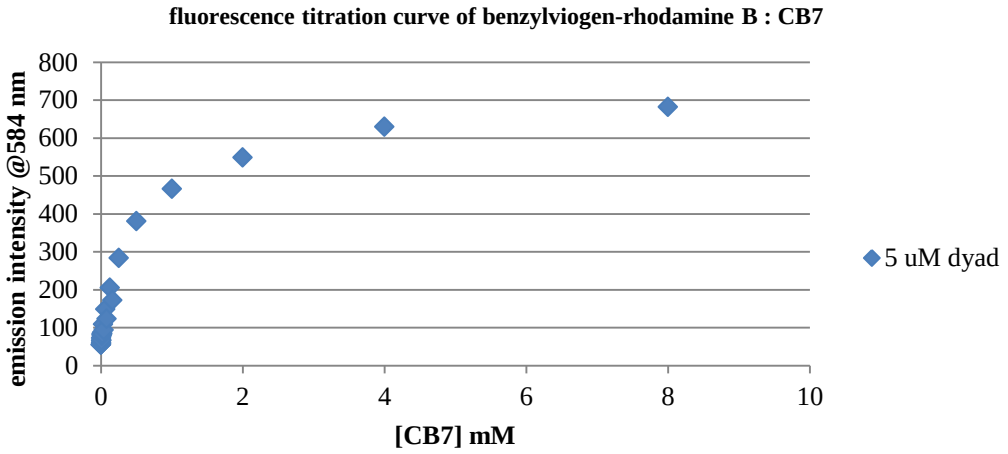

Figure 4.11. Fluorescence titration curve of benzylviologen- rhodamine B (5 μM) titrated with CB7 (0 mM to 8 mM) in water.

To improve our understanding of the nature of the complexation between CB7 and dyad **4.5b** ^{1}H NMR titration experiments were performed where concentration of benzylviologen-rhodamine was held constant and concentration of CB7 was varied from 0 to 2 molar equivalents. The spectral analysis (Figure 4.13) shows binding of benzylviologen with CB7 up to 1 equivalent. Splitting of two aromatic protons (9.05 ppm and 8.4 ppm) of viologen, into total four sets of distinct peaks indicates the slow exchange of included and free viologen of dyad. The α (9.01 ppm) and β (8.4 ppm) protons of uncomplexed pyridine of viologen dyad remains unperturbed , however, α (9.01 ppm) protons of second pyridine found upfield shift (8.9 ppm) whereas β protons shifted to downfield (8.6 ppm). Moreover, upfield shift of benzyl protons (7.4 ppm) clearly indicates the complete inclusion of benzyl into the inner hydrophobic cavity of CB7 and ion dipole

interaction of ureidyl oxygens of the CB7 and one cationic pyridinium of viologen. Above 1 equivalent of CB7, splitting of signal of 3,6-bis(*N*,*N*-diethylanilino) of rhodamine at 3.5 ppm to two sets of broadened signal and upfield shift of peaks supports slow exchange between included and free rhodamine B of dyad. This NMR titration data clearly indicated binding of CB7 with viologen and also with rhodamine B at higher concentration of CB7.

Dyads in Figure **4.5b** possess two binding sites for CB7. In order to confirm this finding and to calculate binding constant, the emission data was further analyzed by curve fitting. The data fits better with two binding sites and a calculated binding constant 1.16 x 10^5 M^{-1}, for the stronger binding with viologen and 1.57 x 10^3 M^{-1} , for the second weekly binding site with rhodamine B.

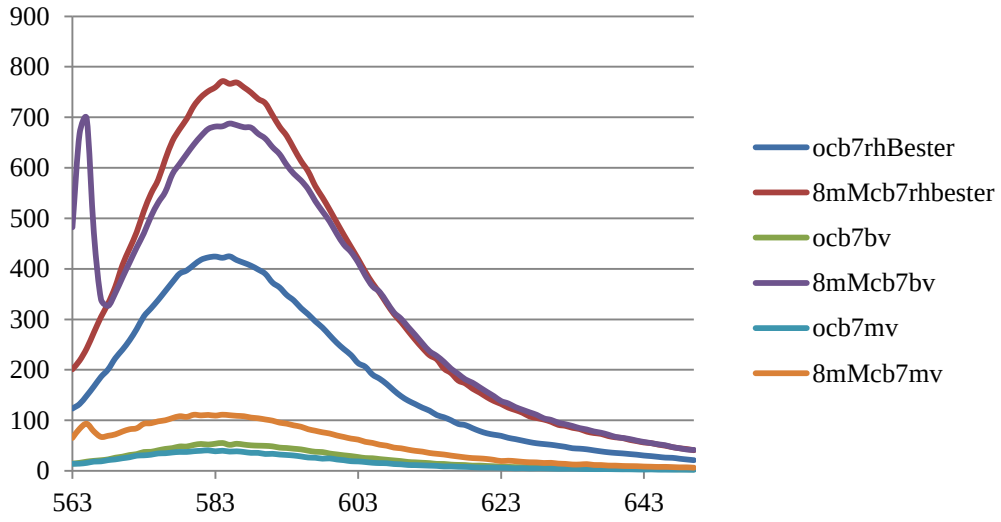

Figure 4.12. Combined emission spectra of **rhodamine B ester** of 2-(3-(2-bromoethoxy)phenoxy)ethanol 2 (labeled as rhbester), methylviologen-rhodamine

B dyad **4.5a** (labeled as mv), benylviologen-rhodamine B dyad **4.5b** (labeled as bv): 5 μM dye and dyad without and and 8 mM CB7 in water.

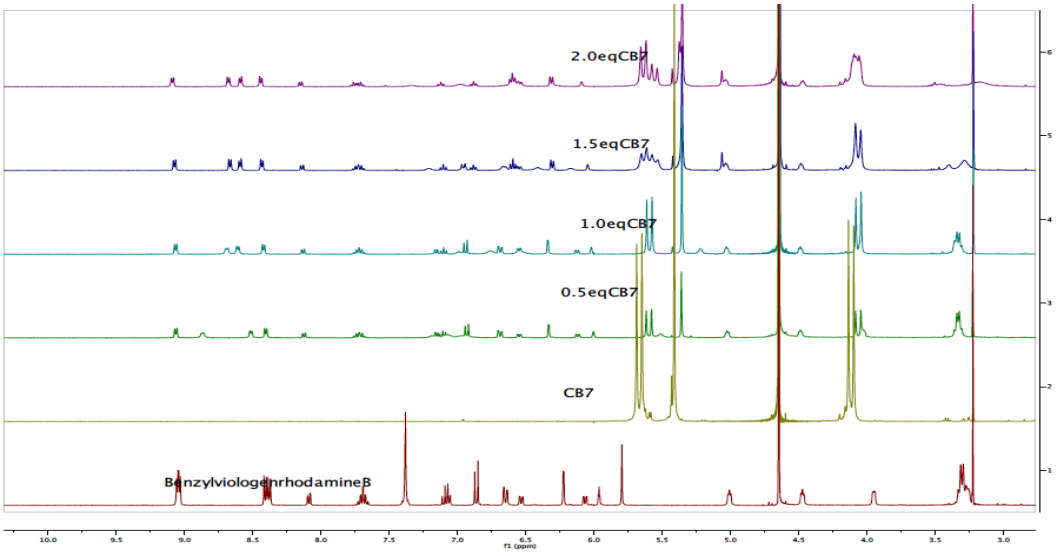

Figure 4.13. ^{1}H NMR spectra (300 MHz, D_2O) of benzylylviologen-rhodamine B dyad (2.9 mM) with CB7 (0 to 2 equivalent).

4.3.3 Spectroscopic Investigation of Benzylviologen-Bodipy Dyad : Cucurbit[7]uril

Due to the cationic nature of rhodamine B, its binding with CB7 could not be avoided. Higher concentrations of CB7 were required to obtain higher emission intensity. Therefore, we wanted to explore the fluorescence switching efficacy by incorporation of neutral dye, Bodipy instead of cationic rhodamine B. Although binding of CB7 with neutral bodipy has not been reported, we thought binding CB7 to bodipy would be negligible as it is not cationic. On this basis, we postulated that dyad incorporating bodipy would produce a large enhancement in the presence of

CB7. Scheme 1 was followed to synthesize the benzylviologen-bodipy dyad as in Figure 4.5c.

In order to study the efficiency of switching fluorescence off to on by benzylviologen-bodipy dyad, UV-Vis absorbance and fluorescence measurements were taken. Absorbance of dyad as in Figure 4.5c (Figure 4.14) shows no significant change in absorbance on the complexation of CB7 with dyads and free dyads. Additionally, no distinct shift for the λ_{max} was observed in the absence and presence of CB7.

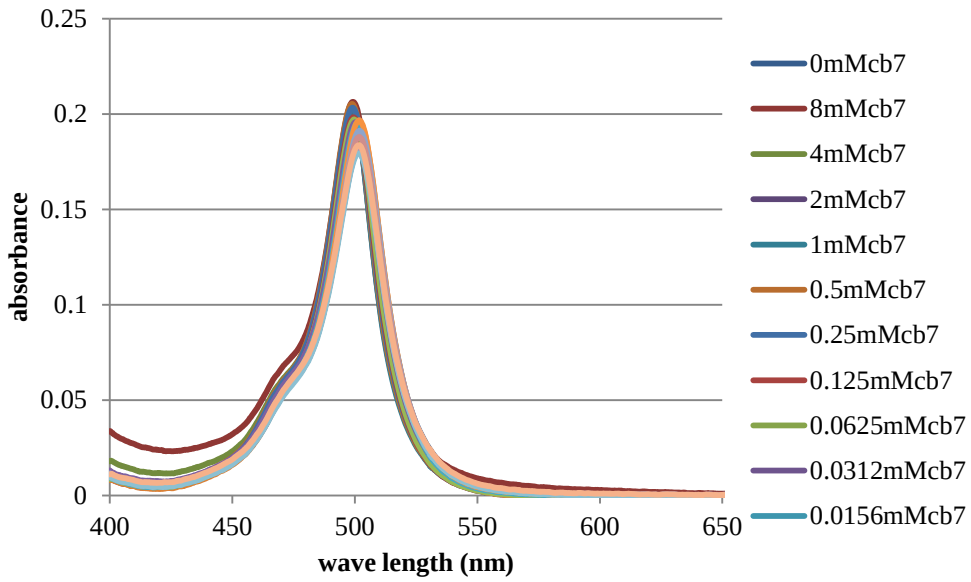

Figure 4.14. UV-vis spectra of benzylviologen-bodipy dyads (5 μM): CB7 (0 mM-8 mM).

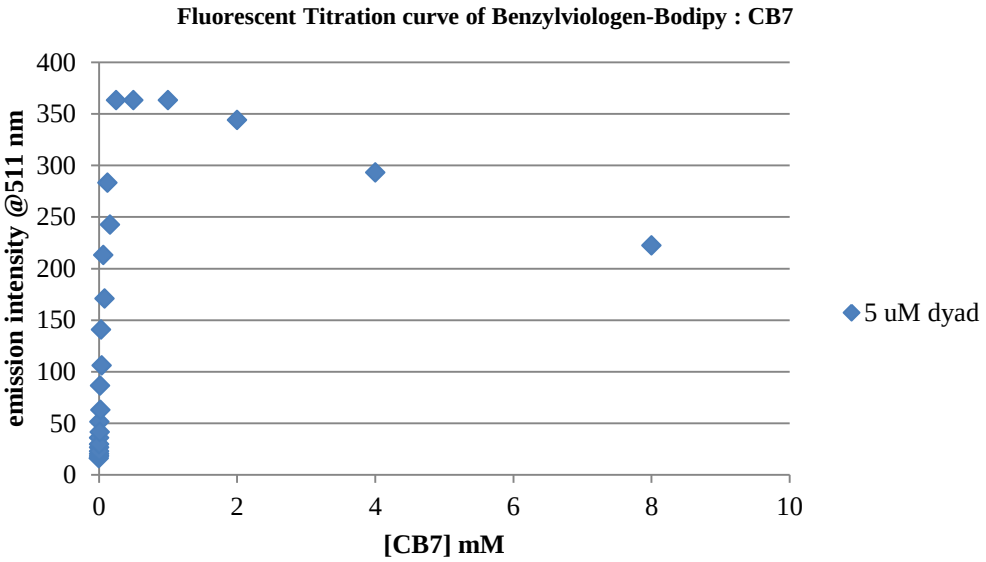

Figure 4.15. Fluorescence titration curve of benzylviologen- bodipy (5 μM) titrated with CB7 (0 mM to 8 mM) in water.

As anticipated, fluorescence titration curve analysis (Figure 4.15) shows 30 fold fluorescence enhancement on the addition of CB7 to the dyad. Emission data indicates the efficient quenching of dyad due to facilitation of electron transfer from the excited bodipy to proximate viologen in the absence of CB7. On the subsequent addition of CB7 fluorescence switches from off to on because of complexation between viologen and CB7 result in the prevention of electron transfer from excied bodipy to viologen. Efficient fluorescence recovery with low concentration CB7 (0.25 mM) indicates binding of CB7 with viologen only and negligible competitive binding with bodipy.

To gain more insight of nature of binding of CB7 with dyad as in Fig 4.5c, ^{1}H NMR titration experiments were performed where the concentration of benzylviologen-bodipy was kept constant and varied the concentration of CB7 from 0 to 2 molar equivalents in D_2O. Unlike the dyads **4.5a** and **4.5 b**, the ^{1}H NMR spectral titration of the dyad **4.5c** looked complicated. Several unsuccessful attempts were performed by increasing the concentration of dyad, and increasing acquisitions. No improvement on the quality of spectra could be due to limited solubility of bodipy in water. However, splitting of α and β protons of viologen signals at 8.5 and 9.4 into four distinct sets of signals (Figure 4.16) clearly supports the binding of CB7 to one pyridinium, proximate to the benzyl group at 0.5 molar

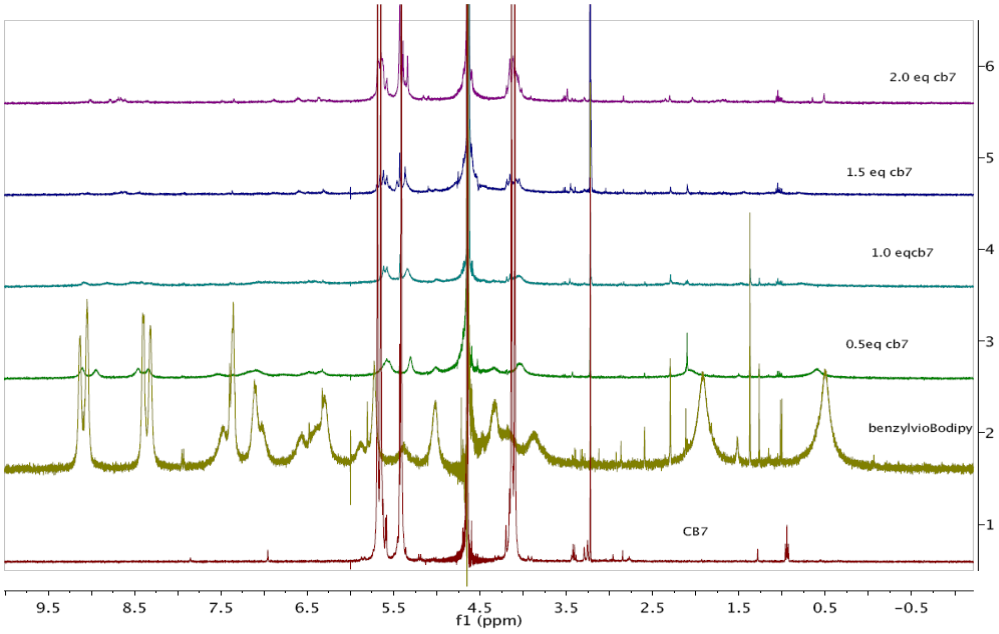

Figure 4.16. ^{1}H NMR spectra (300 MHz, D_2O) of benzylylviologen-bodipy dyad (3.9 mM) with CB7 (0 to 2 equivalent).

equiv. of CB7. This set of splitting signals indicates the slow exchange of included and free viologen of the dyad. The sharp upfield signal of sharp benzyl, proximate to viologen, at 7.5 ppm also supports binding of CB7 to the benzylviologen as shown in Figure 4.17.

Emission data of **4.5c** dyad was employed in curve fitting. The curve fits well with one binding site of dyad that is CB7 binds with only viologen and not with CB7. Binding constant of complexes between dyad **3.5c** and CB7 is 1.2 x 10^4 M^{-1}.

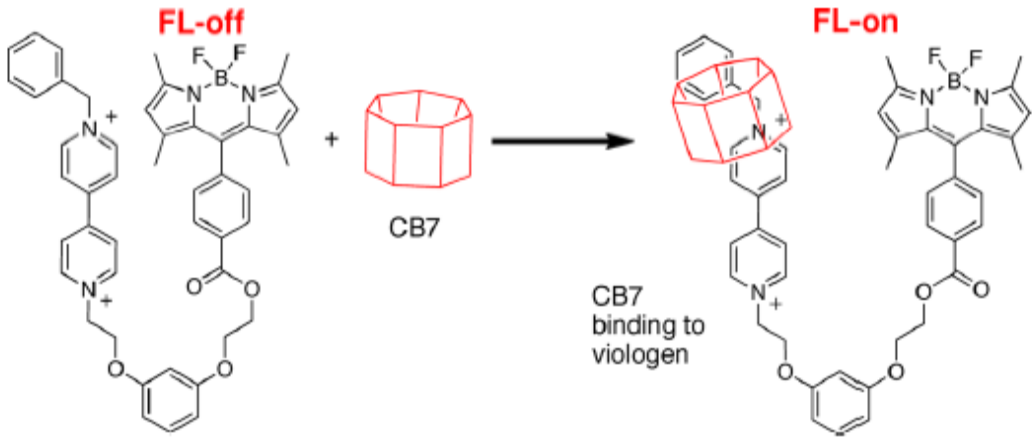

Figure 4.17. Binding of CB7 with benzylviologen of dyads **4.5c**. Diagram produced by Ronald L. Halterman.

This novel approach of tethering a fluorophore with a quencher can be utilized in the construction of sensors. A sensor with two binding sites for CB7 could be intially quenched due to electron transfer from an excited fluorophore to the proximate quencher. The recognition of analytes by receptor diminishes the

binding affinity of CB7 with its initial guest through external stimuli and results shuttling of CB7 to the second binding guest. This shuttling of CB7 switches the fluorescence of fluorophore from off to on. This approach is more attractive as signal unit is electronically independent to the recognition unit. Thus recognition unit can be explored without any change in signal unit and vice-versa. Such an extension of the fluorescence-on signaling will be developed in the followimg chapters.

4.4 Chapter Summary

The efficacy of switching the fluorescence from off to on state of viologen-fluorophore dyads upon addition of cucurbit[7]uril (CB7) was studied. This chapter explains our effort to develop fluorescence off-on signal transduction component which could have potential use in the construction of sensors. The three different dyads were successfully synthesized and characterized by performing NMR spectroscopy and mass spectrometry experiments. The efficiency of fluorescence off-on of dyads was investigated by measuring absorbance and emission dyads. The mode of binding of CB7 with dyads was examined by performing NMR titration experiments. The nature of complexes of dyad with CB7 was further investigated by curve fitting of emission data. Such curve fitting was also used to calculate the binding constant of CB7 and dyads.

Benzylviologen-bodipy dyad exhibits superior fluorescence off-on performance. Addition of CB7 to this dyad increases the emission intensity by 30

fold. Benzylviologen-rhodamineB dyad shows 14 fold enhancement upon binding with CB7. Both dyads indicates the strong binding ($K = 10^4\ M^{-1}$) order of benzylviologen with CB7. Binding of CB7 with only viologen is around $10^6\ M^{-1}$ which indicates the binding interaction between viologen and fluorophore of dyad is $10^2\ M^{-1}$ order. NMR titration data are also consistent with binding of CB7 with benzylviologen of both dyads. However, methylviologen-rhodamine B is able to enhance its fluorescence only by threefold. This could be due to lower viologen-CB7 binding due to limited hydrophobicity of methyl compare to benzyl, allowing rhodamine B to efficiently compete for binding with CB7 over methylviologen. Moreove, curve fitting analysis also supports for two binding events in methylviologen-rhodamineB dyad for CB7.

Finally, a highly efficient novel signal transduction unit was developed by employing a unique approach. The quenching of fluorophore continues until the binding event takes place. Since the signal unit is electronically independent to the recognition unit, recognition unit can be varied according to the analyte of interest without configuring the signal unit. The signal unit can also be varied by using the wide range of other fluorophores and suitable quencher. These features make this approach more promissing over classical photoinduced electron transfer sensors where fluorophore and receptors are electronically dependent.

4.5 Experimental

4.5.1 Experimental Procedures and Spectral Characterization of Synthesized Compounds.

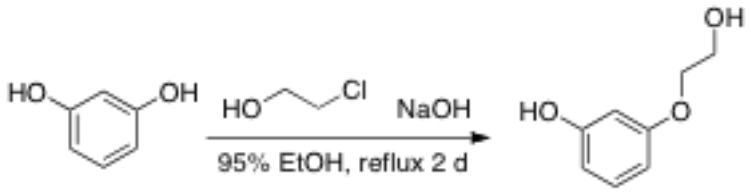

3-(2-Hydroxyethoxy)phenol. In a 250 mL reaction flask, resorcinol (16 g, 149 mmol), 2-chloroethanol (10 g, 124 mmol), sodium hydroxide (5.96 g, 149 mmol) and 95% ethanol (80 mL) were added. The suspension was heated at reflux for 2 d. The flask was cooled to room temperature and ethanol was removed via vacuum evaporation. The residue was extracted with ether (5 x 15 mL). The combined organic portion was dried over anhydrous $MgSO_4$. After filtration the solvent was removed via vacuum evaporation. The compound was purified by column chromatography (SiO_2, 2:1 to 1:1 hexane / ethyl actetate) to provide 3-(2-hydroxyethoxy)phenol (7.5 g, 39% yield) as a white solid. ^{1}H NMR (300 MHz, CD_3COCD_3): δ 8.29 (b, 1H), 7.06 (t, 1H, J = 9 Hz), 6.04 (m, 3H), 4.00 (t, 2H, J = 6 Hz), 3.80 (t, 2H, J = 3 Hz). $^{13}C\{^1H\}$ NMR (75 MHz, CD_3OCD_3): δ 160.47, 158.5, 129.8, 107.7, 105.5, 101.8, 69.4, 60.4. HRMS-ESI: *m/z* calcd for $C_8H_9O_3$ 153.0551; found 153.0557 $[M-H]^+$.

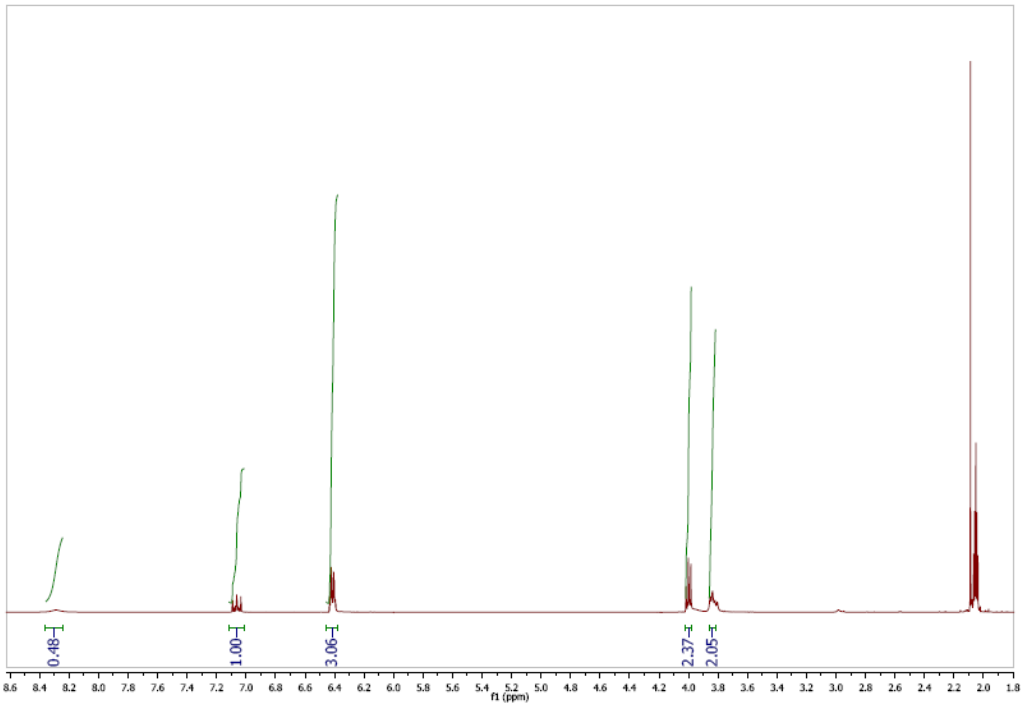

Figure 4.18a. ^{1}H NMR spectrum of **3-(2-Hydroxyethoxy)phenol**.

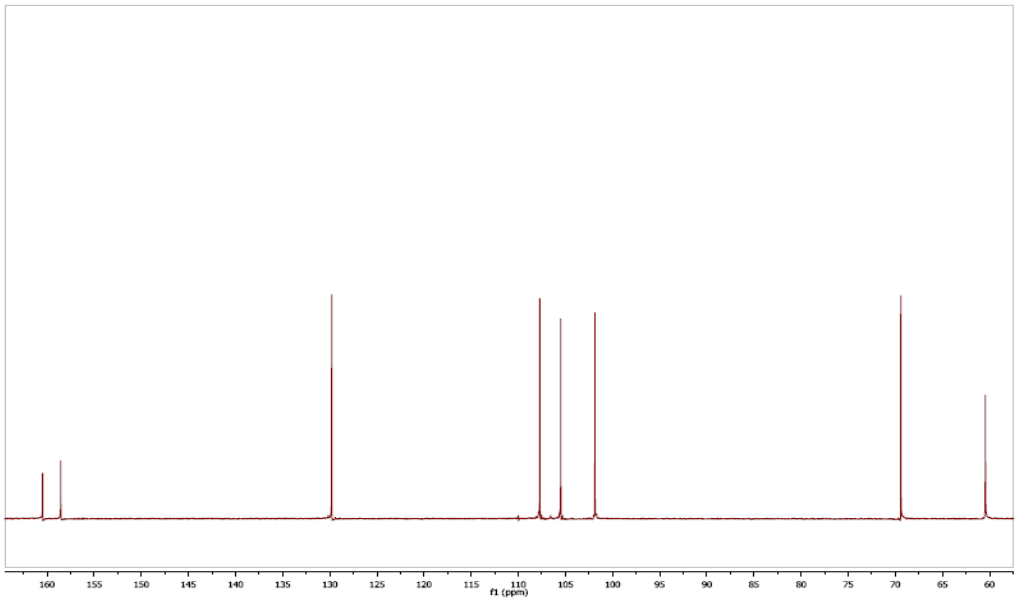

Figure 4.18b. ^{13}C NMR spectrum of **3-(2-Hydroxyethoxy)phenol**.

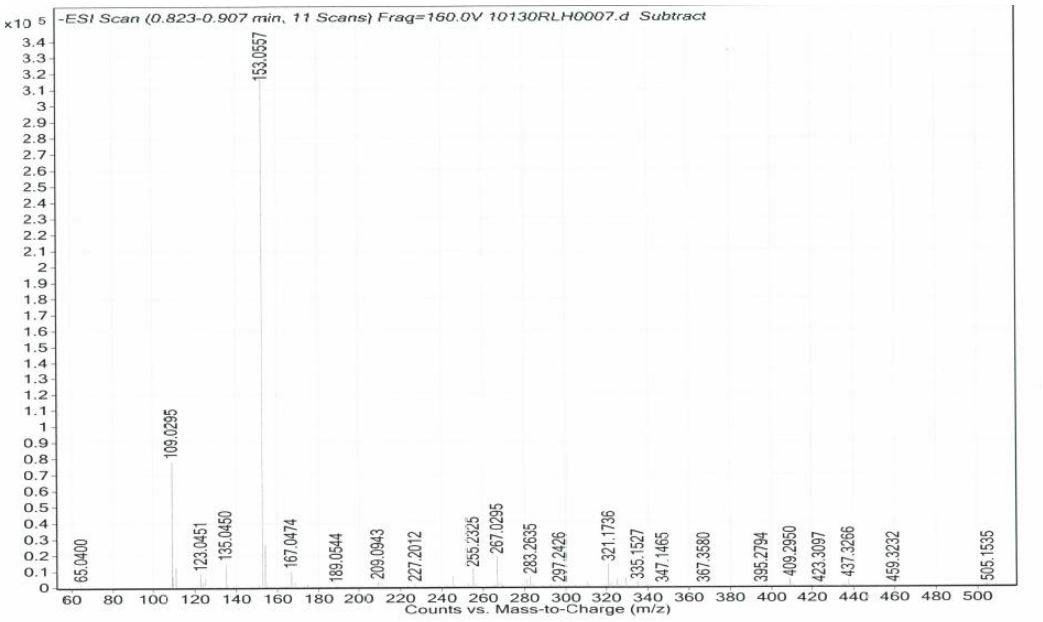

Figure 4.18c. Mass spectrum of **3-(2-Hydroxyethoxy)phenol**.

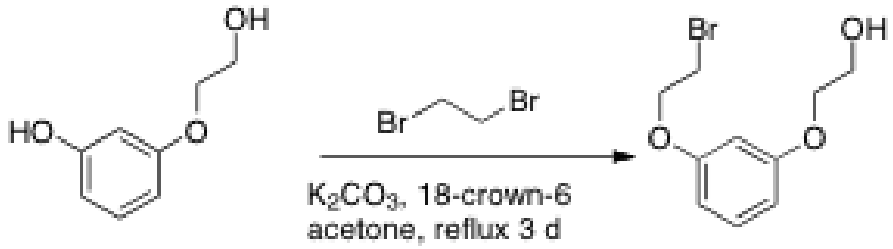

2-(3-(2-Bromoethoxy)phenoxy)ethanol (1). In a 100 mL reaction flask, 3-(2-hydroxyethoxy)phenol (1.2 g, 7.8 mmol), 1,2-dibromoethane (11.7 g , 62.4 mmol), potassium carbonate (2.2 g , 15.6 mmol), 18-crown-6 ether (0.211 g, 0.8 mmol) and acetone (40 mL) were added. The suspension was heated under reflux for 3 d. The flask was cooled to room temperature and acetone was removed via vacuum evaporation. The residue was extracted with dichloromethane (3 x 10 mL). The combined organic portion was washed with water (3 x 10 mL) and dried over anhydrous $MgSO_4$. After filtration the solvent was removed via vacuum

evaporation. The compound was purified by column chromatography (SiO_2, 2:1 to 1:1 hexane / ethyl acetate) to provide 2-(3-(2-bromoethoxy)phenoxy)ethanol (1.15 g, 57% yield) as a colorless oily liquid. ^{1}H NMR (300 MHz, CD_3COCD_3): δ 7.17 (t, 1H, J = 8.7 Hz), 6.57-6.52 (m, 3H), 4.34 (t, 2H, J = 6 Hz), 4.05 (t, 2H, J = 6 Hz), 3.80 (q, 2H, J = 6 Hz), 3.90 (t, 1H, J = 6 Hz), 3.70 (t, 2H, J = 6 Hz). ^{13}C{^{1}H} NMR (75 MHz, CD_3OCD_3): δ 160.4, 159.6, 129.9, 107.3, 106.7, 101.4, 69.6, 67.9, 60.4, 30.1. HRMS-ESI: *m/z* calcd for $C_{10}H_{14}BrO_3$ 261.0126; found 261.0118 $[M+H]^+$.

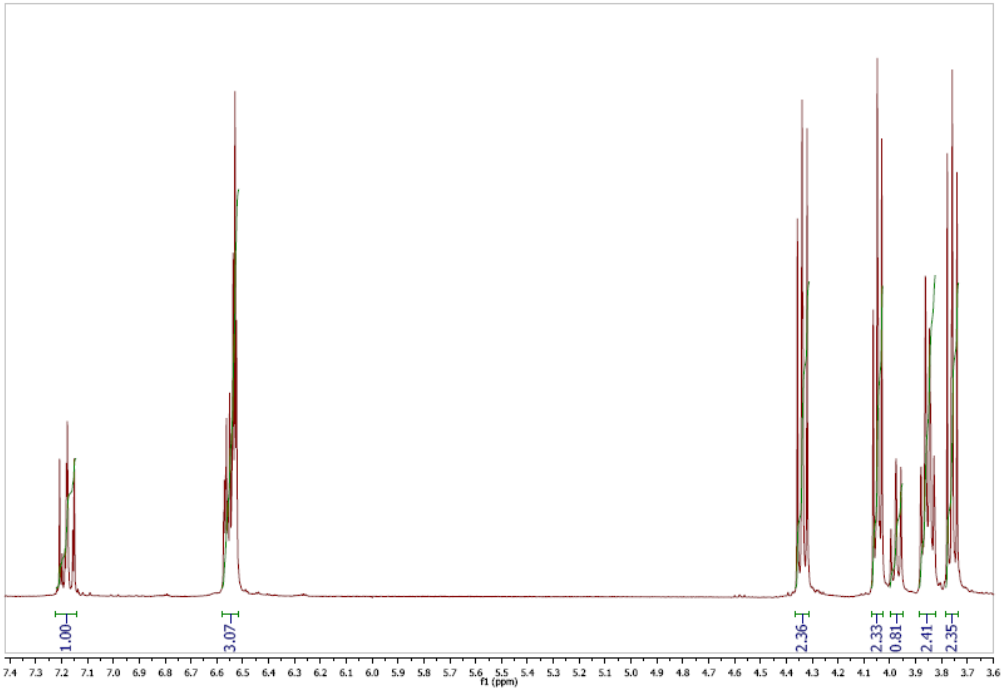

Figure 4.19a. ^{1}H NMR spectrum of **2-(3-(2-Bromoethoxy)phenoxy)ethanol (1).**

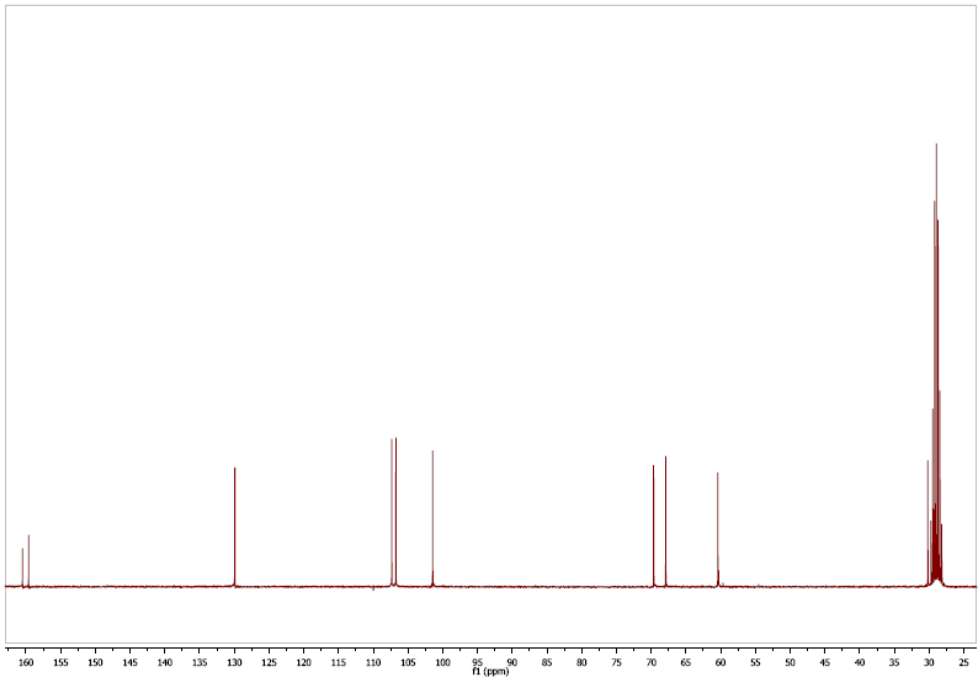

Figure 4.19b. ^{13}C NMR spectrum of **2-(3-(2-Bromoethoxy)phenoxy)ethanol (1).**

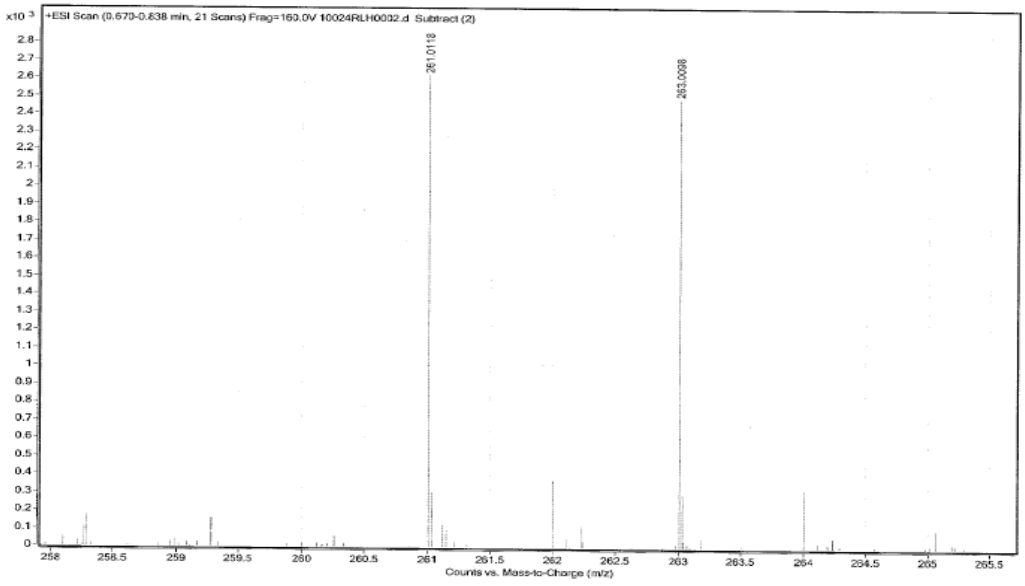

Figure 4.19c. Mass spectrum of **2-(3-(2-Bromoethoxy)phenoxy)ethanol (1).**

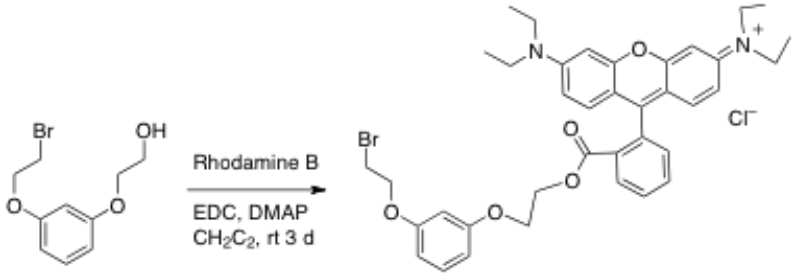

Rhodamine-B ester, 2: In a 100 mL reaction flask, rhodamine B (2.00 g, 4.2 mmol), 2-(3-(2-bromoethoxy)phenoxy)ethanol (1.20 g, 4.6 mmol), 1-ethyl-3-(3-dimethylaminopropyl)carbodiimide (1.2 g, 6.3 mmol), N.N-dimethylaminopyridine (77 mg, 0.63 mmol) and dichloromethane (20 mL) were added. The mixture was stirred for 3 d at room temperature. The solvent was removed via vacuum evaporation. The compound was purified by column chromatography (SiO_2, 99:1 CH_2Cl_2:CH_3OH) to provide Rhodamine- B ester **2** (930 mg, 31% yield) as a purple colored solid. ^{1} H NMR (300 MHz , $CDCl_3$): δ 8.3(dd, 1H, *J* = 7.8 Hz, 1.2 Hz), 7.71-7.81 (m, 2H), 7.3 (dd, 1H, *J = 7.8 Hz,* 1.2 Hz), 7.1 (t, 1H, J 9 Hz), 7.0 (d, 2H, J9Hz), 6.89(dd, 2H, *J = 9.3 Hz,* 2.1 Hz), 6.6 (d, 2H, J 3 Hz), 6.54 (dd, 1H, *J = 7.8 Hz,* 1.8 Hz), 6.3 (m, 2H), 4.32 (t, 2H, J 3 Hz), 4.24 (t, 2H, J 6 Hz), 3.84 (t, 2H, J 6 Hz),3.80(t, 2 H, 3 Hz), 3.59(q, 8H, J 6Hz), 1.3 (t, 12H, J 6Hz). ^{13}C NMR (75MHz , $CDCl_3$): δ 165.11, 159.53, 159.33, 158.29, 157.59, 155.41, 133.39, 133.24, 131.66, 131.27, 130.37, 130.20, 130.06, 129.67, 114.28, 113.54, 107.51, 106.91, 102.08, 96.32, 68.24, 65.68, 63.94, 53.44, 46.18, 42.32, 12.7; HRMS-ESI: *m/z* calcd for $[C_{38}H_{42}BrN_2O_5]^+$ 685.2277; found 685.2251 ($[M]^+$, 3%), 687.2246 ($[M^+ + 2]$, 3 %), 641.3 (100%).

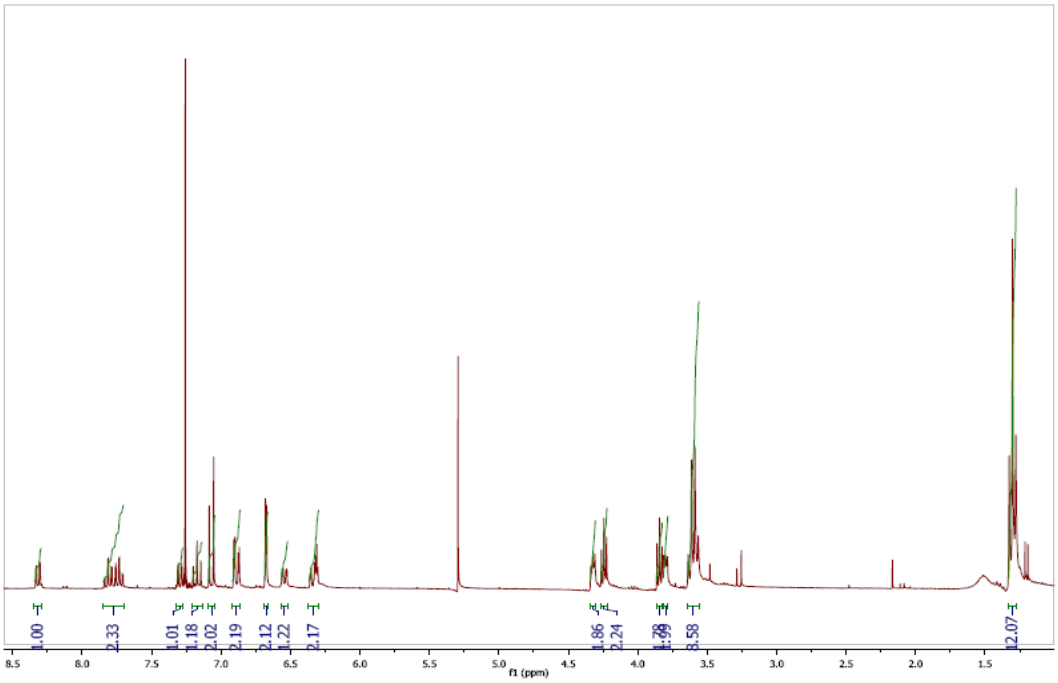

Figure 4.20a. ^{1}H NMR spectrum of **Rhodamine- B ester of 2-(3-(2-Bromoethoxy)phenoxy)ethanol (2).**

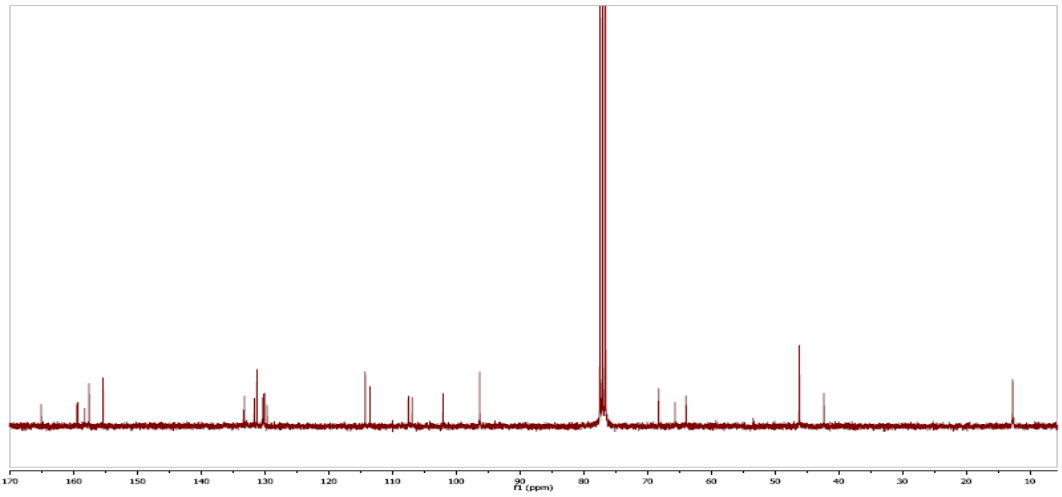

Figure 4.20b. ^{13}C NMR spectrum of **Rhodamine- B ester of 2-(3-(2-Bromoethoxy)phenoxy)ethanol (2).**

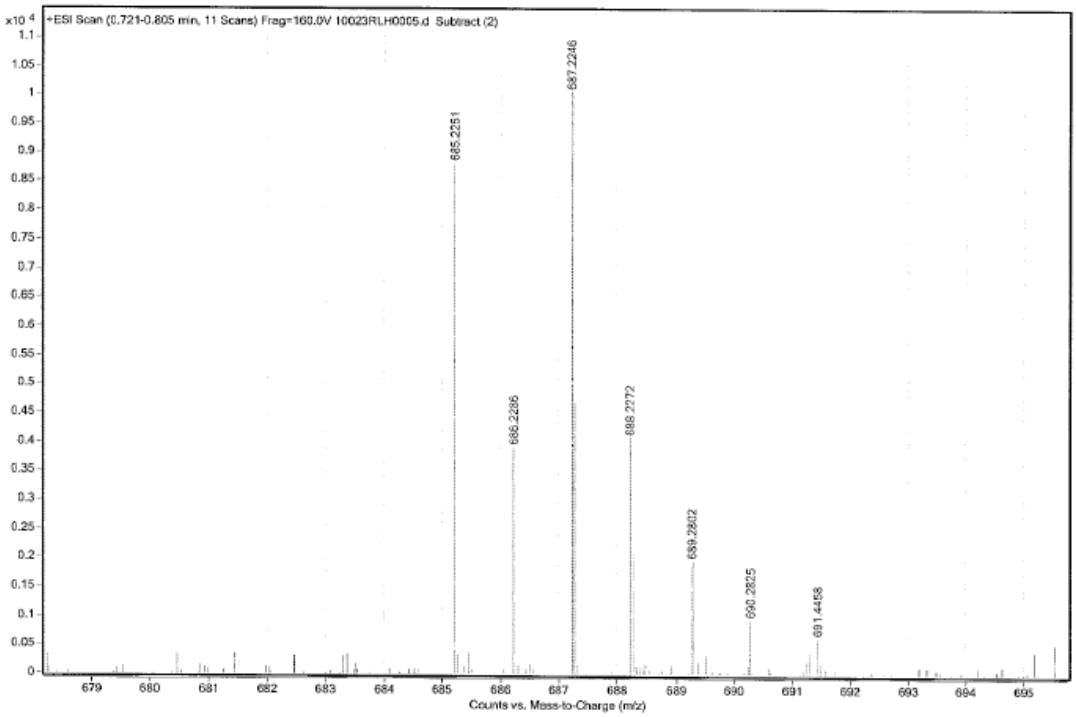

Figure 4.20c. Mass spectrum of **Rhodamine- B ester of 2-(3-(2-Bromoethoxy)phenoxy)ethanol (2).**

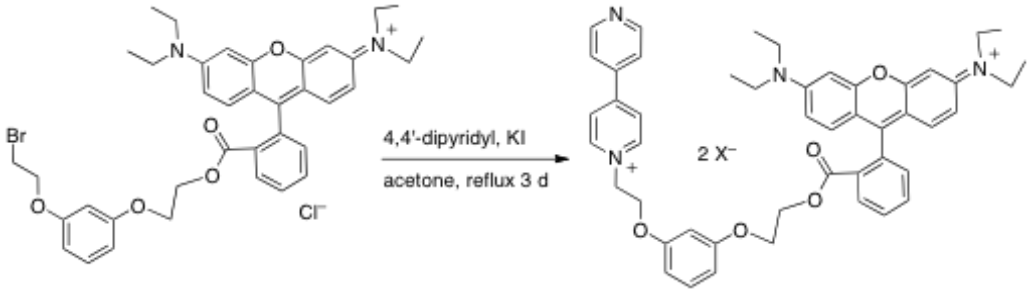

Dipyridyl-rhodamine B ester. In a 100 mL reaction flask, rhodamine B ester (65 mg, 0.09 mmol), 4, 4' dipyridyl (112 mg, 0.72 mmol), potassium iodide (15 mg, 0.09 mmol) and acetone (25 mL) were added. The suspension was refluxed for 3 d. The flask was cooled and acetone was removed via vacuum evaporation. The compound was purified by column chromatography (SiO_2, 9:1 to 8:2 CH_2Cl_2:

CH_3OH) to provide dipyridyl-rhodamine- B ester (80 mg, 96% yield) as a purple colored waxy solid (counter ion not determined). [1] H NMR (300 MHz , CD_3OD): δ 9.2 (d, 2H, *J* = 6Hz), 8.8 (dd, 2H, *J* = 4.8 Hz, 1.8 Hz), 8.6 (d, 2H, *J* = 9Hz), 8.3(dd, 1 H, *J* = 7.8 Hz, 1.8 Hz), 8.0 (dd, 2H, *J* = 4.8 Hz, 1.8 Hz), 7.8 (m, 2H), 7.41(dd, 1H, *J* = 3Hz), 7.15(t, 1H, *J* = 9Hz), 7.1 (d, 2H, *J* = 9Hz), 7.0 (m, 2H), 6.8(2H, d, *J* = 3Hz), 6.6 (dd, 1H, *J* = 8.4 Hz, 2.4 Hz), 6.37(t, 1H, *J* = 3Hz), 6.32(dd, 1H, *J* = 8.4 Hz, 2.4 Hz), 5.15 (t, 2H, *J* 6Hz), 4.58(t, 2H, *J* = 3Hz), 4.24(m, 2H), 3.7 (t, 2H, *J* = 3Hz), 3.6 (q, 8H, *J* = 9 Hz), 1.2 (t, 12H, *J* =6Hz). ^{13}C NMR (75MHz, CD3OD): *δ* 165.25, 159.73, 158.70, 158.37, 157.74, 155.53, 154.10, 150.4, 145.9, 142.12, 133.39, 132.79, 131.07, 130.92, 130.2, 130.05, 129.79, 125.65, 122.23, 114.09, 113.38, 108.13, 106.49, 101.19, 95.85,66.18, 65.73, 63.65,60.45, 45.45, 11.49. HRMS-ESI: *m/z* calcd for $[C_{48}H_{50}N_4O_5]^{++}$ 381.1890; found 381.1886 ($[M^{2+}]^{2+}$, 305.2(22%), 261 (29%), 217(29%).

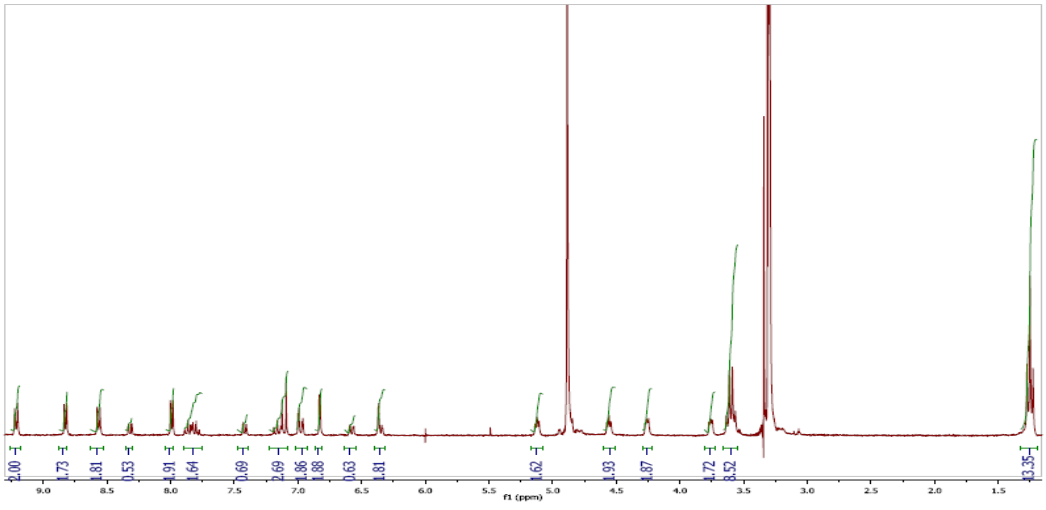

Figure 4.21a. [1]H NMR spectrum of **Dipyridyl-rhodamine B ester, 2.**

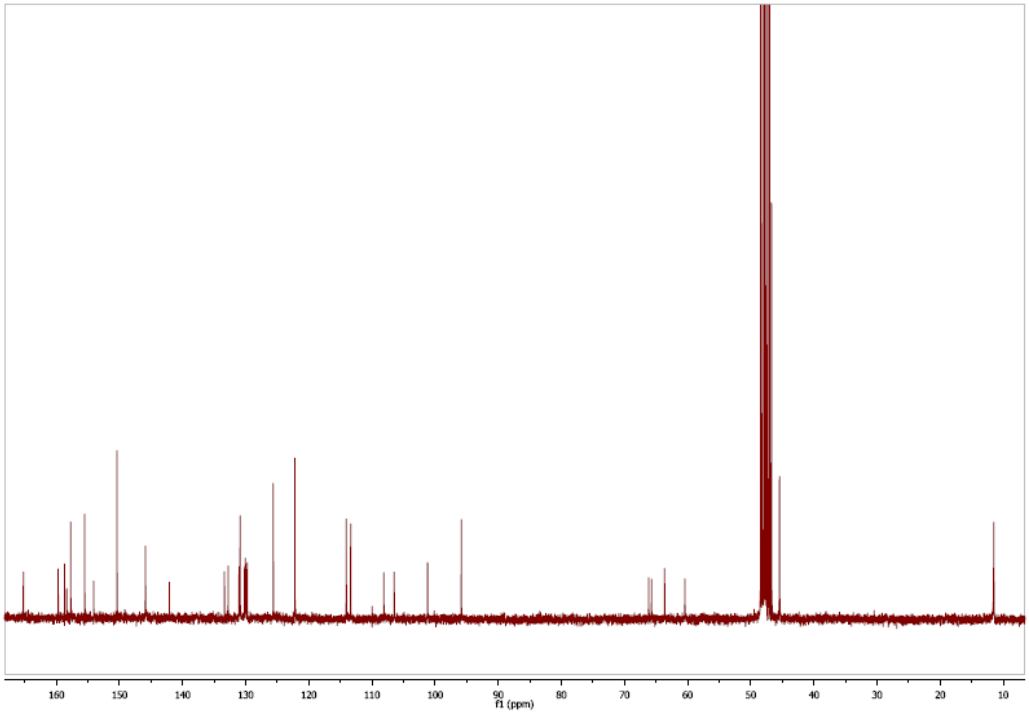

Figure 4.21b. ^{13}C NMR spectrum of **Dipyridyl-rhodamine B ester, 2.**

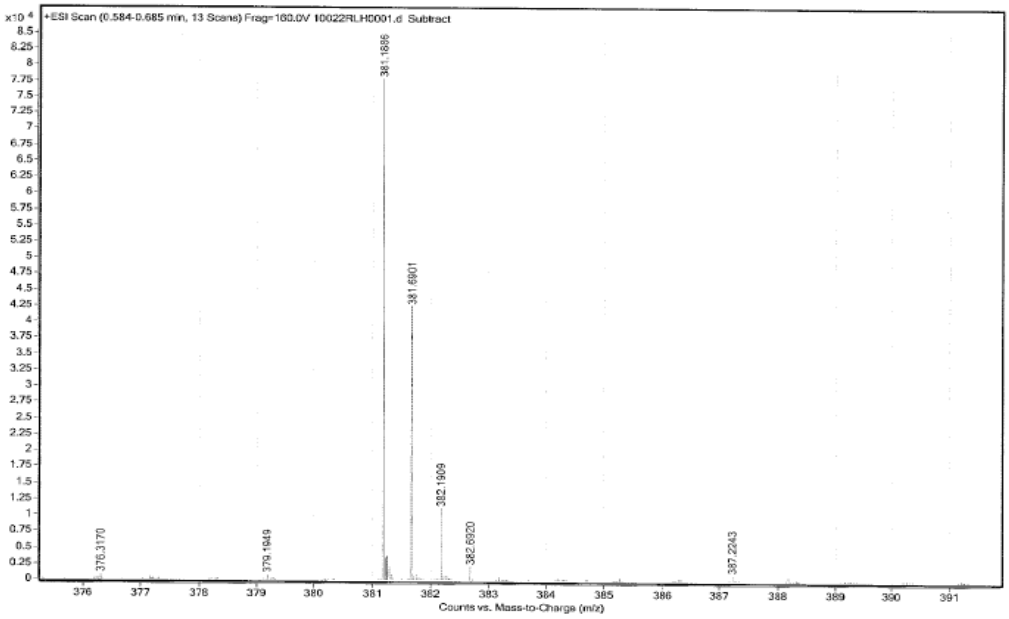

Figure 4.21c. Mass spectrum of **Dipyridyl-rhodamine B ester, 2.**

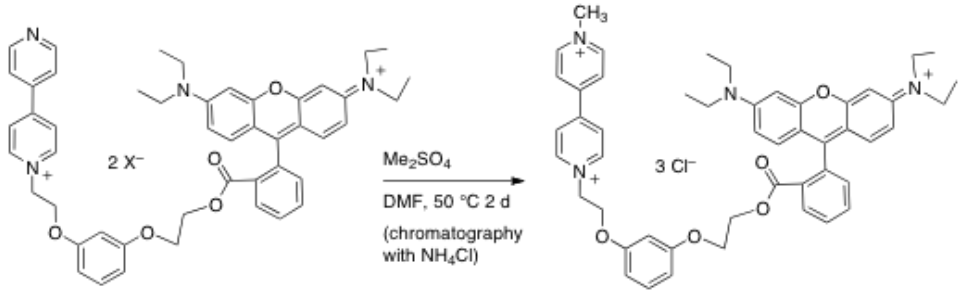

Methylviologen-rhodamine dyad 4.5a. In a 100 mL reaction flask, dipyridyl-rhodamine B ester (60 mg, 0.06 mmol), dimethyl sulfate (38 mg, 0.3 mmol) and DMF (4 mL) were added. The solution was heated at 50 ^{0}C for 2 d. The flask was cooled and DMF was removed via vacuum evaporation. The compound was purified by running column chromatography (SiO_2, 5:5 acetone: (7:2:1 Me OH:2MNH4Cl:CH_3NO_2) to provide methylviologen-rhodamine complex (40 mg, 74% yield) as a purple waxy solid. ^{1} H NMR (300 MHz, CD_3COCD_3,): δ 9.3 (d, 2H, J 9 Hz), 9.15 (d, 2H, J 6Hz), 8.7 (d, 2H, *J* = 6Hz), 8.6 (d, 2H, *J* = 9 Hz), 8.3 (d, 1H, *J* = 6Hz), 7.7-7.8 (m, 2H), 7.42 (dd, 1H, *J* = 7.8 Hz, 1.2 Hz), 7.15 (t, 1H, *J* = 9Hz), 7.1(d, 2H, *J* = 9Hz), 6.9 (m, 2H), 6.82 (d, 2H, *J* = 3Hz), 6.59 (dd, 1H, *J* = 7.5 Hz, 3 Hz), 6.3 (m, 2H), 5.2 (t, 2H, *J* = 3Hz), 4.56 (t, 2H, *J* = 6Hz), 4.52 (s, 3H), 4.25 (t, 2H, *J* = 6Hz), 3.7 (t, 2H, *J* = 3Hz), 3.6 (q, 8H, *J* = 6Hz), 1.2 (t, 12H, *J* = 6Hz). ^{13}C NMR (75MHz, CD3OD): δ 165.19, 159.73, 158.67, 158.46, 157.77, 155.58, 146.59, 146.41, 133.45, 132.82, 131.04, 130.9, 130.2, 130.08, 129.96, 129.82, 126.7, 126.54, 114.02, 113.38, 107.95, 106.59, 101.13, 95.8, 80.48, 67.69, 67.13, 66.03, 65.57, 63.65, 60.94, 45.42, 22.36, 11.45. HRMS-ESI: *m/z* calcd for $[C_{49}H_{53}N_4O_5]^{+++}$ 259.1338; found 259.1344 ($[M^{3+}]$, 100%), 388.7001 ($[M^{3+}]^{2+}$, 63%), 404.2 (63%), 578.2774 (47%), 198.1 (58%), 171.1(58%).

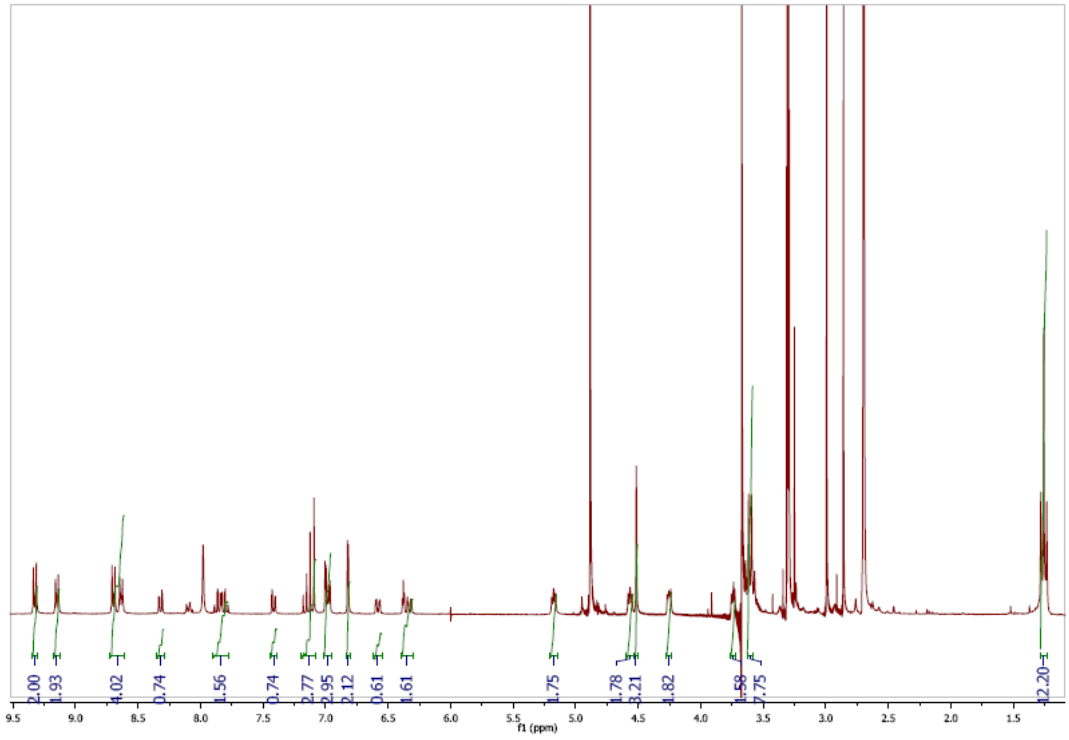

Figure 4.22a. ^{1}H NMR spectrum of **Methylviologen-rhodamine dyad 4.5a.**

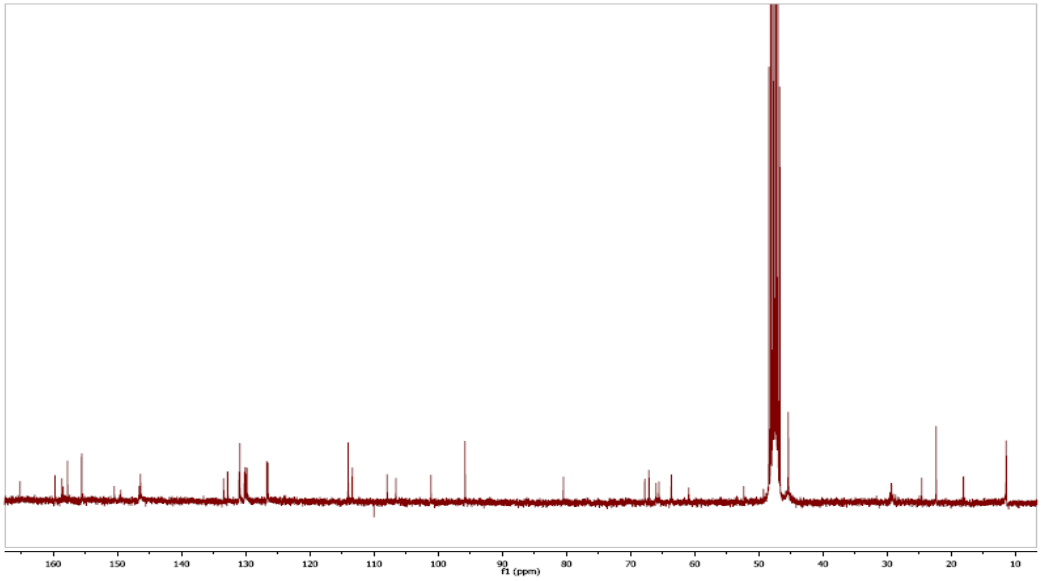

Figure 4.22b. ^{13}C NMR spectrum of **Methylviologen-rhodamine dyad 4.5a.**

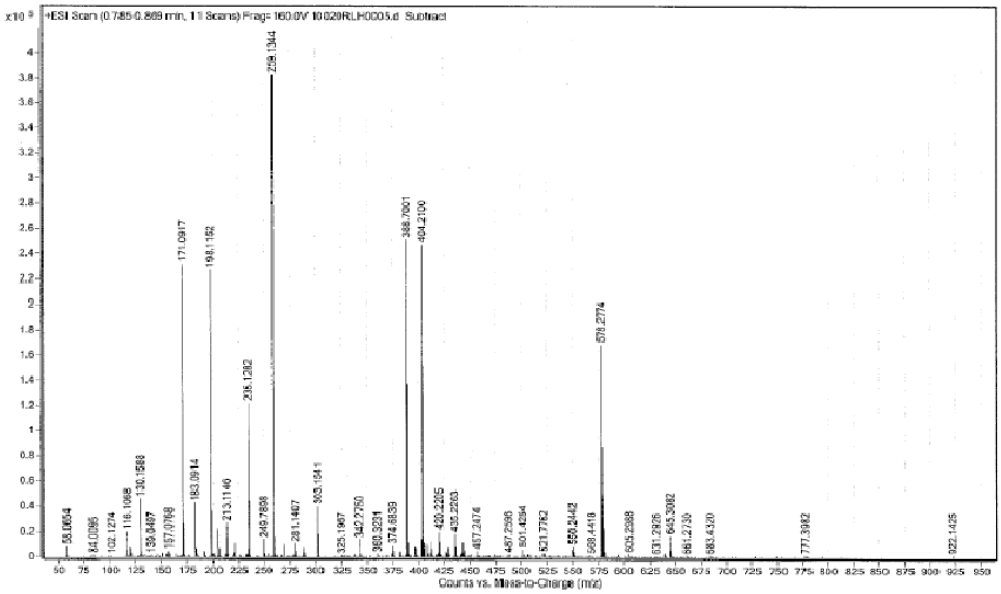

Figure 4.22c. Mass spectra of **Methylviologen-rhodamine dyad 4.5a.**

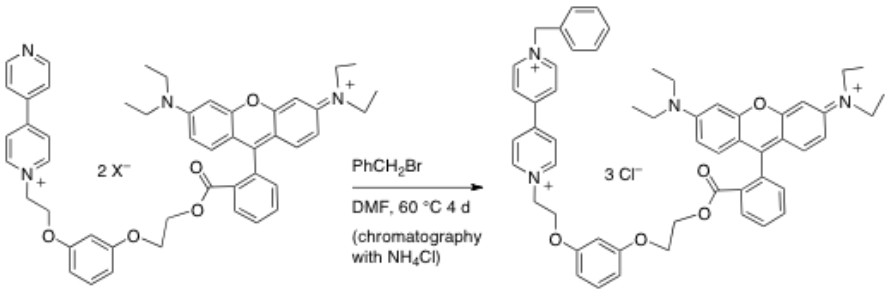

Benzylviologen-rhodamine B dyad 4.5b: In a 100 mL reaction flask, dipyridyl-rhodamine B ester (216 mg, 0.23 mmol), benzyl bromide (200 mg, 1.2 mmol) and DMF (8 mL) were added. The mixture was heated at 60 ^{o}C for 4 d. The flask was cooled and DMF was removed via vacuum evaporation. After separation by column chromatography [SiO_2, 5:5 acetone: (7 : 2 : 1 MeOH : 2M NH_4Cl : CH_3NO_2)] and vacuum evaporation of the solvent, the residue was partially dissolved in dichloromethane to remove ammonium chloride. Evaporation of the

soluble portion provided benzylviologen-rhodamine dyad as a purple waxy solid (171 mg, 67% yield). ^{1}H NMR (300 MHz, CD_3COCD_3): δ 9.4 (t, 4 H, J = 9 Hz), 8.7 (t, 4 H, J = 9 Hz), 8.3 (dd, 1H, J = 1.2 Hz, 7.8 Hz), 7.80-7.87 (m, 2 H), 7.6(m, 2 H), 7.4-7.5 (m, 3 H), 7.4 (d, 1 H, J = 6 Hz), 7.15 (t, 1, J = 6 Hz), 7.1(d, 2 H, J = 9 Hz), 7.0 (dd, 2H, J = 9.3 Hz, 2.4 Hz), 6.82 (d, 2 H, J = 3Hz), 6.6 (dd, 1H, J = 8.4 Hz, 1.8 Hz), 6.37 (t, 1H, J = 3 Hz), 6.32 (dd, 1H, J = 8.1 Hz, 1.8 Hz), 6.01 (s, 2 H), 5.2 (b, 2 H), 4.6 (b, 2 H), 4.2 (b, 2 H), 3.7 (b, 2 H), 3.5 (q, 8 H, J = Hz), 1.2 (t, 12 H, J = 9 Hz). ^{13}C NMR (75 MHz, CD_3OD): δ 165.24, 159.7, 158.69, 158.35, 157.74, 155.55, 150.33, 150.16, 146.44, 145.66, 133.4, 133.01, 132.85, 131.07, 130.92, 130.23, 130.097, 129.97, 129.79, 129.38, 129.12, 127.22, 126.83, 114.10, 113.38, 108.077, 106.56, 101.13, 95.86, 66.12, 65.6, 64.4, 63.7, 60.95, 53.53, 45.46, 11.54. HRMS-ESI: *m/z* calcd for $[C_{48}H_{50}N_4O_5]^{++}$ 381.1890; found 381.1895 ($[M^{2+} - H]^{2+}$, 100%), 426.7 ($[M^{3+}-H]^{2+}$, 33%), 259.1 ($[M^{3+}]$, 39%), 578.2 (44%).

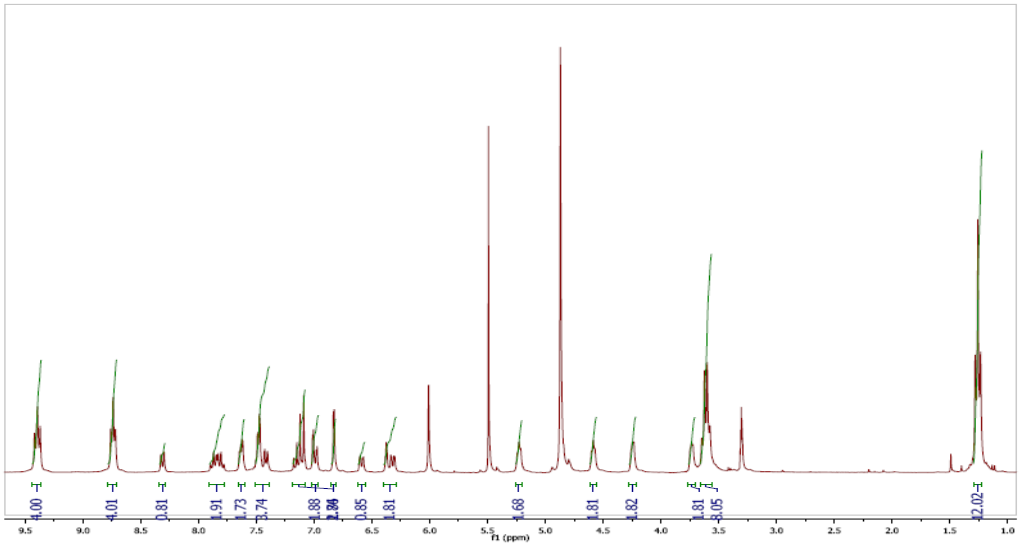

Figure 4.23a. ^{1}H NMR spectrum of **Benzylviologen-rhodamine dyad 4.5b.**

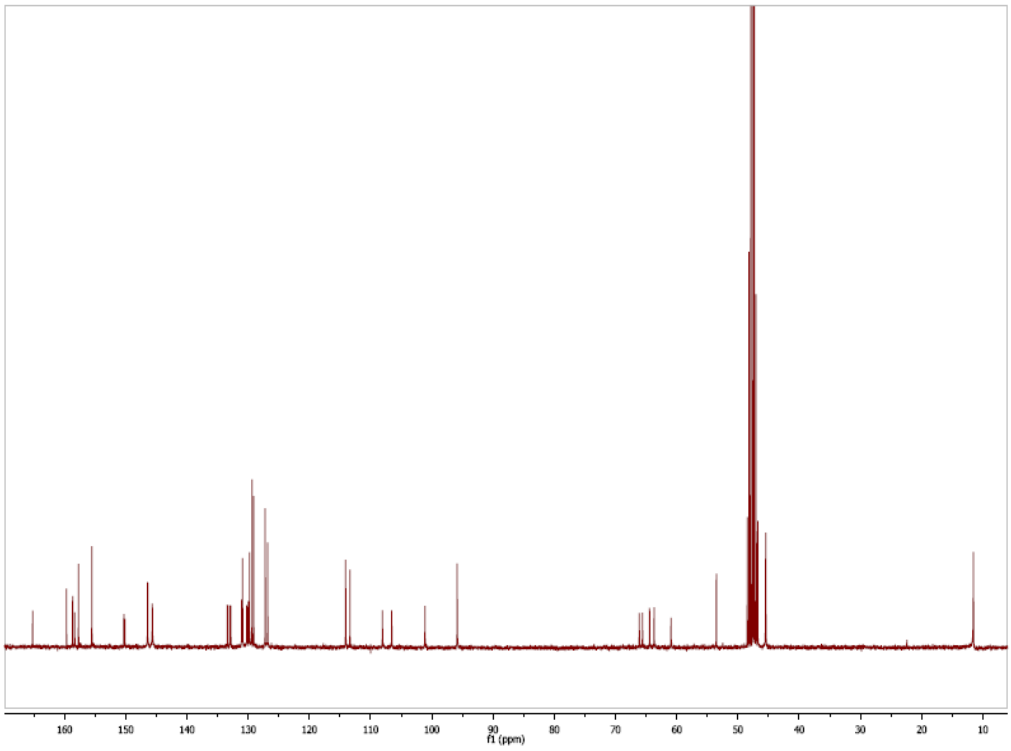

Figure 4.23b. ^{13}C NMR spectrum of **Benzylviologen-rhodamine dyad 4.5b.**

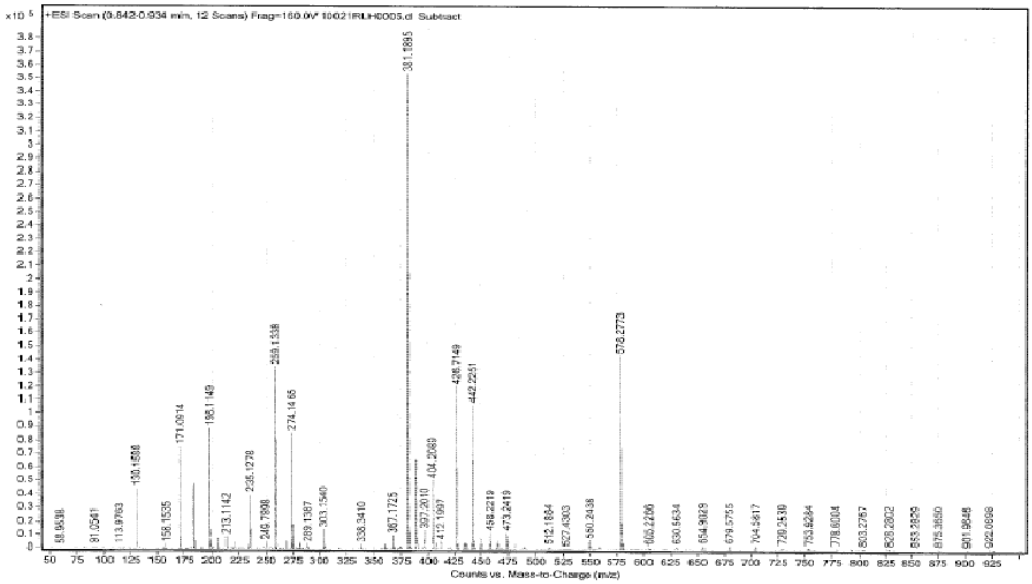

Figure 4.23c. Mass spectra of **Benzylviologen-rhodamine dyad 4.5b.**

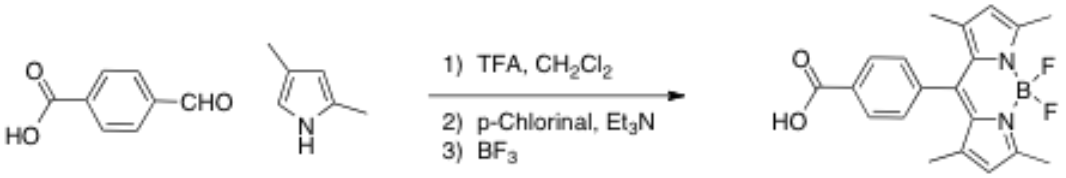

(4-Carboxyphenyl)BODIPY.[1] In a 250 mL reaction flask, 4-formylbenzoic acid (3.7 g, 24.7 mmol), 2,4 dimethylpyrrole (4.7 g, 49.4 mmol) and dichloromethane (35 mL) were added. The mixture was stirred for 20 min at room temperature under nitrogen. Trifluoroacetic acid (0.2 mL) was added and stirred overnight. To the reaction mixture chlorinal (12 g , 49.4 mmol) was added with continuous stirring. After 4 h, triethylamine (29 mL) was added and stirred for 30 min. Boron trifluoride (29 mL) was added and stirred for another 4 h. The mixture was diluted with water (50 mL) and extracted with dichloromethane (6 x 20 mL). The combined organic phase was dried over anhydrous Na_2SO_4 and filtered. The solvent of the filtrate was removed via vacuum evaporation. The compound was purified by column chromatography (SiO_2, 3:1 hexane / ethyl acetate) to provide (4-carboxyphenyl)bodipy (2.807 g, 31% yield) as a brown colored solid. ^{1}H NMR (300 MHz, $CDCl_3$): δ 8.24 (d, 2H, J = 8.1 Hz), 7.46 (d, 2H, J = 8.1 Hz), 6.00 (s, 2H), 2.57 (s, 6H), 1.37 (s, 6H). $^{13}C\{^1H\}$ NMR (75 MHz, $CDCl_3$) δ 143.3, 130.9, 128.5, 121.6, 118.7, 14.6. HRMS-ESI: *m/z* calcd for $C_{20}H_{20}BF_2N_2O_2$ 369.1584; found 369.1581 $[M+H]^+$ (21% intensity), calcd for $C_{20}H_{19}BF_2N_2O_2$ 368.1874; found 368.1575 ($[M]^+$, 5% intensity), 349.2 ($[M-F]^+$, 24%), 282.3 (22%), 116.1 (100%), 144.1 (62%).

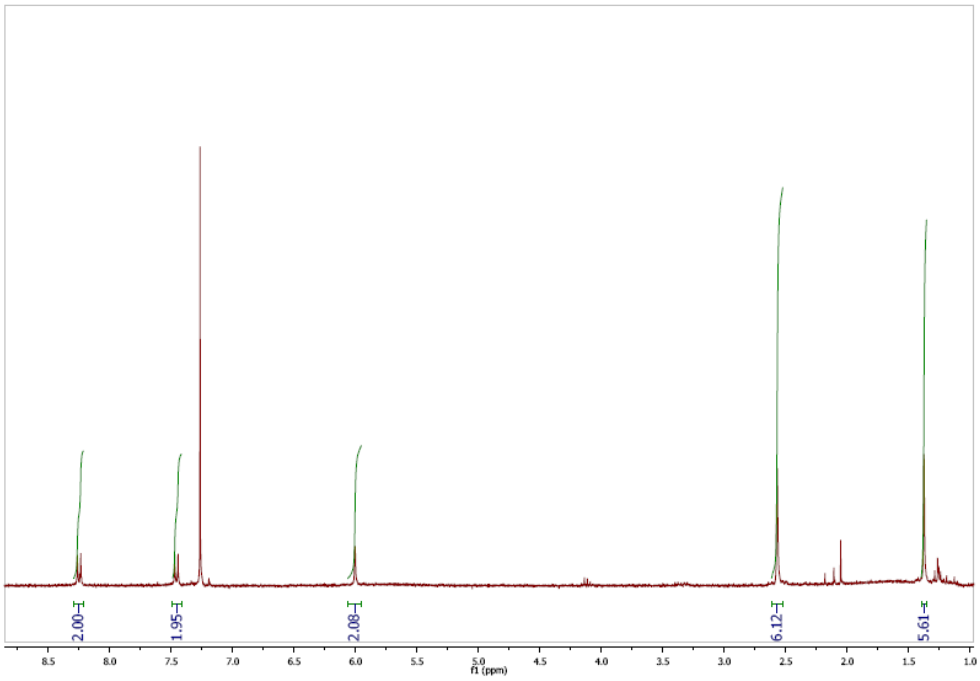

Figure 4.24a. ^{1}H NMR spectrum of (**4-Carboxyphenyl)BODIPY.**

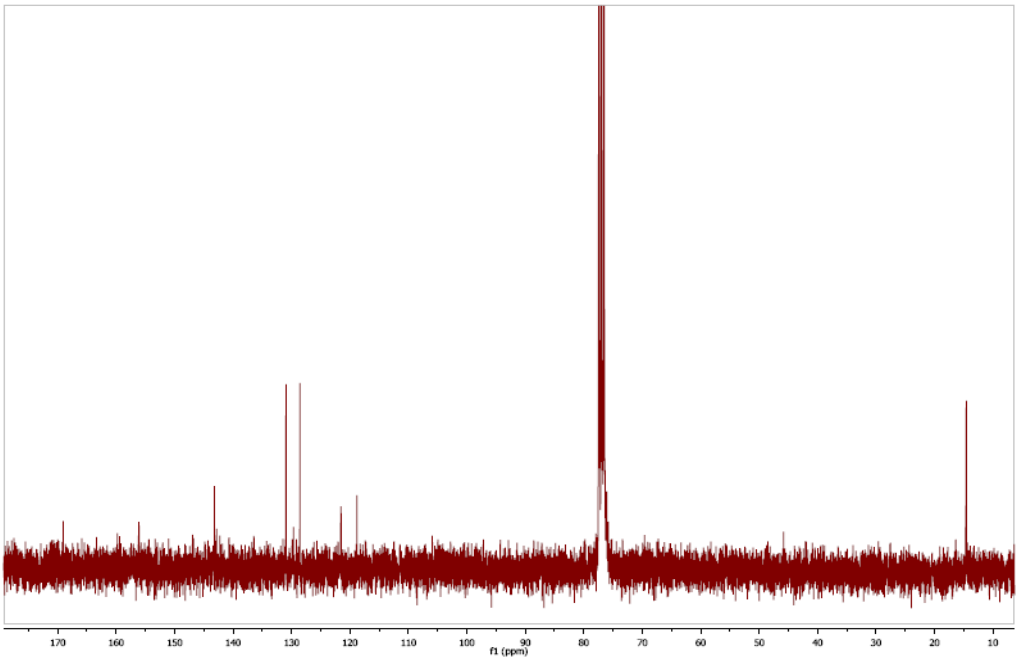

Figure 4.24b. ^{13}C NMR spectrum of (**4-Carboxyphenyl)BODIPY.**

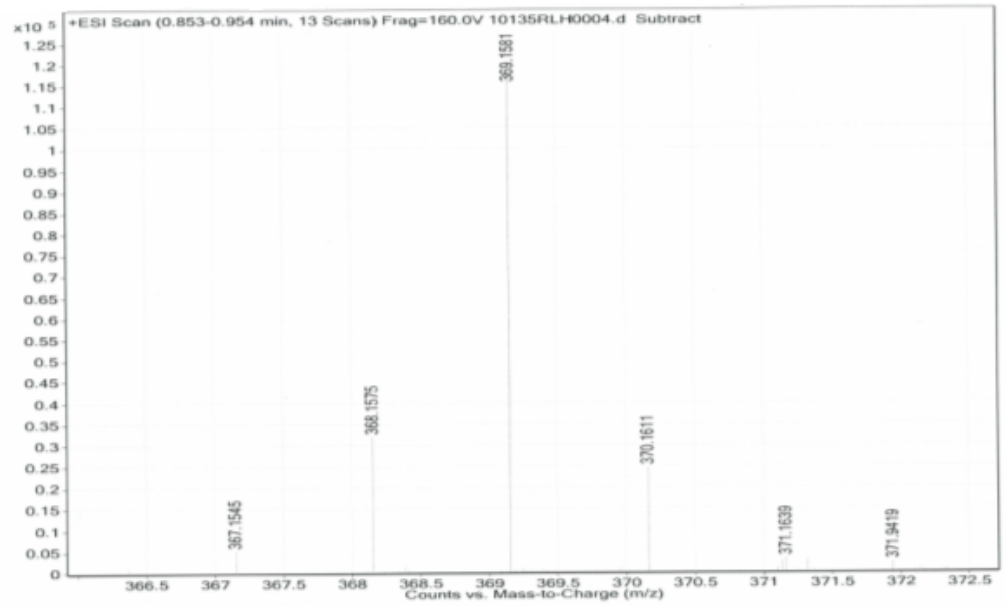

Figure 4.24c. Mass spectra of (**4-Carboxyphenyl)BODIPY.**

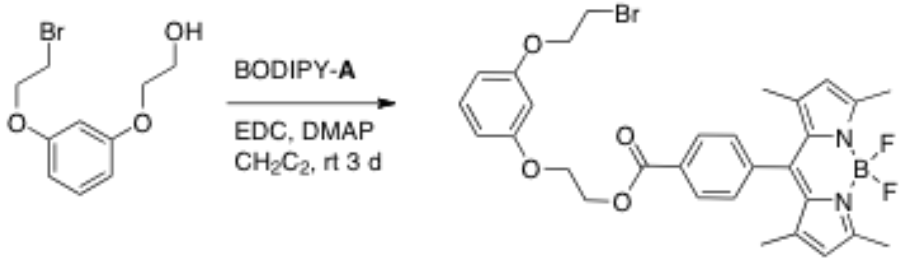

BODIPY ester. In a 100 mL reaction flask, (4-carboxyyphenyl)bodipy (500 mg, 1.36 mmol), 2-(3-(2-bromoethoxy) phenoxy)ethanol (391 mg, 1.5 mmol), 1-ethyl-3-(3-dimethylaminopropyl)carbodiimide (391 mg, 2.04 mmol), *N*,*N*-dimethylaminopyridine (25 mg, 0.204 mmol) and dichloromethane (15 mL) were added. The mixture was stirred for 3 d at room temperature. The solvent was removed via vacuum evaporation. The compound was purified by column chromatography (SiO_2, 3:1 hexane / EtOAc) to provide BODIPY ester (302 mg,

36% yield) as an orange solid. ^{1} H NMR (300 MHz, $CDCl_3$): δ 8.20 (d, 2H, J = 8.1 Hz), 7.40 (d, 2H, J = 8.1 Hz), 7.22 (t, 1H, J = 5.4 Hz), 6.50 (m, 3H), 5.95 (s, 2H), 4.70 (t, 2H, J = 4.5 Hz), 4.30 (t, 2H, J = 3 Hz), 4.20 (m, 2H), 3.40 (t, 2H, J = 6 Hz), 2.55 (s, 6H), 1.35 (s, 6H). $^{13}C\{^{1}H\}$ NMR (75 MHz, $CDCl_3$): δ 164.8, 158.6, 158.13, 154.9, 141.8, 139.0, 138.9, 129.8, 129.4, 129.4, 129.2, 129.1, 120.4,127.3, 106.4,106.3,106.2, 101.0,100.9, 67.5, 66.9, 64.8, 62.6, 13.5, 13.5. HRMS-ESI: *m/z* calcd for $[C_{21}\ H_{21}BF_2N_2O_2\ ]^{+}$ 382.1664 ; found 382.1664 , (46%), 156.1 (93%) , 124.0757 (100%), 382.2 (46%).

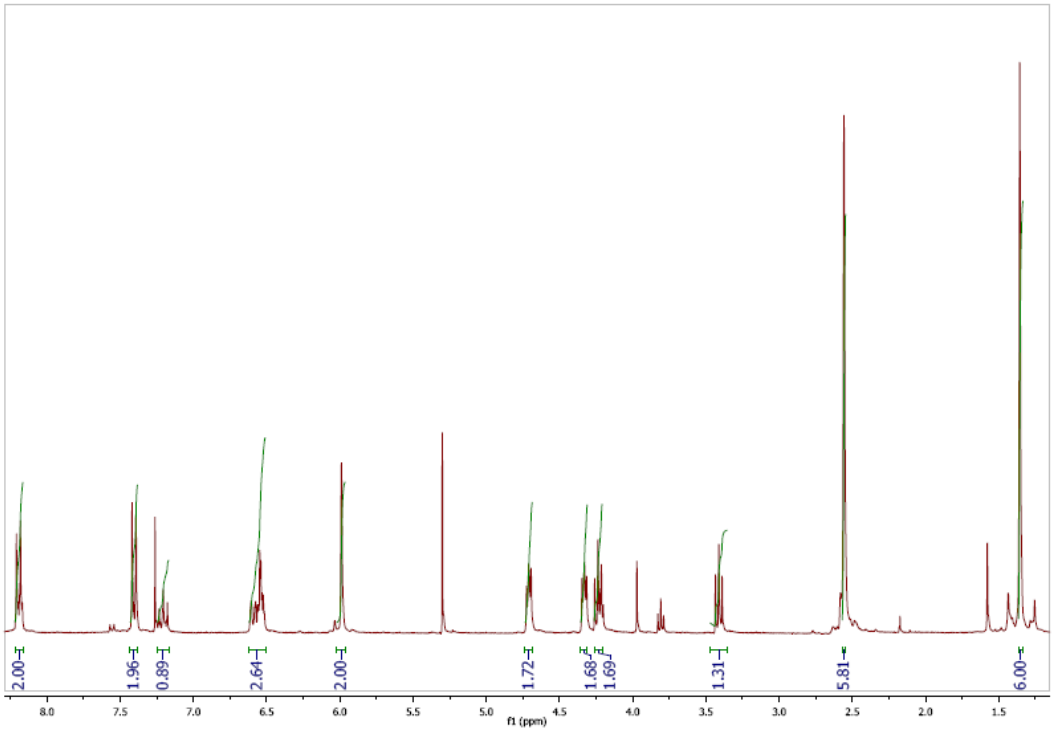

Figure 4.25a. ^{1}H NMR spectrum of **BODIPY ester of 2-(3-(2-bromoethoxy) phenoxy)ethanol.**

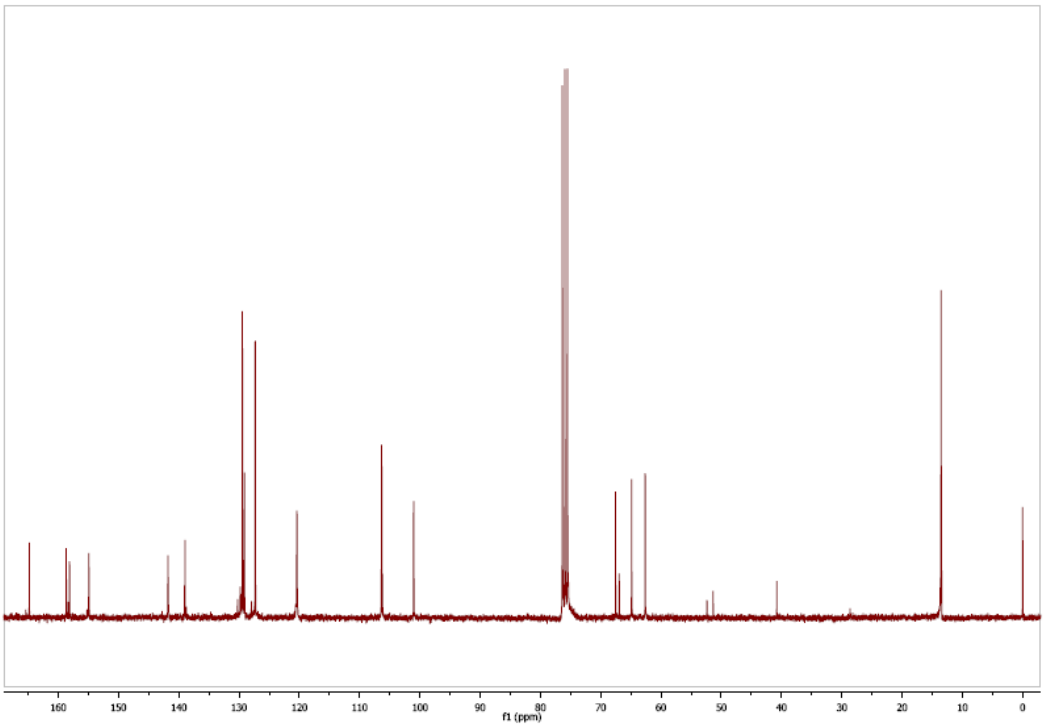

Figure 4.25b. ^{13}C NMR spectrum of **BODIPY ester of 2-(3-(2-bromoethoxy) phenoxy)ethanol.**

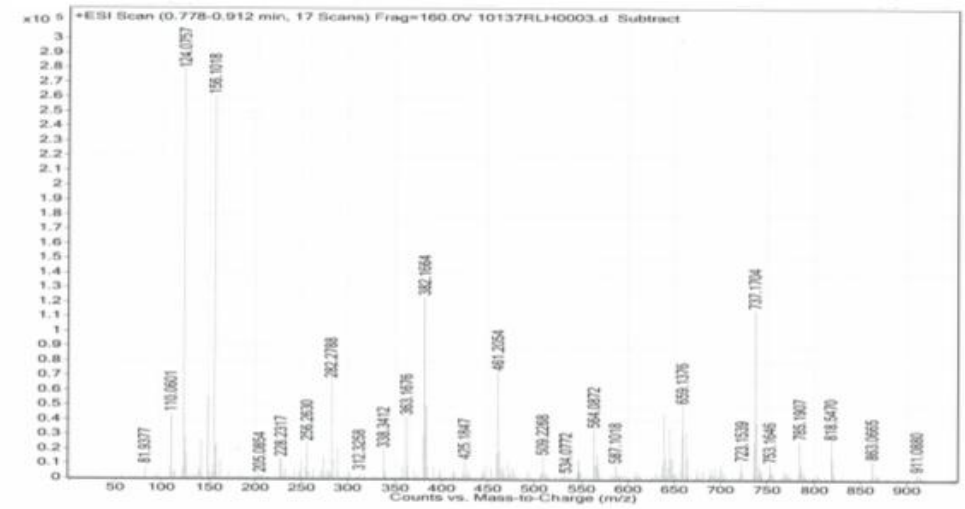

Figure 4.25c. Mass spectrum of **BODIPY ester of 2-(3-(2-bromoethoxy) phenoxy)ethanol.**

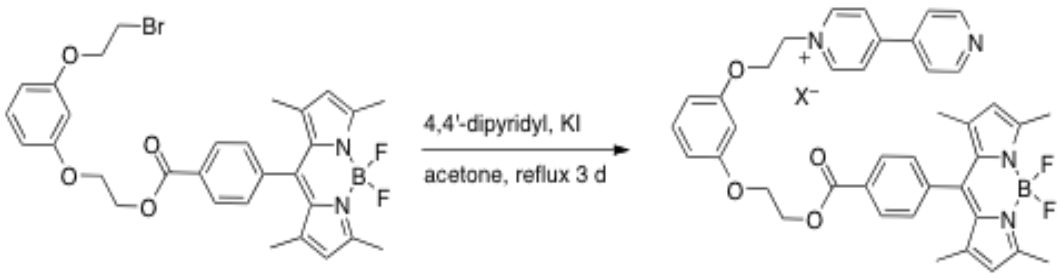

Monocationic dipyridyl-BODIPY. In a 100 mL reaction flask, BODIPY ester (302 mg, 0.5 mmol), 4, 4'-dipyridyl (390 mg, 2.5 mmol), potassium iodide (83 mg, 0.5 mmol) and acetone (15 mL) were added. The suspension was heated under reflux for 3 d. The flask was cooled to room temperature and solvent was removed via vacuum evaporation. The residue was purified by column chromatography (SiO_2, 9:1 to 8:2 CH_2Cl_2 / CH_3OH) to provide monocationic dipyridyl-BODIPY ester (179 mg, 47% yield) as an orange waxy solid (counter ion not determined). [1]

H NMR (300 MHz, CD_3OD): δ 9.24 (d, 2H, J = 9 Hz), 8.80 (d, 2H, J = 6 Hz), 8.50 (d, 2H, J = 9 Hz), 8.17 (d, 2H, J = 9 Hz), 7.90 (2H, d, J = 6 Hz), 7.43 (d, 2H, J = 9 Hz), 7.16 (t, 1H, J = 9 Hz), 6.65 - 6.53 (m, 3H), 6.07 (s, 2H), 5.14 (t, 2H, J = 6 Hz), 4.67 (t, 2H, J = 6 Hz), 4.56 (t, 2H, J = 6 Hz), 4.36 (t, 2H, J = 6 Hz), 2.47 (s, 6H), 1.34 (s, 6H). $^{13}C\{^1H\}$ NMR (75 MHz, CD_3OD): δ 165.7, 159.9, 158.8, 155.8, 153.9, 150.3, 145.9, 142.9, 142.1, 139.7, 130.5, 130.2, 129.8, 128.4, 125.7, 122.3, 121.1, 109.9, 107.9, 106.7, 101.6, 66.1, 66.1, 63.6, 60.5, 13.3, 13.2. HRMS-ESI: *m/z* calcd for $[C_{40}H_{38}BF_2N_4O_4\ ]^+$ 687.2954; found 687.2948 $[M]^+$ (100% intensity), 688.3 ($[M+H]^+$, 40% intensity), 686.3 ($[M-H]^+$,20%), 130.1 (44%), 219.0 (28%), 455.2 (18%).

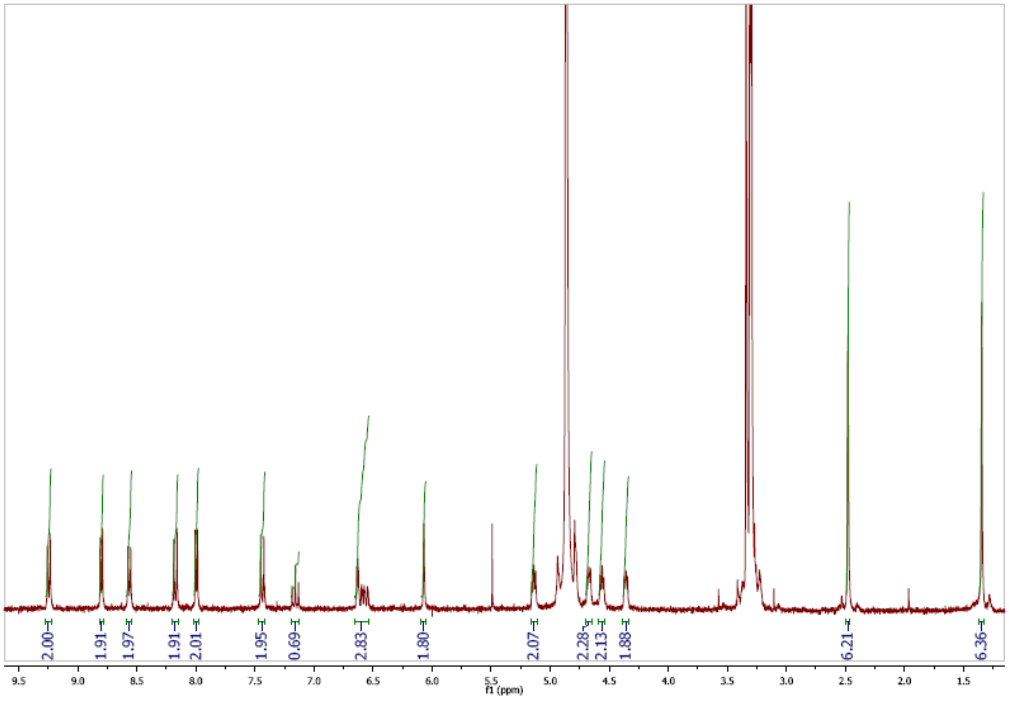

Figure 4.26a. ^{1}H NMR spectrum of **Monocationic dipyridyl-BODIPY.**

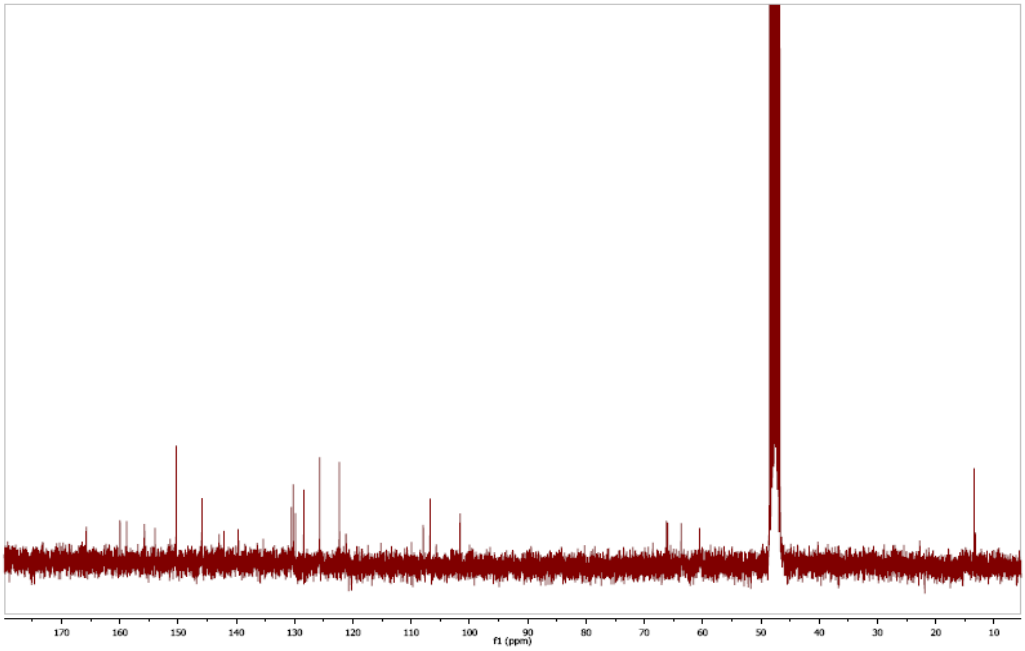

Figure 4.26b. ^{13}C NMR spectrum of **Monocationic dipyridyl-BODIPY.**

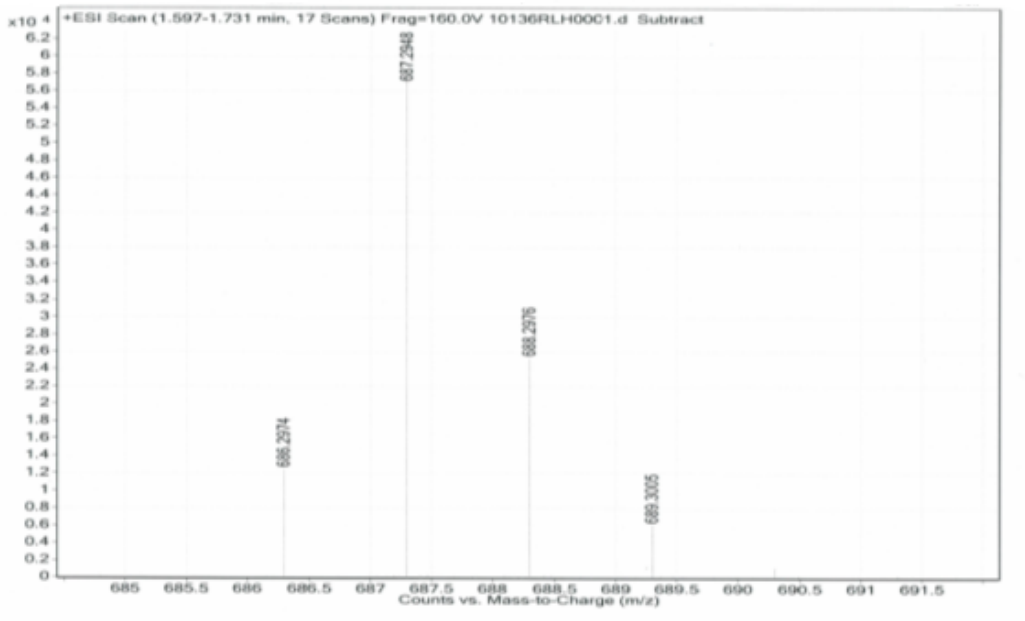

Figure 4.26c. Mass spectrum of **Monocationic dipyridyl-BODIPY.**

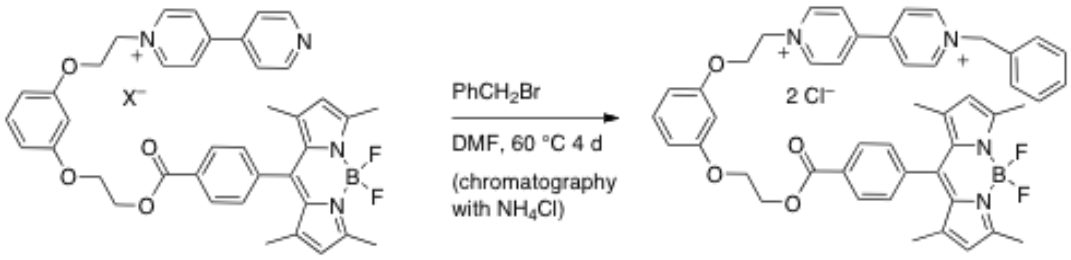

Benzylviologen-BODIPY dyad 4.5c. In a 100 mL reaction flask, monocationic dipyridyl-BODIPY (179 mg, 0.23 mmol), benzyl bromide (222 mg, 1.3 mmol) and DMF (8 mL) were added. The mixture was heated at 60 °C for 4 d. The flask was cooled to room temperature and solvent was removed via high vacuum evaporation. The compound was purified by column chromatography [SiO_2, 5:5 acetone / (7:2:1 MeOH / 2M aq. NH_4Cl / CH_3NO_2)] to provide benzylviologen-BODIPY complex **4** (101 mg, 47% yield) as a purple waxy solid. ^{1}H NMR (400 MHz, CD_3OD): δ 9.30 (dd, 4H, J = 14.8 Hz, 7.2 Hz), 8.68 (dd, 4H, J = 9.6 Hz, 6.8 Hz), 8.16 (d, 2H, J = 8.8 Hz), 7.58 (m, 2H), 7.48-7.42 (m, 5H), 7.16 (t, 1H, J = 8 Hz), 6.60-6.50 (m, 3H), 6.06 (s, 1H), 5.96 (s, 2H), 5.17 (t, 2H, J = 4 Hz), 4.60 (t, 2H, J = 4 Hz), 4.50 (t, 2H, J =4 Hz), 4.30 (t, 2H, J = 4 Hz), 2.47 (s, 6H), 1.35 (s, 6H). $^{13}C\{^1H\}$ NMR (100 MHz, CD_3OD): δ 165.6, 159.9, 158.7, 155.8, 150.3, 150.2, 146.3, 145.6, 142.9, 140.6, 139.7, 132.8, 130.6, 130.2, 130.1, 129.9, 129.8, 129.3, 128.9, 128.4, 127.1, 126.7, 121.1, 107.6, 106.7, 101.6, 65.9, 65.8, 64.5, 63.6, 60.9, 13.3, 13.1. HRMS-ESI: *m/z* calculated for $C_{47}H_{45}BF_2N_4O_4$ 778.3501; found 778.3493 ($[M^{2+}]^+$, 28% intensity), calcd for $[C_{47}H_{45}BF_2N_4O_4]^{++}$ 389.1750 ; found 389.1762 ($[M]^{++}$, 100%), 320.1519 ($[M^{2+}- BF_2]^+$, 30%).

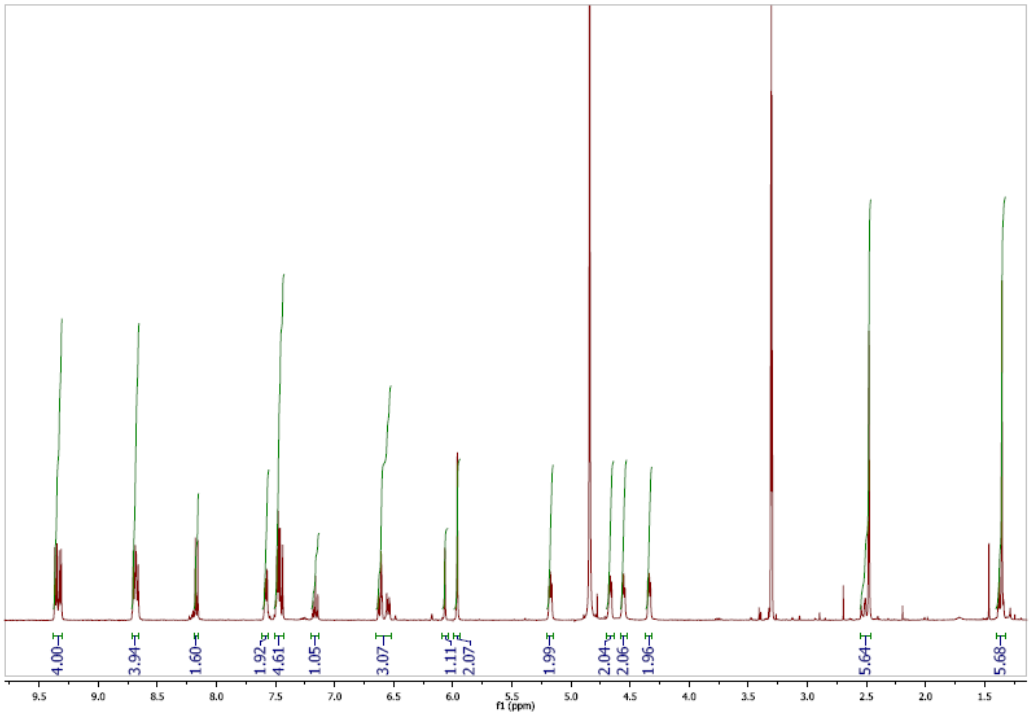

Figure 4.27a. ^{1}H NMR spectrum of **Benzylviologen-BODIPY dyad 4.5c.**

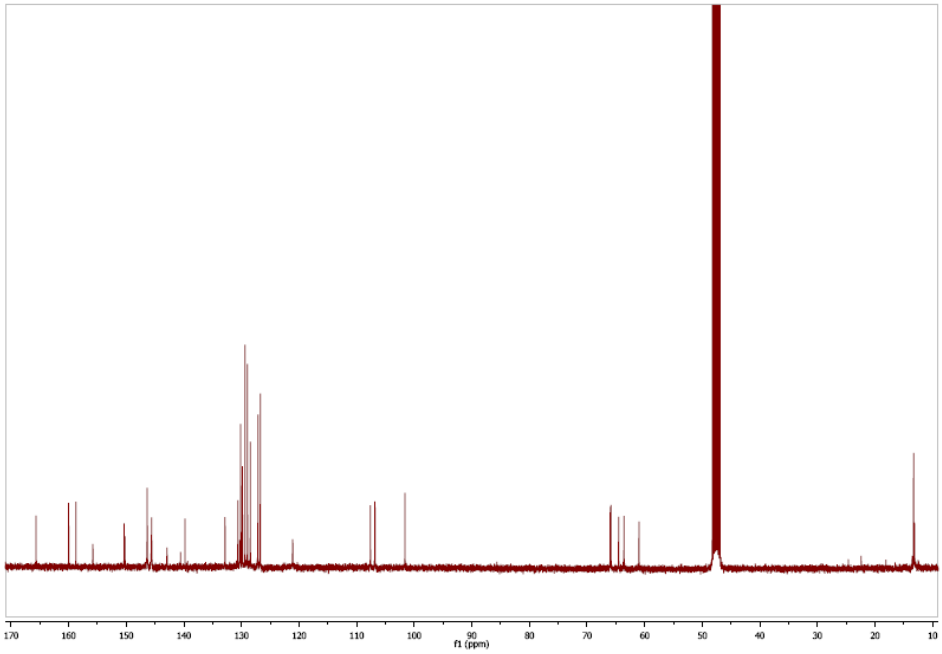

Figure 4.27b. ^{13}C NMR spectrum of **Benzylviologen-BODIPY dyad 4.5c.**

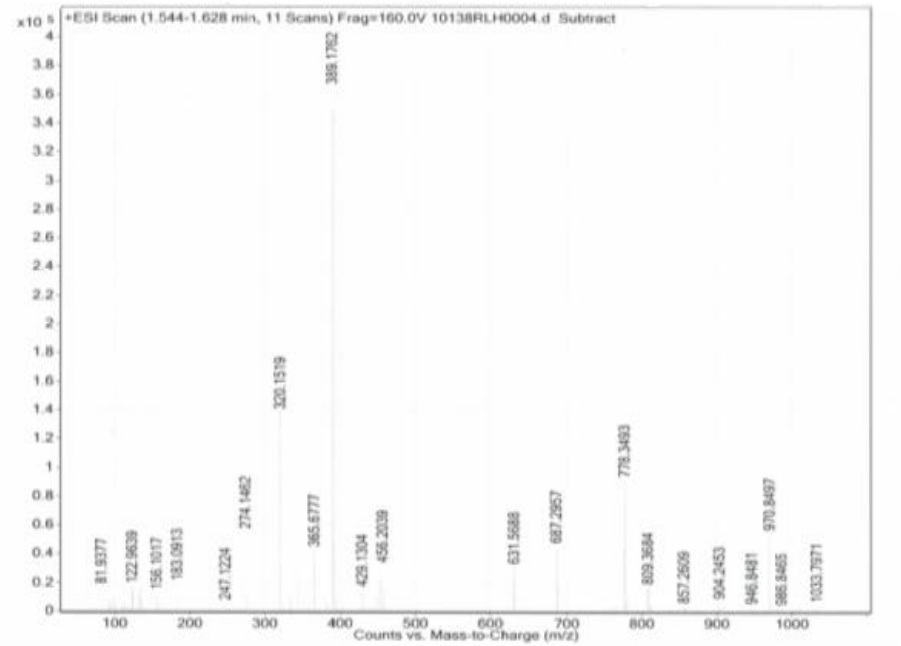

Figure 4.27c. Mass spectrum of **Benzylviologen-BODIPY dyad 4.5c.**

Cucurbit[7]uril (CB[7]).[2] Following the procedure of Day, et al, in a 300 mL beaker, glycouril (20 g, 140.7 mmol), paraformaldehyde (8.45 g, 281.5 mmol) and 5 M HCl (150 mL) were added. The mixture was heated at 80 °C for 8 d. During this period, addition of 5 M HCl was continued to keep the volume constant. The reaction mixture was cooled to room temperature and filtered. To the filtrate, 400 mL of methanol was added and settled for 1 d. The mixture was filtered and washed the solid with methanol (2 x 100 mL). Thus dried solid was dissolved in 20% aq. glycerol (500 mL, v/v). The mixture was heated at 60-80 °C in open atmosphere for 3 h. The mixture was filtered. To the filtrate, methanol (400 mL)

was added and the mixture left undisturbed overnight. The mixture was filtered. The resulting solid was washed with methanol (3 x 100 mL) to obtain CB[7] (6.26 g, 27% yield) as a white solid. ^{1} H NMR (300 MHz, D_2O): δ 5.6 (d, 14 H, J = 15 Hz), 5.37 (s, 14H), 4.06 (d, 14H, J = 15 Hz). $^{13}C\{^{1}H\}$ NMR (75 MHz, D_2O): δ 156.5, 71.1, 52.4. HRMS-ESI: *m/z* calcd for $[C_6H_6N_4O_2\ ]_7Na$ 1185.3333; found 1185.3331 $[M+Na]^+$.

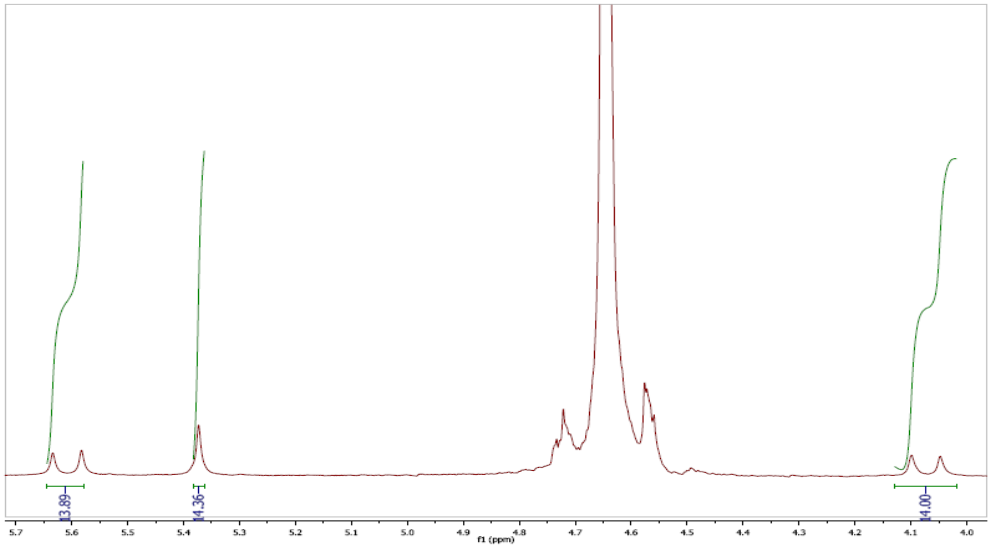

Figure 4.28a. ^{1}H NMR spectrum of **Cucurbit[7]uril (CB[7].**

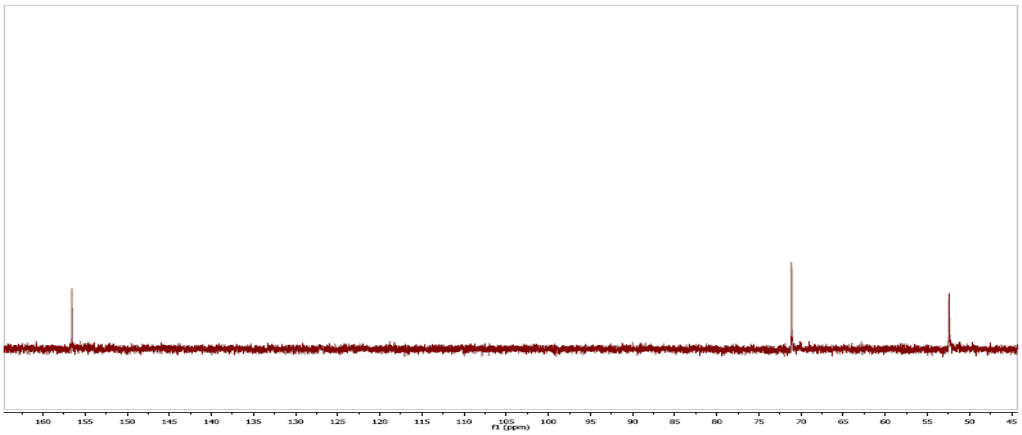

Figure 4.28b. ^{13}C NMR spectrum of **Cucurbit[7]uril (CB[7]).**

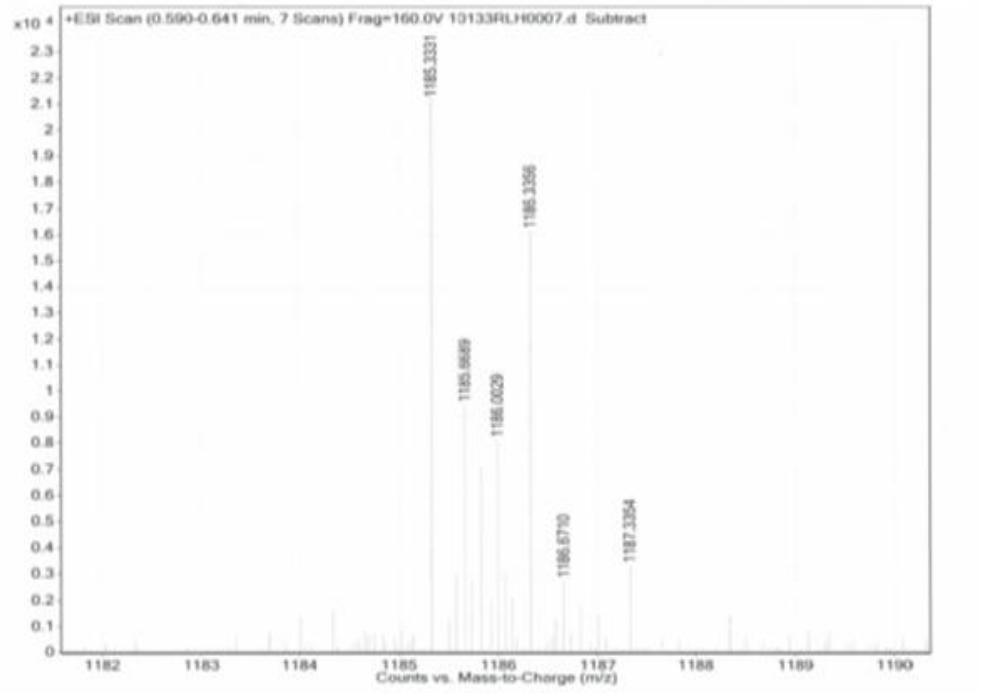

Figure 4.28c. Mass spectrum of **Cucurbit[7]uril (CB[7]).**

Procedure and spectra for absorbance and fluorescence measurements.

Absorbance measurements. Absorbance measurements were done on Shimadzu Scientific Instruments UV-2101 PC UV-Vis scanning spectrophotometer. Measurement was performed in disposable polystyrene cuvettes of 10.0 mm/10.0mm. The baseline was recorded with water in both sample and reference cuvettes. All the measurements were performed at ambient temperature in air. All the measurements were done on 4 mL sample.

Fluorescence measurements. Fluorescence measurements were done on Shimadzu Scientific Instruments RF-5301 PC spectrofluorophotometer equipped with a xenon lamp of 150 W as an excitation source. Measurement was performed in disposable polystyrene cuvettes of 10.0 mm/10.0mm. In all the measurements slit width was adjusted to 1.5. All the measurements were performed at ambient temperature in air. All the measurements were done on 4 mL sample.

Stock solution of methylviologenrhodamine. A methylviologenrhodamine ($C_{49}H_{53}N_4O_5^{3+}SO_4^{2-}Cl^-$, FW = 909.48) stock solution (3.0 mM) was prepared by dissolving methylviologenrhodamine (70 mg, 0.0770 mmol) in 25 mL of deionized water (DI water). A portion of the stock solution (166 μL) was taken in a 50 mL volumetric flask and diluted up to 50 mL with DI water to prepare 10 μM solution.

Stock solution of benzylviologenrhodamine. A benzylviologenrhodamine [$C_{55}H_{57}N_4O_5^{3+}\ Cl^-Br^-\ I^-$; FW = 1096.22] stock solution (1.38 mM) was prepared in a 25 mL volumetric flask by dissolving benzylviologenrhodamine (38 mg, 0.0347 mmol) in DI water. A portion of the stock solution (0.360 mL) was taken in a 50

mL volumetric flask and diluted up to 50 mL with DI water to prepare 10 μM solution.

Stock solution of rhodamine ester. A rhodamine ester [$C_{38}H_{44}BrN_2O_5^+$ Cl^- ; FW =722.11] stock solution (0.19 mM) was prepared by dissolving rhodamine ester (7 mg, 0.0097mmol) in 50 mL of DI water with 4-5 drops of MeOH. A portion of the stock solution (2.6 mL) was taken in a 50 mL volumetric flask and diluted with DI water to prepare 10 μM solution.

Stock solution of benzylviologenbodipy. A benzylviologenbodipy [$C_{47}H_{45}BF_2N_4O_4^{2+}$ Br^- I^- , FW = 985.17] stock solution (3.8 mM) was prepared by dissolving benzylviologenbodipy (37 mg, 0.038 mmol) in a 10 mL volumetric flask with DI water. A portion of the stock solution (132 μL) was taken in a 50 mL volumetric flask and diluted up to 50 mL with DI water to prepare 10 μM solution.

CB7 solution. A CB7 solution (16 mM) was prepared by dissolving CB7 (93 mg, 0.08 mmol) in DI water (5 mL). A portion of the CB7 solution (0.04 mL) was taken and diluted up to 4 mL with DI water to prepare 0.32 mM solution.

Dilution of CB7 for measurement. A CB7 solution (4 mL, 16 mM) was taken in a cuvette. A portion of the CB7 solution (2 mL) was transferred to the second cuvette and DI water (2 mL) was added. The solution was mixed properly. A portion of this solution (2mL) was transferred to the third cuvette and again diluted with DI water (2mL). This way a series of CB7 dilution was done up to 0.0038 mM CB7. After dilution, the dye complex (2 mL, 10 μM) was added to all the cuvettes.

The solution was mixed properly and then absorbance and fluorescence was measured. To perform the second set of dilution, 0.32 mM CB7 was prepared from 16 mM CB7, a series of dilution was done in the cuvettes from 0.16 up to 0.0006 mM and then dye complex (2 mL) was added. After mixing, absorbance and fluorescence was measured. All the measurements were done three times and each time the experiment was performed on two sets. The excited wavelength was 562 nm for rhodamine dye and 490 nm for bodipy.

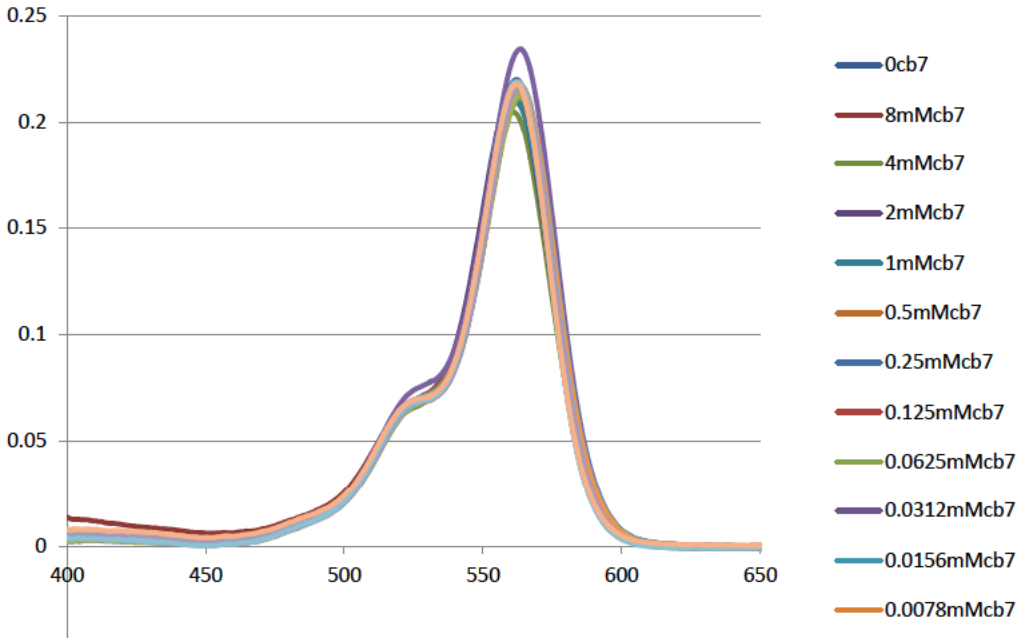

Figure 4.29. Absorbance spectra of methylviologen-rhodamine B dyad 4.5a (5µM in water **+ CB7).**

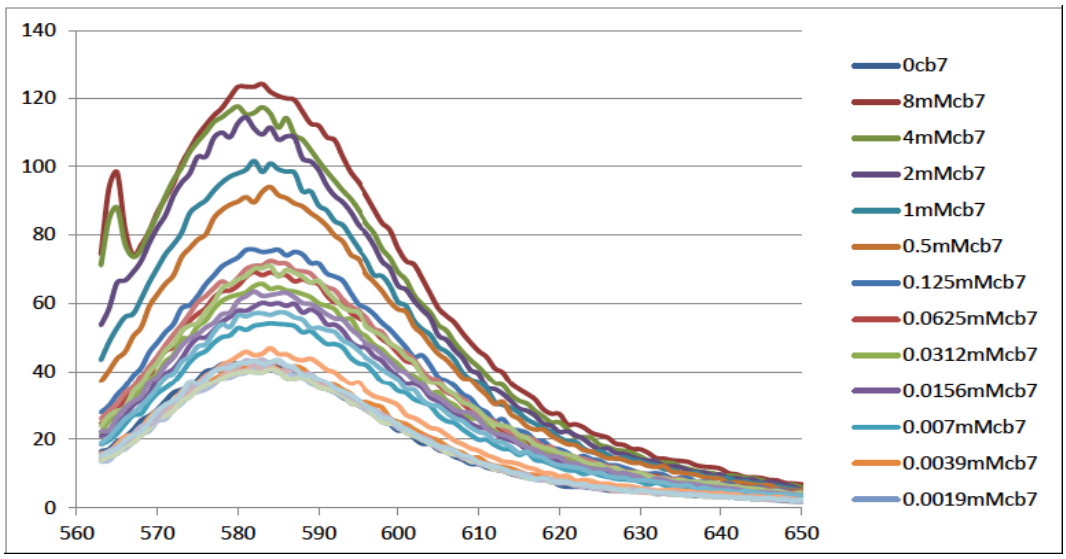

Figure 4.30. Emission spectra of **methylviologen-rhodamine B dyad 4.5a** (5 μM in water + **CB7**, excitation wave length 560 nm).

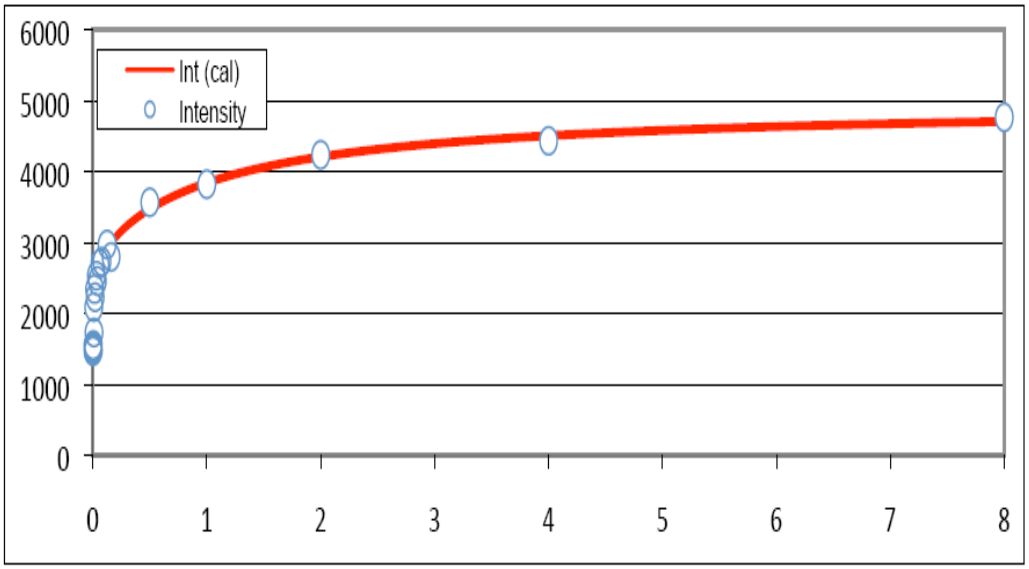

	a0	0.005			
	K1	69.215	mM^{-1}	6.92E+04	M^{-1}
	K2	0.914	mM^{-1}	9.14E+02	M^{-1}
		Enhancement			
no CB7	Ia	2.829			
complex 1	Iy	5.736	2.03		
complex 2	Iz	9.925	1.73	3.51	

Figure 4.31. Emission spectra titration curve of **methylviologen-rhodamine B dyad 3.5a** (5μM in water + **CB7,** excitation wave length 560 nm and two equilibrium curve fitting model): provided by courtesy of Wai Tak Yip.

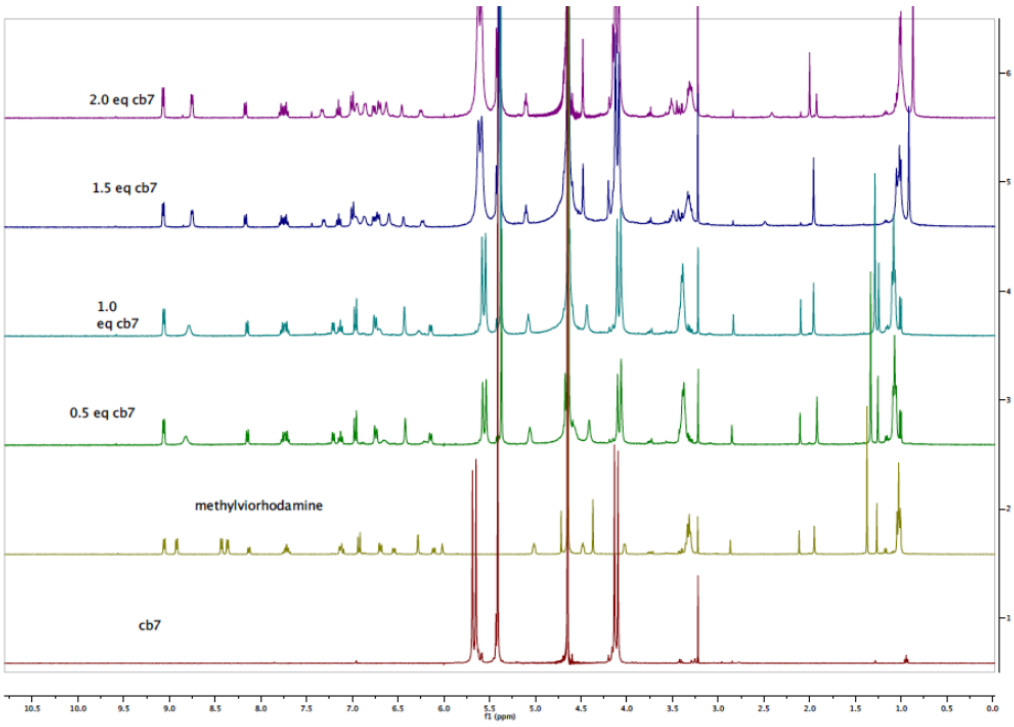

Figure 4.32. ^{1}H NMR spectra of **methylviologen-rhodamine B dyad 4.5a + CB7.**

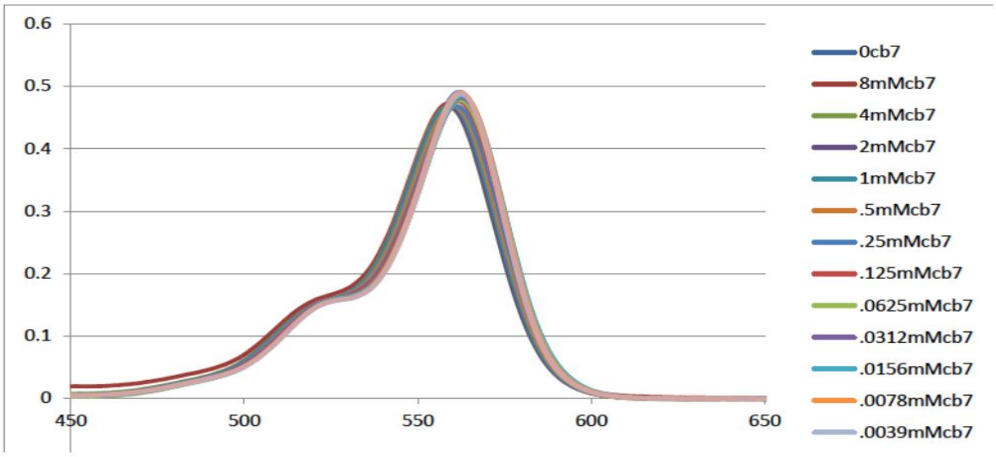

Figure 4.33. Absorbance spectra of **benzylviologen-rhodamine B dyad 4.5b** (5 μM in water + **CB7**).

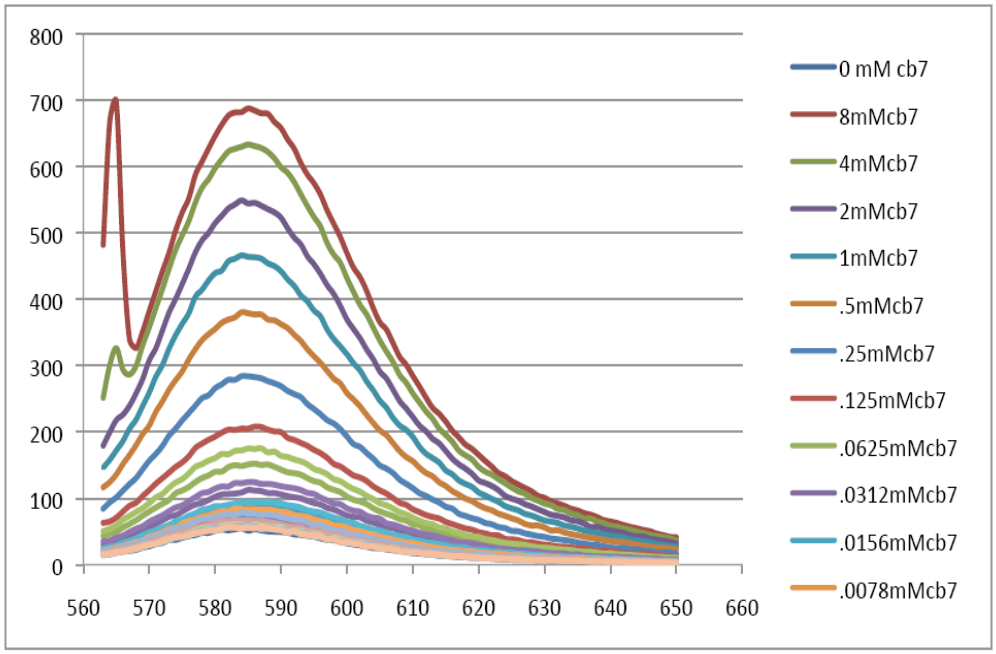

Figure 4.34. Emission spectra of **benzylviologen-rhodamine B dyad 4.5b** (5 μM in water + **CB7**, excitation wave length 560 nm).

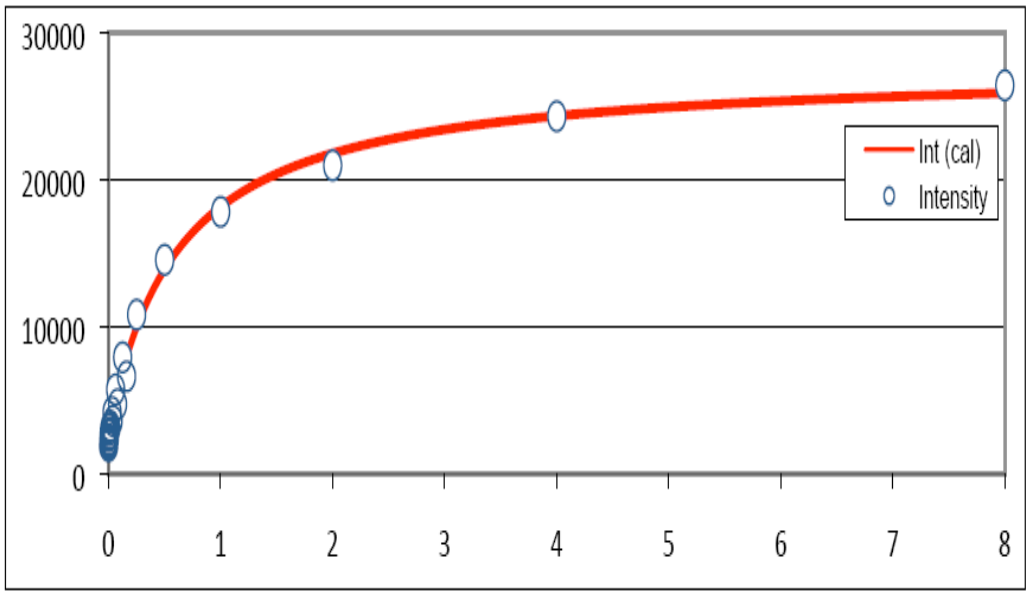

	a0	0.005			
	K1	116	mM^{-1}	1.16E+05	M^{-1}
	K2	1.57	mM^{-1}	1.57E+03	M^{-1}
	Enhancement				
no CB7	Ia	4.0			
complex 1	Iy	7.0	1.7		
complex 2	Iz	55	8.0	13.8	

Figure 4.35. Emission spectra titration curve of **benzylviologen-rhodamine B dyad 3.5b** (5 μM in water + CB7, excitation wave length 560 nm and two equilibrium curve fitting model): provided by courtesy of Wai Tak Yip.

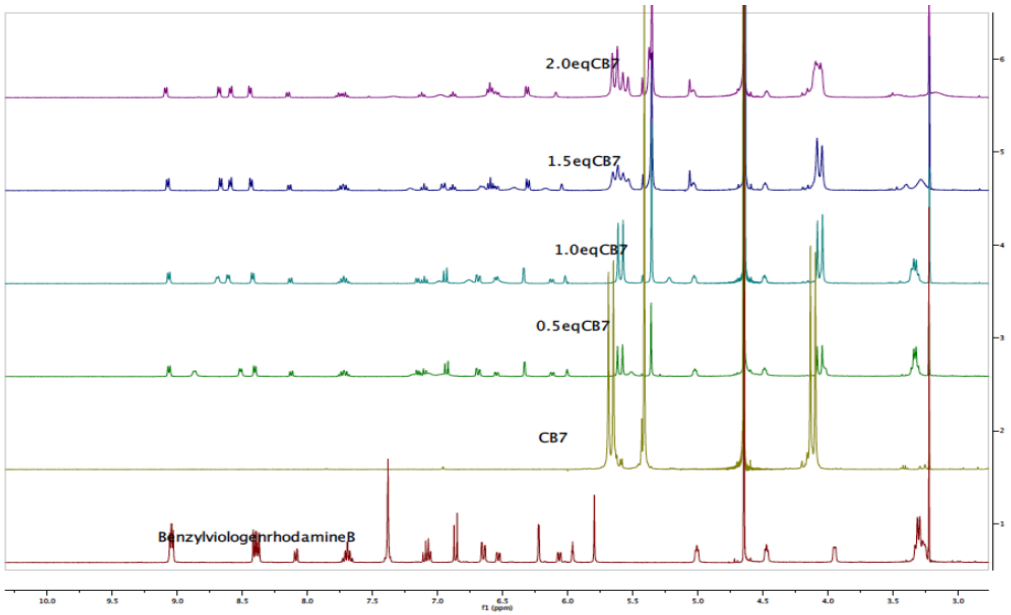

Figure 4.36. ^{1}H NMR spectra of **methylviologen-rhodamine B dyad 4.5a + CB7.**

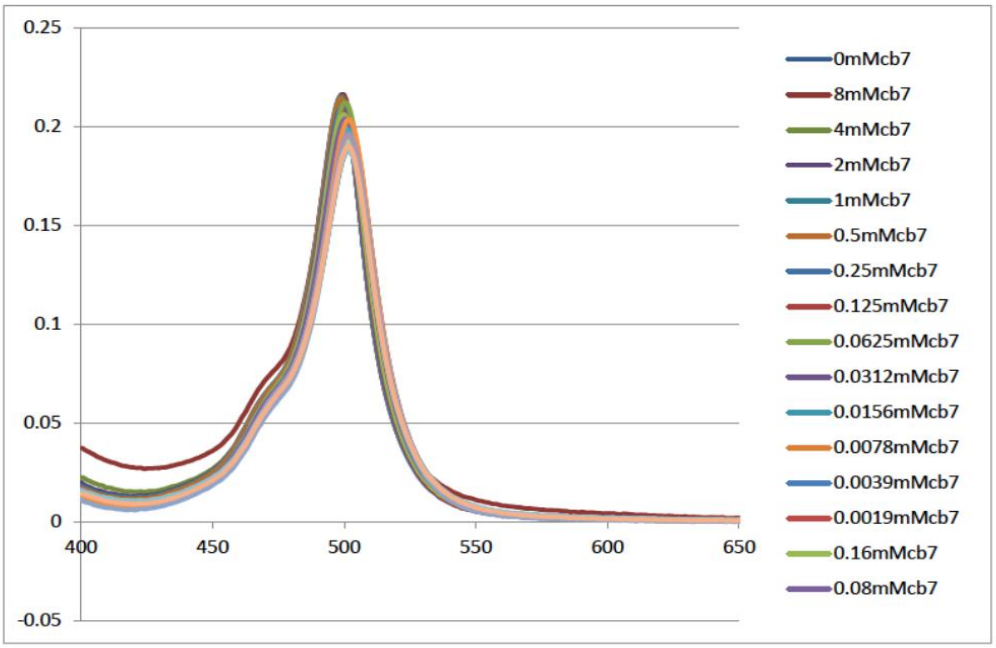

Figure 4.37. Absorbance spectra of **benzylviologen-bodipy 4.5c** (5 μM in water + CB7).

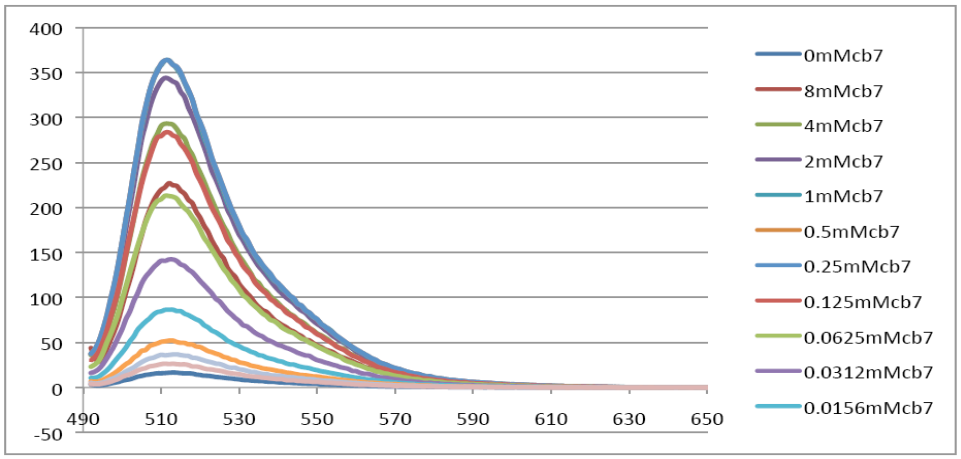

Figure 4.38. Emission spectra of **benzylviologen-bodipy dyad 4.5c** (5 μM in water + CB7, excitation wave length 490 nm.

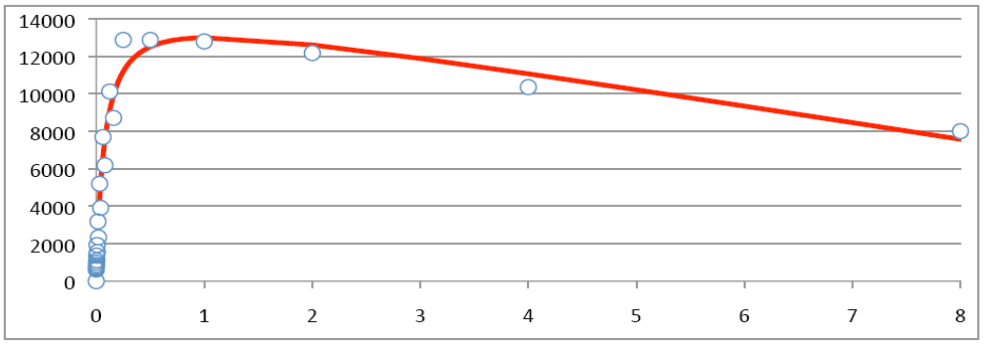

K_C	12.43	mM^{-1}	1.2E+04	M^{-1}
Int(Dye)	9.9E+04			
Int(Complex)	3.0E+06			
CB7 Quenching	910			
Enhancement	**30**			

Figure 4.39. Emission spectra titration curve of **benzylviologen-bodipy dyad 4.5c** (5 μM in water + **CB7,** excitation wave length 490 nm and single equilibrium constant curve fitting model): provided by courtesy of Wai Tak Yip.

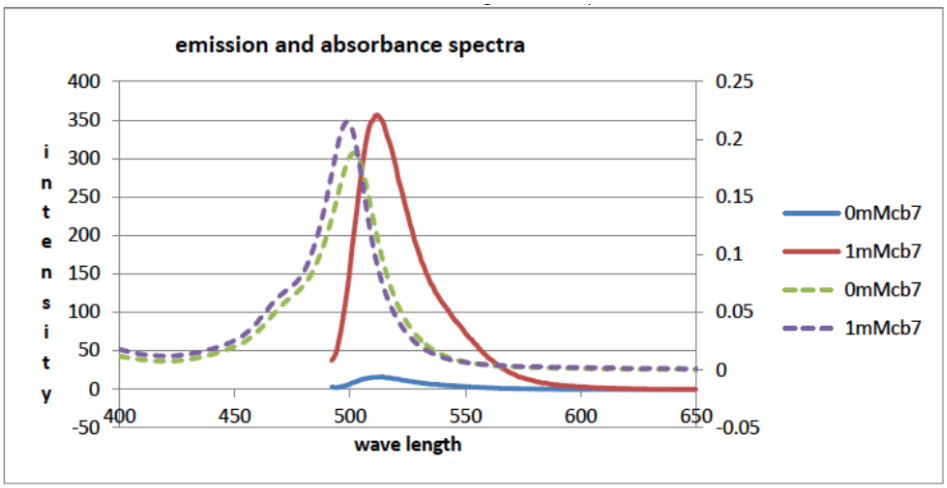

Figure 4.40. Summary of absorbance and emission spectra of **benzylviologen-bodipy 4.5c** (5 μM in water and without and with 1 mM CB7, excitation wave length 490 nm).

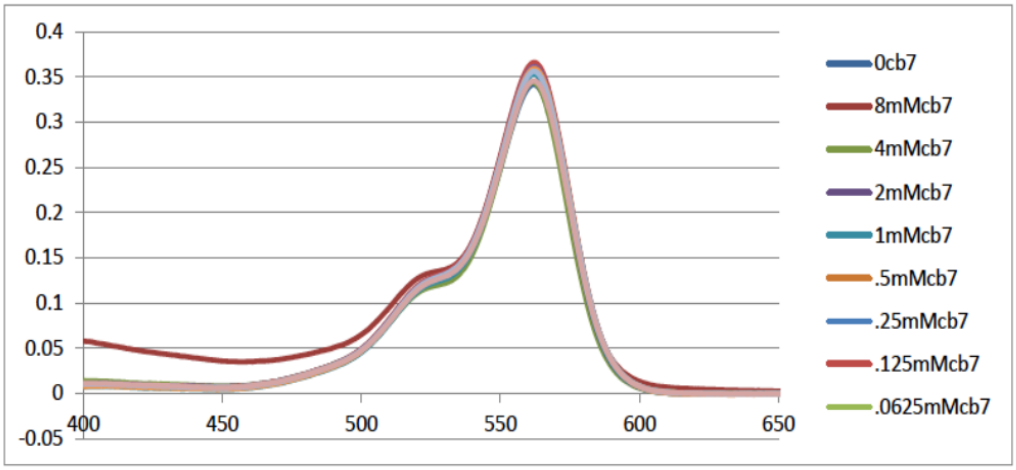

Figure 4.41. Absorbance spectra of **rhodamine B ester 2** (5 μM in water + **CB7**): control dye without tethered viologen.

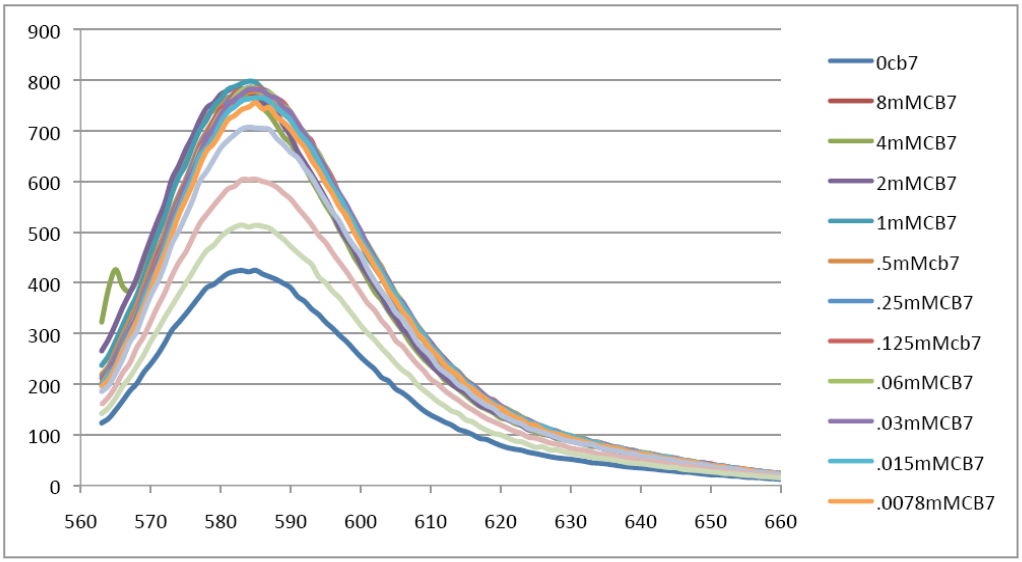

Figure 4.42. Emission spectra of **rhodamine B ester 2** (5 μM in water + **CB7,** excitation wave length 560 nm):control dye without tethered viologen**.**

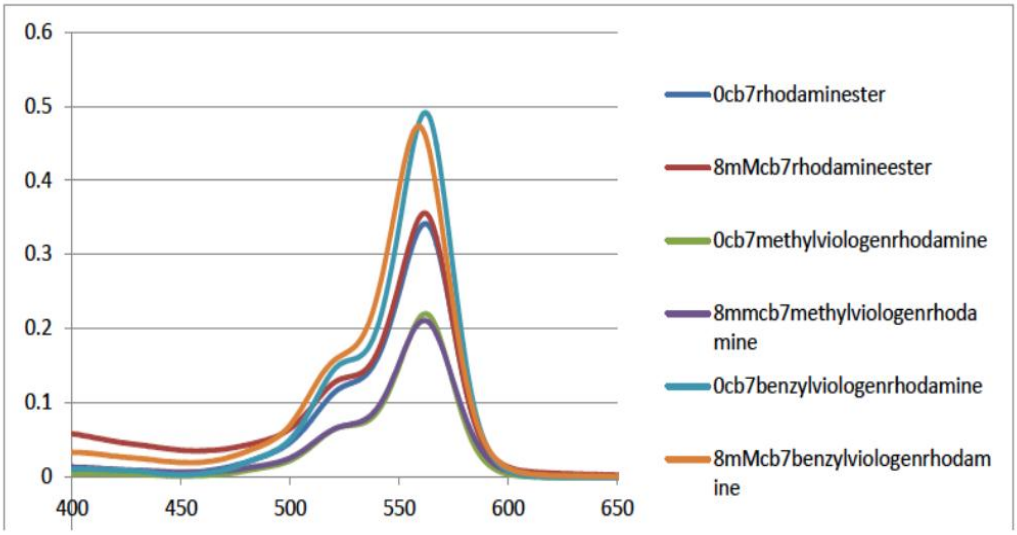

Figure 4.43. Combined absorbance spectra of **rhodamine B ester of 2-(3-(2-bromoethoxy)phenoxy)ethanol 2** (labeled as **rhbester), methylviologen-**

rhodamine B. dyad 3.5a (labeled as **mv), benylviologen-rhodamine B dyad 3.5b (**labeled as **bv) :** 5 μM dye and dyad without and and 8 mM **CB7** in water**.**

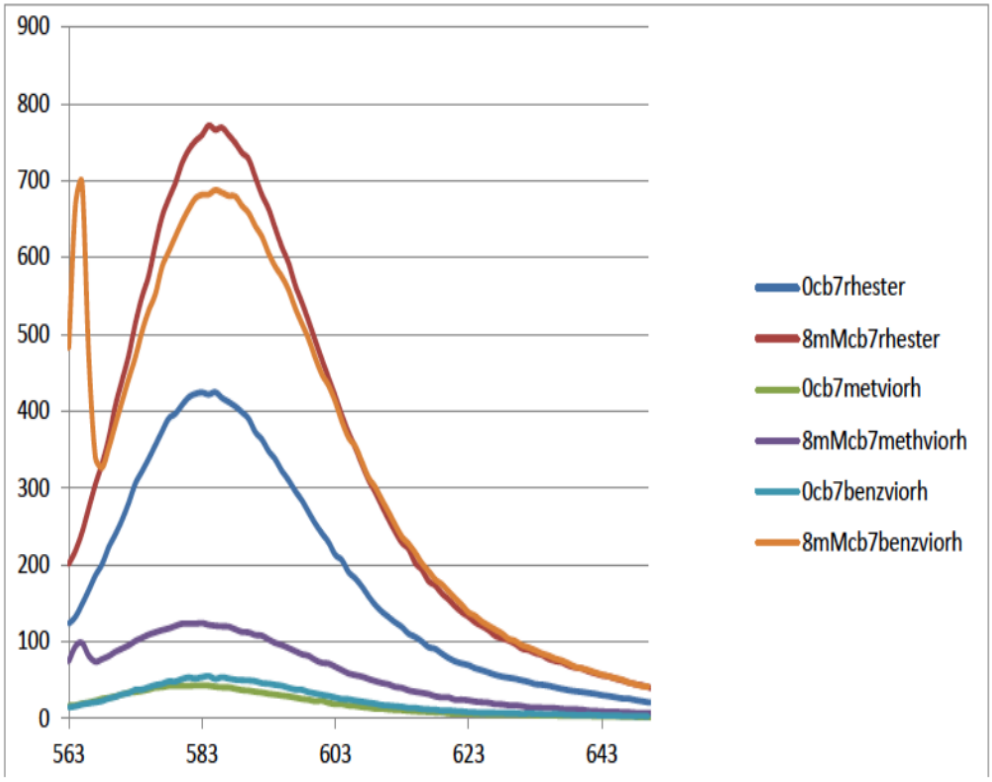

Figure 4.44. Combined emission spectra of rhodamine B ester of 2-(3-(2-bromoethoxy)phenoxy)ethanol 2 (labeled as rhbester), methylviologen-rhodamine B dyad 3.5a (labeled as mv), benylviologen-rhodamine B dyad 3.5b (labeled as bv) : 5 μM dye and dyad without and and 8 mM CB7 in water, excited wavelength 560 nm.

4.6 References

1. Singh, A.; Yip, W.-T.; Halterman, R. L. Fluorescence-On Response via CB7 Binding to Viologen–Dye Pseudorotaxanes. *Org. Lett.* **2012**, *14*, 4046-4049.

2. Tainaka, K; Sakaguchi, R.; Hayashi, H. ; Nakano, S. ; Liew, F. F.; Morii, T. Design Strategies of Fluorescent Biosensors Based on Biological Macromolecular Receptors. *Sensors* **2010**, *10*, 1355-1376.

3. Color Chemistry, Heinrich Zollinger.

4. Johnsson, N.; Johnsson, K. Chemical Tools for Biomolecular Imaging. *ACS Chem. Biol.* **2007**, *2*, 31-38.

5. Rao, J.; Dragulescu-Andrasi, A.; Yao, H. Fluorescence imaging in vivo: recent advances. *Curr.Opin. Biotechnol.* **2007**, *18*, 17.

6. Johnsson, K. Visualizing biochemical activities in living cells. *Nat. Chem. Biol.* **2009**, *5*, 63-65.

7. Wang, H.; Nakata, E.; Hamachi, I. Recent Progress in Strategies for the Creation of Protein-Based Fluorescent Biosensors. *Chem BioChem* **2009**, *10*, 2560-2577.

8. Demchenko, A. P. The future of fluorescence sensor arrays. *Trends Biotechnol.* **2005**, *23*, 456-460.

9. (a) Turfan, B.; Akkaya, E. U. Modulation of boradiazaindacene emission by cation-mediated oxidative PET. *Org. Lett*. **2002**, *4*, 2857-2859. (b) Goze, C.; Ulrich, G.; Charbonnie`re, L.; Cesario, M.; Prange´, T.; Ziessel, R. Cation sensors based on terpyridine-functionalized boradiazaindacene. *Chem. Eur. J*. **2003**, *9*, 3748-3755. (c) Gabe, Y.; Urano, Y.; Kikuchi, K.; Kojima, H.; Nagano, T. Highly Sensitive Fluorescence Probes for Nitric Oxide Based on Boron Dipyrromethene Chromophore－Rational Design of Potentially Useful Bioimaging Fluorescence Probe. *J. Am. Chem. Soc*. **2004**, *126*, 3357-3367. (d) Rurack, K.; Kollmannsberger, M.; Resch-Genger, U.; Daub, J. A Selective and Sensitive Fluoroionophore for HgII, AgI, and CuII with Virtually Decoupled Fluorophore and Receptor Units. *J. Am. Chem. Soc*. **2000**, *122*, 968-969. (e) Coskun, A.; Akkaya, E. U. Ion Sensing Coupled to Resonance Energy Transfer: A Highly Selective and Sensitive Ratiometric Fluorescent Chemosensor for Ag(I) by a Modular Approach. *J. Am. Chem. Soc.* **2005**, *127*, 10464-10465.

10. Yee, M.; Fas, S. C.; Stohlmeyer, M. M.; Wandless, T. J.; Cimprich, K. A. A cell-permeable, activity-based probe for protein and lipid kinases. *J. Biol. Chem.* **2005**, *280*, 29053-29059.

11. (a) Dale, T. J.; Rebek, J., Jr. Fluorescent Sensors for Organophosphorus Nerve Agent Mimics. *J. Am. Chem. Soc.* **2006**, *128*, 4500-4501. (b) Bencic-Nagale, S.; Sternfeld, T.; Walt, D. R. Microbead Chemical Switches: An Approach to Detection of Reactive Organophosphate Chemical Warfare Agent Vapors. *J. Am. Chem. Soc.* **2006**, *128*, 5041-5048. (c) Desmonts, L. B.; Reinhoudt, D. N.; Calama, M. C. Design of fluorescent materials for chemical sensing. *Chem. Soc. Rev.* **2007**, *36*, 993-1017. (d) Tainaka, K.; Sakaguchi, R.; Hayashi, H; Nakano, S; Liew, F. F.; Morii, T. Design Strategies of Fluorescent Biosensors Based on Biological Macromolecular Receptors. *Sensors* **2010**, *10*, 1355-1376.

12. Aye-Han, N.; Ni, Q.; Zhang, J. Fluorescent biosensors for real-time tracking of post-translational modification dynamics. *Curr. Opin. Chem. Bio.* **2009**, *13*, 392-397.

13. Dillingham, M. S.; Wallace, M. I. Protein modification for single molecule fluorescence microscopy. *Org. Biomol. Chem.* **2008**, *6*, 3031-3037.

14. De Silva, P. A.; Gunaratne, N. H. Q.; Gunnlaugsson, T.; Huxley, A. J. M.; McCoy, C. P.; Rademacher, J. T.; Rice, T. E. Signaling Recognition Events with Fluorescent Sensors and Switches. *Chem. Rev.* **1997**, *97*, 1515-1566.

15. (a) Isied, S. S.; Ogawa, M. Y.; Wisharets, J. F. Peptide-mediated intramolecular electron transfer: long-range distance dependence. *Chem. Rev. 1992, 92*, 381-394. (b) Gray, H. B.; Winkler, J. R. Long-Range Electron Transfer Special Feature: Long-range electron transfer. *PNAS* **2005**, *102*, 3534-3539.

16. (a) Tang, X.; Peng, X.; Dou, W.; Mao, J.; Zheng, J.; Qin, W.; Liu, W.; Chang, J.; Yao, X. Design of a Semirigid Molecule as a Selective Fluorescent Chemosensor for Recognition of Cd(II). *Org. Lett.* **2008**, *10*, 3653-3656. (b) Taki, M.; Desaki, M.; Ojida, A.; Lyoshi, S.; Hirayama, T.; Hamachi, I.; Yamamoto, Y. Fluorescence Imaging of Intracellular Cadmium Using a Dual-Excitation Ratiometric Chemosensor. *J. Am. Chem. Soc.* **2008**, *130*, 12564-12565.

17. Wu, Y.; Peng, X.; Guo, B.; Fan, J.; Zhang, Z.; Wang, J. Cui, A.; Gao, Y. Boron dipyrromethene fluorophore based fluorescence sensor for the selective imaging of Zn(II) in living cells. *Org. Biomol. Chem*. **2005**, *3*, 1387-1392.

18. Vedamalai, M; Wu, S. P. A BODIPY-Based Highly Selective Fluorescent Chemosensor for Hg^{2+} Ions and Its Application in Living Cell Imaging. *Eur. J. Org. Chem.* **2012**, 1158-1163.

19. Thompson, R. *Rev. Fluores.* **2005**, *2*, 349.

20. (a) Doose, S.; Neuweiler, H.; Sauer, M. Fluorescence quenching by photoinduced electron transfer: a reporter for conformational dynamics of macromolecules. *Chem. Phys. Chem.* **2009**, *10*, 1389-1398. (b) Gray, H. B.; Winkler, J. R. Long-Range Electron Transfer Special Feature: Long-range electron transfer. *Proc. Natl. Acad. Sci.* U.S.A. **2005**, *102*, 3534-3539. (c)Yang, H.; Luo,G.; Karnchanaphanurach, P.; Louie, T.-M.; Rech, I.;Cova, S.; Xun, L.; Xie, X. S. Protein Conformational Dynamics Probed by Single-Molecule Electron Transfer. *Science* **2003**, *302*, 262-266. (d)Marquez, C.; Huang, F.; Nau,W. M. Cucurbiturils: Molecular Nanocapsules for Time-Resolved Fluorescence-based Assays. *IEEE Trans.Nanobiosci*. **2004**, *3*, 39-45.

21. (a) Setiawan, D.; Kazaryan, A.; Martoprawiro, A. M.; Filatov, M. A first principles study of fluorescence quenching in rhodamine B dimers: how can quenching occur in dimeric species? *Phys. Chem. Chem. Phys*. **2010**, *12*, 11238-11244. (b) Rohatgi, K. K.; Singhal, G. S. Nature of Bonding in Dye Aggregates. *J. Phys. Chem*. **1966**, *70*, 1695-1701. (c) Halterman, R.L.; Moore, J.L.; Mannel, L.M. Disrupting aggregation of tethered rhodamine B dyads through inclusion in cucurbit[7]uril. *J. Org. Chem.* **2008**, *73*, 3266-3269. (d) Gutierrez, M.C.; Hortiguela, M. J.; Ferrer, M.L.; delMonte, F. Highly Fluorescent Rhodamine B Nanoparticles Entrapped in Hybrid Glasses. *Langmuir* **2007**, *23*, 2175-2179. (e) Klika, Z.; Weissmannova, H.; Capkova, P.; Pospisil, M. The rhodamine B intercalation of montmorillonite. *J. Coll. Interface Sci*. **2004**, *275*, 243-250. (f) Halterman, R. L.; Moore, J. L.; Yakshe, K. A.; Halterman, J. A.; Woodson, K. A. Inclusion complexes of cationic xanthene dyes in cucurbit[7]uril. *J. Incl. Phenom. Macrocycl. Chem.* **2010,** *66*, 231-241. (g) Andrews, D. L. in *Lasers in Chemistry*, Ed.; Springer-Verlag, Berlin, 1997. (h) Fujihara, M. ; Kubota M. ; Osa, T. *J. Electroanal. Chem.* **1981**, *119*, 379. (i) Ward, R. K. ; Nation, P. N. ; Maxwell, M. ; Barker, C. L. ; Clothier, R. H. *Toxicol. in Vitro*, **1997**, *11*, 633.

22. (a) Loudet, A.; Burgess, K. BODIPY Dyes and Their Derivatives: Syntheses and Spectroscopic Properties. *Chem. Rev.* **2007**, *107*, 4891-4932. (b) Krumova, K.; Cosa, G. Bodipy Dyes with Tunable Redox Potentials and Functional Groups for Further Tethering: Preparation, Electrochemical, and Spectroscopic Characterization. *J. Am. Chem. Soc.* **2010**, *132*, 17560-17569. (c) Liu, J.-Y.; Ermilov, E. A.; Rader, B.; Ng, D. K. P. Switching the photo-induced energy and electron-transfer processes in BODIPY–phthalocyanine conjugates. *Chem. Commun.* **2009**, 1517-1519.

23. (a) Yee, M.C.; Fas, S. C.; Stohlmeyer, M. M.; Wandless, T. J.; Cimprich, K. A. A cell-permeable, activity-based probe for protein and lipid kinases. *J. Biol. Chem.* **2005**, *280*, 29053-29059. (b) Golovkova, T. A.; Kozlov, D. V.; Neckers, D. C. Synthesis and Properties of Novel Fluorescent Switches. *J. Org. Chem.* **2005**, *70*,

5545-5549. (c) Turfan, B.; Akkaya, E. U. Modulation of boradiazaindacene emission by cation-mediated oxidative PET *Org. Lett.* **2002**, *4*, 2857-2859.

24. (a) Bhasikuttan, A. C.; Mohanty, J.; Nau, W. M.; Pal, H. Supra-bimolecular Host-protein Assembly. *Angew. Chem., Int. Ed.* **2007**, *46*, 4120-4122. (b) Nau, W. M.; Mohanty, J. Taming fluorescent dyes with cucurbituril. *Inter. J. Photoenergy* **2005**, *7*, 131-141. (c) Mohanty, J.; Nau, W. M. Ultrastable rhodamine with cucurbituril. *Angew. Chem., Int. Ed.* **2005**, *44*, 3750-3754. (d) Lagona, J.; Mukhopadhyay, P.; Chakrabarti, S.; Isaacs, L. The Cucurbit[n]uril Family *Angew. Chem., Int. Ed.* **2005**, *44*, 4844-4870. (e) Dsouza, R. N.; Pischel, U.; Nau, W. M. Fluorescent dyes and their supramolecular host/guest complexes with macrocycles in aqueous solution. *Chem. Rev.* **2011**, *111*, 7941-7980.

25. (a) Ueno, A.; Moriwaki, F.; Osa, T.; Hamada, F.; Murai, K. Fluorescence and circular dichroism studies on host-guest complexation of γ-cyclodextrin bearing two 2-naphthyl moieties. *Bull. Chem. Soc. Jpn.* **1986**, *59*, 465-470. (b) Ueno, A.; Minato, S.; Osa, T. Host-guest sensors of 6A,6B-, 6A,6C-, 6A,6D-, and 6A,6E-bis(2-naphthylsulfenyl)-.gamma.-cyclodextrins for detecting organic compounds by fluorescence enhancements. *Anal. Chem.* **1992**, *64*, 1154-1157. (c) Moriwaki, F.; Kaneko, H.; Ueno, A.; Osa, T.; Hamada, F.; Murai, K. Excimer formation and induced-fit type of complexation of β-cyclodextrin capped by two naphthyl moieties. *Bull. Chem. Soc. Jpn.* **1987**, *60*, 3619-3623. (d) Ogoshi, T.; Harada, A**.** Chemical Sensors Based on Cyclodextrin Derivatives. *Sensors* **2008**, *8*, 4961-4982.

26. Guo, D.-S.; Uzunova,V. D.; Su, X.; Liu, Y.; Nau, W. M. Operational calixarene-based fluorescent sensing systems for choline and acetylcholine and their application to enzymatic reactions. *Chem. Sci.,* **2011**, *2*, 1722-1734.

27. (a) Freeman, W.A.; Mock, W.L.; Shih, N.Y. Cucurbituril. *J. Am. Chem. Soc*. **1981**, *103*, 7367-7368. (b) Day, A., Arnold, A.P., Blanch, R.J., Snushall, B. Controlling Factors in the Synthesis of Cucurbituril and Its Homologues. *J. Org. Chem*. **2001**, *66*, 8094-8100. (c) Kim, J., Jung, I., Kim, S., Lee, E., Kang, J., Sakamoto, S., Yamaguchi, K., Kim, K. New Cucurbituril Homologues: Syntheses, Isolation, and X-ray Crystal Structures of Cucurbit[n]uril (n = 5, 7, and 8. *J. Am. Chem. Soc.* **2000,** *122*, 540-541. (d) Lagona, J., Mukhopadhyay, P., Chakrabarti, S., Isaacs, L. The Cucurbit[n]uril Family. *Angew. Chem., Int. Ed.* **2005**, *44*, 4844-4870.

28. (a) Lee, J. W. ; Samal, S. ; Selvapalam, N. ; Kim, H.-J. ; Kim, K. Cucurbituril Homologues and Derivatives: New Opportunities in Supramolecular Chemistry. *Acc. Chem. Res.* **2003**, *36*, 621-630. (b) Ong, W.; Kaifer, A. E. *Organometallics* **2003**, *22*, 4181. (c) Isaacs, L. Cucurbit[*n*]urils: from mechanism to structure and function**.** *Chem. Commun*. **2009**, 619-629.

29. Liu, S.; Ruspic, C.; Mukhopadhyay, P.; Chakrabarti, S.; Zavalij, P. Y.; Isaacs, L. The Cucurbit[*n*]uril Family: Prime Components for Self-Sorting Systems. *J. Am. Chem. Soc*. **2005**, *127*, 15959-15967.

30. (a) Halterman, R. L.; Moore, J. L.; Mannel, L. M. Disrupting aggregation of tethered rhodamine B dyads through inclusion in cucurbit[7]uril *J. Org. Chem.* **2008,** *73*, 3266-3269. (b) Halterman, R. L.; Moore, J. L.; Yip, W. T. Cucurbit[7]uril Disrupts Aggregate Formation Between Rhodamine B Dyes Covalently Attached to Glass Substrates. *J. Fluoresc.* **2012**, *21*, 1467-1478. (c) Martyn, T. A.; Moore, J. L.; Halterman, R. L.; Yip, W. T. Cucurbit[7]uril induces superior probe performance for single-molecule detection. *J. Am. Chem. Soc*. **2007**, *129*, 10338-1039.

31. Fischer, A. B.; Bronstein-Bonte, I. Photoinduced electron transfer quenching of rhodamine B in polymer films. *J. Photochem.* **1985**, *30*, 475-485.

32. (a) Ong, W.; Gomez-Kaifer, M.; Kaifer, A. E. Cucurbit[7]uril: a very effective host for viologens and their cation radicals. *Org. Lett.* **2002**, *4*, 1791-1794. (b) Kim, H.-J.; Jeon, W. S.; Ko, Y. H.; Kim, K. Inclusion of methylviologen in cucurbit[7]uril. *Proc. Natl. Acad. Sci. U.S.A.* **2002**, *99*, 5007-5011**.** (c) Moon, K.; Kaifer, A. E. Modes of Binding Interaction between Viologen Guests and the Cucurbit[7]uril Host. *Org. Lett.* **2004**, *6*, 185-188. (d) Sindelar, V.; Moon, K.; Kaifer, A. E. Binding Selectivity of Cucurbit[7]uril: Bis(pyridinium)-1,4-xylylene versus 4,4‘-Bipyridinium Guest Sites. *Org. Lett.* **2004**, *6*, 2665-2668.

33. Kalmar, J.; Ellis, S. B.; Ashby, M. T.; Halterman, R. L. Kinetics of Formation of the Host–Guest Complex of a Viologen with Cucurbit[7]uril. *Org. Lett.* **2012,** *14*, 3248-3251.

34. Bhattacharya, P.; Kaifer, A. E. Preparation, characterization, and electrochemical properties of a new series of hybrid dendrimers containing a viologen core and Frechet and Newkome dendrons. *J. Org. Chem.* **2008**, *73*, 5693-5698.

35. Cui, A.; Peng, X.; Fan, J.; Chen, X.; Wu, Y.; Guo, B. Synthesis, spectral properties and photostability of novel boron–dipyrromethene dyes. *J. Photochem. Photobiol. A* **2007**, *186*, 85-92.

36. Halterman, R. L.;Moore, J. L.; Yakshe, K. A.; Halterman, J. A. I.;Woodson, K. A. Inclusion complexes of cationic xanthene dyes in cucurbit[7]uril. *J. Incl. Phenom. Macro. Chem.* **2010**, *66*, 231-241.

Chapter V: Investigation of pH Responsive Fluorescence off-on Fluorophore-Viologen Dyads

5.1 Chapter Overview

This chapter presents the effects of cucurbit[7]uril (CB7) on the fluorescence off-on efficiency of fluorophore-viologen dyads in the presence of another competing guest molecules at different pH. Shuttling of CB7 from one binding site to another on alteringpH has already been reported. There are only few reports on switching fluorescence off-on due to displacement of CB7. Since we were interested in construction of biosensor with a novel approach where recognition of target cause the CB7 shuttles from its intial binding station to another station and result switching the fluorescence –off to –on, we put our effort to investigate the fluorescence off-on mechanism in the presence of dyads and another competing guest for CB7 on varying pH of solution. We also wanted to study the effect on the spectroscopic behavior of dyads on switching the position of substituent on viologen of dyads. ^{1}H NMR, UV-Vis absorbance, fluorescence titration, and pH titration experiments were conducted to investigate the fluorescence off-on efficacy of dyads. Data collected from fluorescence titration was further examined through curve fit to determine binding constant.

5.2 Introduction

Development of advanced techniques to monitor molecular or cellular processes *in vivo* for physicochemical alteration and theranostic application is a

current focus in cellular and materials research.[1] In particular conversion of molecular signals into nanometer scale event for biorecognition process into a readable macroscopic property is a challenge.[2] Fluorescence techniques have been becoming more promising to overcome these challenges as fluorescence sensing is highly sensitive, selective, and inexpensive, which detect the signals in the molecular level.[3] The fluorescence-on sensors seem to be more advantageous because these could provide higher target to background ratio thereby reducing the noise significantly.[4]

Switching a fluorescence-off biosensor to fluorescence-on could be based on shuttling of a host from its initial binding guest to second guest upon binding of recognition unit to target. Shuttling of host from one station to another could be driven by varying external stimuli[5] such as alternation of solvent,[6] pH of solution, and various ionic strnegth.[7] Herein we report control and selective fluorescent off-on pseudorotaxane by employing a displacement property. This model system study is crucial for the development of fluorescent off-on biosensor. Previously we have reported fluorescence-on dyads due to the disruption of aggregrate of fluorophore and quencher upon binding of cucurbit[7]uril (CB7) to the quencher shut off the electron transfer from an excited fluorophore to viologen.[8] The macrocyclic host CB7[9] binds to the cationic species in broad range K_a from 10^4 to 10^{12} M^{-1}.[10] Because of the presence of carbonyl groups at the both portal ends and an inner hydrophobic pocket, CB7 binding with cationic species is driven by ion-dipole interaction interaction and as well as hydrophobic interaction.[11] Extensive

efforts towards the study of binding of CB7 with cationic fluorophore,[12] viologen,[13] and ammonium species[10] have been documented. Furthermore binding of CB7 is highly dependent on pH of solution and can be utilized in the construction of pH sensitive molecular shuttles.[14] The displacement principle was exploited to displace dapoxyl fluorophore from CB7 on the addition of DBO as a competitive guest accompanied by deprotonation of dapoxyl fluorophore.[15]

5.3 Results and Discussion

In our previous report,8 we were able to develop highly efficient fluorescence off-on dyads which inspired us to pursue our research towards the development of biosensors. A biosensor based on this approach would posessess two binding sites for CB7. In the absence of target the fluorescence of fluorophore (rhodamine B or bodipy) will be quenched (or fluorescence-off) due to photoinduced electron transfer[16] from the excited fluorophore (Figure 5.1) to the quencher (viologen). In the presence of target CB7 will shuttle from initial binding station to the second binding station or viologen due to the change in external stimuli results the interuption of electron transfer and fluorescent enhancement (fluorescent-on) from fluorophore. The two more dyads azidotetraethyleneglycol benzylviologen-rhodamine B (Figure 4.1a) and azidotetraethyleneglycol benzylviologen-bodipy (Figure 4.1b) were syntnesized to explore the efficiency of fluorescence off-on dyad on changing the position of benzyl group from top pyridinium to bottom pyridinum of viologen. The current aim is to investigate the control fluorescent off-on efficiency of dyads at different pH solution in the

presence of competitive guest molecules as means to establish signaling through shuttling.

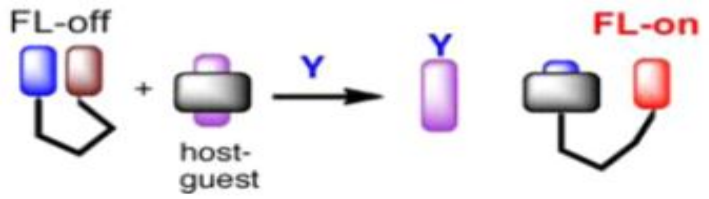

Figure 5.1. Binding of Y displaces host from initial binding site to another binding site to disrupt fluorophore aggregation. Diagram produced by Ronald L. Halterman.

The azidotetraethyleneglycol benzylviologen-rhodamine B (Figure 5.1a) and azidotetraethyleneglycol benzylviologen-bodipy (Figure 5.1b) were synthesized by following scheme 5.5. These two dyads are different in position of benzyl group than the dyads described in Chapter IV. The dyads that have benzyl positioning above viologen (Figure 5.2) needed higher concentration of CB7 to gain complete recovery because after complexation of benzyl pyridinium of viologen, the another pyridinium could still in contact with fluorophore. Thus due to a perfect height match between viologen and fluorophore a stronger aggregate (around $K= 10^2\ M^{-1}$) was formed in the case of benzyl positioning above viologen. Placing of benzyl group at the bottom of viologen (Figure 5.3) would change the fluorescence off-on efficiency since this group provides more flexibility compare to ethyl group. We posulated that this flexibility may be beneficial in terms of binding affinity with CB7 and faster recovery. Thus we aimed to synthesize dyads that possess benzyl group below viologen to gain better understanding on binding of CB7 and

fluorescence-on efficiency. Above viologen azido terminated tetraethylene glycol was placed. The azido group was for tethering with alkyne terminated another CB7 binding guest molecules via click chemistry to establish a rotaxane for the construction of biosensor.

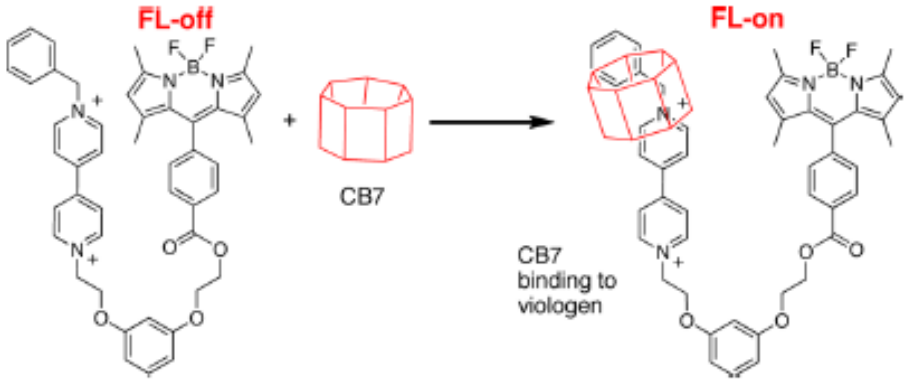

Figure 5.2. Binding of CB7 with benzylviologen of dyads **4.5c**. Diagram produced by Ronald L. Halterman.

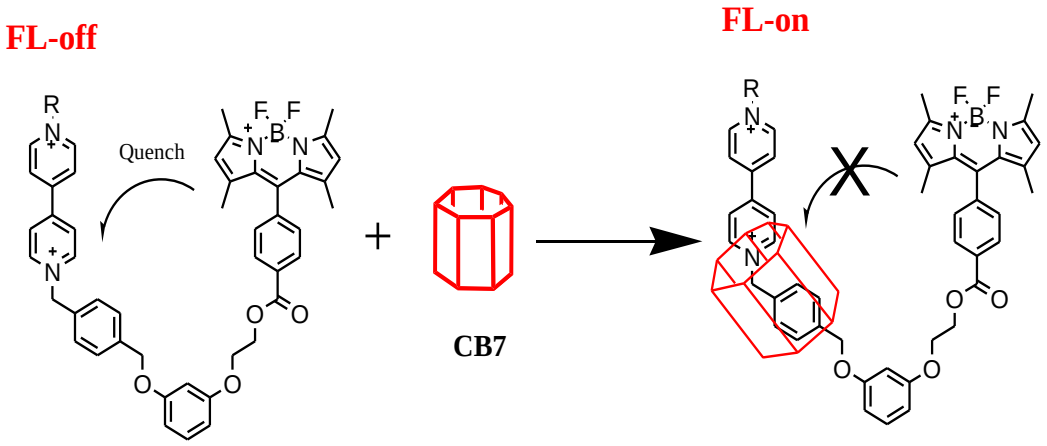

Figure 5.3. Binding of CB7 with reverse benzylviologen of dyads **5.4b**.

One hydroxy group of resourcinol was alkylated with 2-bromoethanol and a second alkylation with *p*-xylene dibromide to obtain 2-(3-(4-(bromomethyl)benzyloxy)phenoxy) ethanol. In both steps desire compound was isolated by column chromatography using hexane : ethyl acetate solvent as an eluent. This compound was exploited to anchor fluorophore and viologen on each end.

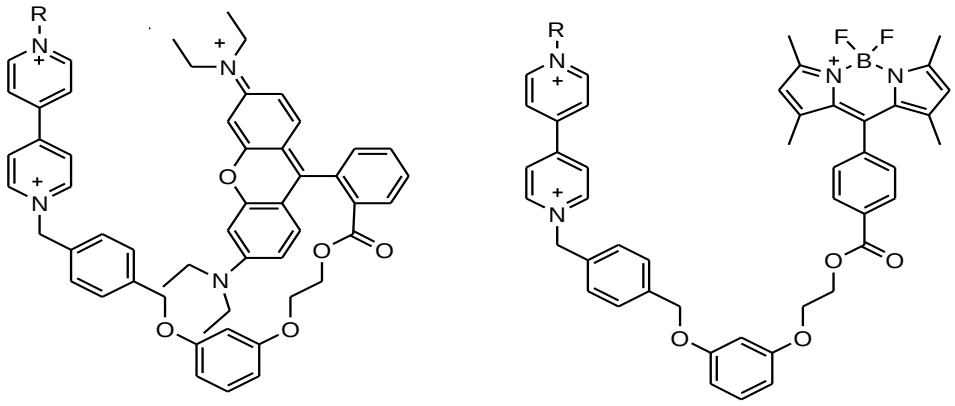

Figure 5.4a and b. Reverse benzyl azido tetraethylene glycol viologen-rhodamine B dyad (Left, Figure **5.4a**) and Reverse benzyl aido tetraethylene glycol viologen-bodipy dyad (Right, **Figure 5.4b**), R = 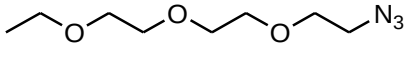

EDC promoted coupling was utilized to attach carboxy fluorophore, rhodamine B or bodipy, with hydroxy terminated dialkylated resourcinol to obtain rhodamine ester and bodipy ester respectively. Rhodamine B ester was isolated by column chromatography using dicholoromethnae : methanol (v/v 98: 2) as an eluent. The eluting solvent composition hexane : ethylacetate (v/v 3: 1) was used

to isolate bodipy ester. Tetraethylene glycol was ditosylated and one tosylate functionality was substituted by azido group.[17] The resulting monoazidomonotosyltetraethylene glycol was utilized for the monoalkylation of bipyridine.[18] Thus prepared monocationic azidotetraethylene glycol viologen was tethered with rhodamine B or bodipy ester by nucleophilic substitution of bromine to produce fluorophore tethered dicationicviologen. The polycationic dyads

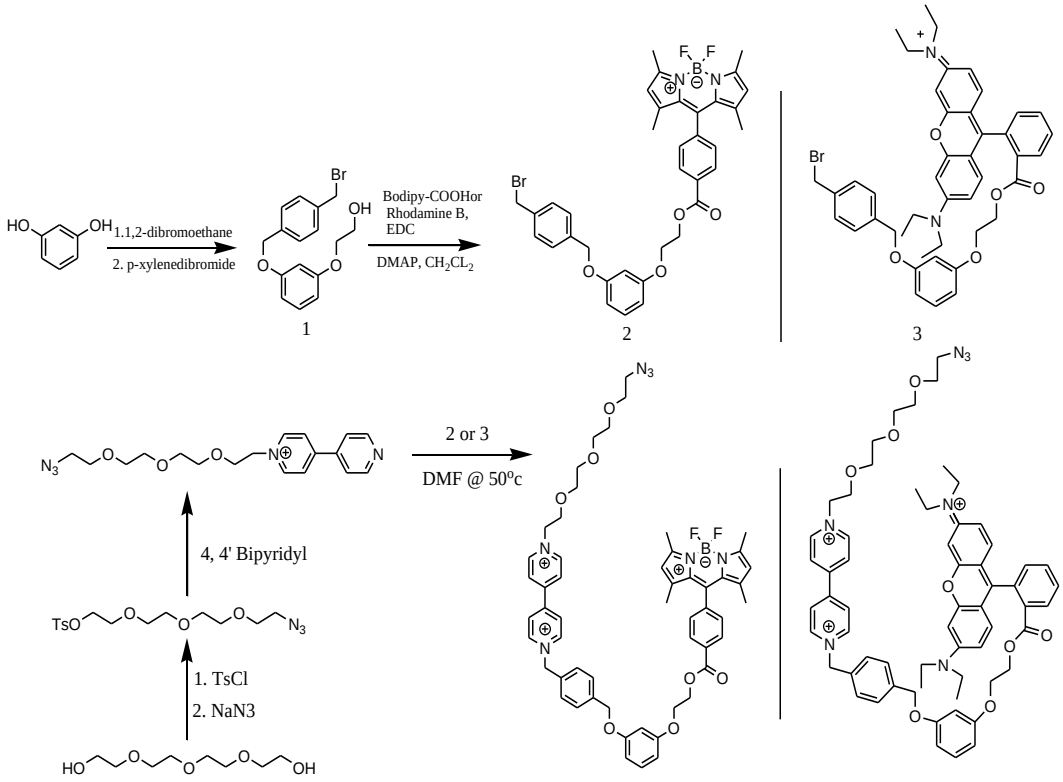

Scheme 5.5. Synthesis of reverse benzyl azidotetraethylene glycol viologen bodipy and reverse benzyl azidotetraethylene glycol viologen rhodamine B.

(Figure 5.4a and 5.4b) were purified through silica gel chromatography by using a mixture of acetone (50%) and methanol, nitromethane, and aqueous ammonium

chloride (50%, 7:2:1) as an eluent.[19] The dyad was dissolved in dichloromethane leaving behind ammonium chloride.

5.3.1. Spectroscopic Investigation of Benzyllviologen-Rhodamine B Dyad (5.4a) with Cucurbit[7]uril

Quenching and fluorescence recovery efficacy of dyad **5.4.a** was investigated by performing a CB7 titration. There was no significant spectral shift observed in the absorbance spectra in CB7 titration. Also no detectable change in absorbance was observed in the presence and absence of CB7. However, the brightness of benzylviologen dyad was fivefold lower than free rhodamine B (without viologen). Addition of CB7 resulted an efficient fluorescence recovery (*ca.* 88%), about eight fold enhancement, (Figure 5.6) due to the halting of electron transfer from excited rhodamine to the CB7 bound viologen. Fluorescent titration data was analyzed further through curve fit and this experiment was performed by Wai Tak Yip. Thus fitted curve showed two binding site, one stronger for viologen guest ($K_1 = 1.47 \times 10^5\ M^{-1}$) and second weaker could be for rhodamine B ($K_2 = 7.15 \times 10^4\ M^{-1}$). The two binding constants are very close. On the addition of CB7, CB7 forms inclusion complex with bottom benzyl and lower cationic pyridinium of viologen (Figure 5.3). Also another molecule of CB7 can still bind with cationic rhodamine B due to the presence of more flexible benzyl group resulted height mismatch between viologen and rhodamine B.

To further analyze regarding the binding site, NMR titration (Figure 5.7) was performed on constant concentration of dyad and varying concentration of CB7. The upfield shift of two α protons at 9 ppm of viologen and unshifting other two α protons at 8.9 ppm clearly indicated the binding of CB7 with one pyridinium of

viologen. Furthermore, benzyl peaks at 7.5 ppm shifted to 7.0 ppm which evidenced the inclusion of benzyl into CB7 host and at 1.5 equiv of CB7 complete dispperance of benzyl peaks also supported binding of CB7 to the lower pyridinum of viologen or pyridnium that is closer to benzyl group.[20] Curve fit data showed two binding site for CB7 one for benzylviologen and another we assume for rhodamine B. Binding of CB7 with rhodamine B of dyad **5.4a** could be possible due to its cationic behavior and also benzyl group keeps rhodamine B away from viologen so as to allow steric CB7 binding possible more efficiently than the dyads having benzyl group above viologen. Binding of CB7 with rhodamine B can easily be followed by observing perturbation of 3,6-bis(*N*,*N*-diethylanilino) signals.[21] Unavoidable binding of CB7 with rhodamine B evidenced the splitting of anilinium ethyl peak at 3.3 ppm and methyl pekas at 1.0 ppm into two sets of signals. This two sets of signal indicated slow exchange between bound and free rhodamine B.

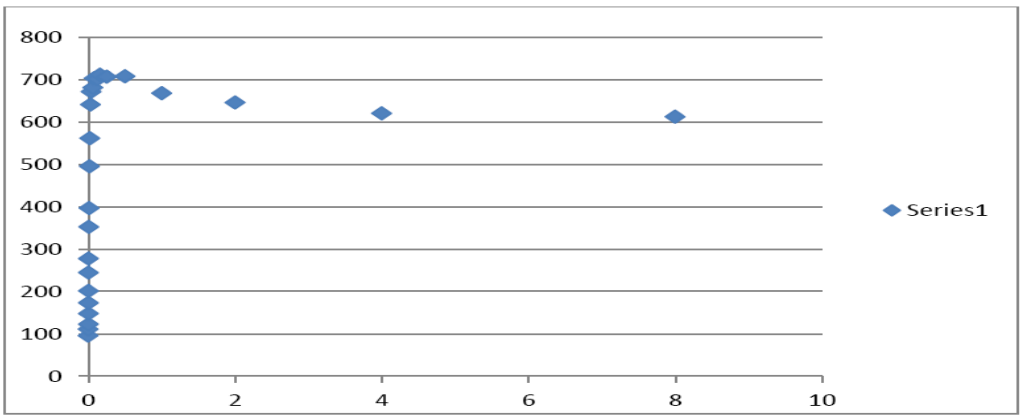

Figure 5.6. Fluorescence titration curve of **5.4a** dyad (5 μM) titrated with CB7 (0 mM, 8mM - 0.0019 mM, 0.16 mM- 0.0003 mM) in millipore water at 585 nm.

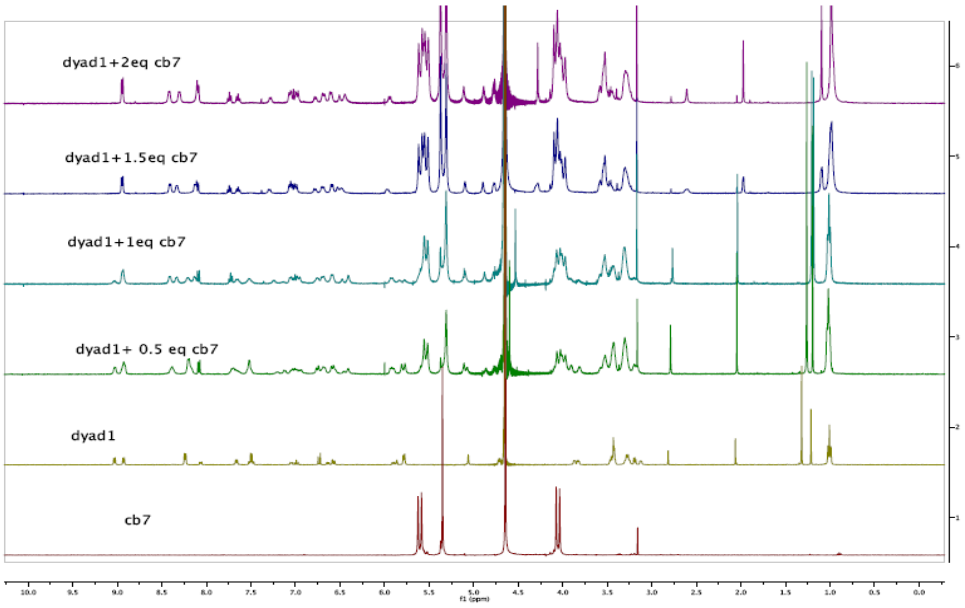

Figure 5.7. ^{1}H NMR spectra (400 MHz, D_2O) of **5.4a** dyad (2.1 mM) with CB7 (0 to 2 equivalent).

5.3.2 Spectroscopic Investigation of Reverse Benzyl Azido Tetraethylene Glycol Viologen-Bodipy Dyad (5.4.b) with Cucurbit[7]uril

Similar to dyad **5.4a**, no significant spectral shift and change in absorbance was noticed in the absence and presence of CB7 in the case of benzyl azido tetraethylene glycol viologen-bodipy dyad . Quenching was observed in the absence of CB7 while fluorescence titration with CB7 a large enhancement, 20 fold, in emission intensity (Figure 5.8) was observed. Fluorescence titration data was used for curve fitting and as expected curve was nicely fitted with one CB7 binding mode. This curve fitting was also performed by Wai Tak Yip. Interestingly, strong binding constant was calculated ($K = 2.72 \times 10^6\ M^{-1}$) for **5.4b** dyad which is comparable to the literature binding constant of free viologen.[13, 10]

This result is crucial large enhancement due to binding of CB7 with viologen only not as with efficient quenching when CB7 is on rhodamine B.

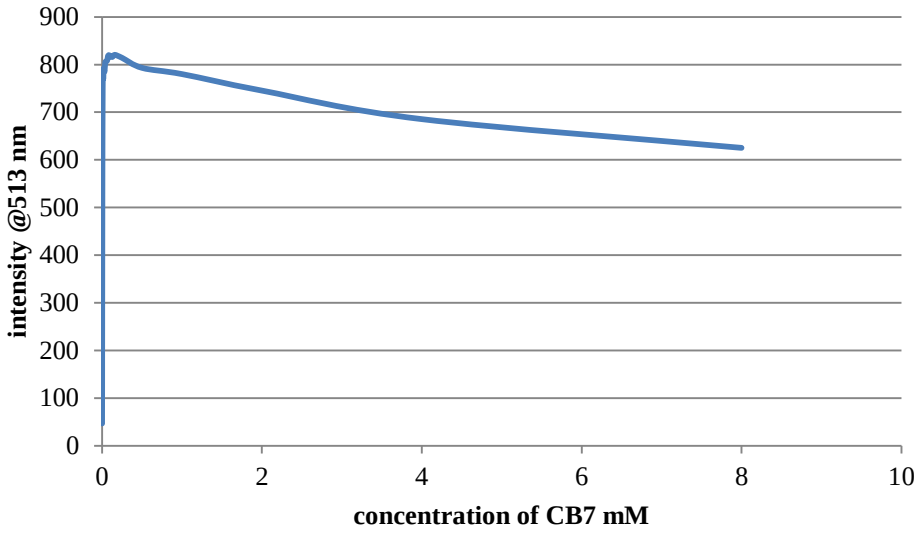

Figure 5.8. Fluorescence titration curve of reverse benzylviologen- bodipy (5 μM) titrated with CB7 (0 mM, 8mM - 0.0019 mM, 0.16 mM- 0.0003 mM) in Millipore water.

The mode of binding of CB7 with dyad **5.4b** was further investigated by performing NMR titrations (Figure 5.9) with CB7. In this case also upfield shift two α protons around 9.1 ppm while no shift of two other α protons at 9.0 ppm, pyridinium tethered to tetraethylene glycol, of viologen indicated binding of CB7 to the one of the pyridiniums of viologen. Complete disappearance of benzyl peak at 7.5 supported binding of CB7 with one pyridinum and benzyl group.

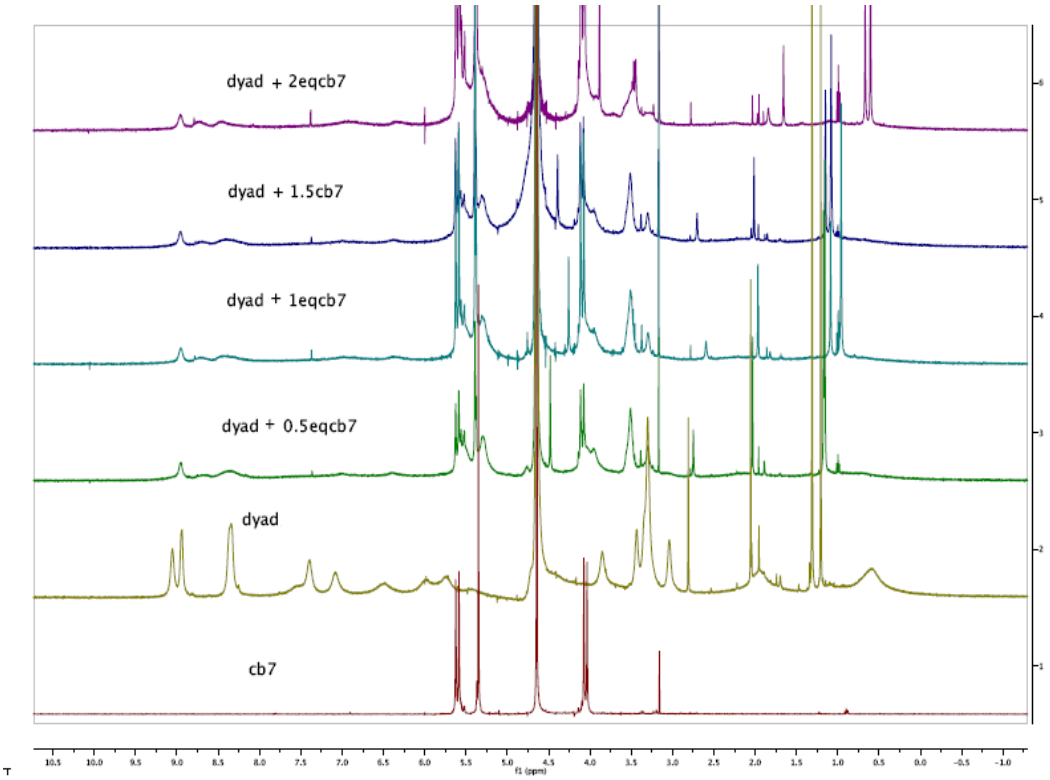

Figure 5.9. ^{1}H NMR spectra (400 MHz, D_2O) of 5.4b dyad (2.95 mM) with CB7 (0 to 2 equivalent).

Dyads having benzyl group at the bottom of viologen showed very efficient fluorescent off-on in the absence and presence of CB7 respectively. After this exciting result it was important to investigate the shuttling efficiency of CB7 from its initial binding station to quencher viologen binding station on changing external stimuli since working of our biosensor depends on shuttling of CB7. Thus we pursue the research towards the examination of fluorescence off-on efficacy of dyads at different pH solutions with CB7.

5.3.3 Investigation of Efficacy of Control and Selective Fluorescence Off-On of 5.4a and 5.4b Dyads by Displacement Principle at Different pH.

The main aim of this experiment was to observe the control fluorescence off-on process. For this *p* -xylyl diamine was selected as a competitor guest since its binding constant is higher than that of viologen.[10] As expected at lower pH, CB7 preferred to bind with protonated *p*-xylyldiamine and quenching of dyad was observed. The pH titration performed from pH 2 to pH 8 and quenching was continued to pH 8. It could be due to the higher pK_a of amine (*ca.* 9)[22] there was still protonated amine and CB7 prefers to bind with xylyl amine. Also, at higher pH the system turned to complex because of higher ionic strength as well as cleavage of viologen and ester bond of dye.

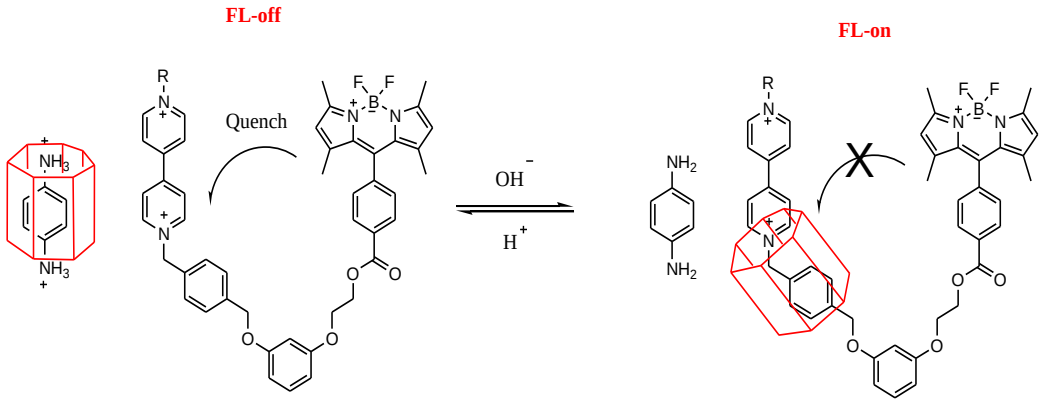

Figure 5.10. Mechanism for fluorescence off-on at different pH.

Thus we chose 1,4-diaminobenzene (pK_a 4-5)[22] as it possesses a lower pK_a . The binding of this amine and viologen is the same at the order of 10^6 M^{-1}.[10] Unsurprisingly, binding of CB7 at lower pH was observed with both protonated

amine and viologen of dyads. As a control quenching could be observed in the absence of CB7 at all pH's studied and also no effect on quenching was observed in the presence amine at all pH's studied. As the pH of solution increased dramatic increase in enhancement was noted (Figure 5.11 and 5.12) due to the displacement of deprotonated 1,4-diaminobenzene amine from CB7 and more binding of CB7 to the viologen (Figure 5.10) of dyads. At pH 6 complete recovery of fluorescence of dyads were observed as no CB7 prefers to bind with neutral amine and can completely bind viologen to disrupt quenching aggregation. Therefore, fluorescence off-on could be controlled by using suitable guest on the basis of binding constant.

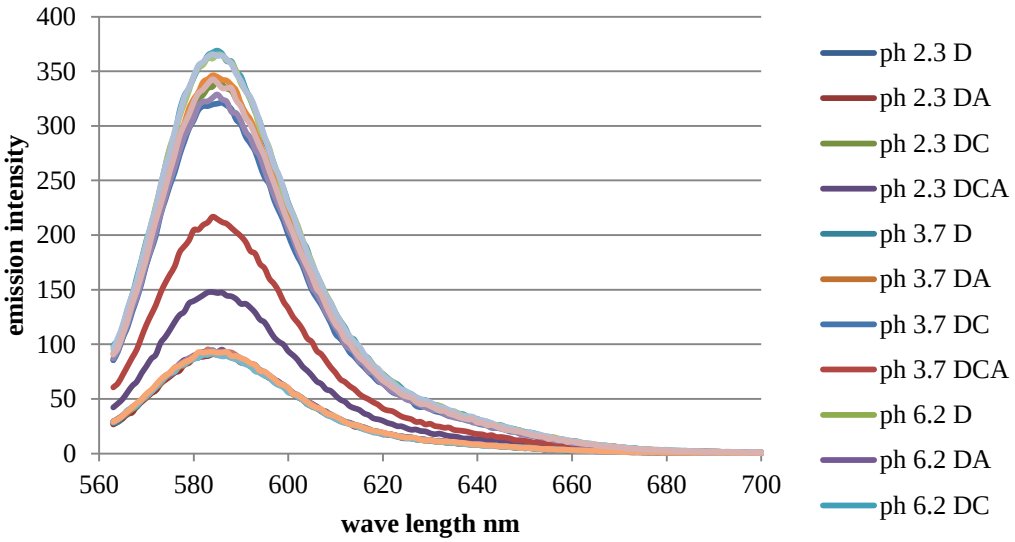

Figure 5.11. Emission spectra of reverse benzylviologen-rhodamine B dyad (5 μM dyad + 6.25 μM CB7 + 10 μM 1,4-diaminobenzene, D = dyad, A= diaminobenzene, C= CB7, excitation wavelength = 562 nm).

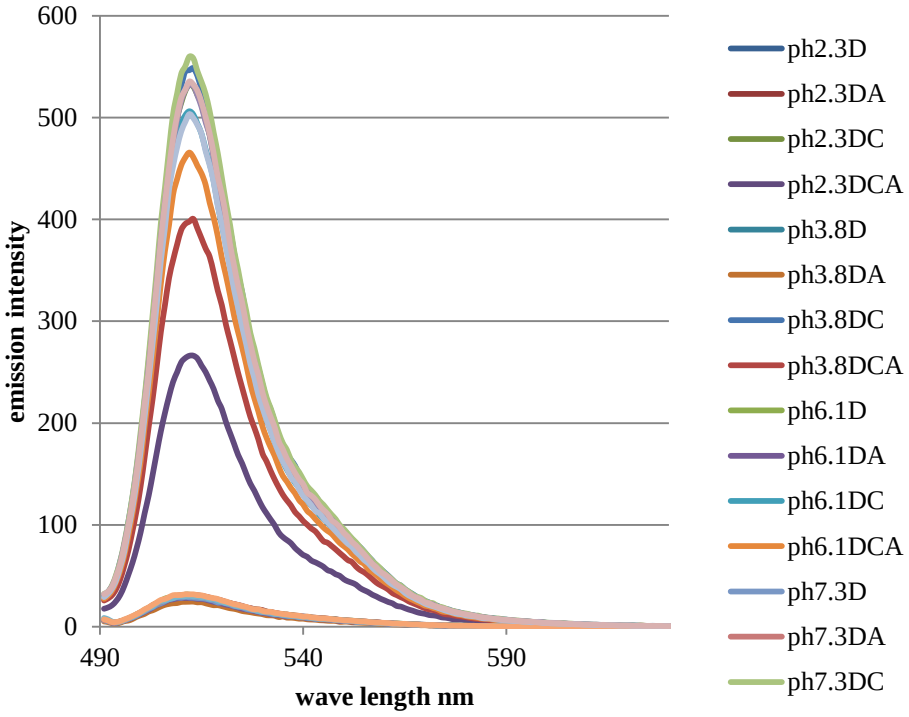

Figure 5.12. Emission spectra of reverse benzylviologen-BODIPY dyad (5 μM dyad + 6.25 μM CB7 + 10 μM 1,4-diaminobenzene, D=dyad, A= diaminobenzene, C= CB7, excitation wavelength = 490 nm).

In conclusion, we have developed two more new dyads that exhibit very efficient fluorescence off-on in the absence and presence of CB7 respectively. More importantly, we have demonstrated shuttling of CB7 from one station to another dyad employing displacement property of CB7. This study was crucial before construction of biosensors.

5.4 Chapter Summary

The displacement of Cucurbit[7]uril (CB7) from one guest molecule, 1,4-diaminobenzene, to another, viologen of dyads, and its effect on fluorescence off-on mechanism was studied. ^{1}H NMR, UV-Vis absorbance, fluorescence titration, and pH titration experiments were conducted to investigate the effect on photophysical properties of the dyads on the displacement of CB7 and also to study the effect on photophysical properties of the dyads on changing the position of substituent on viologen of dyads . Fluorescence titration data was utilized in curve fitting to determine binding contant and ^{1}H NMR titration experiments were used to analyze the binding mode of CB7 to the dyads.

On changing the position of benzyl group from terminal pyridinum of viologen to the bottom pyridinium, quenching was still in existence in the absence of CB7. Addition of CB7 showed emission enhancement due to interruption electron transfer from excited fluorophore to the viologen of dyads. Collected fluorescence titration data was further utilized to determine binding constant by curve fitting. Binding was found to be higher around 10^{6} which was comparable to the binding contant of isolated viologen. Furthermore, the curve was fitted well to two and single binding curve with viologen-rhodamine dyad and viologen-bodipy dyad respectively. ^{1}H NMR titration data was consistent to the curve fitting data. As expected the pH titration data showed quenching of fluorescence due to binding of CB7 with protonated amine at lower pH. However, complete recovery of fluorescence was found at higher pH. This finding could be utilized to control

fluorescence off-on mechanism by varying pH solution. This preliminary finding will be utilized in the construction of biosensor.

5.5 Experimental

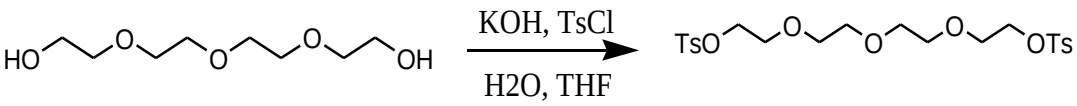

Tetraethyleneglycol ditosylate .[17] In a 250 mL reaction flask, tetraethylene glycol (2.2 mL, 12.87 mmol), tosyl chloride (7.36 g, 38.6 mmol), and THF (50 mL) were added.The mixture was cooled to 0 ^{o}C and then potassium hydroxide (5.05 g, 90.1 mmol, 25 mL H_2O) solution was added dropwise to the reaction mixture over 1 h. The mixturewas stirred for additional 2 h. The crude reaction mixture was poured into water/diethylether (50 mL/50 mL) and the organic layer was separted. The aqueous layer was extracted with diethylether (3 x 20 mL). The combined organic portion was washed with sat. ammonium chloride (1 x 20 mL) and water (3 x 20 mL). The organic phase was dried over anhydrous $MgSO_4$, filtered and removed solvent via vacuum evaporation to give **1** (5.969 g, 92% yield) as a colorless oily liquid. ^{1}H NMR 7.78 (d, 4H, *J* = 9 Hz), 7.32 (d, 4H, *J* = 9 Hz), 4.15 (t, 4H, *J* = 6 Hz) 3.68 (t, 4H, *J* = 6 Hz), 3.56 (s, 8H), 2.44 (s, 6H).

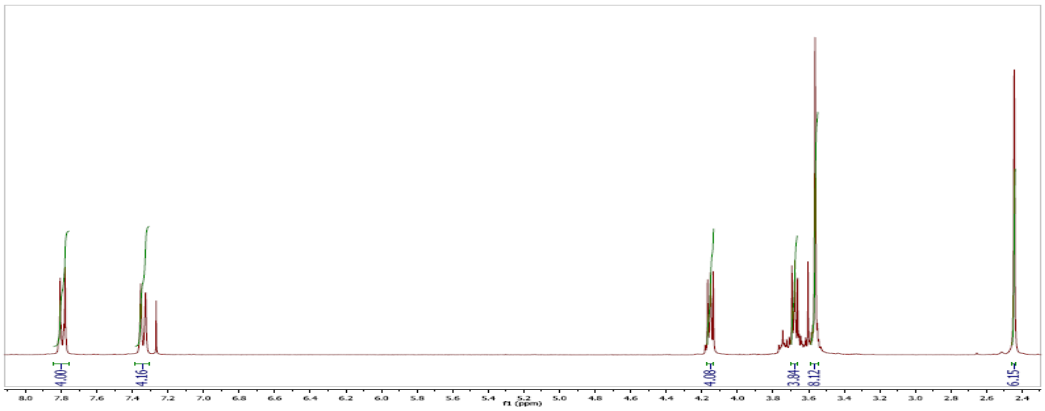

Figure 5.13. ^{1}H NMR spectrum of **Tetraethyleneglycol ditosylate.**

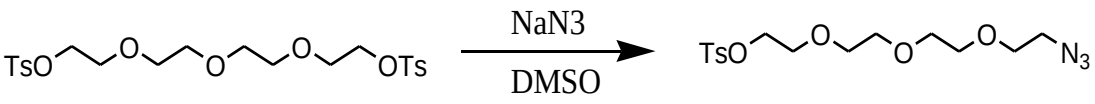

Azidotetraethyleneglycol tosylate.[17] The tetraethyleneglycol ditosylate (4.185 g, 8.3 mmol) was dissolved in DMSO (25 mL). To this solution was added NaN_3 (182 mg, 2.8 mmol) portion wise and the mixture was stirred overnight under nitrogen at room temperature. The reaction was quenched with H_2O (50 mL) and stirred for 5 min. The reaction mixture was extracted with diethyl ether (3 x 15 mL). The combined ether portion was washed with brine (1 x 15 mL) and water (3 x 15 mL). The ether portion was dried over anhydrous $MgSO_4$, filtered and concentrated under reduced pressure. The crude compound was purified by silica gel column chromatography (hexane/ethylacetate, 1:1) to give **2** (0.5 g, 48% yield) as a colorless oily liquid. ^{1}H NMR (300 MHz, $CDCl_3$) δ 7.80 (d, 2H, J = 9 Hz), 7.34 (d, 2H, J = 9 Hz), 4.16 (t, 2H, J = 6 Hz) 3.64-3.70 (m, 8H), 3.60 (s, 4H), 3.38 (t, 2H, J = 6Hz), 2.45 (s, 3H).

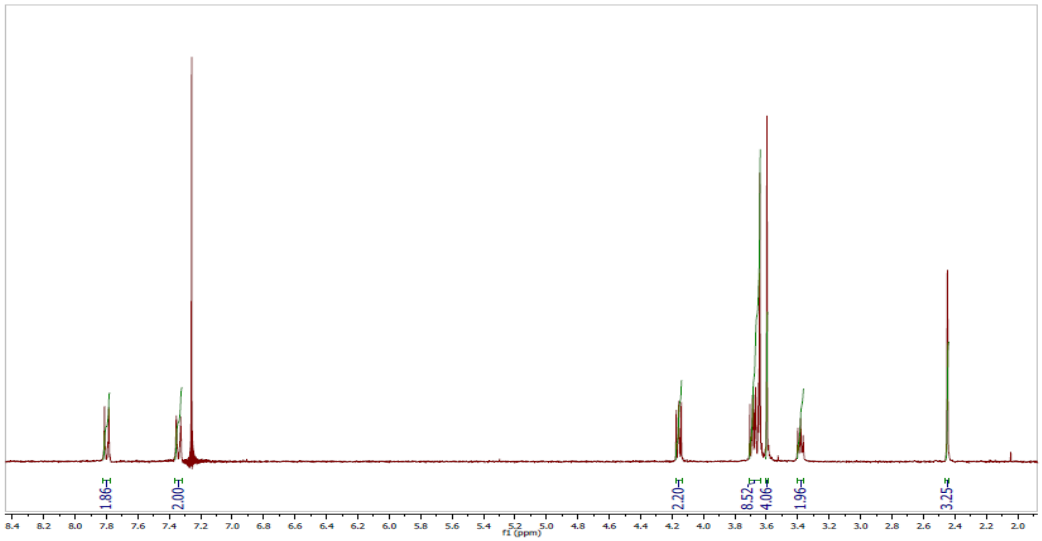

Figure 5.14. ^{1}H NMR spectrum of **azidotetraethyleneglycol tosylate.**

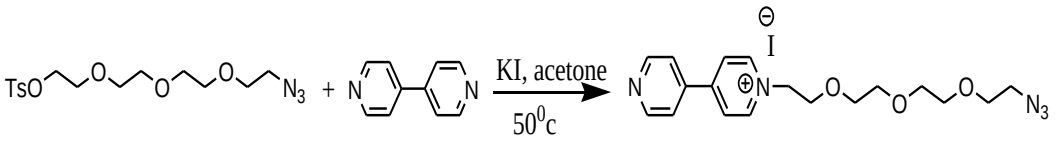

AzidoTetraethylene glycol viologen. In a 100 mL reaction flask, azidotetraethyleneglycol tosylate (206 mg, 0.55 mmol), 4, 4'-dipyridyl (345 mg, 2.2 mmol), potassium iodide (91 mg, 0.55 mmol), and acetone (20 mL) were added. The suspension was heated under reflux for 4 d. The flask was cooled to room temperature and solvent was removed via vacuum evaporation. The residue was purified by column chromatography (SiO_2, 9:1 to 8:2 CH_2Cl_2 / CH_3OH) to provide **3** (95 mg, 36% yield) as a yellow oily liquid. ^{1} H NMR (300 MHz, $CDCl_3$) δ 8.57 (2H, d, J = 6 Hz), 8.89 (2H, d, J = 6 Hz), 8.30 (2H, d, J = 6Hz), 7.7 (2H, d, J = 6 Hz), 5.24 (2H, t, J = 6Hz), 4.14 (2H, t, J = 6Hz), 3.6-3.7 (10 H, m), 3.42 (2H, t, J = 6 Hz) 13C NMR (75MHz, CD_3OD) δ 150.68, 145.78, 142.57, 125.06,

122.14, 70.18, 70.08, 69.57, 68.72, 50.34. MS-ESI:*m/z* calcd for $[C18H24N_5O_3]^+$ 358.4167; found 358.1867 $[M]^+$.

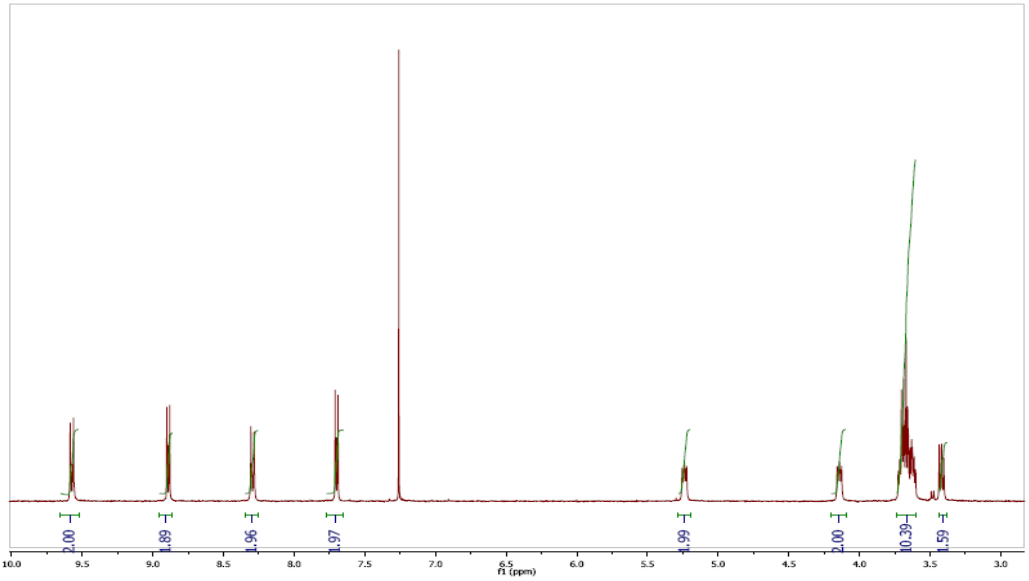

Figure 5.15a. ^{1}H NMR spectrum of **azidotetraethylene glycol viologen.**

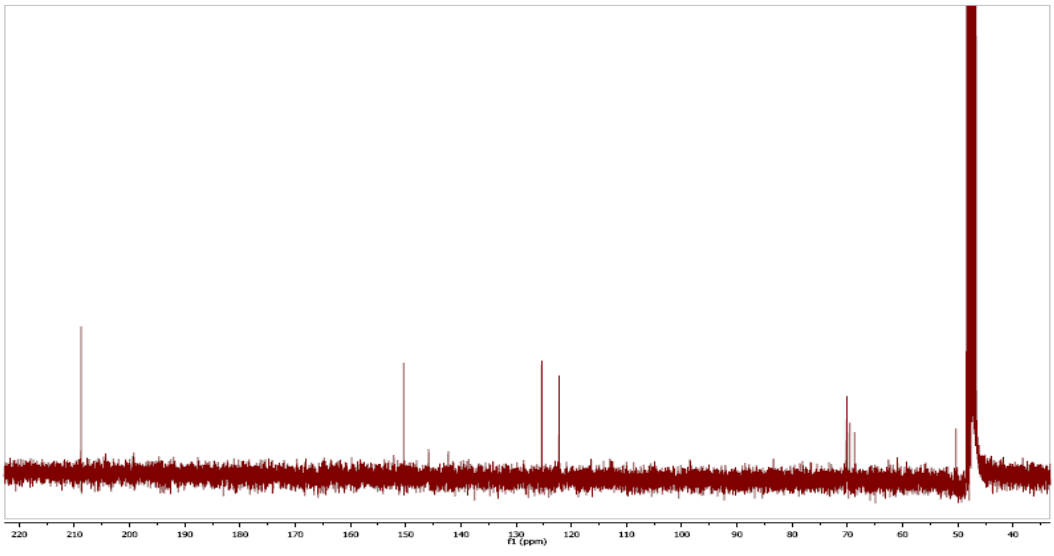

Figure 5.15b. ^{13}C NMR spectrum of **azidotetraethylene glycol viologen.**

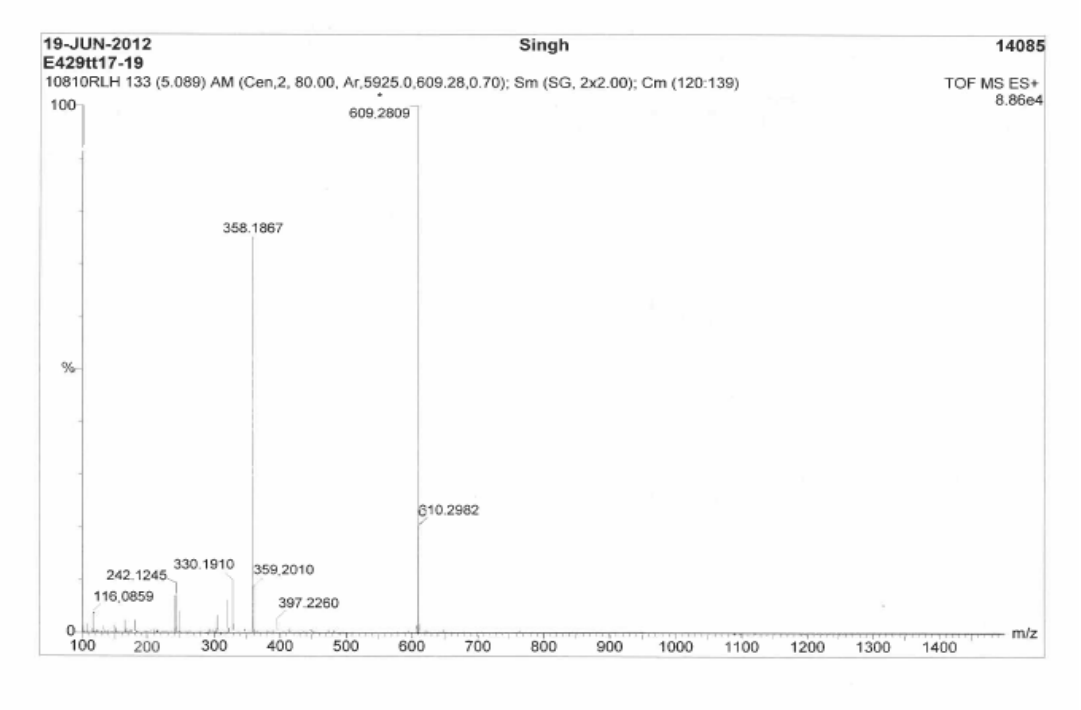

Figure 5.15c. Mass spectrum of **AzidoTetraethylene glycol viologen.**

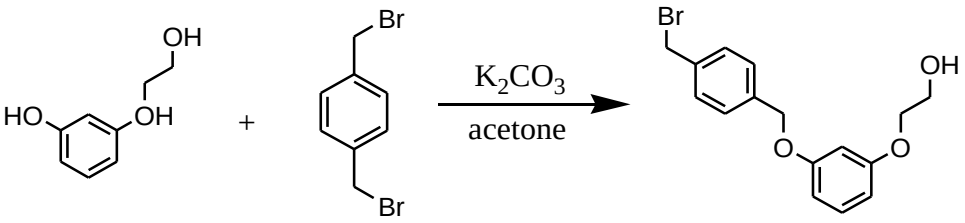

2-(3-(4-Bromomethyl)benzyloxy)phenoxy)ethanol. In a 250 mL reaction flask, 3-(2-hydroxyethoxy)phenol (1.86 g, 12.06 mmol), 1,4-bis(bromomethyl)benzene (19.11 g , 72.39 mmol), potassium carbonate (1.833 g , 13.26 mmol), 18-crown-6 ether (0.319 g, 1.2 mmol), and acetone (100 mL) were added. The suspension was heated under reflux for 1 d. The flask was cooled to room temperature and acetone was removed via vacuum evaporation. Recrystallization of the crude product was performed to remove most of 1,4-bis(bromomethyl)benzene that separated by

filtration as a white crystals. The filtrate was concentrated and the crude product was purified by silica gel column chromatography (2:1 to 1:1 hexane / ethyl acetate) to provide 2-(3-(4-bromomethyl)benzyloxy)phenoxy)ethanol, **4** (2.845 g, 70% yield) as a white solid. ^{1}H NMR(300 MHz, CD_3COCD_3) 7.49 (s, 4H), 7.17 (t, 1H, *J* = 9 Hz), 6.51-6.61 (m, 3H), 5.12 (s, 2H), 4.67 (s, 2H), 4.04 (t, 2H, *J* = 6 Hz), 3.8 (q, 2H, *J* = 5 Hz) ^{13}C NMR (400 MHz, CD_3COCD_3) 160.47, 160.03, 137.85, 129.83, 129.28, 127.77, 107.05, 101.71, 69.66, 69.08, 60.44, 33.20 HRMS- ESI *m/z* calculated for [$C_{16}H_{17}BrO_3Na$] 359.025; found 359.025 [M + Na] and 361.023 [M+2 + Na].

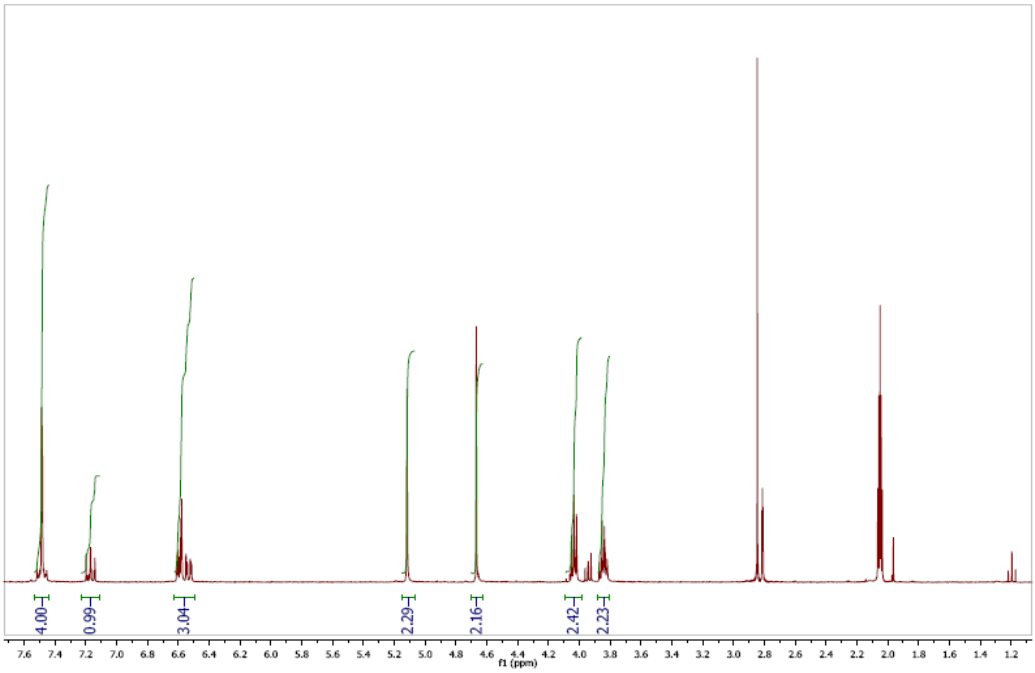

Figure 5.16a. ^{1}H NMR spectrum of **2-(3-(Bromomethyl)benzyloxy)phenoxy)ethanol.**

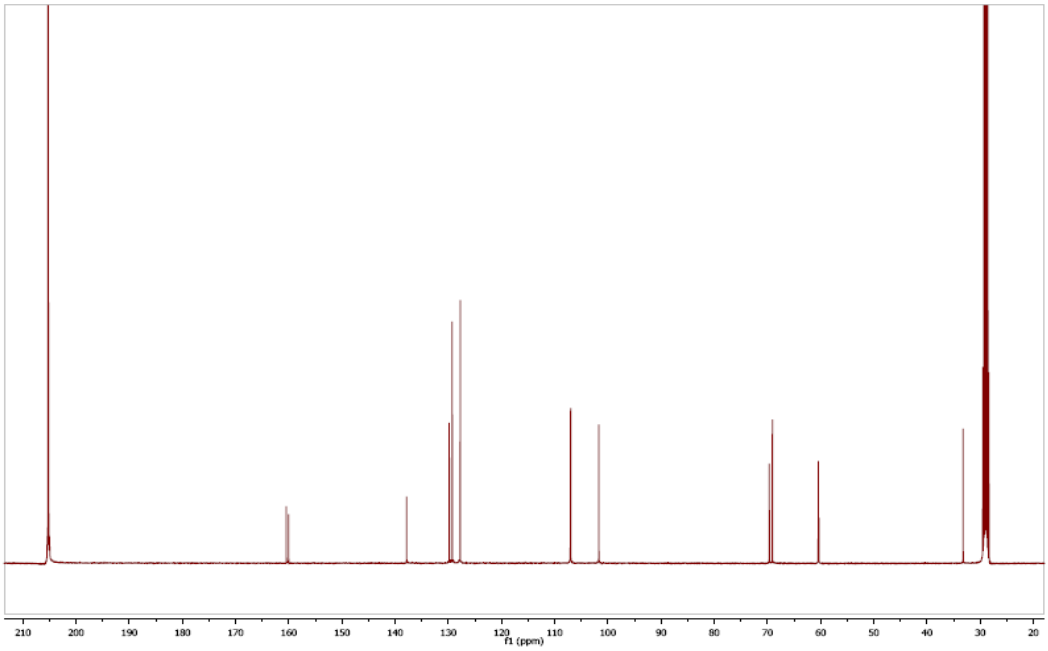

Figure 5.16b. ^{13}C NMR spectrum of **2-(3-(Bromomethyl)benzyloxy)phenoxy)ethanol.**

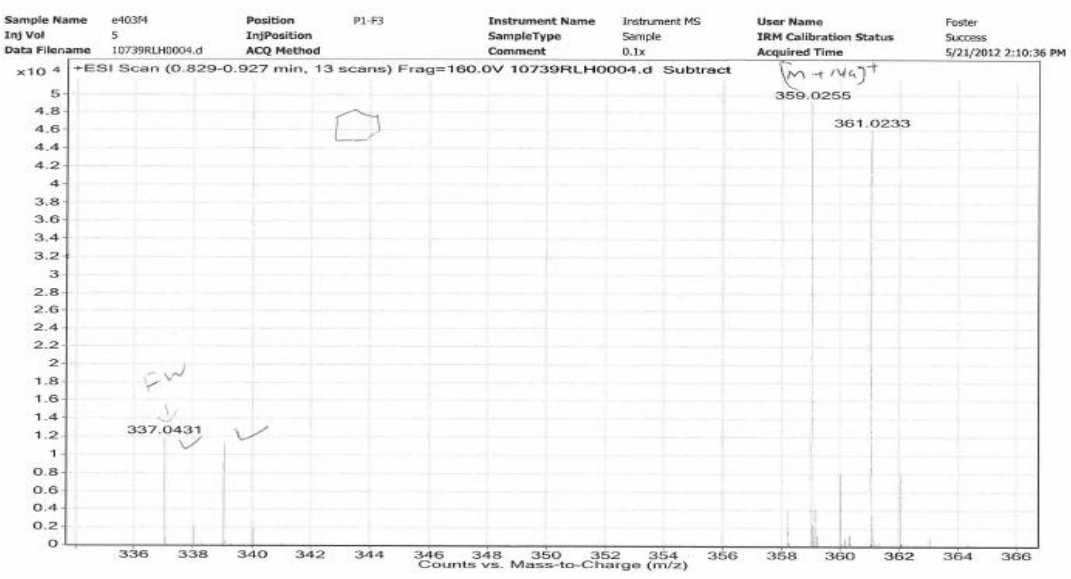

Figure 5.16c. Mass spectrum of **2-(3-Bromomethyl)benzyloxy)phenoxy)ethanol.**

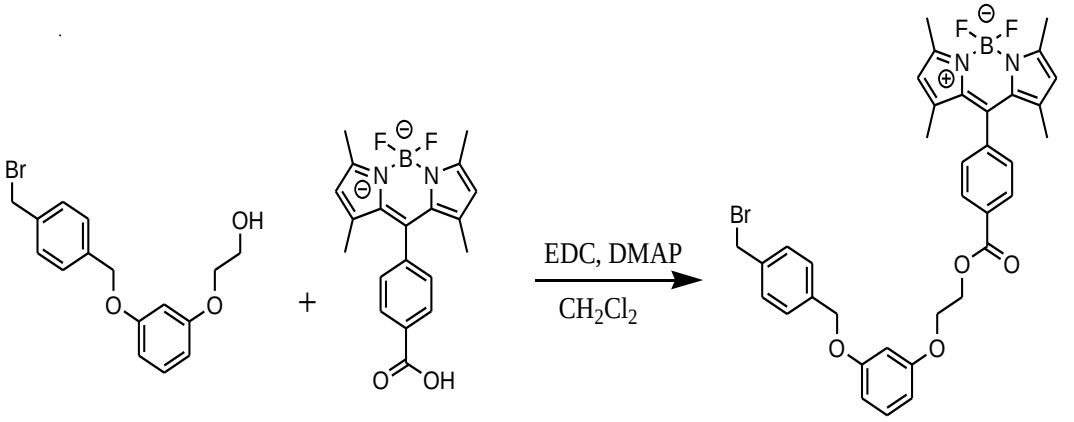

Bodipy ester. In a 50 mL reaction flask, (4-carboxyyphenyl)bodipy (189 mg, 0.5 mmol), 2-(3-(2-bromomethyl)benzyloxy) phenoxy)ethanol (189 mg, 0.56 mmol), 1-ethyl-3-(3-dimethylaminopropyl)carbodiimide (148 mg, 0.77 mmol), *N*,*N*-dimethylaminopyridine (10 mg, 0.08 mmol), and dichloromethane (15 mL) were added. The mixture was stirred for 3 d at room temperature. The solvent was removed via vacuum evaporation. The compound was purified by column

chromatography (SiO_2, 3:1 hexane / EtOAc) to provide **5** (66 mg, 17% yield) as an orange solid. ^{1}H NMR (300MHz $CDCl_3$) 8.18 (d, 2H, *J* = 6 HZ), 7.4 (d, 2H, *J* = 6 Hz), 7.41 (s, 4H), 7.21 (t, 1H, *J* = 6Hz), 6.56-6.62 (m, 3H), 5.99 (s, 2H), 5.05 (s, 2H), 4.70 (t, 2H, *J* = 6Hz), 4.59 (s, 2H), 4.33 (t, 2H, *J* = 6 Hz) 2.56 (s, 6H), 1.35 (s, 6H) ^{13}C NMR (75MHz $CDCl_3$) 165.89, 159.93, 159.73, 156.02, 142.88, 140.13, 140.04, 137.25, 137.12, 130.54, 130.47, 130.09, 128.87, 128.38, 127.77, 121.50, 107.46, 107.22, 102.15, 69.57, 69.94, 63.76, 45.90, 14.62 HRMS- ESI *m/z* calculated for $[C_{36}H_{34}BBrF_2N_2O_4]$ 686.1763 found; 687.1584 $(M + H)^+$ and 689.1828 for $(M+2 + H)^+$.

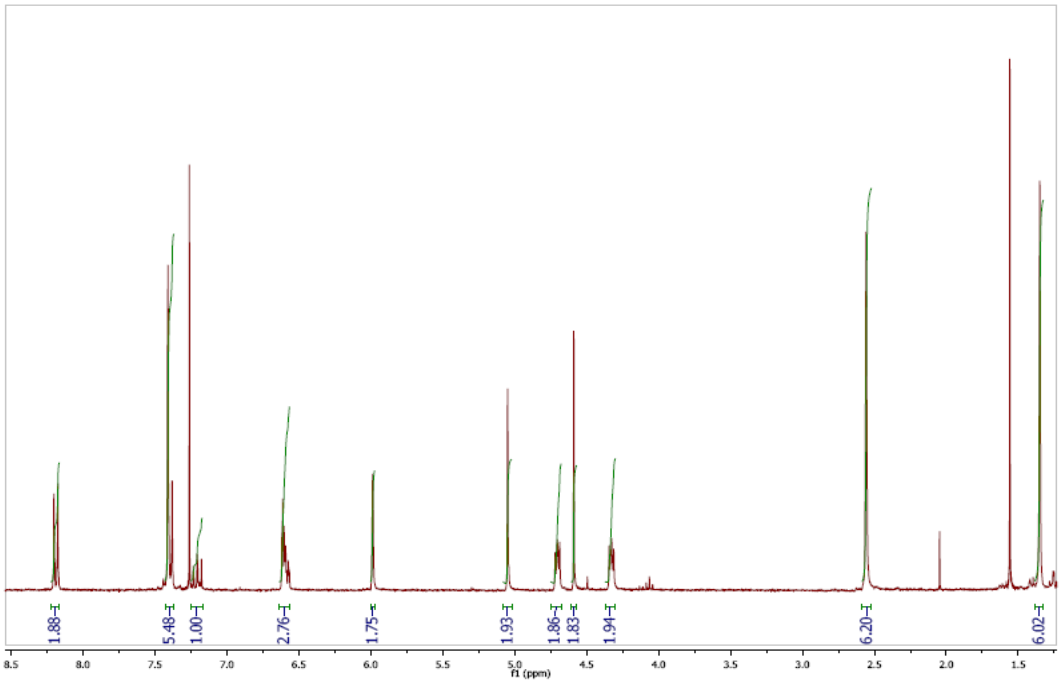

Figure 5.17a. ^{1}H NMR spectrum of **Bodipy ester.**

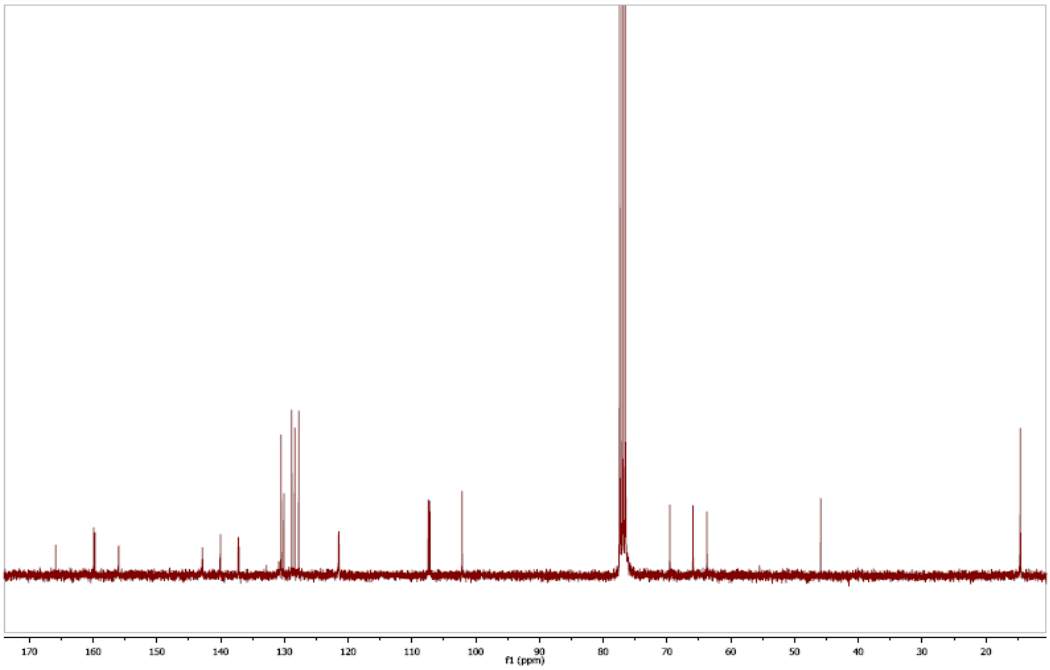

Figure 5.17b. ^{13}C NMR spectrum of **Bodipy ester.**

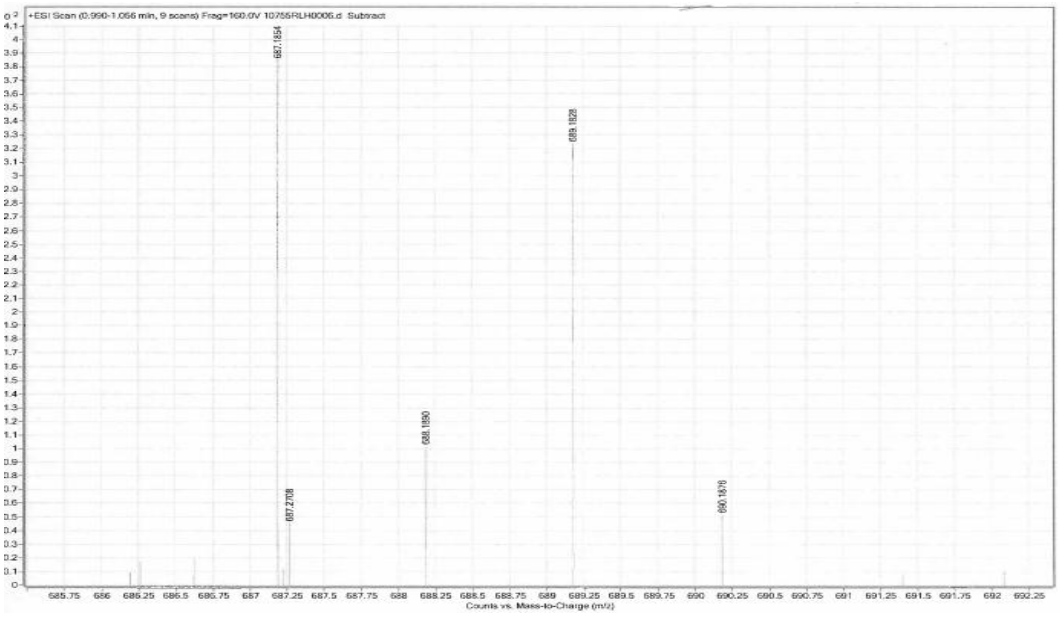

Figure 5.17c. Mass spectrum of **Bodipy ester.**

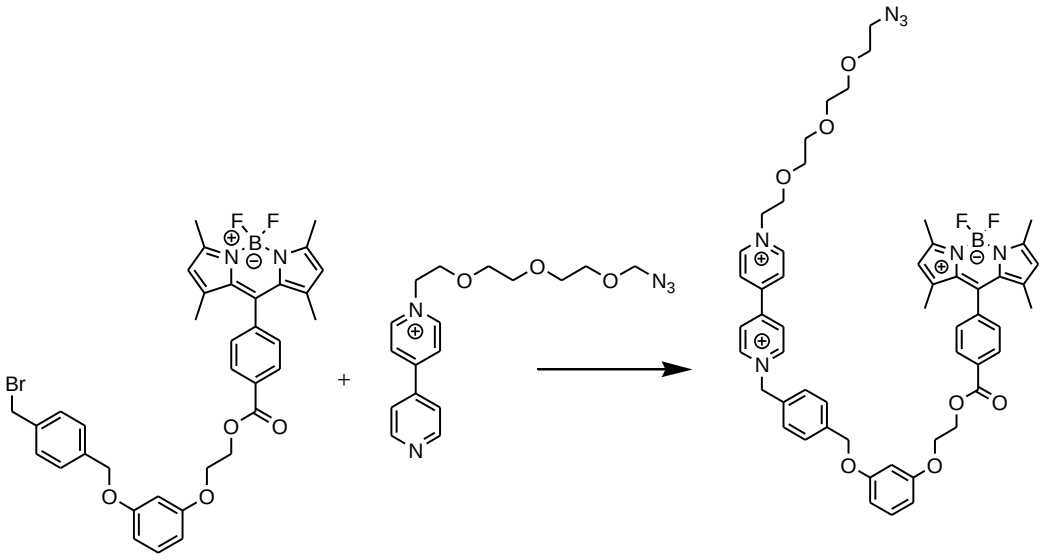

Benzyl azidotetraethylene glycol viologen-BODIPY dyad 5.4b. In a 100 mL reaction flask, bodipy ester (66 mg, 0.1 mmol), tetraethyleneglycol viologen (98 mg, 0.2 mmol), and DMF (5 mL) were added. The mixture was heated at 50 °C for 4 d. The flask was cooled to room temperature and solvent was removed via high vacuum evaporation. The compound was purified by column chromatography [SiO_2, 5:5 acetone / (7:2:1 MeOH / 2M aq. NH_4Cl / CH_3NO_2)] to provide reverse benzylviologen-BODIPY dyad **1** (41 mg, 36% yield) as an orange solid. ^{1}H NMR (CD_3OD 400 MHz) δ 9.29 (m, 4H), 8.66 (b, 4H), 8.16 (d, 2H, J = 12 Hz), 7.57 (s, 4H), 7.44 (d, 2H, 8 = Hz), 7.15 (t, 1H, J = 8 Hz), 6.56- 6.64 (m, 3H), 6.07 (s, 2H), 5.96 (s, 2H), 5.11 (s, 2H), 4.93 (b, 2H), 4.66 (t, 2H, J = 4 Hz), 4.35 (t, 2H, J = 4 Hz), 4.04 (b, 2H), 3.57- 3.68 (m, 10H), 3.34 (m, 2H), 2.48 (s, 6H), 1.36 (s, 6H) ^{13}C NMR (100 MHz, CD_3OD) δ 165.73, 160.01, 159.77, 155.80, 150.38, 150.01, 146.36, 145.65, 143.00, 140.63, 139.82, 139.77, 132.27, 130.66, 130.20, 129.70, 129.14, 128.46, 128.24, 127.12, 126.43, 121.10, 121.10, 107.22, 107.04, 101.92,

70.17, 70.06, 70.04, 69.99, 69.49, 68.69, 68.63, 65.85, 64.21, 63.78, 61.46, 50.33, 49.30, 24.62, 22.57, 22.54, 13.31, 13.16 ^{19}F NMR -146.90 (q) HRMS- ESI *m/z* calculated for $[C_{54}H_{58}BF_2N_7O_7]^{2+}$ 482.7229; found 482.7216 for [M/2].

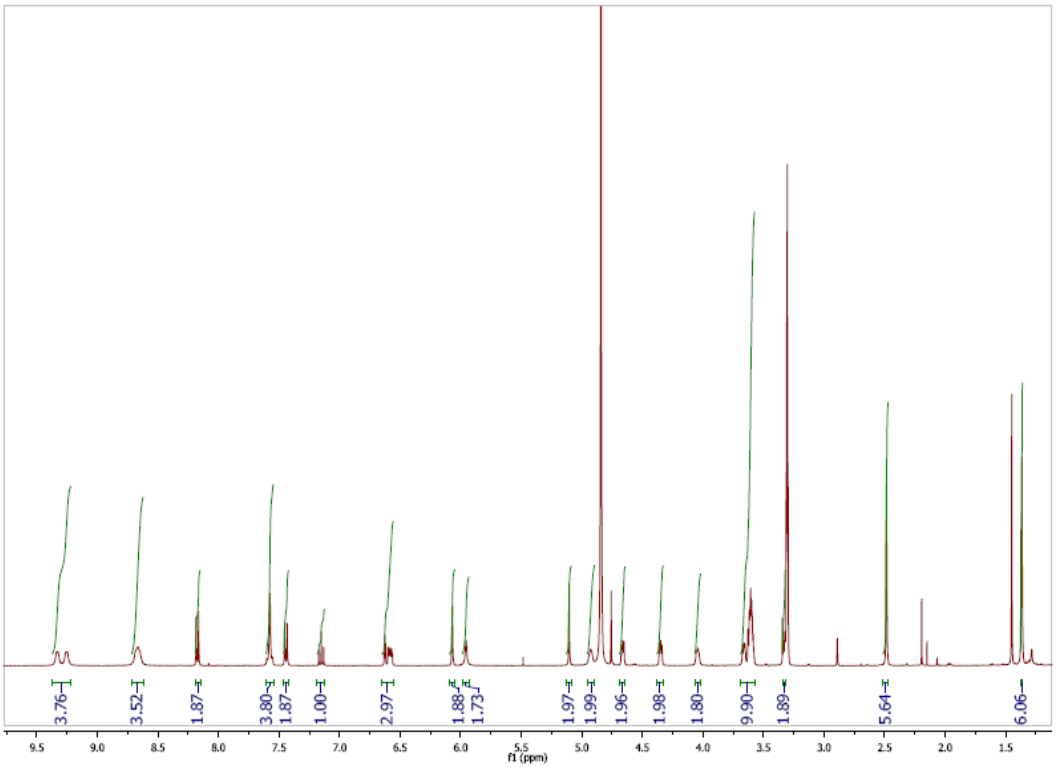

Figure 5.18a. ^{1}H NMR spectrum of **benzyl azidotetraethylene glycol viologen-Bodipy dyad 5.4b.**

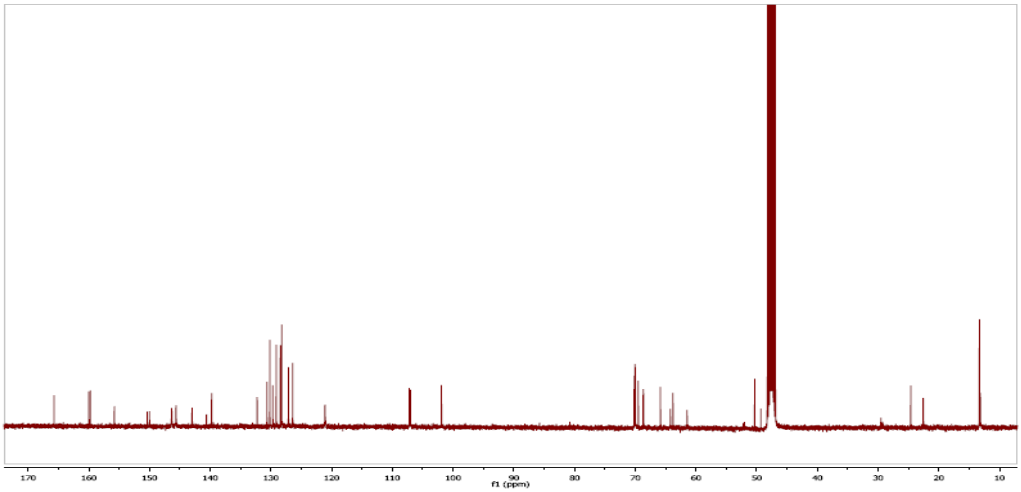

Figure 5.18b. ^{13}C NMR spectrum of **benzyl azidotetraethylene glycol viologen-Bodipy dyad 5.4b.**

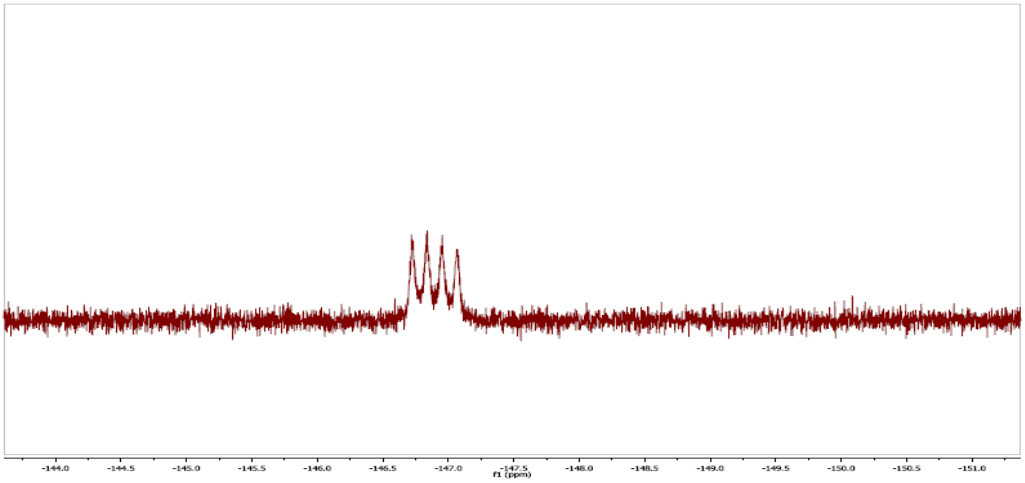

Figure 5.18a'. ^{19}F NMR spectrum of **Benzyl azidotetraethylene glycol viologen-BODIPY dyad 5.4b.**

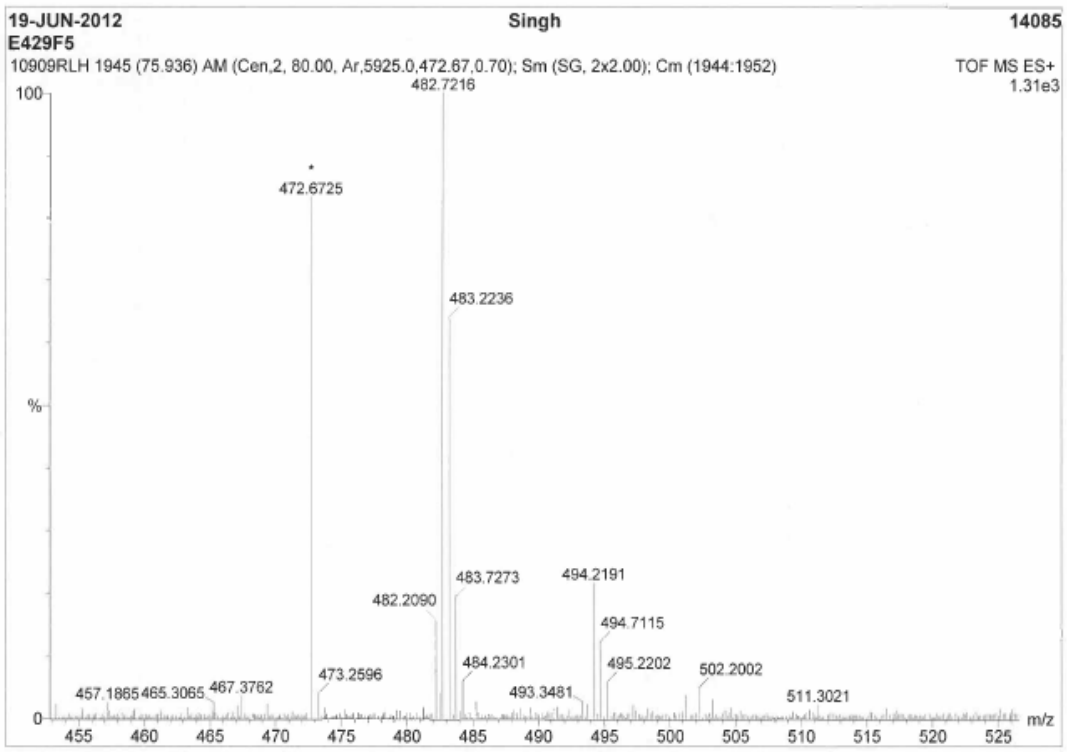

Figure 5.18c. Mass spectrum of **Benzyl azidotetraethylene glycol viologen-Bodipy dyad 5.4b.**

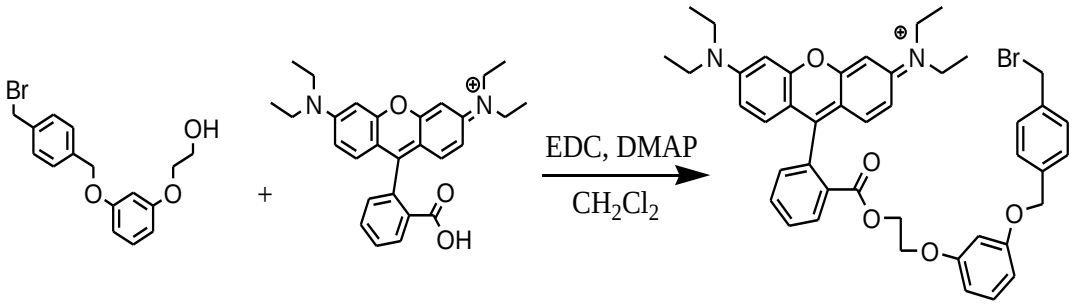

Rhodamine- B ester. To a 100 mL reaction flask, rhodamine B (1.25 g, 2.61 mmol), 2-(3-(2-bromomethyl)benzyloxy)phenoxy)ethanol (.968 g, 2.87 mmol), 1-ethyl-3-(3-dimethylaminopropyl)carbodiimide (0.751 g, 3.92 mmol), *N,N*-dimethylaminopyridine (48 mg, 0.39 mmol) and dichloromethane (20 mL) were

added. The mixture was stirred for 3 d at room temperature. The solvent was removed via vacuum evaporation. The compound was purified by column chromatography (SiO_2, 98:2 CH_2Cl_2:CH_3OH) to provide Rhodamine- B ester **2** (717 mg, 34% yield) as a purple colored solid. ^{1} H NMR (400 MHz , $CDCl_3$): δ 8.31 (d, 1H, J = 8 Hz), 7.81 (t, 1 H, J = 8 Hz), 7.72 (t, 1H, J = 8 Hz), 7.42 (s, 4H), 7.30 (d, 1H, J = 8 Hz), 7.16 (t, 1H, J = 8 Hz), 7.06 (dd, 2H, J = 9.4 Hz, 1 Hz), 6.88 (m, 2H), 6.68 (d, 2H, J = 2.4 Hz), 6.6 (m, 1H,), 6.31- 6.36 (m, 2H), 5.04 (s, 2H), 4.59 (s, 2H), 4.32 (t, 2H, J = 4 Hz), 3.81 (t, 2H, J = 4 Hz), 3.57 (q, 8H, J = 7.2 Hz), 1.28 (t, 12H, J = 7 Hz) ^{13}C NMR (100 MHz, CD_3 $COCD_3$) δ 164.99, 159.93, 159.78, 158.52, 157.73, 155.63, 137.71, 133.48, 133.08, 131.29, 130.44, 130.36, 130.13, 129.91, 128.93, 127.88, 114.44, 113.56, 107.17, 107.01, 101.95, 95.99, 69.24, 65.68, 63.89, 45.68, 45.64, 11.95 HRMS- ESI *m/z* calculated for$[C_{44}H_{46}BrN_2O_5]^+$ 761.2590; found 761.2586,763.2577 for $[M]^+$ and $[M+2]^+$.

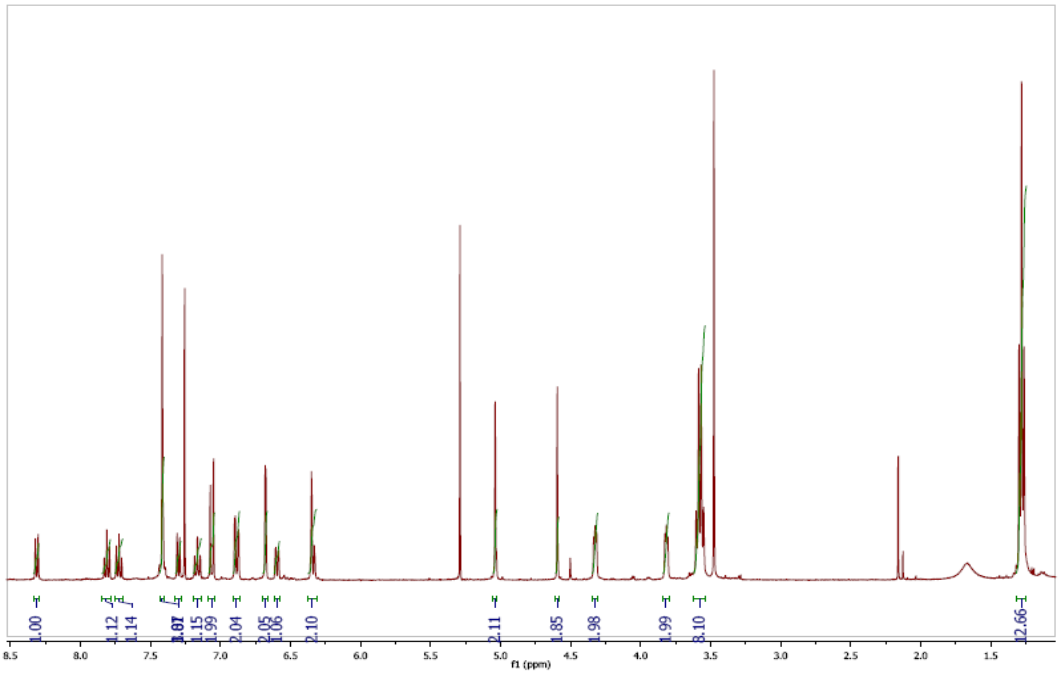

Figure 5.19a. ^{1}H NMR spectrum of **Rhodamine B ester.**

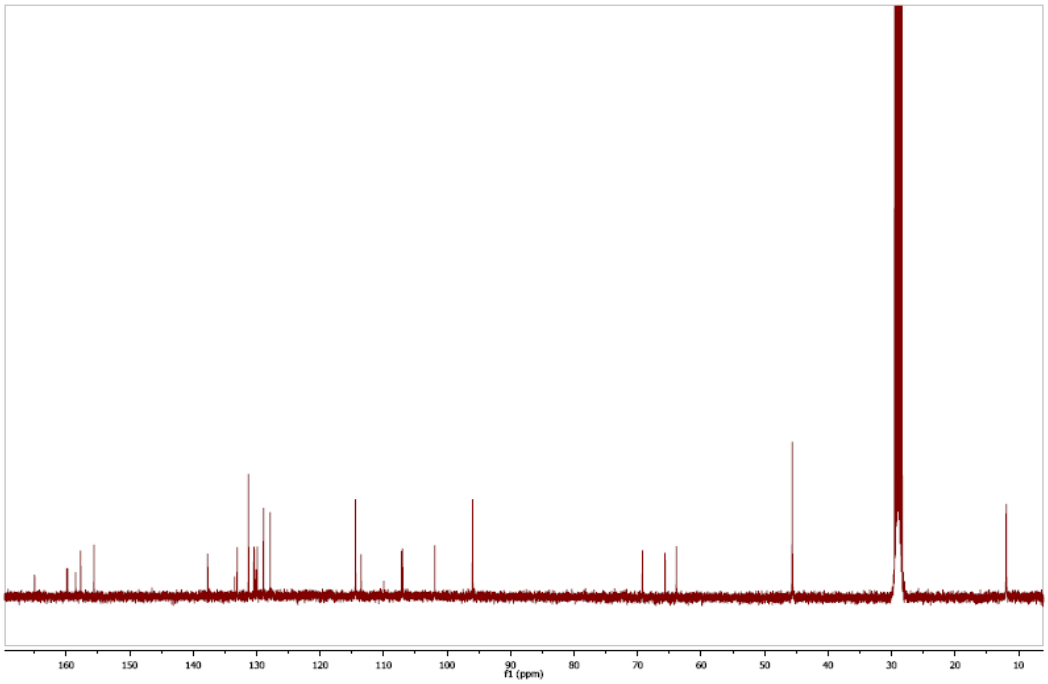

Figure 5.19b. ^{13}C NMR spectrum of **Rhodamine B ester.**

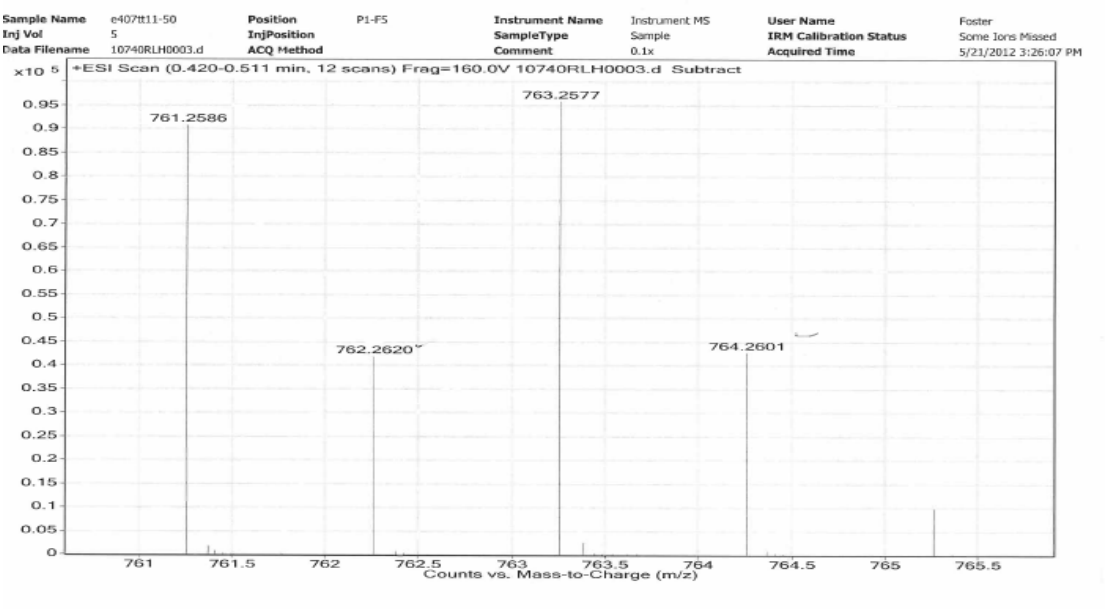

Figure 5.19c. Mass spectrum of **Rhodamine B ester.**

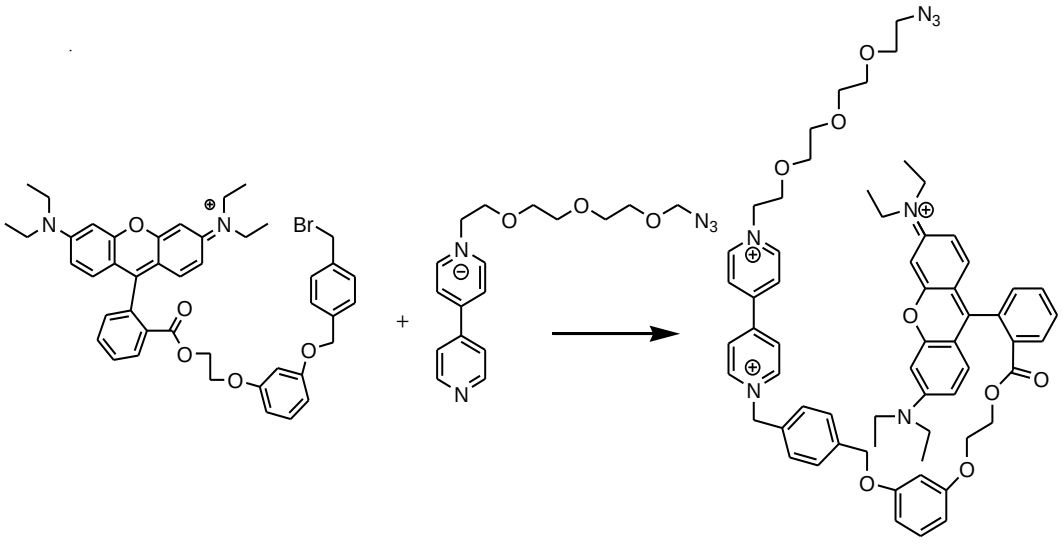

Benzyl azidotetraethylene glycol viologen-Rhodamine B 5.4b dyad. In a 100 mL reaction flask**,** azidotetraethylene glycol viologen (130 mg, 0.3 mmol), rhodamine B ester (45 mg, 0.06 mmol) and DMF (5 mL) were added. The mixture was heated at 50 °C for 4 d. The flask was cooled to room temperature and solvent was removed via high vacuum evaporation. The compound was purified by column

chromatography [SiO_2, 5:5 acetone / (7:2:1 MeOH / 2M aq. NH_4Cl / CH_3NO_2)] to provide **4** (45 mg, 59% yield) as a purple waxy solid. ^{1}H NMR (300 MHz, CD_3OD): δ 9.32 (m , 4H), 8.70 (m, 4H), 8.34 (d, 1H, J = 5.7 Hz), 7.78-7.89 (m, 2H), 7.62 (m, 4H), 7.41(d, 1H, J = 5.7 Hz), 7.14 (m, 3H), 7.00 (m, 2H), 6.75 (s, 2H), 6.63 (d, 1H, J = 6.3 Hz), 6.30 (m, 2H), 6.00 (s, 2H), 5.13 (s, 2H), 4.94 (b, 2H), 4.24 (b, 2H), 4.05 (b, 2H), 3.61 (m, 20 H), 3.34 (m, 2H), 1.25 (t, 12H, J = 5.7 Hz) ^{13}C NMR (100 MHz, CD_3 OD) δ 165.33, 159.68, 159.61,158.40, 157.75, 155.56, 150.39, 150.01, 146.37, 145.70, 139.62, 133.25, 132.75, 132.47, 131.10, 130.94, 130.19, 130.06, 129.61, 129.24, 128.26, 127.15, 126.46, 114.04, 113.47, 107.07, 106.68, 101.80, 95.83, 80.54, 70.18, 70.05, 70.00, 69.51, 68.81, 68.65, 65.49, 64.16, 63.77, 61.46, 52.34, 52.01, 50.39, 49.35, 45.39, 29.58, 24.62, 22.42, 11.43. HRMS- ESI *m/z* calculated for $[C_{62}H_{69}N_7O_8]^{2+}$ 519.7603; found 519.7612 for $[M/2-H]^{2+}$.

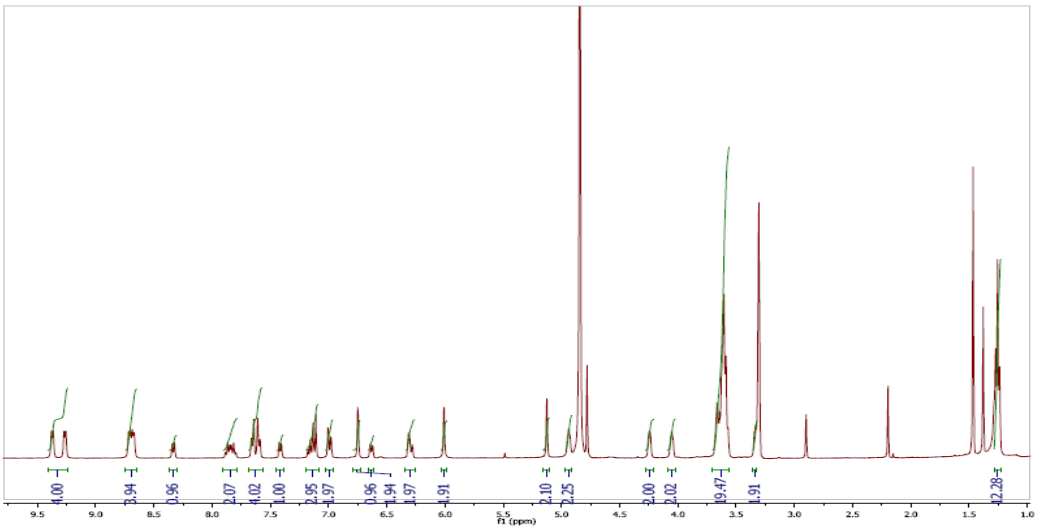

Figure 5.20b. ^{1}H NMR spectrum of **Benzyl azidotetraethylene glycol viologen-Rhodamine B 5.4a dyad.**

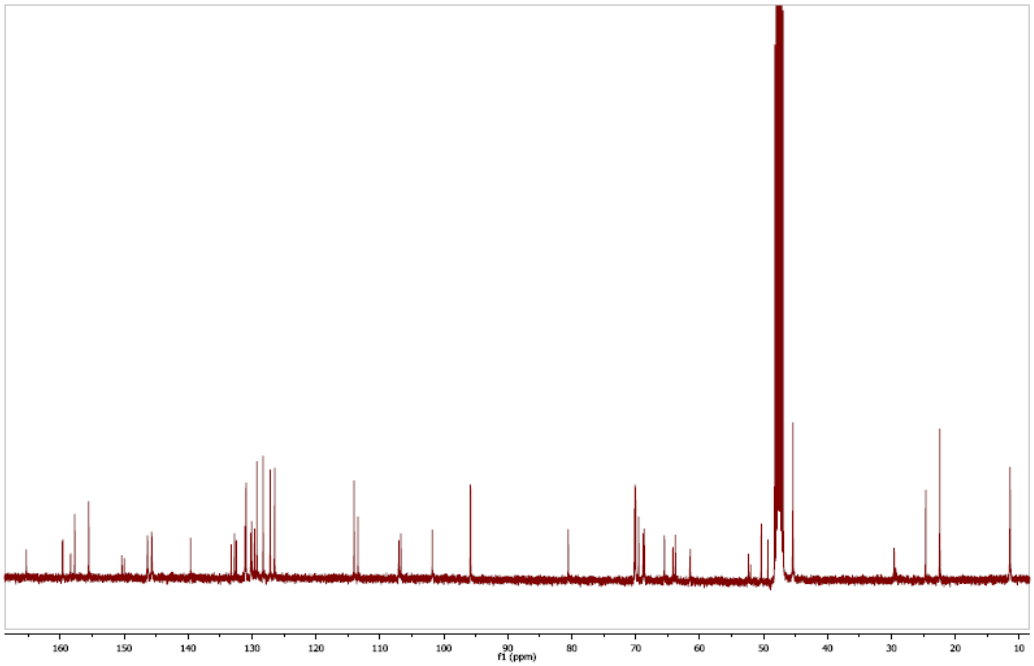

Figure 5.20b. ^{13}C NMR spectrum of **Benzyl azidotetraethylene glycol viologen-Rhodamine B 5.4a dyad.**

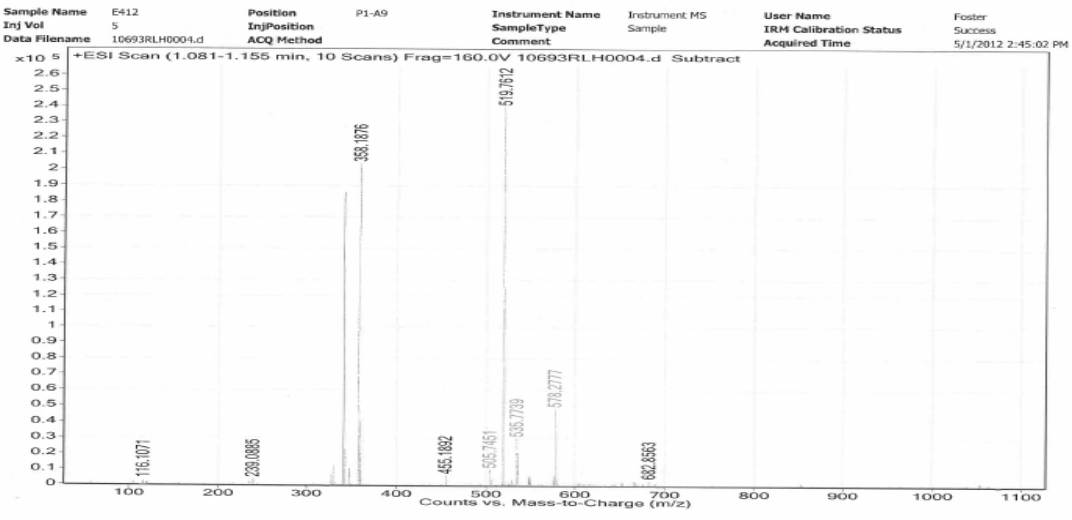

Figure 5.20c. Mass spectrum of **Benzyl azidotetraethylene glycol viologen-Rhodamine B 5.4a dyad.**

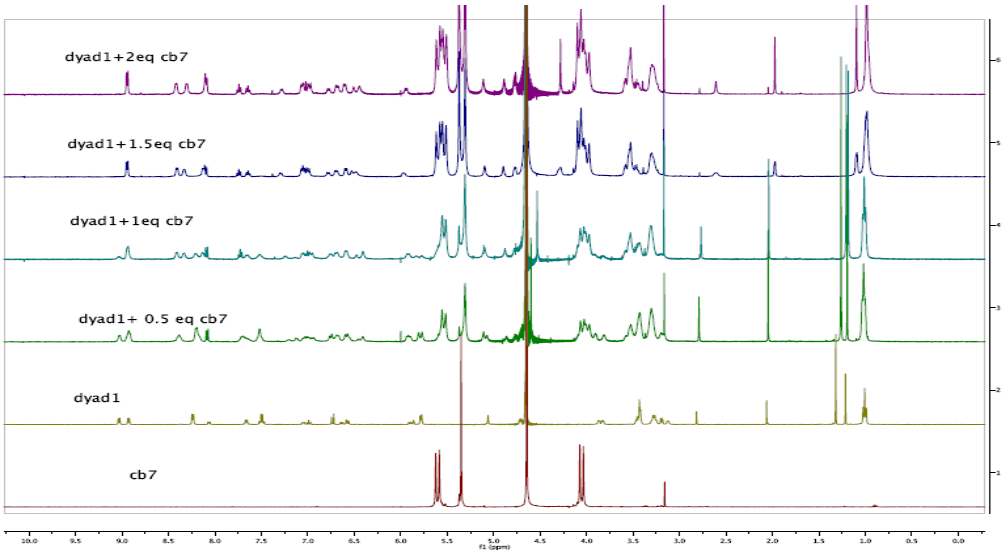

Figure 5.21. ^{1}H NMR spectra (400 MHz, D_2O) of **5.4a** dyad (2.1 mM) with CB7 (0 to 2 equivalent).

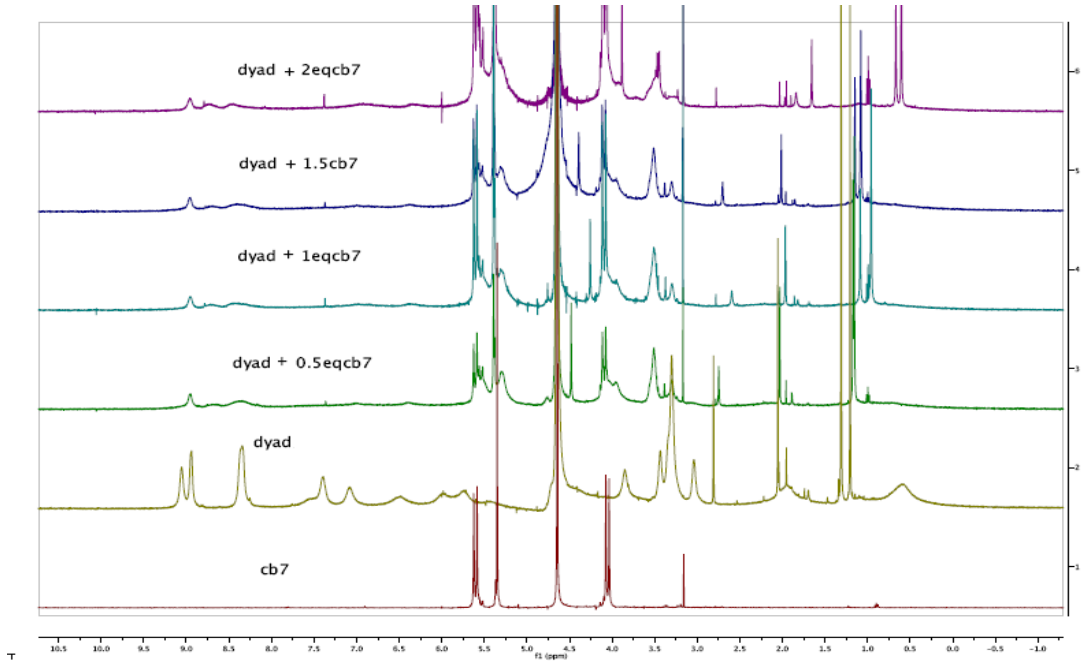

Figure 5.22. ^{1}H NMR spectra (400 MHz, D_2O) of **5.4b** dyad (2.95 mM) with CB7 (0 to 2 equivalent).

Procedure and spectra for absorbance and fluorescence measurements.

Absorbance measurements. Absorbance measurements were done on Shimadzu Scientific Instruments UV-2101 PC UV-Vis scanning spectrophotometer. Measurement was performed in disposable polystyrene cuvettes of 10.0 mm/10.0 mm. The baseline was recorded with water in both sample and reference cuvettes. All the measurements were performed at ambient temperature in air. All the measurements were done on 4 mL sample.

Fluorescence measurements. Fluorescence measurements were done on Shimadzu Scientific Instruments RF-5301 PC spectrofluorophotometer equipped with a xenon lamp of 150 W as an excitation source. Measurement was performed in disposable polystyrene cuvettes of 10.0 mm/10.0mm. In all the measurements slit width was adjusted to 1.5. All the measurements were performed at ambient temperature in air. All the measurements were done on 4 mL sample.

Stock solution of 5.1a dyad. A stock solution (2.367 mM) of dyad 5.1a [$C_{62}H_{70}N_7O_7^{3+}$ Cl^-Br^- I^- ; FW = 1267.52 g/mol] was prepared by dissolving dyad **5.1a** (30 mg, 0.024 mmol) in deionized water (DI water, 25 mL). A portion of the stock solution (211 μL) was taken in a 50 mL volumetric flask and diluted up to 50 mL with DI water to prepare 10 μM solution.

Stock solution of 5.1b dyad. A stock solution (4.6 mM) of dyad **5.1b** [$C_{54}H_{58}BF_2N_7O_7^{2+}$ Br^- I^- ; FW = 1172.6973] was prepared by dissolving **5.1 b** (27 mg, 0.023 mmol) in DI water (10 mL). A portion of the stock solution (109 μL)

was diluted up to 50 mL in 50 mL volumetric flask with DI water to prepare 10 μM solution.

CB7 solution. A CB7 solution (16 mM) was prepared by dissolving CB7 (93 mg, 0.08 mmol) in DI water (5 mL). A portion of the CB7 solution (0.08 mL) was taken and diluted up to 4 mL with DI water to prepare 0.32 mM solution.

Dilution of CB7 for measurement. To a cuvette CB7 solution (4 mL, 16 mM) was added and then portion of the CB7 solution (2 mL) was transferred to the second cuvette and DI water (2 mL) was added to the second cuvette. After mixing the solution properly a portion of this solution (2mL) was transferred to the third cuvette and diluted with DI water (2 mL). Repeating the procedure a series of CB7 dilution was carried out up to 0.0038 mM CB7. Similarly by using stock CB7 (0.32 mM) solution another series of diluted CB7 (0.16- 0.0003 mM) solution was prepared.To the entire cuvettes of CB7 (2 mL) the dyad (2 mL, 10 μM) was added. The solution was mixed properly and then absorbance and fluorescence was measured. The CB7 and dyad solution was mixed properly and then absorbance and fluorescence was measured. All the measurements were done three times and each time the experiment was performed on two sets. The excited wavelength was 562 nm for rhodamine dye and 490 nm for bodipy.

pH titration. A stock solution of HCl (1M) was prepared by taking 2.066 mL HCl (12.1 M) and diluted up to 25 mL. A portion of this stock solution (1 mL) was taken in a 10 mL volumetric flask and diluted up to the mark to obtain pH 1

solution. A portion of pH 1 solution (1 mL) was taken in another 10 mL volumetric flask and diluted up to the mark. This way a series of different pH solutions was prepared from pH 1 to pH 6. A stock solution of KOH (0.5 M) was prepared by dissolving it (0.701 g) in DI water (25 mL). pH 12 solution was prepared by diluting stock solution (0.2 mL)into 10 mL volumetric flask with DI water. A portion of pH 12 solution (1 mL) was transferred to another 10 mL volumetric flask and diluted with DI water. In this way dilution was continued to get different pH solutions from pH 12 to pH 6. The pH value was measured on a pH meter.

A stock solution (18.5 mM) was prepared by dissolving 1,4-diaminobenzene (10 mg, 0.092 mmol) in DI water (5 mL). Measurement was performed with 2 (10 μM) equivalent of amine, 1.25 equivalents (6.25 μM) of CB7 and 1 equivalent (5 μM) of dyad. The required concentration of amine, CB7 and dyad was obtained by dilution of stock solution of each.

Absorbance and fluorescence measurement. To the different pH solutions (4 mL) in a 20 mL vial, 1,4-diaminobenzene (50 μL), CB7 (50 μL), and dyad (50 μL) were added respectively and mixed well. Finally total volume (5 mL) was obtained by the addition of suitable amount of respective pH solution. In the solution the concentration of dyad, CB7 and 1,4-diaminobenzene was 5 μM, 6.25 μM and 10 μM respectively. For the measurement of UV-absorbance and fluorescence, 4 mL of the solution was taken in a cuvette and the measurements were carried out.

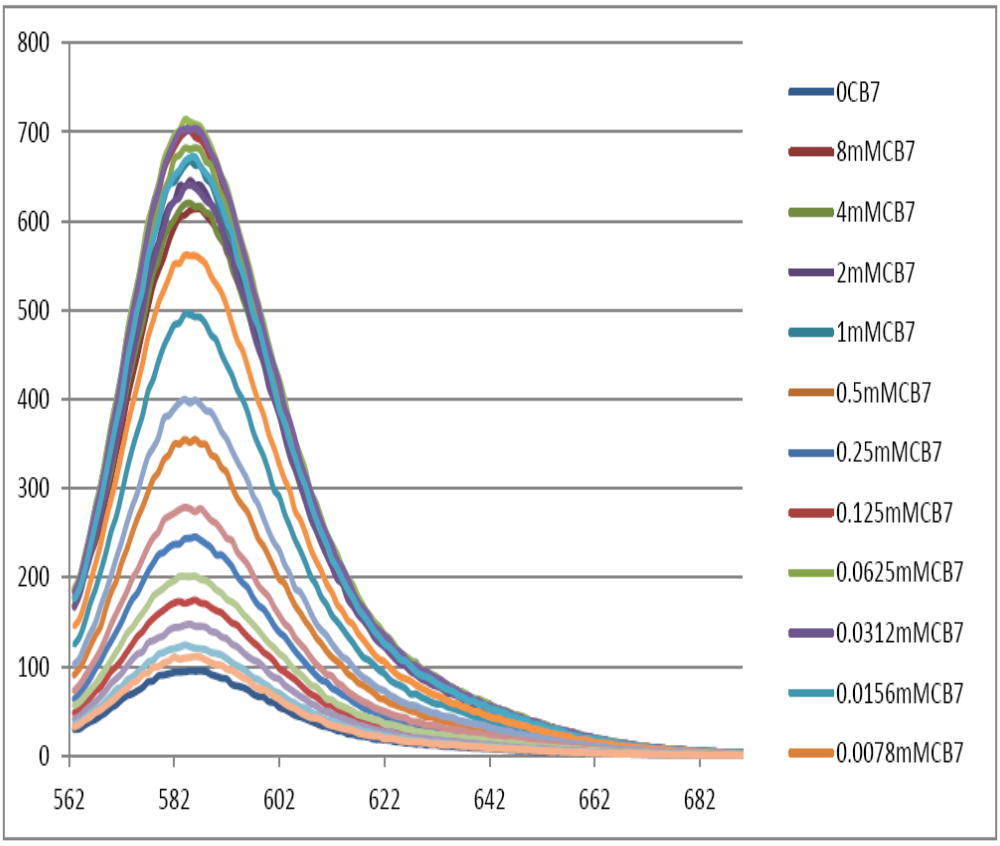

Figure 5.23. Emission spectra of reverse benzyl azido tetraethylene glycol viologen-rhodamine B dyad **5.4a** dyad (5 μM dyad with CB7 (0 mM, 8mM - 0.0019 mM, 0.16 mM- 0.0003 mM) in Millipore water, excitation wavelength = 560 nm).

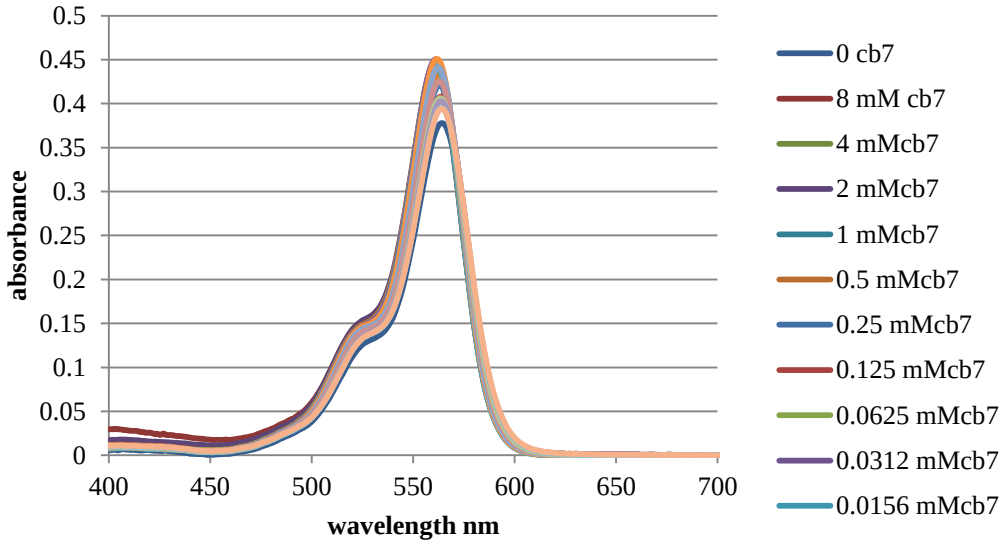

Figure 5.24. UV-Vis absorption spectra of reverse benzyl azido tetraethylene glycol viologen-rhodamine B dyad (5 μM): CB7 (0 mM, 8mM - 0.0019 mM, 0.16 mM- 0.0003 mM) in Millipore water.

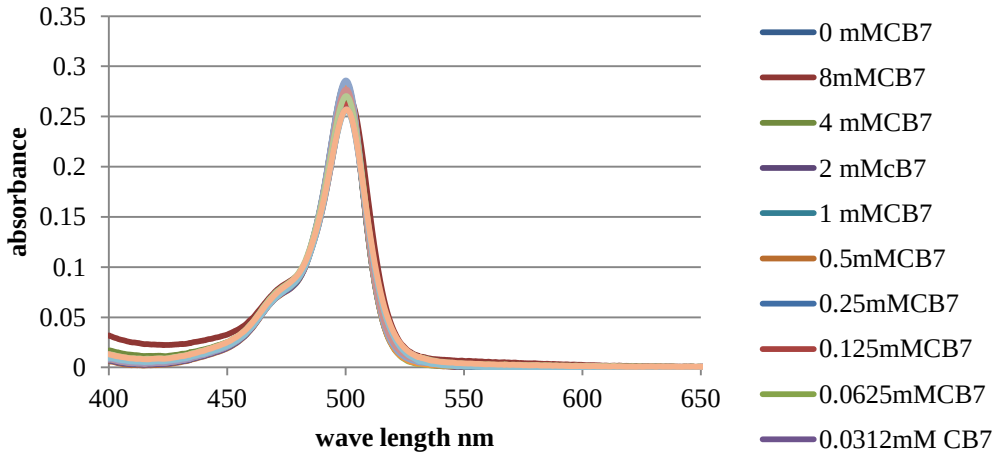

Figure 5.25. UV-Vis absorption spectra of reverse benzyl azido tetraethylene glycol viologen-bodipy dyad (5 μM): CB7 (0 mM, 8mM - 0.0019 mM, 0.16 mM-0.0003 mM) in Millipore water.

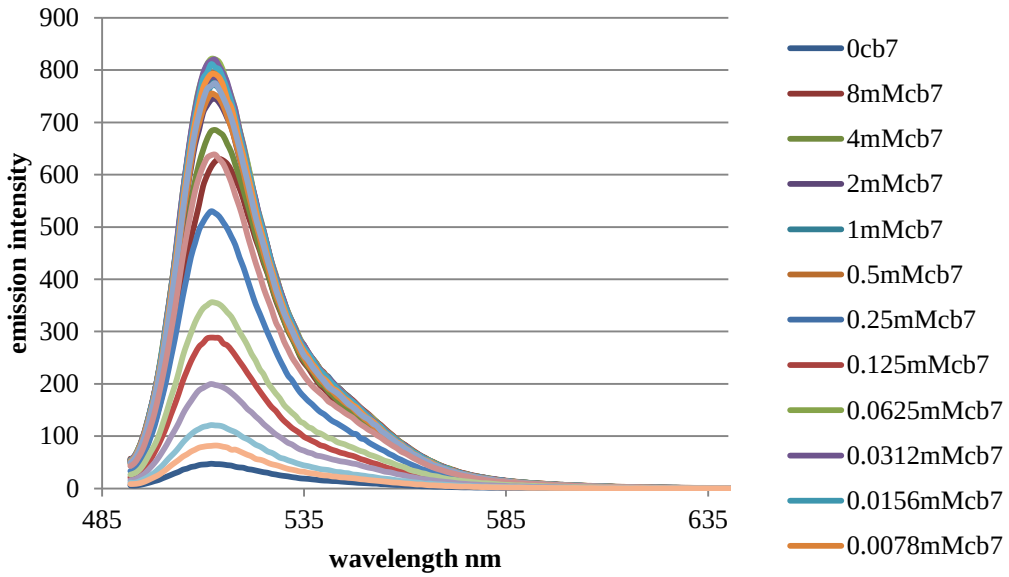

Figure 5.26. Emission spectra of reverse benzyl azido tetraethylene glycol viologen-bodipy 5.4b dyad (5 μM dyad with CB7 (0 mM, 8mM - 0.0019 mM, 0.16 mM- 0.0003 mM) in Millipore water, excitation wavelength = 490 nm).

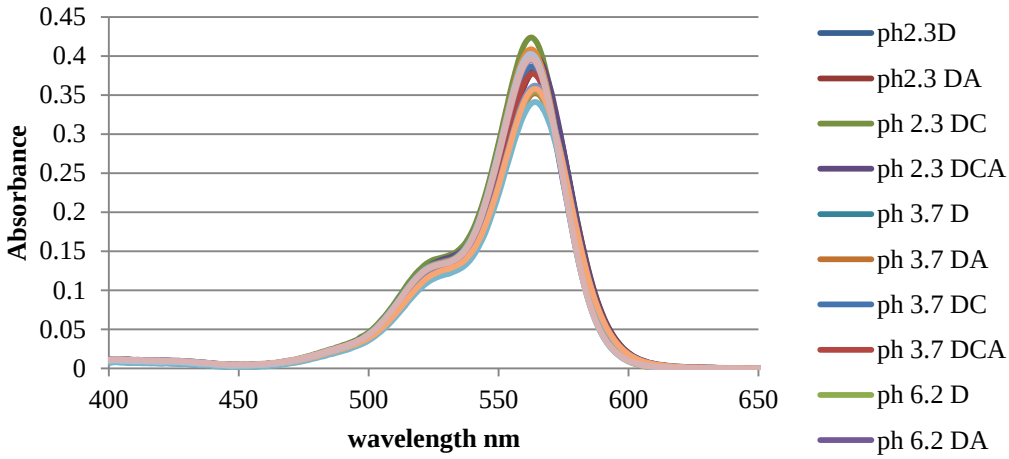

Figure 5.27. Absorbance spectra of reverse benzylviologen-rhodamine B dyad (5

μM dyad + 6.25 μM CB7 + 10 μM 1,4-diaminobenzene, D = dyad, A = diaminobenzene, C= CB7).

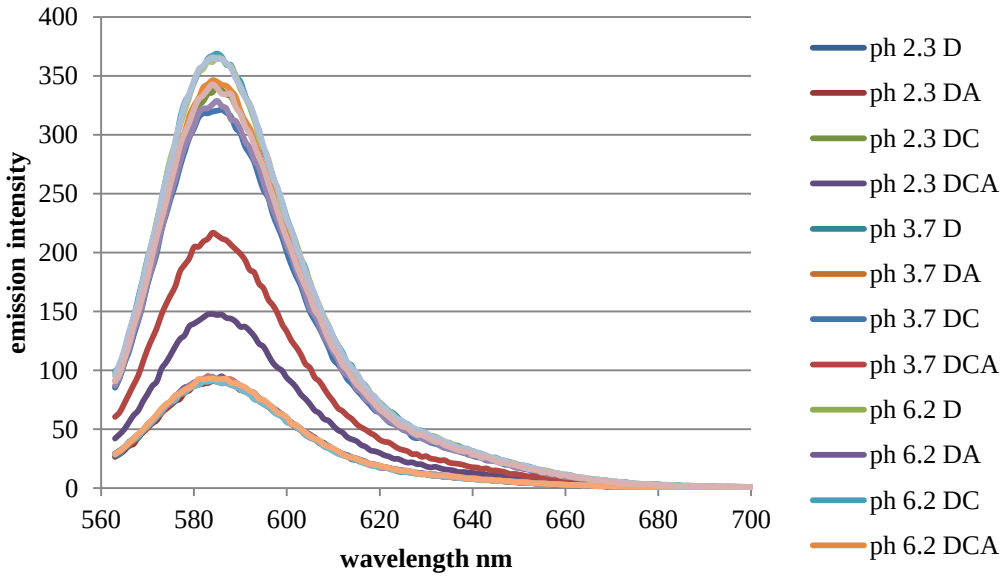

Figure 5.28. Emission spectra of reverse benzylviologen-rhodamine B dyad (5 μM dyad + 6.25 μM CB7 + 10 μM 1,4-diaminobenzene, D =dyad, A= diaminobenzene, C = CB7, excitation wavelength = 560 nm).

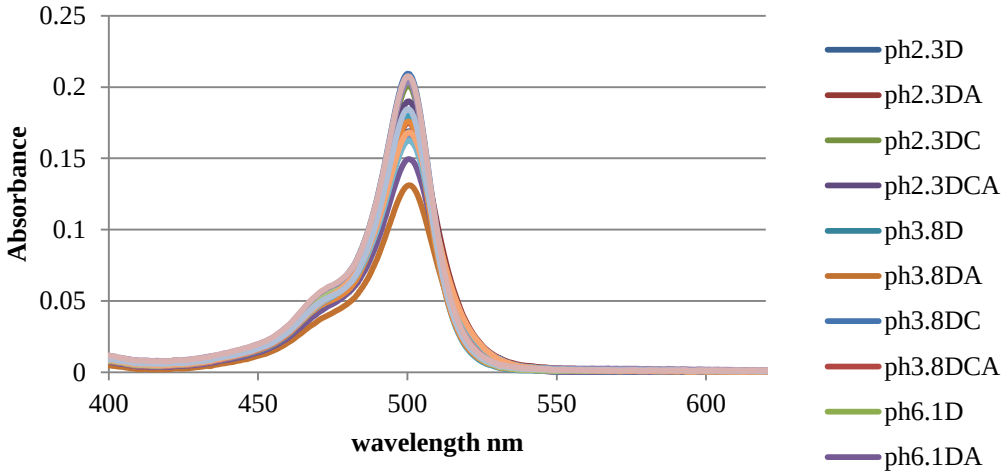

Figure 5.29. Absorbance spectra of reverse benzylviologen-bodipy dyad (5 μM dyad + 6.25 μM CB7 + 10 μM 1,4-diaminobenzene, D=dyad, A= diaminobenzene, C= CB7).

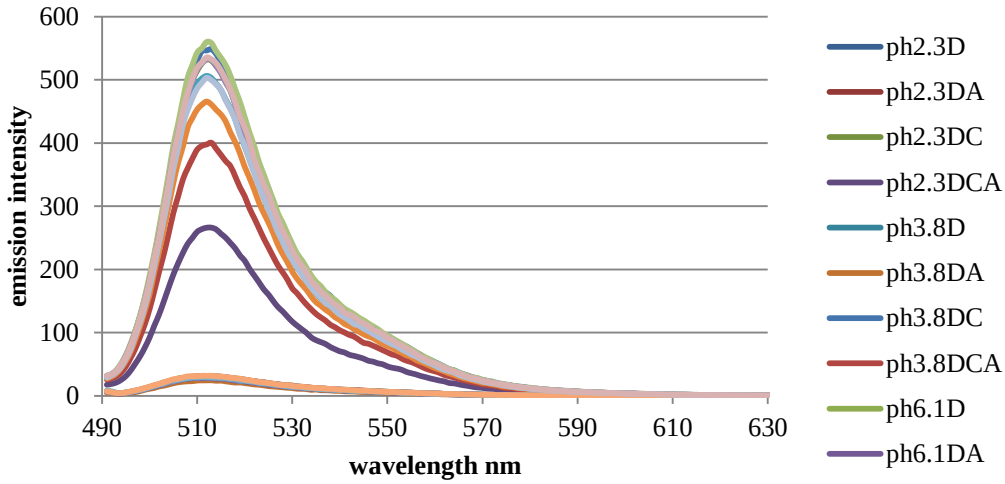

Figure 5.30. Emission spectra of reverse benzylviologen-BODIPY **5.4b** dyad (5 μM dyad + 6.25 μM CB7 + 10 μM 1,4-diaminobenzene, D =dyad, A= diaminobenzene, C= CB7, excitation wavelength = 490 nm).

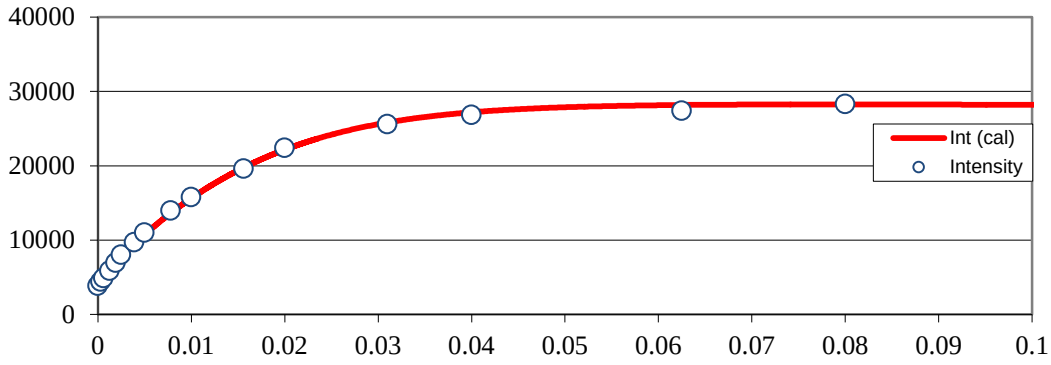

a0	0.013393		
K1	147.450	mM^{-1}	1.474E+05
K2	71.518	mM^{-1}	7.152E+04
CB7 quench	307.143		
Ia	3.219		
Iy	25.461	7.91	
Iz	20.565	0.81	6.39

Figure 5.31. Emission spectra titration curve of reverse benzylviologen-rhodamine B dyad **3.5b** (5 μM in water + CB7, excitation wave length 562 nm and two equilibrium curve fitting model): curve provided by courtesy of Dr. Wai Tak Yip.

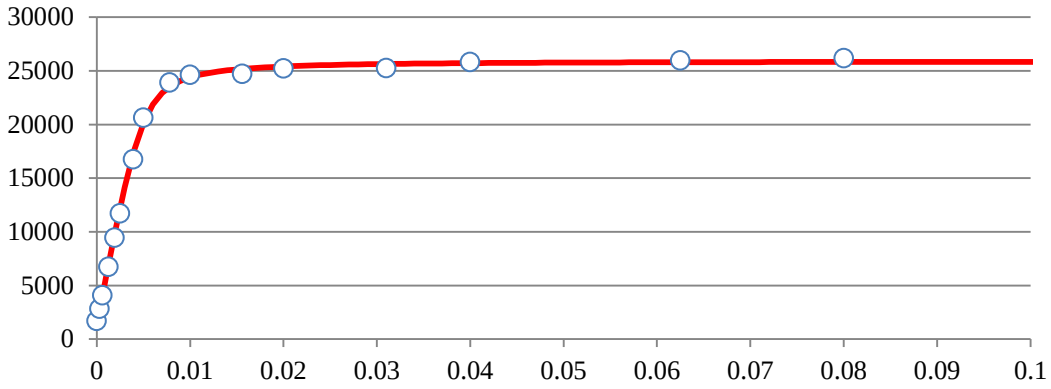

K_C	2718.33	mM^{-1}	2.718E+06	M^{-1}
Int(Dye)	257703			
Int(Complex)	5200217			
CB7 Quenching	689.3572			
Enhancement	20.18			

Figure 5.32. Emission spectra titration curve of reverse benzylviologen-bodipy dyad **3.5c** (5 μM in water + CB7, excitation wave length 490 nm and single equilibrium constant curve fitting model): curve provided by courtesy of Dr. Wai Tak Yip.

5.6 References

1. (a) Weissleder, R; Mahmood, U. Molecular imaging. *Radiology* **2001**, *219*, 316. (b) Thakur, M.; Lentle, B. C. Report of a summit on molecular imaging. *Radiology* **2005**, *236*, 753-755.

2. Ibraheem, A.; Campbell, R. E. Designs and applications of fluorescent protein-based biosensors. *Curr. Opin. Chem. Bio.* **2010**, *14*, 30-36.

3. (a) Giepmans, B.N.; Adams, S.R.; Ellisman, M.H.; Tsien, R.Y. The Fluorescent Toolbox for Assessing Protein Location and Function. *Science* **2006**, *312*, 217-224. (b) Johnsson, N.; Johnsson, K. Chemical Tools for Biomolecular Imaging. *ACS Chem. Biol.* **2007**, *2*, 31-38. (c) Rao, J.; Dragulescu-Andrasi, A.; Yao, H. Fluorescence imaging in vivo:recent advances. *Curr. Opin. Biotechnol.* **2007**, *18*, 17-25. (d) Johnsson, K. Visualizing biochemical activities in living cells**.***Nat. Chem. Biol.* **2009**, *5*, 63-65. (e) Wang, H.; Nakata, E.; Hamachi, I. Recent Progress in Strategies for the Creation of Protein-Based Fluorescent Biosensors. *ChemBioChem* **2009**, *10*, 2560-2577.

4. (a) Funovics, M; Weissleder, R; Tung, C. H. *Anal. Bioanal. Chem*. **2003**, *377*, 956. [PubMed: 12955390]. (b) Weissleder, R; Tung, C. H.; Mahmood, U.; Bogdanov, A. Jr. In vivo imaging of tumors with protease-activated near-infrared fluorescent probes. *Nat. Biotechnol.* **1999**, *17*, 375-378. [PubMed: 10207887].

5. (a) Balzani,V.; Credi, A. ; Raymo, F. M. ; Stoddart, J. F. Molecular Machines. *Angew. Chem.* **2000**, *112*, 3484 – 3530. (b) Kay, E. R. ; Leigh, D. A. ; Zerbetto, F. Synthetic Molecular Motors and Mechanical Machines. *Angew. Chem., Int. Ed.* **2007**, *46*, 72–91. (c) Tian,H.; Wang, Q.-C. *Chem. Prod. Chem. Soc., Rev.* **2006**, *35*, 361 – 374.

6. (a) Lane, A. S.; Leigh, D. A.; Murphy, A. *J. Am. Chem. Soc*. **1997**, *119*, 11092–11093. (b) Mateo-Alonso, A.; Fioravanti, G.; Marcaccio, M.; Paolucci, F.; Jagesar D. C.; Brouwer, A. M.; Prato, M. *Org. Lett.* **2006**, *8*, 5173–5176. (c) Huang, F.; Nagvekar, D. S. ; Slebodnick, C.; Gibson, H. W. A Supramolecular Triarm Star Polymer from a Homotritopic Tris(Crown Ether) Host and a Complementary Monotopic Paraquat-Terminated Polystyrene Guest by a Supramolecular Coupling Method *J. Am. Chem. Soc.* **2005**, *127*, 484–485. (d) Zhou, W.; Zhang, S.; Li, G.; Zhao, Y.; Shi, Z.; Liu, H.; Li, Y. Fluorescent Alteration on a Bistable Molecular Shuttle. *ChemPhysChem* **2009**, *10*, 2066 – 2072.

7. Jiang, W.; Winkler, H. D. F.; Schalley**,** C. A. Integrative Self-Sorting: Construction of a Cascade-Stoppered Hetero[3]rotaxane. *J. Am. Chem. Soc.* **2008**, *130*, 13852–13853. (b) Coutrot, F.; Busseron, E. A New Glycorotaxane Molecular

Machine Based on an Anilinium and a Triazolium Station. *Chem. Eur. J.* **2008**, *14*, 4784–4787.

8. Singh, A.; Yip, W. T.; Halterman, R. L. Fluorescence-On Response via CB7 Binding to Viologen–Dye Pseudorotaxanes. *Org. Lett*. **2012**, *14*, 4046-4049.

9. Kim, J.; Jung, I. S.; Kim, S. Y.; Lee, E.; Kang, J. K.; Sakamoto, S.; Yamaguchi, K.; Kim, K. New Cucurbituril Homologues: Syntheses, Isolation, and X-ray Crystal Structures of Cucurbit[n]uril (n = 5, 7, and 8). *J. Am. Chem. Soc.* **2000**, *122*, 540–541. (b) Day, A.; Arnold, A. P.; Blanch, R. J.; Snushall, B. Controlling Factors in the Synthesis of Cucurbituril and Its Homologues. *J. Org. Chem.* **2001**, *66*, 8094–8100. (c) Kim, K. Mechanically interlocked molecules incorporating cucurbituril and their supramolecular assemblies. *Chem. Soc. Rev.* **2002**, *31*, 96–107. (d) Lagona, J.; Mukhopadhyay, P.; Chakrabarti, S.; Isaacs, L. The Cucurbit[n]uril Family. *Angew.Chem., Int.Ed.* **2005**, *44*, 4844–4870. (e) Isaacs, L. Cucurbit[n]urils: from mechanism to structure and function *Chem.Commun.* **2009**, 619–629. (f) Masson, E.; Ling, X.; Joseph, R.; Kyeremeh-Mensah, L.; Lu, X. Cucurbituril chemistry: a tale of supramolecular success. *RSC Adv.* **2012**, *2*, 1213–1247.

10. Liu, S.; Ruspic, C.; Mukhopadhyay, P.; Chakrabarti, S.; Zavalij, P. Y.; Isaacs L. The Cucurbit[n]uril Family: Prime Components for Self-Sorting Systems. *J. Am. Chem. Soc*. **2005**, *127*, 15959-15967.

11. (a) Lee, J. W. ; Samal, S. ; Selvapalam, N. ; Kim, H.-J. ; Kim, K. *Acc. Chem. Res.* **2003**, *36*, 621–630. (b) Ong, W.; Kaifer, A. E. *Organometallics* **2003**, *22*, 4181–4183. (c) Isaacs, L. *Chem. Commun*. **2009**, 619–629.

12. (a) Bhasikuttan, A. C.; Mohanty, J.; Nau, W. M.; Pal, H. Efficient Fluorescence Enhancement and Cooperative Binding of an Organic Dye in a Supra-biomolecular Host–Protein Assembly. *Angew. Chem., Int. Ed.* **2007**, *46*, 4120–4122. (b) Nau, W. M.; Mohanty, J. Taming Fluorescent Dyes with Cucurbituril. *Inter. J. Photoenergy* **2005**, *7*, 133-141. (c) Mohanty, J.; Nau, W. M. Ultrastable Rhodamine with Cucurbituril. *Angew. Chem*. **2005**, *117*, 3816-3820 (d) Mohanty, J.; Nau, W. M. Ultrastable Rhodamine with Cucurbituril. *Angew. Chem., Int. Ed.* **2005**, *44*, 3750–3754. (e) Dsouza, R. N.; Pischel, U.; Nau, W. M. Fluorescent dyes and their supramolecular host/guest complexes with macrocycles in aqueous solution. *Chem. Rev.* **2011,** *111*, 7941–7980. (f) Halterman, R. L.; Moore, J. L.; Mannel, L. M. Disrupting Aggregation of Tethered Rhodamine B Dyads through Inclusion in Cucurbit[7]uril *J. Org. Chem.* **2008**, *73*, 3266–3269. (g) Halterman, R. L.; Moore, J. L.; Yip, W. T. Cucurbit[7]uril Disrupts Aggregate Formation Between Rhodamine B Dyes Covalently Attached to Glass Substrates. *J. Fluoresc.* **2012**, *21*, 1467–1478. (h) Martyn, T. A.;Moore, J. L.; Halterman, R. L.;Yip, W. T. Cucurbit[7]uril Induces Superior Probe Performance for Single-Molecule Detection. *J. Am. Chem. Soc.* **2007,** *129*, 10338–10339.

13. (a) Ong, W.; Gomez-Kaifer, M.; Kaifer, A. E. Cucurbit[7]uril: A Very Effective Host for Viologens and Their Cation Radicals. *Org. Lett.* **2002**, *4*, 1791–1794. (b) Kim, H.-J.; Jeon, W. S.; Ko, Y. H.; Kim, K. Inclusion of methylviologen in cucurbit[7]uril. *Proc. Natl. Acad. Sci. U.S.A.* **2002**, *99*, 5007–5011. (c) Moon, K.; Kaifer, A. E. Modes of Binding Interaction between Viologen Guests and the Cucurbit[7]uril Host. *Org. Lett.* **2004**, *6*, 185–188. (d) Kalmar, J.; Ellis, S. B.; Ashby, M. T.; Halterman, R. L. Kinetics of Formation of the Host–Guest Complex of a Viologen with Cucurbit[7]uril. *Org. Lett.* **2012**, *14*, 3248–3251.

14. (a) Mock, W. L.; Pierpont, J. A cucurbituril-based molecular switch. J. Chem. Soc., *Chem. Commun.* **1990**, 1509–1511. (b) Tuncel, D.; Özsar, Ö.; Tiftika, H. B.; Salih, B. Molecular switch based on a cucurbit[6]uril containing bistable [3]rotaxane. *Chem. Commun.* **2007**, 1369–1371. (c) Tuncel, D.; Katterle, M. pH-Triggered Dethreading Rethreading and Switching of Cucurbit[6]uril on Bistable [3]Pseudorotaxanes and [3]Rotaxanes. *Chem. Eur. J.* **2008**, *14*, 4110-4116. (d) Sindelar, V.; Silvi, S.; Kaifer, A. E. Switching a molecular shuttle on and off: simple, pH-controlled pseudorotaxanes based on cucurbit[7]uril. *Chem. Commun.* **2006**, 2185–2187.

15. Koner, A. L.; Nau, W. M. Enhancing Fluorescence and Photostability Properties of Dyes. *Supramol.Chem.* **2007**, *19*, 55-66.

16. (a) de Silva, A. P.; Gunaratne, H. Q.; Gunnlaugsson, T.; Huxley, A. J. M. McCoy, C. P.; Rademacher, J. T.; Rice, T. E. Signaling Recognition Events with Fluorescent Sensors and Switches. *Chem. Rev.* **1997**, *97*, 1515–1566. (b) Tang, X.; Peng, X.; Dou, W.; Mao, J.; Zheng, J.; Qin, W.; Liu, W.; Chang, J.; Yao, X. Design of a Semirigid Molecule as a Selective Fluorescent Chemosensor for Recognition of Cd(II). *Org. Lett.* **2008**, *10*, 3653–3656. (c) Taki, M.; Desaki, M.; Ojida, A.; Lyoshi, S.; Hirayama, T.; Hamachi, I.; Yamamoto, Y. Fluorescence Imaging of Intracellular Cadmium Using a Dual-Excitation Ratiometric Chemosensor . *J. Am. Chem. Soc.* **2008**, *130*, 12564-12565.

17. Schmidt, F. ; Rosnizeck, I. C.; Spoerner, M. ; Kalbitzer, H. R.; König, B. Zinc(II)cyclen–peptide conjugates interacting with the weak effector binding state of Ras. *Inorg. Chim. Acta* **2011**, *365*, 38-48.

18. Nagamura, T.; Sakano, T.; Ozawa, M.; Tanaka, A.; Hirata, O.; Odoi, K.; Electrochromic material. *PCT Int. Appl.* **2009,** WO 2009136626 A1 20091112**.**

19. Bhattacharya, P.; Kaifer, A. E**.** Preparation, Characterization, and Electrochemical Properties of a New Series of Hybrid Dendrimers Containing a Viologen Core and Frechet and Newkome Dendrons. *J. Org. Chem.* **2008,** *73*, 5693–5698.

20. Sindelar, V.; Moon, K.; Kaifer, A. E. Binding Selectivity of Cucurbit[7]uril: Bis(pyridinium)-1,4-xylylene versus 4,4'-Bipyridinium Guest Sites. *Org. Lett.* **2004,** *6*, 2665–2668.

21. Halterman, R. L.;Moore, J. L.; Yakshe, K. A.; Halterman, J. A. I.; Woodson, K.A. Inclusion complexes of cationic xanthene dyes in cucurbit[7]uril. *J. Incl.Phenom. Macro.Chem.* **2010**, *66*, 231–241.

22. Bitter, J. H.; Dommele, S. van; Jong, K. P. On the virtue of acid–base titrations for the determination of basic sites in nitrogen doped carbon nanotubes *Catal. Today* **2010,** *150*, 61-66.